FAILURE ANALYSIS OF UNIQUE CHILD PASSENGER SAFETY SCENARIOS

by

KRISTY DAWN BRINKER BROUWER

A dissertation submitted in partial fulfillment of the
requirements for the degree of

DOCTOR OF PHILOSOPHY IN MECHANICAL ENGINEERING

2025

Oakland University
Rochester, Michigan

Doctoral Advisory Committee:

Michael A. Latcha, Ph.D., Chair
Yin-Ping Chang, Ph.D.
Alexey Tonyushkin, Ph.D.
Theresa Atkinson, Ph.D.

ACKNOWLEDGMENTS

This project would not be complete without the excellent guidance and expert counsel from Michael Latcha, Patrick Atkinson, Theresa Atkinson, Brenda Lemke, Jennifer Bastiaan, as well as, my legion of colleagues who encouraged and supported me continuously at Kettering University.

I am deeply grateful to my husband, Chris, and my son, Drew, for amending all three of our lives to make my academic goal a priority for our family. I truly could not complete this challenging journey without their unwavering support and unconditional love and understanding. Thank you both for never asking “when will you be done?”

Kristy Dawn Brinker Brouwer

PREFACE

Child passenger safety is a topic I have been passionate about for decades beginning with my undergraduate studies. I received both a Bachelor of Science and Master of Science from Kettering University in Mechanical Engineering - Bioengineering Applications. My diverse work background includes 25 years of wide-ranging experience in several industries including: driveline components (GKN Automotive), safety restraints and federal regulation testing (Autoliv), military robotics and autonomous vehicles (TARDEC and US Army), as well as, athletic shoe testing, osteoarthritis and breast cancer research in biomechanics laboratories at Michigan State University and Oakland University. I hold two US patents in airbag technologies including one that reduces airbag deployment risk with rear-facing child seats. For the past 17 years, I have been actively teaching, serving as a board member, and volunteering as a certified Child Passenger Safety Technician and Instructor for Safe Kids Worldwide, all over the United States, advocating for the safe transportation of our most precious cargo.

ABSTRACT

"FAILURE ANALYSIS OF UNIQUE CHILD PASSENGER SAFETY SCENARIOS"

by

Kristy Dawn Brinker Brouwer

Adviser: Michael A. Latcha, Ph.D.

Special circumstance scenarios exist where a child safety seat (CSS) cannot be, or is not, used according to best practices recommended by the American Academy of Pediatrics. This research identifies three such scenarios that uniquely affect the safe use of CSS. The first scenario examines children fitted with a lower extremity body cast due to developmental dysplasia of the hip (DDH) or femur fracture that prevent proper CSS fit for the child or the caregiver's vehicle. A CSS must be used properly, according the user manual and vehicle owner's manual, to ensure the child's safety in and around vehicles. However, even with these available instructions, it is very common for caregivers to misuse the CSS. The second scenario in this research looks specifically at when the CSS is improperly used as a child restraint outside of a vehicle. Finally, the future of mobility is trending towards an incorporation of autonomous ride-share vehicles on public roads. Proposed automated vehicles (AV) vary greatly in size and shape, both on the exterior and the interior. With these changes, along with the likelihood of bi-directional drive AVs, CSS best practices for use may no longer be able to be followed. The third scenario develops a Design Failure Mode and Effects Analysis (DFMEA)

specific to children being transported in AVs operating at Society of Automotive Engineers (SAE) Level 4 or Level 5 Driving Automation to investigate the specific potential failure modes and effects of child passenger safety in automated vehicles.

TABLE OF CONTENTS

TABLE OF CONTENTS—Continued

LIST OF TABLES

LIST OF FIGURES

LIST OF ABBREVIATIONS AND UNITS

AAP	American Academy of Pediatrics
ADAS	Advanced Driver Assistance Systems
ADS	Automated Driving Systems
ATD	Anthropomorphic Test Dummy
AV	Automated Vehicle
b	Damping Coefficient
BSD	Booster Spring-Dampers
CAV	Connected and Automated Vehicles
C.F.R.	Code of Federal Regulations
CHI	Closed Head Injury
cm	Centimeters
CPS	Child Passenger Safety
CPST	Child Passenger Safety Technician
CRS	Child Restraint System
CSS	Child Safety Seat
DOE	Design of Experiments
DDH	Developmental Dysplasia of the Hip
DFMEA	Design Failure Modes and Effects Analysis
E	Modulus of Elasticity
ED	Emergency Department
EMS	Emergency Medical Services

FMVSS	Federal Motor Vehicle Safety Standards
g	Acceleration Due to Gravity in meters per second
Gx	Global x position
Gy	Global y position
h	height
HIC	Head Injury Criterion
HIC36	Head Injury Criterion Over a 36 millisecond Time Interval
IC	Infant Carrier
IRB	Institutional Review Board
ISOMME	International Organization for Standardization Measurement Metadata Exchange
k	Spring Constant
kg	kilograms
LATCH	Lower Anchors and Tether for Children
LBSD	Lap Belt Spring-Damper
m	Meters
ms	Milliseconds
μ_s	Coefficient of Static Friction
μ_k	Coefficient of Kinetic Friction
NEISS	National Electronic Injury Surveillance System
NHTSA	National Highway Traffic Safety Administration

N	Newtons
N_{ij}	Normalized Neck Injury Criterion
N-s	Newton-seconds
NSC	National Safety Council
NSD	Neck Spring-Damper
OOP	Out Of Position
ρ	Density
SAE	Society of Automotive Engineers
SARC	Scholarly Activity Review Committee
SBSD	Shoulder Belt Spring-Damper
SKAVA	Safe Kids in Advancing Vehicle Alliance
SKW	Safe Kids Worldwide
STAC	Safe Travel for All Children
SUV	Sport Utility Vehicle
SWE	Society of Women Engineers
UTSD	Upper Tether Spring-Damper
w	width
2D	2-Dimensional

INTRODUCTION

Since the 1960s, a vast number of studies have been conducted on the safe transportation of children. Durbin et al. (2018b) presented the current best practices, based on these previous research studies, for age-appropriate vehicle restraint from the American Academy of Pediatrics (AAP). Child Safety Seats (CSS) have been proven to be effective in reducing motor vehicle crash injuries and deaths in children aged 12 and under if all three of the following conditions are simultaneously true

- the CSS fits the child;
- the CSS fits the vehicle;
- the CSS is used properly every single time.

However, there are special circumstance scenarios where one or more of these conditions cannot be met. This research identifies three such scenarios that uniquely affect the safe use of CSS.

Part One

The first scenario examines children fitted with a lower extremity body cast due to Developmental Dysplasia of the Hip (DDH) or femur fracture. This cohort typically cannot fit in the traditional, commercially-available CSS due to the fixed angles of the child's hips, knees, and ankles in the cast. In addition, the rigid cast can also interfere with the interior architecture of the vehicle transporting the child. These challenges resulted in the first two research questions that will be analyzed in Part One:

1. For children fitted with spica casts, is there a low-cost, commercially available CSS option that fits a range of child ages, heights, weights, and cast configurations?
2. Can children fitted with varying spica cast configurations be safely restrained in a variety of modern vehicles by their caregivers?

Part Two

A CSS must be used properly to ensure the child's safety in and around vehicles. The CSS instruction manual provided by the manufacturer lists the acceptable usage ranges based on the child's height, weight, age, and when to stop usage due to CSS expiration. The manual provides step-by-step instructions for caregivers on how to correctly install the CSS in a vehicle using the vehicle's owner's manual, the seat belt restraint system, and the Lower Anchors and Tether for Children (LATCH). The manual educates caregivers on how to properly position the child in the seat, how to adjust and tighten the harness and crotch buckle straps, and provides safety recommendations for CSS use inside and outside of the vehicle. Nevertheless, it is very common for caregivers to misuse the CSS. Part Two, looks specifically at when the CSS is improperly used as a child restraint outside of a vehicle. The third question to be investigated by this study is:

3. What is the most common non-transportation related misuse scenario of a CSS that resulted in an injury requiring emergency department visitation?

Part Three

Finally, the future of mobility is trending towards an incorporation of autonomous ride-share vehicles on public roads. Proposed automated vehicles (AV) vary greatly in size and shape, both on the exterior and the interior. Seating rows, positions, and directions now all have the possibility to change when a driver's seating position is removed from the AV layout. With these changes, along with the likelihood of bi-directional drive AVs, CSS best practices advised by Durbin et al. (2018a, 2018b) may no longer be able to be followed. This results in the final two questions to ensure child passenger safety has been adequately considered in the development of AVs:

4. How will we ensure that child restraints will be compatible with upcoming automated vehicles when currently no federal standards exist?
5. What are the potential failure modes and effects of child passenger safety in automated vehicles?

This dissertation aims to address the questions posed by exploring previous studies and their limitations, ultimately leading to the formulation of a hypothesis for each question. The methods used to test these hypotheses will be outlined, and the results will be summarized to support the conclusions drawn. The primary objective is to enhance child passenger safety by examining the specific safety scenarios considered.

PART ONE

SCENARIO 1: CHALLENGES WITH SAFELY POSITIONING CHILDREN TREATED WITH A HIP SPICA CAST

1.1 Literature Review

Motor vehicle collisions are the leading cause of death for children in the United States. (Durbin et al., 2018a, 2018b). Yet, the risk of traumatic injury or death can be significantly reduced when children are correctly restrained in the vehicle, with some studies reporting a risk reduction of injury by up to 82% (Durbin et al., 2018a, 2018b; Zaloshnja et al., 2007). Safe restraint can be difficult when children do not easily fit in a child safety seat (CSS), such as when they are placed in a hip spica cast typically used to treat developmental dysplasia of the hip (DDH) and femur fractures. Hip spica casts come in various configurations, which include the bilateral-leg hip spica with some designs incorporating wood dowels connecting the knees, as well as single-leg hip and one-and-a-half-leg hip designs that allow for limited walking.

The casting can represent a significant burden of care for the family, not only for managing daily activities but also for ensuring safe transportation to medical appointments and other essential travel. Gockley et al. (2015) studied challenges in safely transporting children by investigating 52 children treated with hip spica casts. They document that 75% of the children were restrained with either a special CSS designed for the spica cast or a harness commonly used for special needs children. The remaining children were either transported in an ambulance (17%) or the family's original CSS (8%). Since 92% of the cases utilized a specialized CSS or ambulance transport other than the family's original CSS, there appear to be issues with safely positioning a child fitted with a hip spica cast. Several studies have commented on the fixed posture of the spica cast and how it affects the positioning of the child in a CSS. (Zielinski et al.,2009; Mead et al., 2020; Collins, McKean, et al., 2022) For DDH-styled casts, a typical, traditional CSS includes side bolsters and/or arm rests that interfere with the lateral casted thighs as the child is slid rearward into the CSS. Interference with the lateral thighs is common for the DDH cast due to fixed hip abduction of ~60° per leg (~120° between thighs) with the net effect that the child typically sits forward in the CSS. In addition, the hips and knees are typically flexed ~80° for the DDH cast. This can lead to contact between the posterior aspect of the casted calf area with the front of the seat pan. Such contact can also force the child to sit forward on the child seat. For femur fracture-styled casts, while the hip abduction is typically less (~30°), the hips are typically only flexed ~30°. This relatively low hip flexion magnitude also causes the casted child to also sit forward on the seat and there is a large gap between the spine and seat back of the CSS.

For both cast types, the groin strap anchor on a traditional CSS is positioned too far back on the CSS seating surface and is typically positioned under the child's buttocks. As such, the groin strap must wrap over the perineal region and groin as it buckles with the shoulder straps between the child's legs (Collins et al., 2020). In addition, if the groin strap is not sufficiently long, the buckle will sit low on the child's groin. This is an issue for the femur fracture styled cast which has a relatively narrow space between the casted thighs due to the smaller hip abduction angles and the added size of the thigh due to the cast material. Longer groin straps anchored farther forward on the CSS seating surface raises the buckle sufficiently superior on the child's lower body to allow the two shoulder straps to attach to the groin strap buckle.

It is worth noting that a variety of laboratory studies have investigated children with a hip spica cast. This work used child-sized anthropomorphic test dummies (ATD), typically used in automotive crash testing, fitted with DDH or fracture-styled casts and subjected to frontal and side impact crash tests per Federal testing guidelines set forth in the Federal Motor Vehicle Safety Standard (FMVSS) No. 213 (NHTSA, 2024b). The casted ATDs were restrained in a variety of CSS and yielded data on the relative safety of a child with a hip spica cast in a vehicle collision. However, there were some key limitations in each of the previous studies that required investigation. First, these laboratory studies all utilized a standard seat assembly, commonly referred to as a bench seat, as called for in FMVSS No. 213 and resulted in test set-ups not representative of current real-world vehicle seating positions. The bench seat used in regulation testing is based on typical rear seats from the 1970s to represent a typical vehicle seat (Wietholter et al., 2021). Studies conducted by Oliver II et al. (2009), Collins et al. (2020), Zielinski et al. (2009), Mead et al. (2020), Collins, Adams, et al. (2022), and Collins, McKean, et al. (2022) were performed on the sled bench. In contrast, modern vehicle seats are typically 'bucket' designs intended for one occupant and include raised side bolsters on the lateral aspect of the thighs (Maltese et al., 2014).

In addition, the testing guidelines allow the research team unrestricted access to the bench seat from the front, sides, and behind the bench seat. Unobstructed CSS installation was shown by Patton et al. (2022) to be not representative of the actual installation constraints experienced by CSS end-users due to interference from the front seating row, door opening width, interior trim, and headliner.

In contrast, access for the real-world in-vehicle environment is limited by seating in the row forward of the child. This can be an issue since some rear-facing seats occupy a great deal of fore-aft space and may prevent the occupants in the forward row from adjusting their seat rearward. Additional sources of interference not represented in FMVSS No. 213 include the roof and the vehicle door which must be able to close and not encroach on the child. As well as, access from the rear of the vehicle is typically eliminated in cases such as the second row of a pickup truck or passenger car. As such, it would be helpful to explain the extent to which the hip spica cast affects the ability to safely restrain a casted child in typical modern vehicles.

"Spica casted child may require specialized restraint", but no additional guidance was provided from AAP. (Durbin et al., 2018b). Oliver II et al. (2009) and Herman et al. (2011) both noted that a lack of U.S. Standards for safe transportation of children in spica casts exists. Safe transportation options have been investigated in several other studies (Bull et al., 1999; Gockley et al., 2015; Herman et al., 2011; Collins et al., 2020; Zielinski et al., 2009); however, the options are either expensive, difficult to use, or not approved for spica cast use by the CSS manufacturer. In 2020, Collins et al. found that safe transport of spica-casted children using commercially available car seats is viable, and O'Neil et al. stated in 2009 that CSS restraints should not be modified unless that modified system has been crash tested.

To aid caregivers with the challenges they face with transporting their casted children, Herman et al. (2011) and Adams et al. (2019) performed patient observation studies that encompassed hospital loaner-CSS programs, rental-CSS programs, ambulance transport, hospital discharge guidance adherence, and the associated monetary costs and discharge delays incurred by families. Overwhelmingly, they found that caregivers became frustrated and resorted to ignoring advice given at hospital discharge (Oliver II et al., 2009; Herman et al., 2011; Zielinski et al., 2009), attempting to use ill-fitting, non-approved personal CSS (Adams et al., 2019), improper vehicle seat belt routing (Oliver II et al., 2009; Herman et al., 2011), or in some cases no safety restraint use at all (Herman et al., 2011).

The literature demonstrates that spica-specific hospital discharge improvements are needed. Gockley et al. (2015) and Collins et al. (2020) suggest spica-specific trained medical staff for hospital discharge. Oliver II et al. (2009) believes that clearer discharge education and resources for caregivers would result in better outcomes for patient safety. Other studies focus on the need for more cost-effective options for caregivers and/or improved hospital-based CSS loaner programs (Herman et al., 2011; Adams et al., 2019).

1.2 Hypothesis Development

Previous research has concluded that transportation of spica-casted children during their 6-12 weeks of cast wear is extremely difficult and frustrating for caregivers. This difficulty was due to many factors, either individually or in combination, such as cast type, CSS installation direction based on child age, spica-specific CSS cost, and spica-specific CSS installation fit in the caregiver's private vehicle. This study aims to test and provide evidence in support of two hypotheses:

- *Hypothesis 1:* A low-cost, commercially available CSS option exists for spica-casted children that will meet the requirements for the FMVSS No. 213 injury threshold criteria in crash testing.
- *Hypothesis 2:* Caregivers are able to successfully transport a spica-casted child using a low-cost, commercially available CSS option installed independently in their personal vehicle.

1.3 Concept Preparation

Two child-sized anthropomorphic test dummies (ATD) shown in Figure 1 representing a 3-year-old (Model 020-0100, Humanetics, Farmington Hills, MI) and a 1-year-old (Model 921022-000-H, Humanetics, Farmington Hills, MI) child were used as surrogates for children in the current study. These ATDs are typically used in automotive crash tests due to being representative of the typical size and weight for a child of the given age. Anatomical terms used to describe methods and results in this study are presented in Figure 2.

Figure 1

ATDs Used in Study

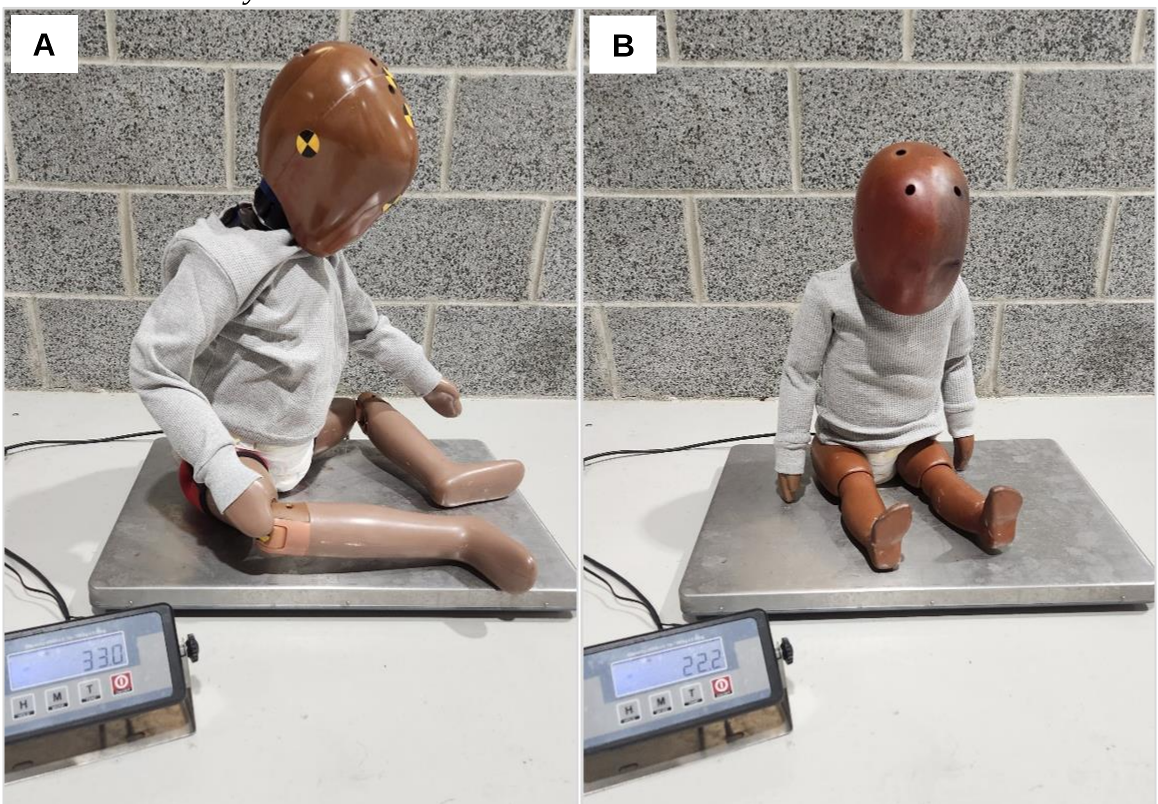

Note. (A) 3-year-old ATD. (B) 1-year-old ATD.

Figure 2

Anatomical Terms

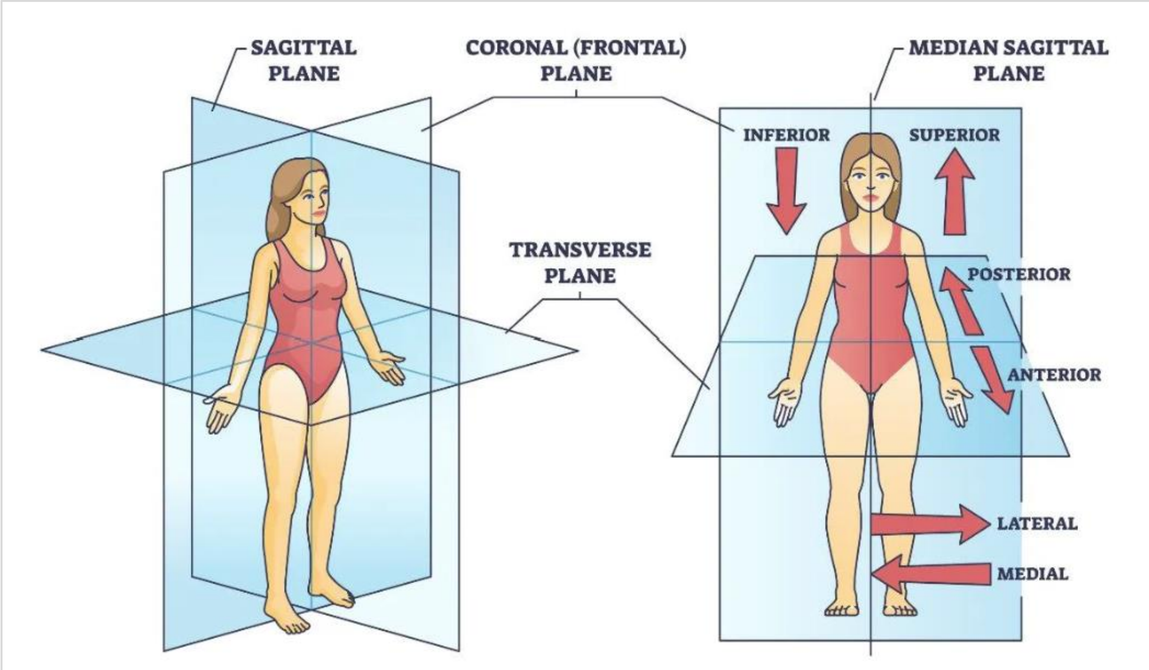

Note. Image sourced *Anatomical terms for location and relative position* (n.d.), by 3D Muscle Lab. Retrieved from https://3dmusclelab.com/anatomical-terms-location-position.

Three cast designs were applied to each ATD by a 5th year Orthopaedic Surgery resident, who had clinical experience applying these casts a using a custom-fabricated hip spica casting table shown in Figure 3. Multiple casts were fabricated during periods of availability of the Orthopaedic Surgery resident and subsequently reserved for use in the testing procedures described later. The casts were designed to treat: 1) developmental dysplasia of the hip (DDH) with complete coverage of both lower extremities, 2) femur fracture with complete coverage of both lower extremities, and 3) femur fracture with complete coverage of one lower extremity and a short portion of the contralateral limb (a

‘1½ Leg’ or ‘Walking’ cast). The ATDs were first positioned supine with the hips and knees in neutral orientation.

Figure 3

Custom Fabricated Hip Spica Casting Table

Next, in the sagittal plane, both lower extremities of the 1-year-old and 3-year-old surrogates were flexed at the hip and knee followed by hip abduction as shown in Figure 4; the same hip and knee joint angles were used for both ATDs. For the casts which extended the full length of the limb, the cast extended to the toes. For the “1½ Leg” cast for the femur fracture design, a coin toss was used to decide that the left limb would receive the ½ leg cast; this shortened cast terminated at approximately the mid-thigh.

The 3-year-old ATD is designed with mobile ball-and-socket hip joints that were sufficiently flexible to accommodate the positions needed for each cast. However, the native hips of the 1-year-old ATD were not sufficiently flexible for the DDH cast position. This is because the hips of the 1-year-old use a screw axis and rubber plug assembly that primarily only allows hip flexion-extension in the sagittal plane. Thus, while relevant magnitudes of hip flexion and extension range of motion were possible, abduction/adduction was limited to approximately 20°. To allow a greater range of motion for the casts intended for the current study, the native hip joint mechanisms were replaced with a stiff elastic band that maintained the approximate hip center of rotation and flexion-extension motion while also allowing increased hip abduction.

Figure 4

Hip and Knee Angles Used in Casting

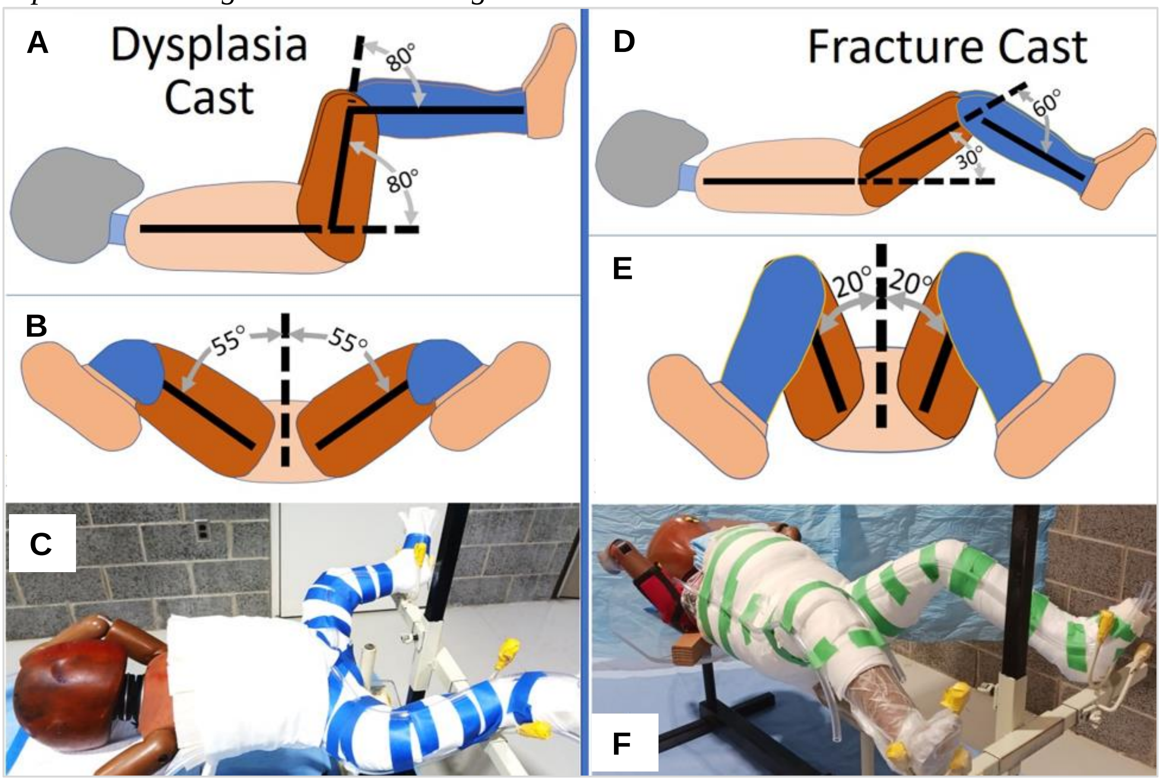

Note. (A) Hip and knee flexion angles for DDH casting. (B) Hip abduction angles for DDH casting. (C) Example DDH casting using provided angles. (D) Hip and knee flexion angles for femur fracture and 1½ Leg casting. (E) Hip abduction angles for femur fracture and 1½ Leg casting. (F) Example femur fracture casting using provided angles.

Prior to casting, the ATD's torso and lower extremities were covered in a polyethylene sheeting as a vapor barrier to protect the ATD from the subsequent moistened casting material. Approximately 50 mm of cotton padding material was placed over the chest and abdomen to simulate the potential space that is created for breathing as shown in Figure 3. Stockinette was placed over the torso and legs followed by spiral wrapped cotton and finally felt over the ankles and chest. Small diameter rubber tubing was placed along both sides of the torso and lower extremities to protect the ATD's vinyl 'skin' during later cast removal via a cast saw. Fiberglass casting tape was finally spiral-wrapped around the torso and lower extremities until several layers of fiberglass were applied.

Following the curing of a given cast, the chest/abdomen pad was removed followed by cast removal via a cast saw by cutting along the lines established by the rubber tubing. This cast separation technique essentially created a clamshell whereby the anterior half of the cast could be removed in a single piece and the ATD was removed from the posterior half of the cast. Minimal fragments of cotton padding were damaged during the cast removal process and any pieces deemed loose were manually removed. To re-establish the space occupied by the cotton padding, the ATDs were each fitted with cotton long sleeve undergarments. Each ATD could then be placed into any of the three casts shown in Figures 5 and 6 to re-establish a given casted position. The anterior and posterior halves of a given cast were held in place with self-sealing 60-gauge polyvinyl chloride sheeting wrapped circumferentially around the cast at the legs, thighs, and torso. The wrapped sheeting layer had the benefit of securing the ATD in the cast while not adding any appreciable thickness to the cast. The polyethylene polyvinyl chloride sheeting was also transparent such that the entire cast was still visible. Finally, a diaper was placed over the perineal area by tucking it anteriorly and posteriorly between the ATD and the cast. A second diaper was attached over the cast and securing it over the hips to replicate the same process used by caregivers. Each casted and diapered ATD was weighed and the overall height was measured and summarized in Table 1.

Figure 5

Cast Variations Used for 1-year-old ATD

Note. Cast types from left to right: DDH, Femur Fracture, 1½ Leg.

Figure 6

Cast Variations Used for 3-year-old ATD

Note. Cast types from left to right: DDH, Femur Fracture, 1½ Leg.

Table 1

Anthropomorphic Data Summary

Child Age	Cast Type	Height (cm)	Mass (kg)
1-year-old	Control	76.2	10.1
	DDH	67.3	11.6
	Fracture	73.7	11.4
	1½ Leg	73.7	11.2
3-year-old	Control	100.3	15.0
	DDH	91.9	16.4
	Fracture	95.0	16.8
	1½ Leg	95.0	16.5

Note. Two crash test ATDs representing 1- and 3-year-old children served as surrogates for the current study. The ATDs were laid supine to record their length from head-to-toe along a superior-inferior axis, coaxial to the spine. The mass was recorded with the cast on the ATD.

Preceding research has found that CSS options for spica-casted children are either expensive, difficult to use, or not approved for spica cast use by the CSS manufacturer. To support *Hypotheses 1* and *2,* a successfully developed CSS concept must effectively address all three of these challenges.

As of 2025, there are currently only four approved transportation options for spica-casted children: 1) EZ-ON Lay Down Vest, 2) Inspired by Drive Spirit Spica Car Seat, 3) Wallenberg Hip Cast Seat by Merritt, and 4) Ambulance Transport. The EZ-ON

Lay Down Vest has been tested for spica use in 1999, 2015, and 2020 (Bull et al., 1999; Gockley et al., 2015; Collins et al., 2020). While a considerably low-cost option at $212 USD (eSpecial Needs, 2025), the drawback to its use is that the child must be positioned supine on a flat bench-style seat in the rear seating row of the vehicle with their head placed in the maximum car in-board position. Proper positioning is not feasible in caregiver's personal vehicles that have individual bucket seats or bench seats with deep recessed areas of the seat pan between the hip and side bolsters in the second row. Supine positioning in the second row also will take up at least two available seating positions and this may not be an option for caregivers who must also transport additional persons with the casted child. Furthermore, maneuvering a casted child to be restrained into a third-row bench seat by the caregiver is highly unfeasible. Transportation Options 2 and 3, the Inspired by Drive Spirit Spica Car Seat and the Wallenberg Hip Cast Seat by Merritt, are financially impractical for many caregivers, given their purchase cost exceeds $2,200 USD and the limited period of use (approximately 6 to 12 weeks) prior to the child transitioning back to their conventional CSS uncasted (Adaptive Specialties, 2025a, 2025b). The final transportation option available to caregivers is also cost-prohibitive since ambulance transport is documented to cost approximately $1200 USD for each round-trip occurrence (City of Livonia, 2025; Gockley et al., 2015).

Accordingly, a viable concept developed for this study must accommodate a spica-casted child, be low-cost and commercially available, comply with FMVSS No. 213 performance requirements, and be capable of independent installation by a caregiver in a personal passenger vehicle. Using these concept guidelines and taking into the consideration the Anthropomorphic Data Summary presented in Table 1, a novel CSS combination was proposed for investigation. This CSS configuration consists of an adjustable travel vest designed to accommodate a broad range of spica cast types and sizes, paired with a booster seat that vertically elevates the casted child to mitigate dimensional conflict between the rigid lower extremities of the spica cast and the vehicle seat contour.

The RideSafer Travel Vest Gen 5 was selected for the forward-facing, 3-year-old only and is shown in Figure 7 (Safe Traffic System, Inc., n.d.). This vest is designed for vehicle forward-facing children aged 2-years and older, and thus was not utilized for the 1-year-old ATD testing. The RideSafer Travel Vest is not a typical 'seat-type' CSS, but is a harness that attaches to the child's body, similar to a conventional rock-climbing harness: four straps that secure over both shoulders and hips. An optional fifth strap connects between the legs to ensure a proper fit of the harness such that it does not migrate superiorly on the child's body. The vehicle's lap and shoulder seat belt then secures the child in the vehicle seat by attaching to distinct landmarks on the RideSafer Travel Vest. The RideSafer Travel Vest offers several advantages for caregivers, including infinite adjustability; the ability to be harnessed within the home; suitability for use during non-transportation activities; compatibility with all vehicle types and non-first-row seating positions; continued usability for non-casted children; and affordability, with a retail price of $180 USD (Safe Ride 4 Kids, 2025).

Figure 7

Safe Travel System RideSafer Travel Vest, Gen5

The booster seat chosen for use in conjunction with the RideSafer Travel Vest was the backless BubbleBum Booster Seat shown in Figure 8 (BubbleBum USA LLC, n.d.). This specific booster seat was selected for testing since it does not include seat-side bolsters or arm rests in its design and only served to raise the height of the seated 3-year-old ATD to aid in vehicle seat and seat belt positioning for the RideSafer Travel Vest. Similar to the Travel Vest, the booster seat is compatible with any passenger vehicle type and any non-first-row seating position equipped with a headrest; it can also be used by non-casted children and is highly affordable, with a retail price of $40 USD (BubbleBum, 2025). Of note, the RideSafer Travel Vest only allows that the Travel Smarter Booster be paired with the Travel Vest. However, the current study was seeking the safe positioning and restraint for a challenging group of children that do not properly fit into typical CSS configurations. The Travel Smarter Booster Seat has arm rests and small seat pan side bolsters which would have prevented the safe positioning of a casted child that requires additional seating width at the hip. Thus, the BubbleBum Booster was carefully chosen for its aforementioned characteristics.

Figure 8

BubbleBum Booster Seat

The development of a novel CSS option for spica-casted children, by combining the RideSafer Travel Vest Gen 5 with the BubbleBum Booster Seat at a total cost of $220 USD, provides support for both *Hypothesis 1* and *Hypothesis 2*. This CSS configuration is a low-cost and commercially available alternative when compared to existing approved transportation solutions, such as the Inspired by Drive Spirit Spica Car Seat, the Wallenberg Hip Cast Seat by Merritt, and ambulance transport.

1.4 Verification

The purpose of verification testing in product development is to determine whether the product complies to specific requirements, specifications, and regulations imposed on the product. O'Neil et al. (2009) stated that CSS restraints should not be modified for the transportation of children with special health care needs unless that modified system has been crash tested. To verify that the RideSafer Travel Vest and BubbleBum Booster Seat combination is a safe and viable option for forward-facing spica-casted children, a dynamic, frontal sled test series utilizing the FMVSS No. 213 methods and injury criteria thresholds was performed since the combination has not yet been crash tested nor approved by either CSS manufacturer.

1.4.1 FMVSS No. 213 Test Methodology

A pneumatic deceleration sled, commonly referred to as a sled, is an industry standard testing device used in automotive engineering to simulate a vehicle crash. Automotive manufacturers, vehicle component suppliers, and the National Highway Traffic Safety Administration (NHTSA) rely on sled outcome to evaluate crashworthiness, safety restraint system performance, and occupant injury values due to the device's controlled, repeatable, and cost-effective advantages over full-vehicle crash tests.

According to NHTSA, the purpose of dynamic frontal sled testing for child restraint systems used in motor vehicles is to reduce the number of children injured or killed in motor vehicle crashes by testing the child restraint system integrity and the following three measured injury criteria from the child surrogates: head acceleration, chest acceleration, and occupant excursion (NHTSA, 2024b). Unlike FMVSS No. 208, Occupant Crash Protection (NHTSA, 2024a), the child restraint systems tested under FMVSS No. 213 do not measure and evaluate neck injury criterion directly. Instead, neck injury minimization is assumed using the results from FMVSS No. 213 testing as confirmation of a restraint system's ability to protect and properly contain the child during a crash.

To properly assess a child restraint system according to FMVSS No. 213, the following overarching ten steps must be followed in order:

1. Ensure standard seat assembly mounted to the testing sled is configured according to FMVSS No. 213, S6.1 Dynamic systems test for child restraint systems.
2. Install CSS onto the standard seat assembly securing it by using the appropriate method: vehicle seat belt, LATCH system, and/or tether anchors according to CSS manufacturer's user manual.
3. Correctly position the anthropomorphic test ATD based on age, height, weight, and CSS specifications presented in CSS manufacturer's user manual.
4. Restrain the test ATD using the CSS harness system following CSS manufacturer's user manual.
5. Collect measurements and pre-test still camera photos of test configuration and set up.
6. Conduct dynamic crash tests using the sled testing system following S6.1.1(b)(1) Test Configuration I for child restraints manufactured on or after August 1, 2005.
7. Record test ATD kinematics, including head, chest, and knee excursions using internal test ATD sensors, sled device sensors, high-speed video cameras, physical measurements, and post-test still camera photos.

8. Using collected sensor data, calculate injury criteria including Head Injury Criterion, chest acceleration, and occupant excursion based on test ATD and CSS configuration.
9. Evaluate post-test CSS integrity by checking device for separations, displacements, or damage to any structural components.
10. Document all measurements, observations, and deviations from the expected performance.

1.4.2 Injury Assessment Criteria

Head Acceleration is measured to determine the likelihood of a closed head (brain) injury due to a severe motor vehicle crash in which the velocity change is 30 miles-per-hour (NHTSA, 2024b). This first injury criteria, named HIC36, refers to the maximum Head Injury Criterion over a 36-millisecond time interval. The equation for calculating this injury criteria is as follows:

$$\boldsymbol{HIC36} = \left[\frac{\mathbf{1}}{(\boldsymbol{t_2} - \boldsymbol{t_1})}\int_{t_1}^{t_2} \boldsymbol{a}\, \boldsymbol{dt}\right]^{\mathbf{2.5}} (\boldsymbol{t_2} - \boldsymbol{t_1}) \tag{1}$$

where,

$\boldsymbol{a}$ = resultant head acceleration, expressed in multiples of the acceleration due to gravity (g), at the center of gravity for the head;

$\mathbf{2.5}$ = weighting exponent based on empirical test data (Gadd, 1966);

$(\boldsymbol{t_2} - \boldsymbol{t_1})$ = any two points in time, t_1 and t_2, during the crash event separated by not more than 36 milliseconds; and

$\boldsymbol{HIC36}$ = maximum calculated Head Injury Criterion that shall not exceed 1000.

Chest Acceleration is measured to determine the likelihood of an internal vital organ injury due to a severe motor vehicle crash in which the velocity change is 30 miles per hour (NHTSA, 2024b). The second injury criteria named Chest Acceleration, 3 ms clip, refers to the Thoracic Spine Acceleration, expressed in multiples of the acceleration of gravity (g), over a continuous 3-millisecond time interval. The equation for calculating this injury criteria is as follows:

$$\boldsymbol{Chest\ Acceleration, 3\ ms\ clip = \ max\left(\frac{1}{n} \cdot \sum_{i=k}^{k+n-1} a\right)} \tag{2}$$

where,

$\boldsymbol{a}$ = resultant thoracic spine acceleration, expressed in multiples of the acceleration of gravity (g);

$\boldsymbol{n}$ = number of acceleration samples taken in 3 milliseconds;

$\boldsymbol{k}$ = starting time sample for 3 millisecond time intervals; and

$\boldsymbol{Chest\ Acceleration, 3\ ms\ clip}$ = maximum calculated chest acceleration, expressed in multiples of acceleration of gravity (g), that shall not exceed 60g.

The third injury criteria measured by FMVSS No. 213 is Occupant Excursion. Occupant Excursion is measured at two locations, the head and the knee, to determine if either will contact the vehicle interior during a 30 mile-per-hour crash event or determine impact velocity if contact is unavoidable (Hu et al., 2014). Both excursion values are expressed as a measurement in millimeters parallel to the Seat Orientation Reference Line (SORL) located at the center of the sled bench seat shown in Figure 9. Figure 10 displays the maximum excursion measurement for the head, 813 mm, and the knee, 915 mm, in relation to the standard sled bench used in FMVSS No. 213 testing.

Figure 9

SORL on the Standard Seat Assembly

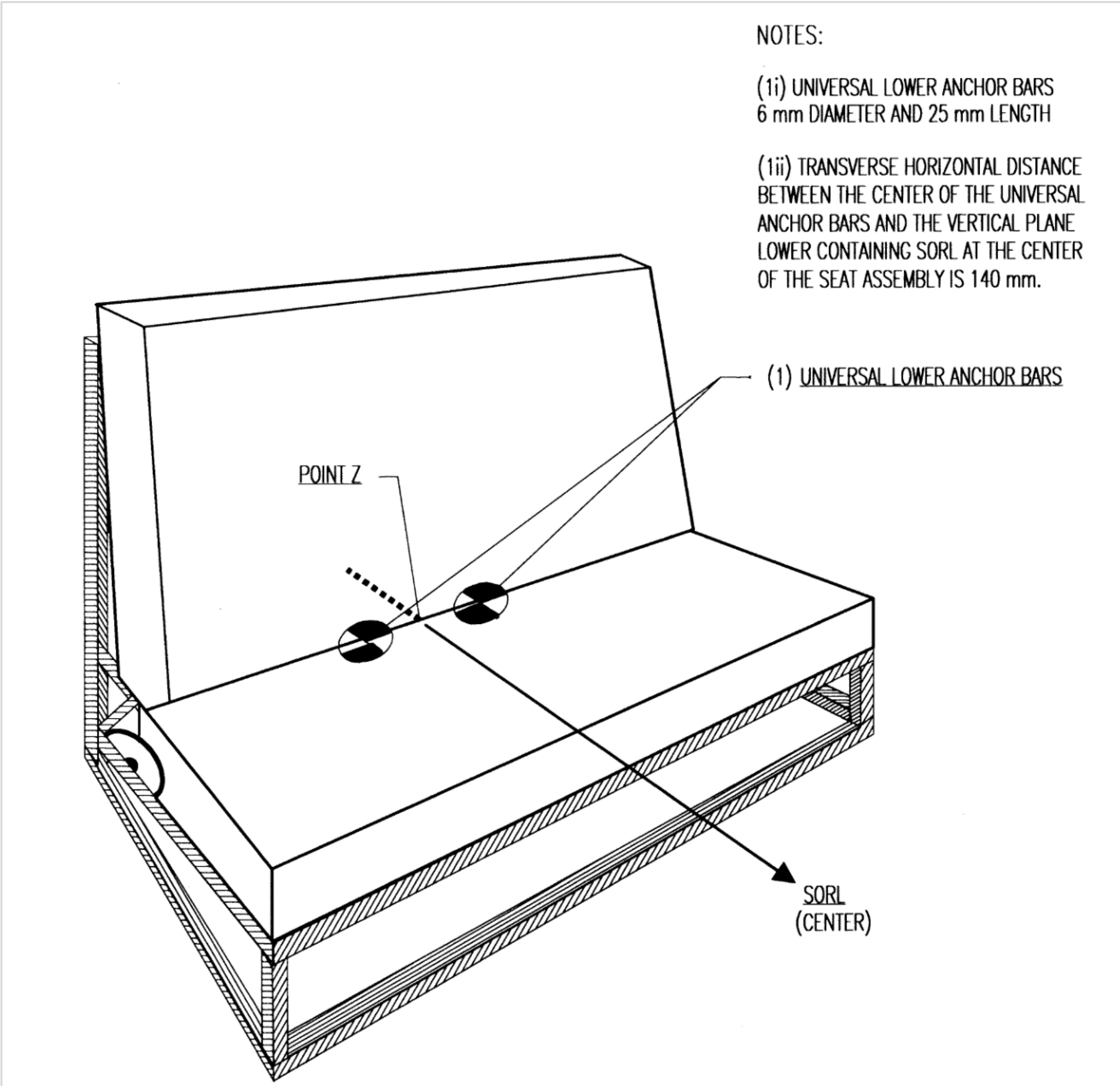

Note. Image sourced from Figure 1A of Federal Motor Vehicle Safety Standard No. 213; Child Restraint Systems, Child Restraint Systems—Side Impact Protection, Incorporation by Reference, 49 CFR Part 571, published on October 1, 2024.

Figure 10

Forward Excursion Limits on the Standard Seat Assembly

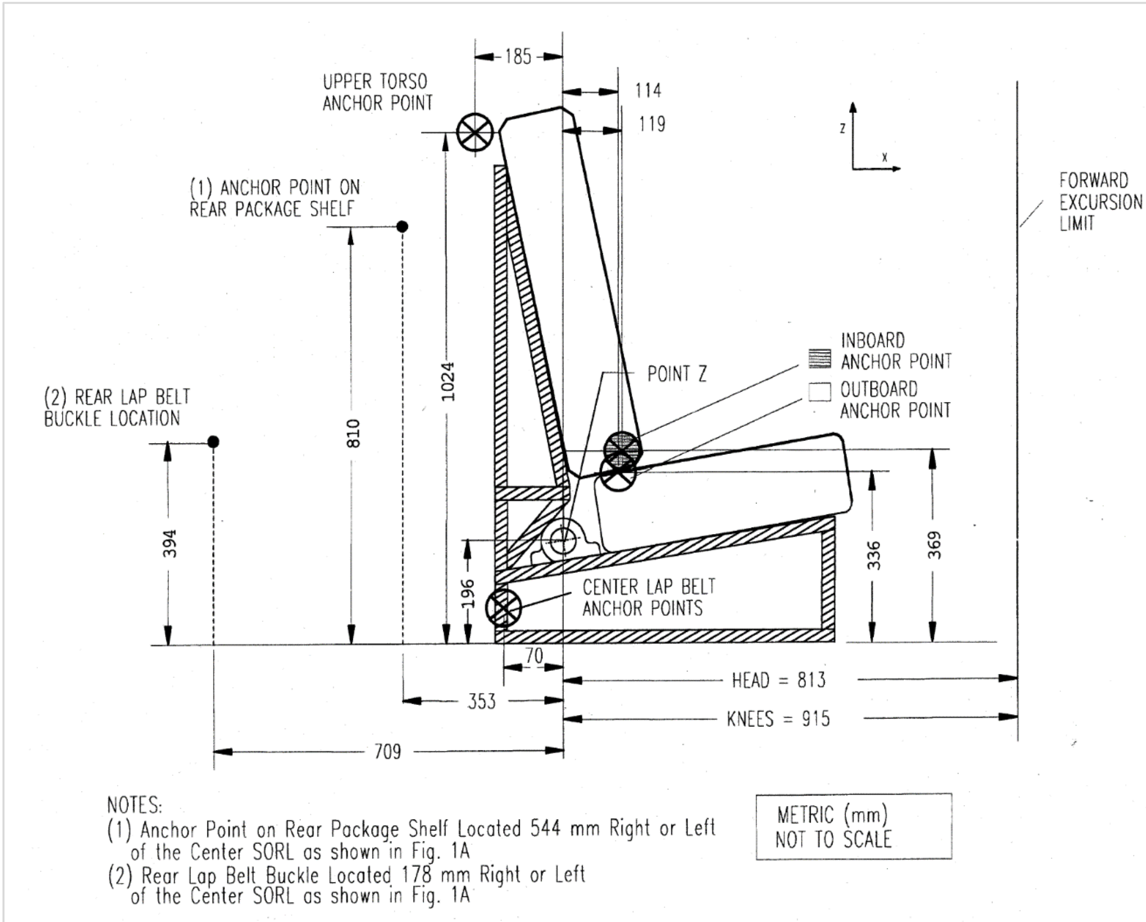

Note. Image sourced from Figure 1B of Federal Motor Vehicle Safety Standard No. 213; Child Restraint Systems, Child Restraint Systems—Side Impact Protection, Incorporation by Reference, 49 CFR Part 571, published on October 1, 2024.

To determine if the CSS proposed combination of vest and booster is safe and viable, the dissertation study will dynamically sled test the configuration and compare the HIC36 and Chest Acceleration, 3 ms clip, injury criteria values to the summarized maximum thresholds set by NHTSA as the safety standard requirements for child restraint systems shown in Table 2. Head and Knee Excursion measurements will not be evaluated during sled test because the knees of the casted child surrogate will be fixed by the cast.

Table 2

FMVSS No. 213 Maximum Injury Criteria Thresholds

Injury Metric	Maximum Threshold Value
HIC36	1000
Chest Acceleration, 3 ms clip	60 g
Head Excursion	813 mm
Knee Excursion	915 mm

1.4.3 Materials and Methods: Sled Testing

Two low-cost, commercially available child restraint systems were dynamically investigated using a pneumatic deceleration sled device located at the Kettering University Crash Safety Center in Flint, Michigan to test *Hypothesis 1* presented in Section 1.2. The sled used in this study has a 900 kg payload capacity, can reach 67.5 kph (42 mph), and is able to attain peak decelerations of greater than 70 g. With these maximum performance capabilities, the sled device employed for this study is the appropriate device for testing according to FMVSS No. 213.

Design of the frontal impact dynamic test series was constructed as directed by NHTSA's Laboratory Test Procedure for FMMVSS No. 213. Section 12.A.3.(1) of the test procedure states that "One (1) CRS is required for EACH TEST according to frontal impact dynamic test Configuration I. One or more tests are possible depending on the number of installation modes (forward facing/infant mode), adjustment positions (upright/recline), and height and weight recommendations of the manufacturer" (NHTSA, 2023, p. 17). Since both the SafeRider Travel Vest and the BubbleBum, Booster only have singular installation modes and adjustment positions, one test is required. The sled test verification series includes three installation configurations using the 3-year-old ATD to determine if the novel concept CSS combination resulted in acceptable injury criterion values limited by FMVSS No. 213 and thereby confirming the *Hypothesis 1* presented in Section 1.2. The series included four sled test trials overall denoted by A, B, C, and D and shown in Table 3.

Table 3

Sled Test Verification Series

Trial	ATD	Cast Type	CSS Configuration
A	3-year-old	Control	RideSafer Travel Vest
B	3-year-old	Control	RideSafer Travel Vest & BubbleBum Booster
C	3-year-old	Femur	RideSafer Travel Vest & BubbleBum Booster
D	3-year-old	Femur	RideSafer Travel Vest & BubbleBum Booster

Note. Control cast type refers to an uncasted ATD. Femur cast type refers to a bilateral femur fracture casted ATD.

Trial A served as the overall sled testing control to verify the baseline performance of the RideSafer Travel Vest when used in a forward-facing configuration with an uncasted 3-year-old ATD child surrogate as shown in Figure 11. Data collected from this trial establishes the reference condition against which all subsequent test configurations are compared.

Figure 11

Trial A Pre-Test Photos

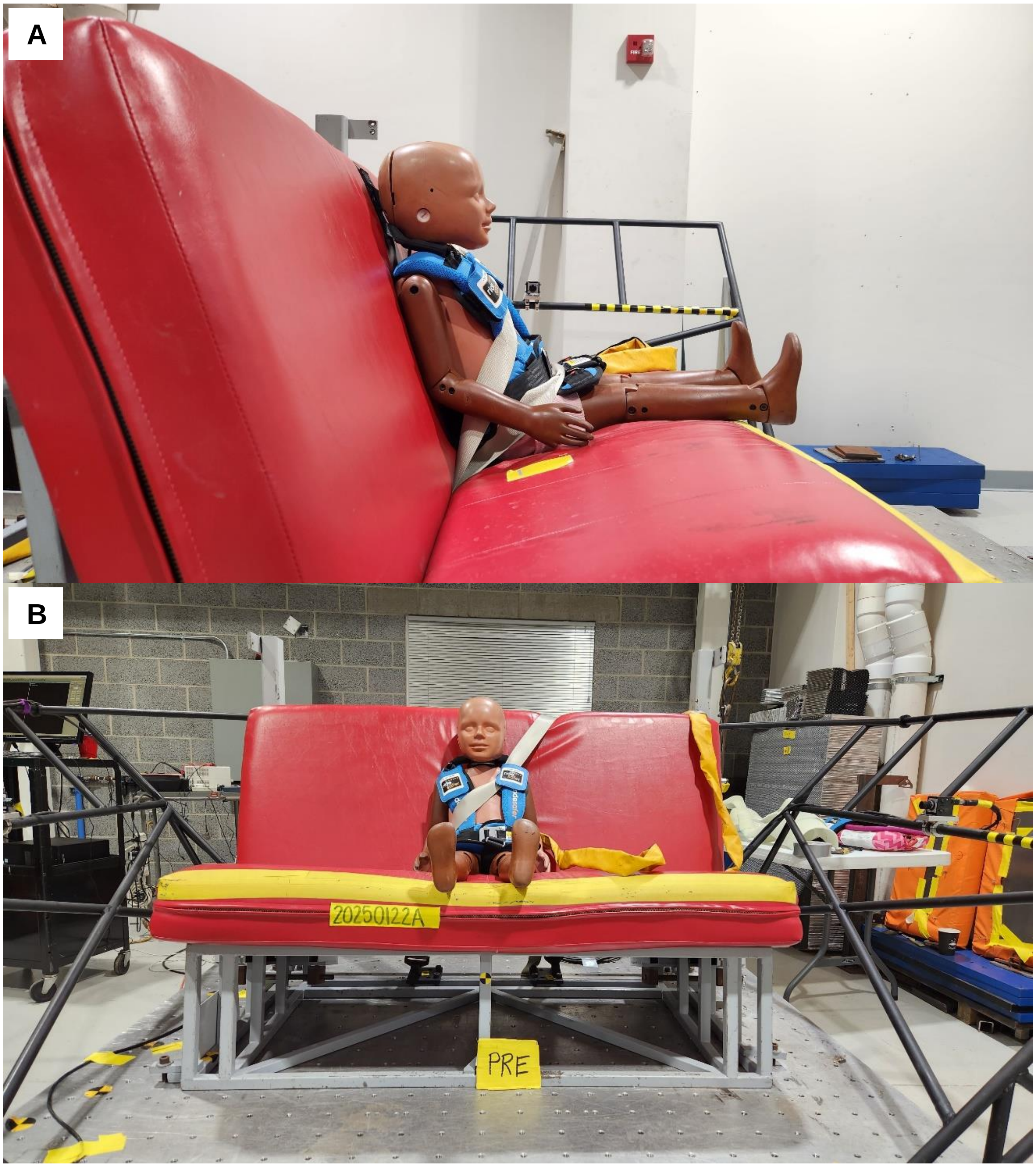

Note. (A) Side view. (B) Front view.

Trial B evaluated the concept CSS combination, consisting of the RideSafer Travel Vest and the BubbleBum Booster, using the same uncasted, forward-facing 3-year-old ATD as shown in Figure 12. Since this configuration concept combined CSS systems from two separate manufacturers and had not been previously tested, it functions as the baseline for assessing future trials involving spica-casted ATDs.

Figure 12

Trial B Pre-Test Photos

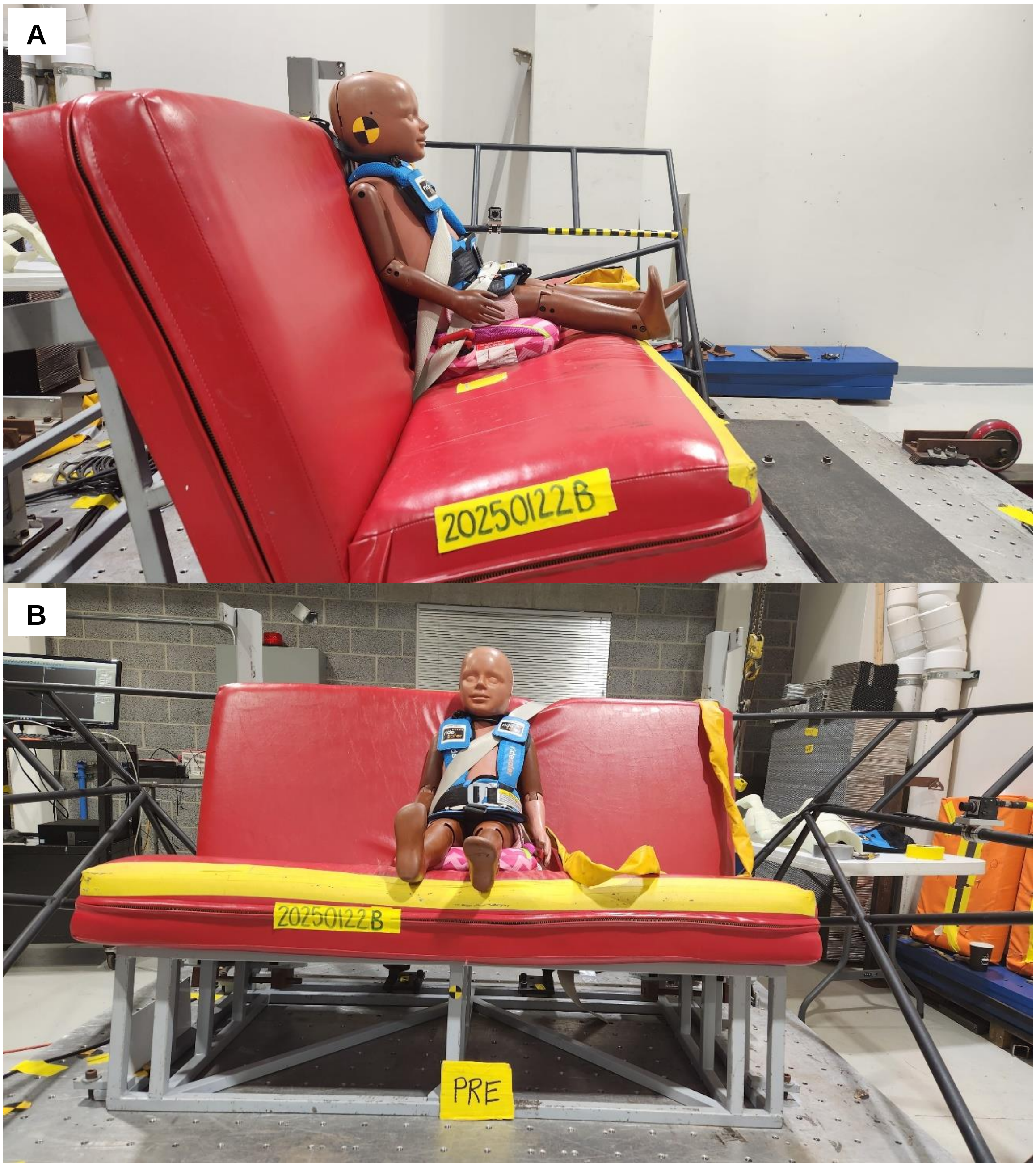

Note. (A) Side view. (B) Front view.

Trial C was the first trial to incorporate a spica-casted 3-year-old ATD with the proposed CSS combination concept as shown in Figure 13. A bilateral femur fracture cast was selected to represent a worst-case scenario due to the extreme hip flexion it imposes, which significantly complicates achieving a vertical seated posture within the vehicle seat.

Figure 13

Trial C Pre-Test Photos

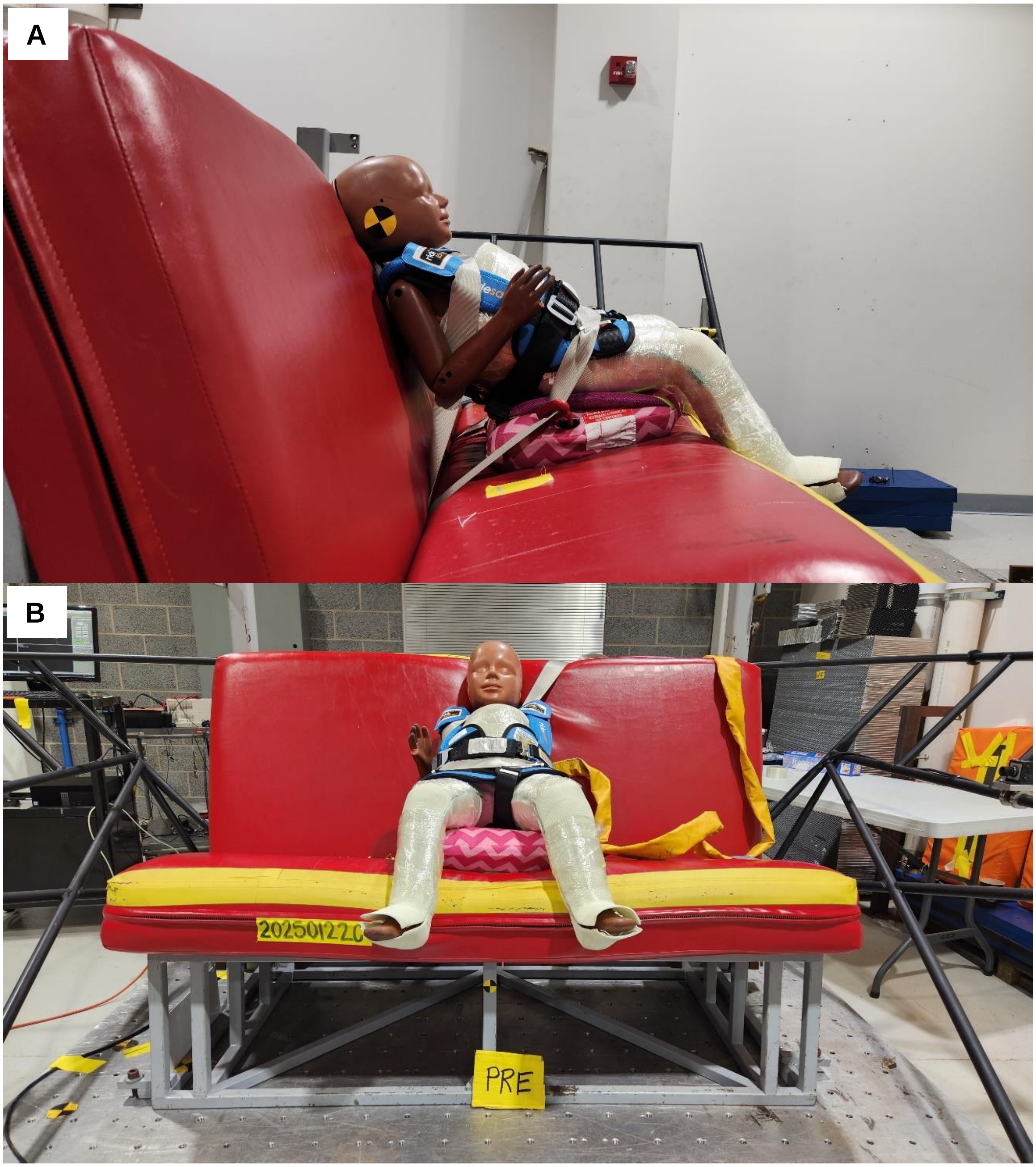

Note. (A) Side view. (B) Front view.

Trial D replicated the conditions of Trial C, as shown in Figure 14, to assess test-retest reliability and strengthen the validity of the findings derived from the spica-casted configuration. For all trials, CSS installation and ATD positioning and harnessing were conducted in accordance with the CSS manufacturer's specifications by certified Child Passenger Safety Technician (CPST).

Figure 14

Trial D Pre-Test Photos

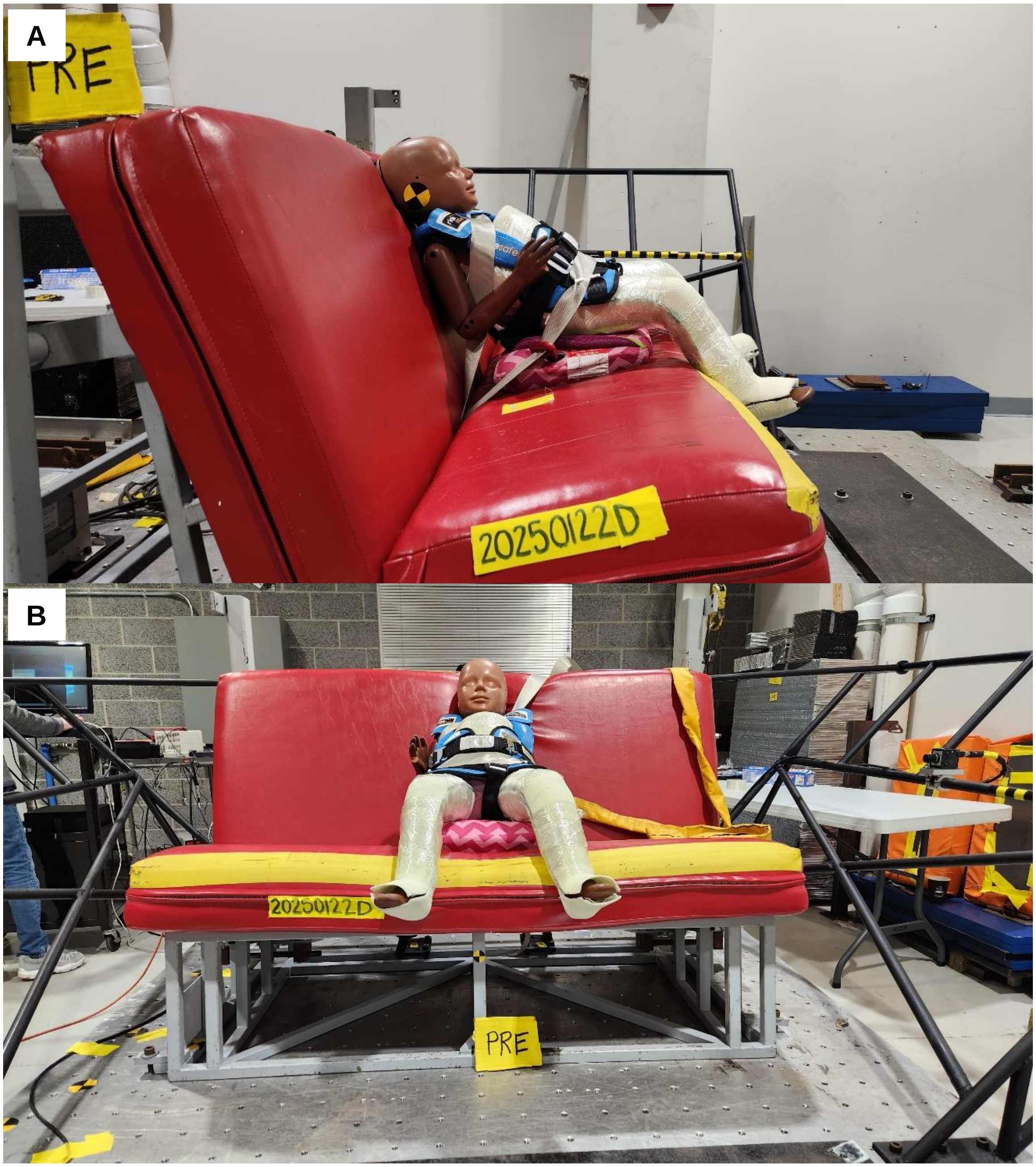

Note. (A) Side view. (B) Front view.

The Kettering University Crash Safety Center employs Kistler's onboard data acquisition system, KiDAU, integrated with the 2024 version of CrashDesigner software, to perform sled-based crash testing and capture measurement data (Kistler, 2025). Following each test trial, CrashDesigner generates output reports containing channel-specific data, which are subsequently analyzed and compared against the injury threshold criteria established in FMVSS No. 213.

1.4.4 Results: Sled Testing

Table 4 summarizes the injury outcomes from the sled test verification series, based on data acquired through the sled device's Kistler CrashDesigner software. The full output report pages from each trial prepared by CrashDesigner can be found in Appendix C. It is noted that all test trials complied with the specified excursion requirements in FMVSS No. 213.

Table 4

Sled Test Verification Results

Trial	Cast Type	CSS Configuration	HIC36	Chest Acceleration, 3 ms clip (g)
			LV = 1000	LV = 60
A	Control	Vest	289	35.22
B	Control	Vest & Booster	312	31.28
C	Femur	Vest & Booster	418	45.096
D	Femur	Vest & Booster	424	42.638

Note. LV refers to the limiting value set by FMVSS No. 213. Control cast type refers to an uncasted ATD. Femur cast type refers to a bilateral femur fracture casted ATD. Vest CSS configuration type refers to the RideSafer Travel Vest only. Vest & Booster CSS configuration type refers to the RideSafer Travel Vest and BubbleBum Booster combination.

During each sled test trial, two acceleration sensors were affixed to the standard seat assembly to measure acceleration data, commonly referred to as the deceleration pulse when expressed in units of g. These signals were recorded through Channels 1 and 2 of the data acquisition system. The use of dual sensors enhances confidence in the integrity of the recorded data by allowing for cross-verification. Figure 15 presents an overlay of the acceleration data from Channels 1 and 2 in Trial A. The close alignment of the deceleration pulse profiles between the two channels supports the reliability and consistency of the data collection process for this trial. Figure 16 presents an overlay of the Channel 1 deceleration pulse profiles across all four sled test trials. Channel 2 data has been omitted to enhance visual clarity in the figure. The similarity among the pulse profiles indicates a high degree of consistency, attributed to the controlled and repeatable test methods used in this study.

Figure 15

Trial A Deceleration Pulse

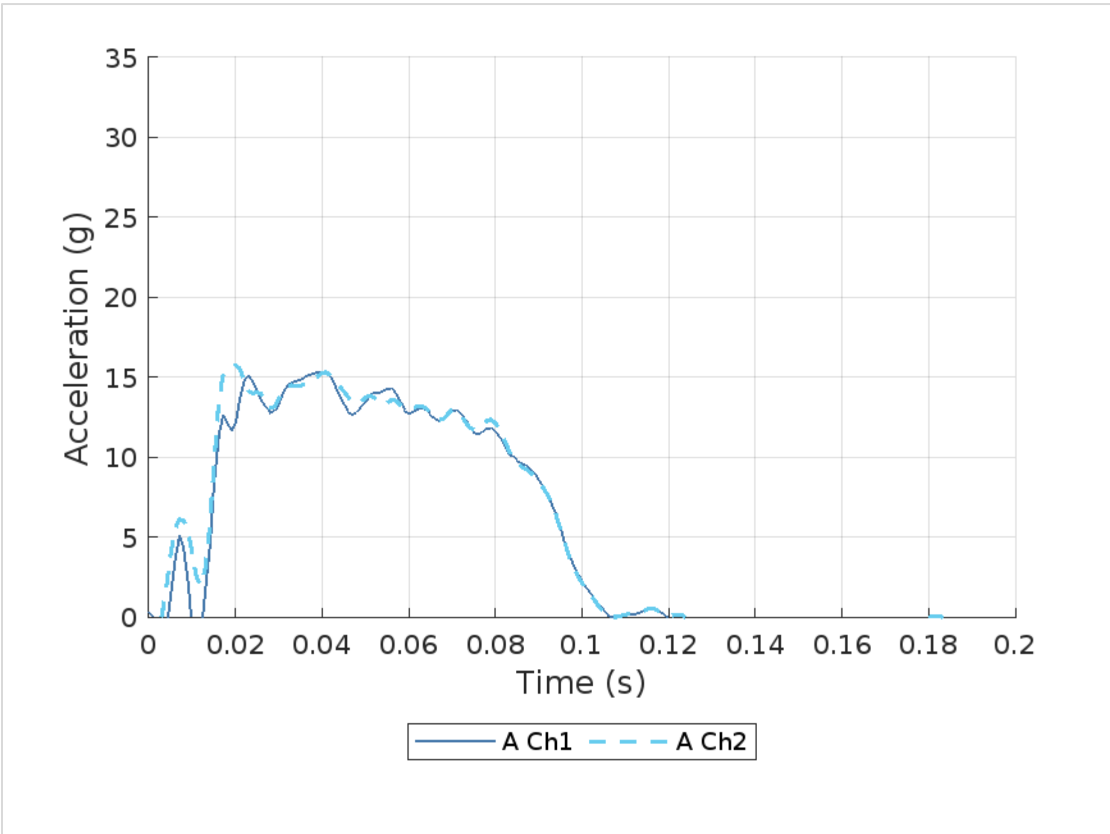

Figure 16

Deceleration Pulse Comparison for All Trials

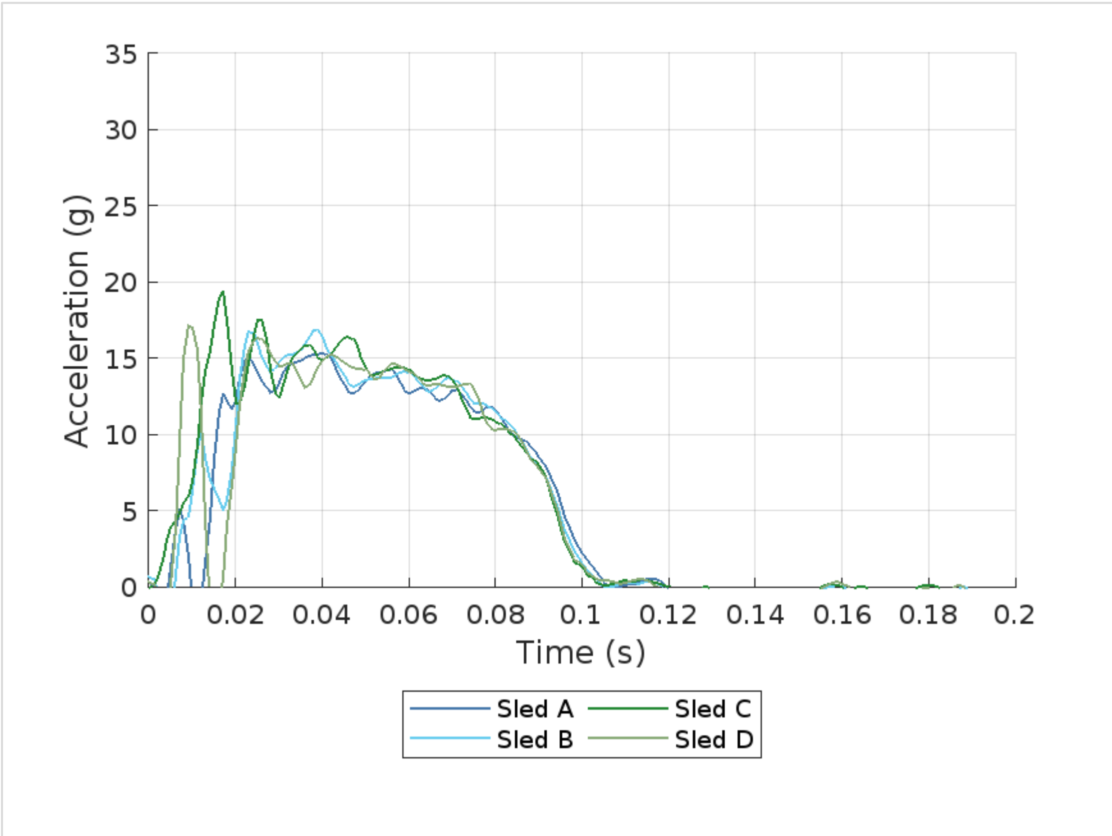

1.4.5 Discussion: Sled Testing

The injury criteria measured in sled test Trials A-D all fell well below the thresholds set by NHTSA in FMVSS No. 213. Therefore, the test results shown in Section 1.4.4 support *Hypothesis 1:* A low-cost, commercially available CSS option exists for spica-casted children that will meet the requirements for the FMVSS No. 213 injury threshold criteria in crash testing.

The HIC36 injury criteria has a federal limiting value of 1000, representing the threshold above which the risk of closed head (brain) injury increases significantly in a frontal impact scenario (NHTSA, 2024b). In Trial B, which simulated an uncasted child restrained using the combined RideSafer Travel Vest and the BubbleBum Booster, the resulting HIC36 was 312, approximately 69% below the federal threshold. When the bilateral femur fracture casts were introduced, as in Trials C and D, the HIC36 value increased by approximately 10%. Even with this increase, the values remained well within the allowable safety margin and still under threshold.

HIC36 is derived from the resultant head acceleration over time and a comparison of this measurement between trials is shown in Figure 17. Peak head acceleration of 44.2 g was recorded at 83 ms during Trial A. This maximum occurred as the head reached its most car-forward excursion along the SORL in the +x direction, as depicted in the video frames in Figure 18. The motion of the head was constrained by the vehicle's shoulder belt, which was routed through the RideSafer Travel Vest. According to Newton’s First Law of Motion, “a particle remains at rest or continues to move with uniform velocity if there is no unbalanced force acting on it” (Meriam, Kraige, & Bolton, 2018, p. 5). This physical phenomenon is demonstrated through the restraint sequence as follows: the vehicle’s shoulder belt stops the forward motion of the Travel Vest, thereby restricting chest displacement at 56 ms. This restraint subsequently limits the forward motion of the head, which occurs at 65 ms. However, the head continues its rotational momentum momentarily, resulting in a collision of the chin with the chest at 83 ms. At this time, forward motion of the head has ceased, and in a human subject, this would correspond to when the brain impacts the interior surface of the skull with maximum acceleration, producing the highest force and potential for traumatic brain injury. This sequence explains the double-peak data profile observed in the head acceleration data. After 83 ms, the head decelerates during ride-down into a deceleration trough after the crash event as illustrated in the head acceleration profile shown in Figure 19. All acceleration versus time figures presented in this study have been time-aligned to compensate for the sampling frequency discrepancy between Kistler's CrashDesigner software, which operates at 20,000 Hz, and the 1,000 Hz sampling rate utilized by the *Chest G and HIC Calculator.xls*. The specific shift applied to each figure is documented within the MATLAB Script for Data Visualization provided in Appendix F.

Figure 17

Sled Trials A-D Head Acceleration vs. Time Comparison

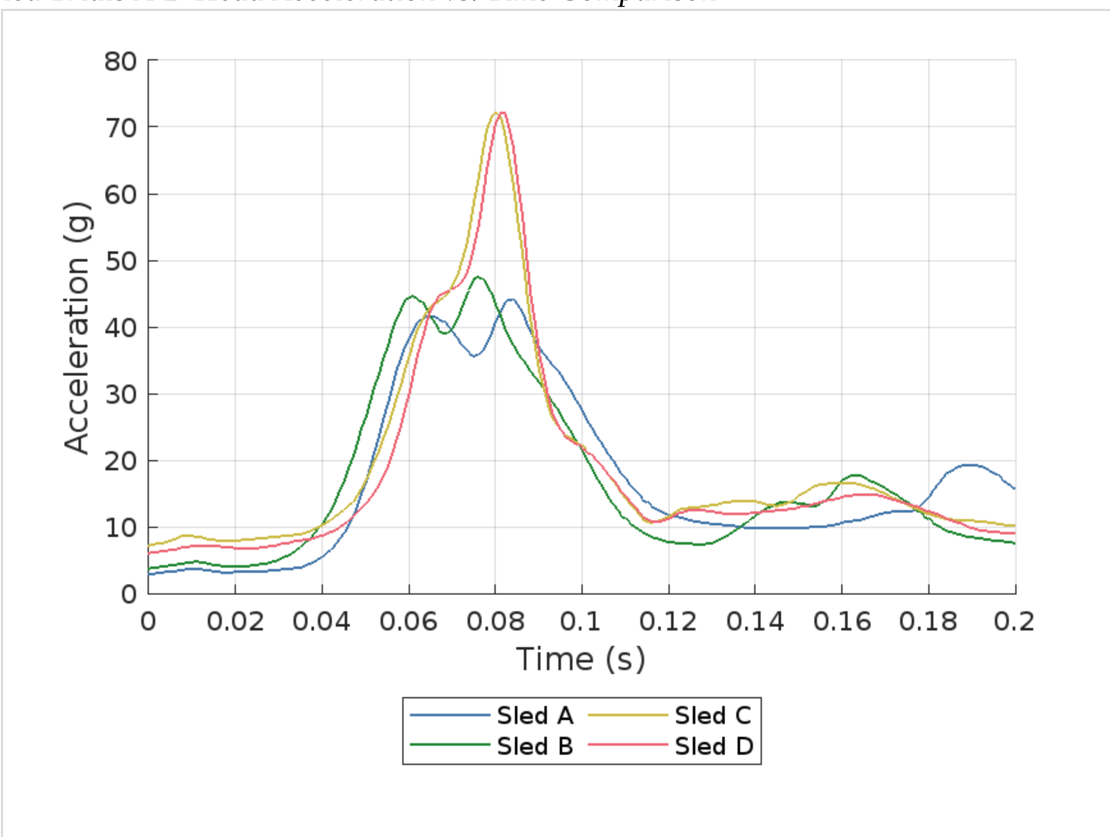

Figure 18

Trial A Test Video Frames

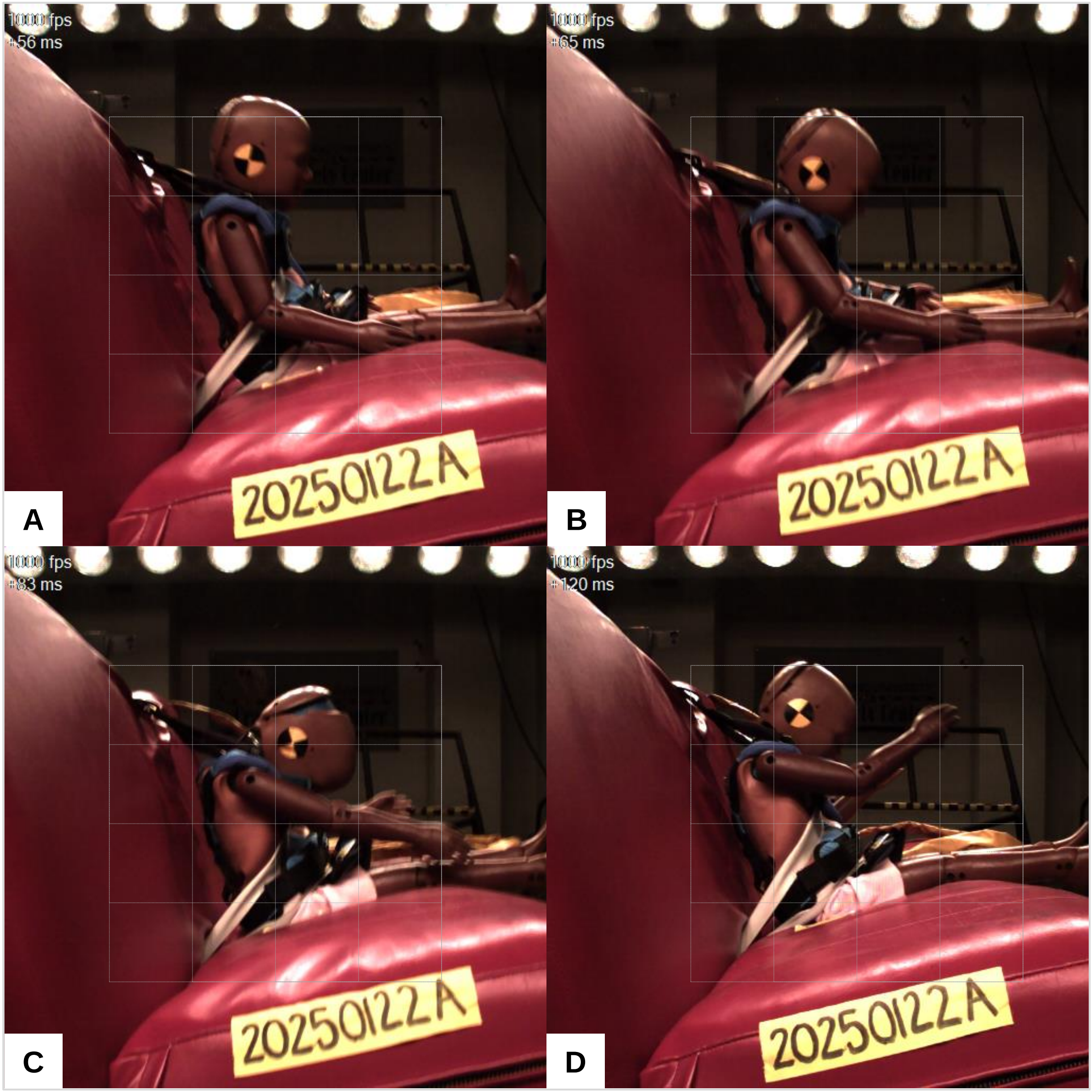

Note. (A) Peak Chest Acceleration at time = 0.056 seconds. (B) Increased Head Acceleration due restrained chest at time = 0.065 seconds. (C) Peak Head Acceleration at time = 0.083 seconds. (D) Head Deceleration shown at time = 0.120 seconds.

Figure 19

Sled Trial A Head Acceleration vs. Time

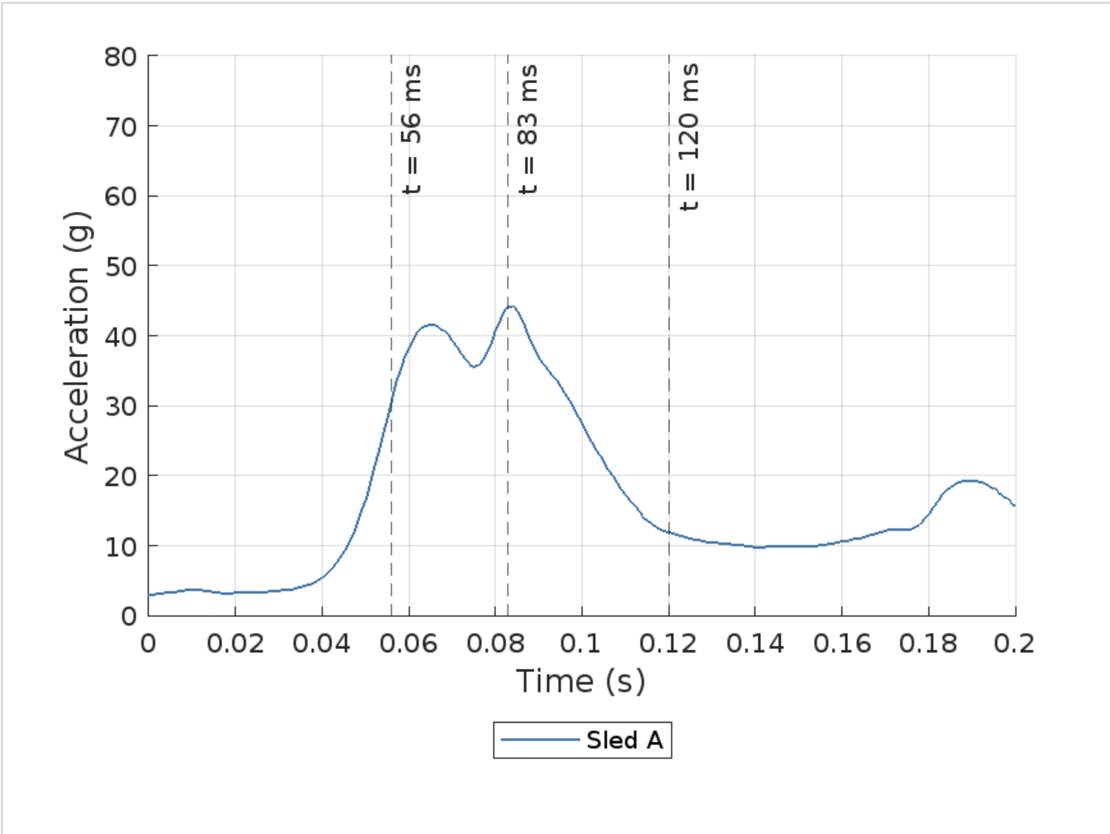

Note. Peak Chest Acceleration at time = 0.056 seconds. Increased Head Acceleration due restrained chest at time = 0.065 seconds. Peak Head Acceleration at time = 0.083 seconds. Head Deceleration trough shown at approximately 0.120 seconds.

The head acceleration profile for Trial B closely mirrors that of Trial A, exhibiting only a minimal time offset. In Trial B, the CSS configuration results in increased engagement between the vehicle's seat belt and the chest of the ATD which is enclosed by the vest (Figure 20). This larger contact area starts the restraint sequence approximately 3 ms earlier than that of Trial A as shown in Figure 21. The peak head acceleration recorded for Trial B is 47.3 g and occurs 0.007 seconds earlier than that of Trial A, and represents an earlier onset of head deceleration when the two trial are compared (Figure 22).

Figure 20

Trial B Test Video Frames

Note. (A) Peak Chest Acceleration at time = 0.056 seconds. (B) Increased Head Acceleration due restrained chest at time = 0.062 seconds. (C) Peak Head Acceleration at time = 0.076 seconds. (D) Head Deceleration shown at time = 0.120 seconds.

Figure 21

Sled Trial B Head Acceleration vs. Time

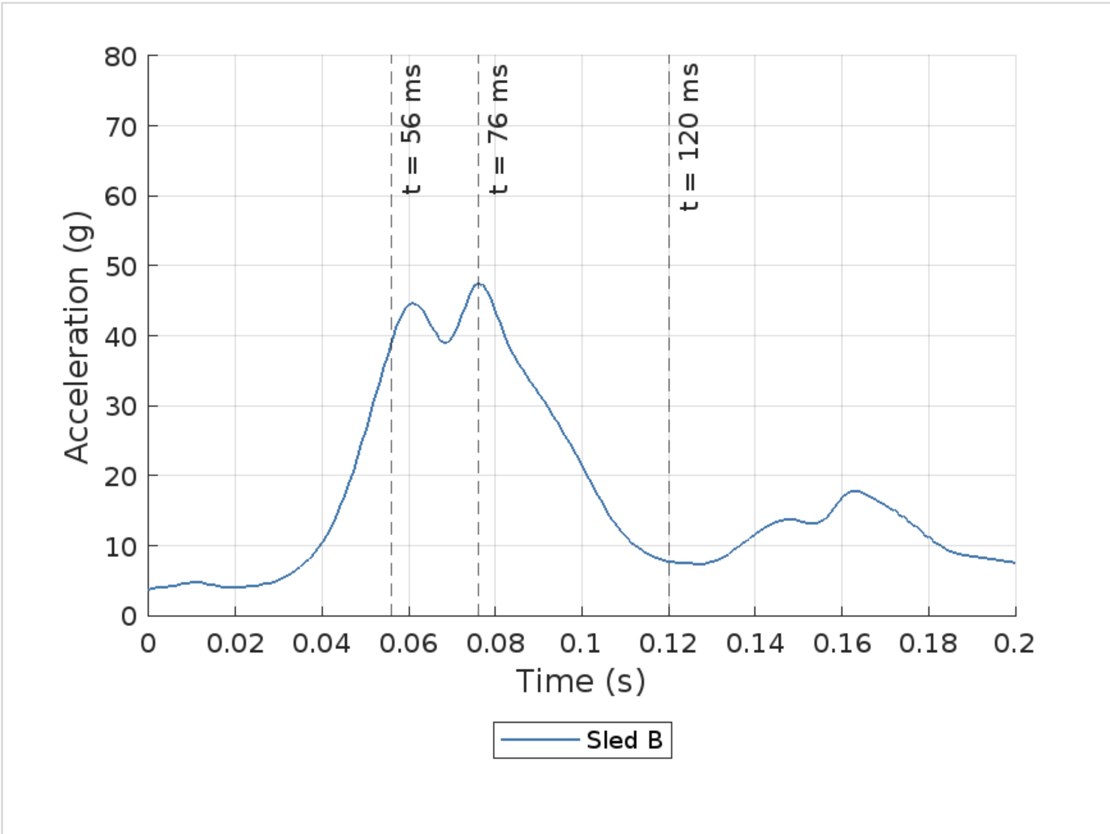

Note. Peak Chest Acceleration at time = 0.056 seconds. Increased Head Acceleration due restrained chest at time = 0.062 seconds. Peak Head Acceleration at time = 0.076 seconds. Head Deceleration trough shown at approximately 0.120 seconds.

Figure 22

Sled Trials A & B Head Acceleration Comparison

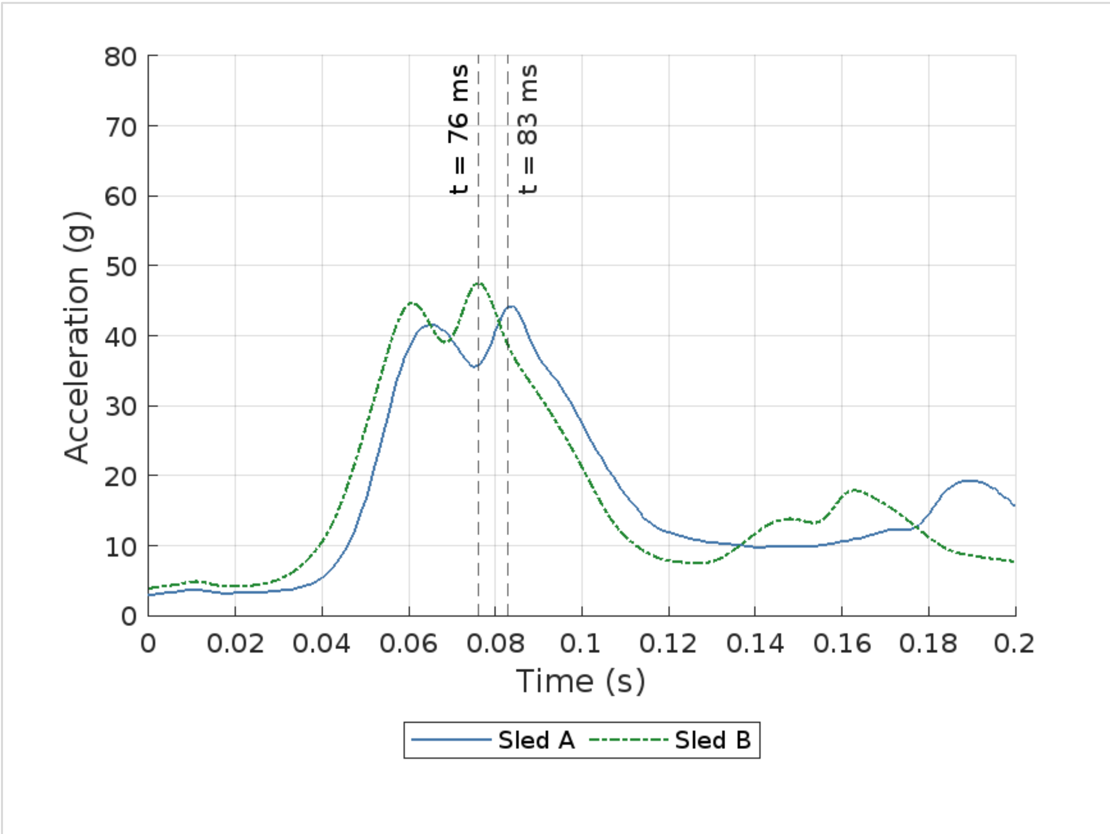

Note. Trial B Peak Head Acceleration at time = 0.076 seconds. Trial A Peak Head Acceleration at time = 0.083 seconds.

In Trials C and D, the addition of the spica cast in the test configuration prevents the ATD from sitting in an upright position (Figure 13, Figure 14). This position change produces two notable effects on the resulting head acceleration profile. First, the characteristic double-peak pattern observed in Trials A and B is absent. Instead, the head acceleration has an initial increase that then plateaus for approximately 10 ms, followed by a sharp rise in slope over the next 5 ms before achieving the peak head acceleration value as shown in Figure 23. This change in response is attributed to the ATD's neck being in flexion at the beginning of the test, which limits forward rotational motion compared to the neutral positioning of the ATD neck in the previous non-casted trials. As a result, the acceleration rate between 0.065 and 0.075 seconds is reduced as shown by the plateau. The subsequent abrupt increase in acceleration slope after 0.075 seconds is due to the head impacting the anterior edge of the spica cast (Figure 24c, Figure 26c). This impact abruptly stops the head's rotational motion leading to the observed peak in head accelerations in Figures 25 and 27.

Figure 23

Sled Trials C & D Head Acceleration Comparison

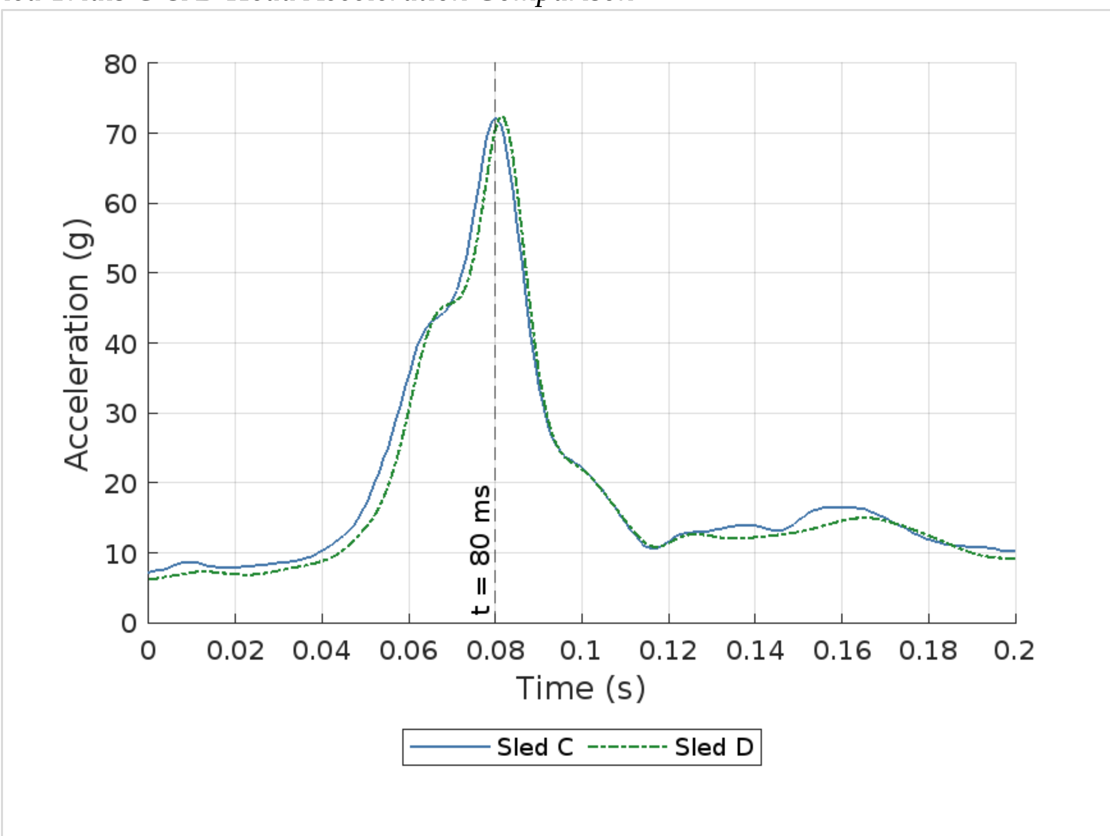

Note. Trial C Peak Head Acceleration at time = 0.080 seconds. Trial D Peak Head Acceleration at time = 0.081 seconds (not shown for figure clarity).

Figure 24

Trial C Test Video Frames

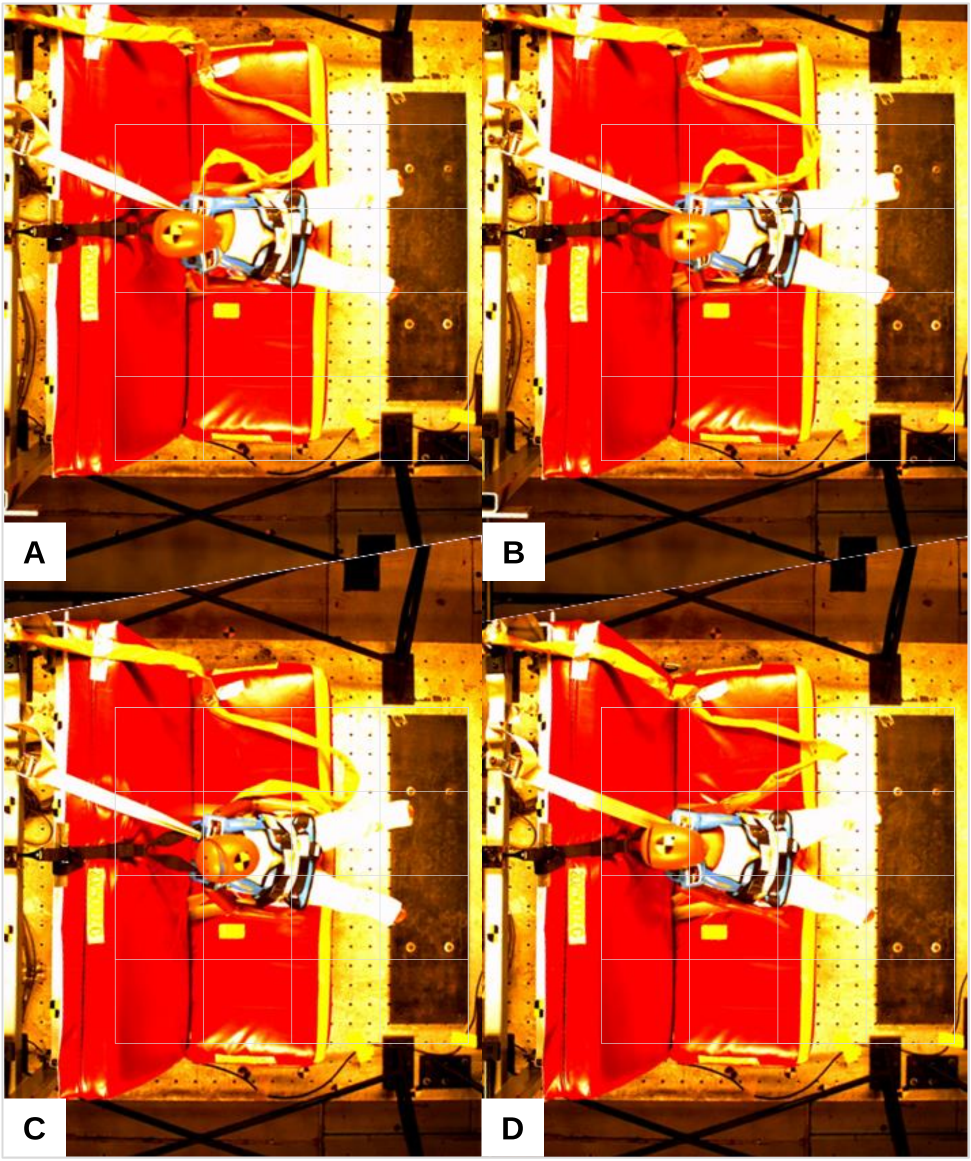

Note. (A) Peak Chest Acceleration at time = 0.058 seconds. (B) Increased Head Acceleration due restrained chest at time = 0.066 seconds. (C) Peak Head Acceleration due to head impact with cast at time = 0.080 seconds. (D) Head Deceleration shown at time = 0.120 seconds.

Figure 25

Sled Trial C Head Acceleration vs. Time

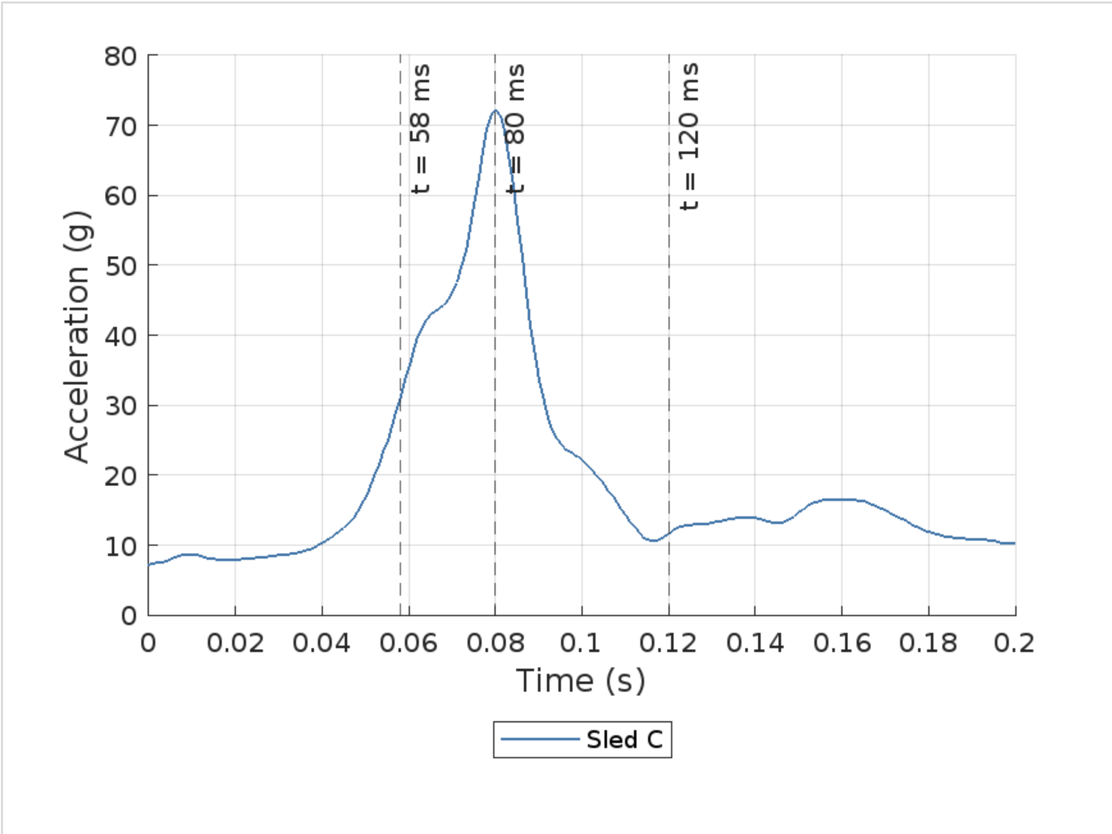

Note. Peak Chest Acceleration at time = 0.058 seconds. Increased Head Acceleration due restrained chest at time = 0.066 seconds. Peak Head Acceleration due to head impact with cast at time = 0.080 seconds. Head Deceleration trough at approximately 0.120 seconds.

Figure 26

Trial D Test Video Frames

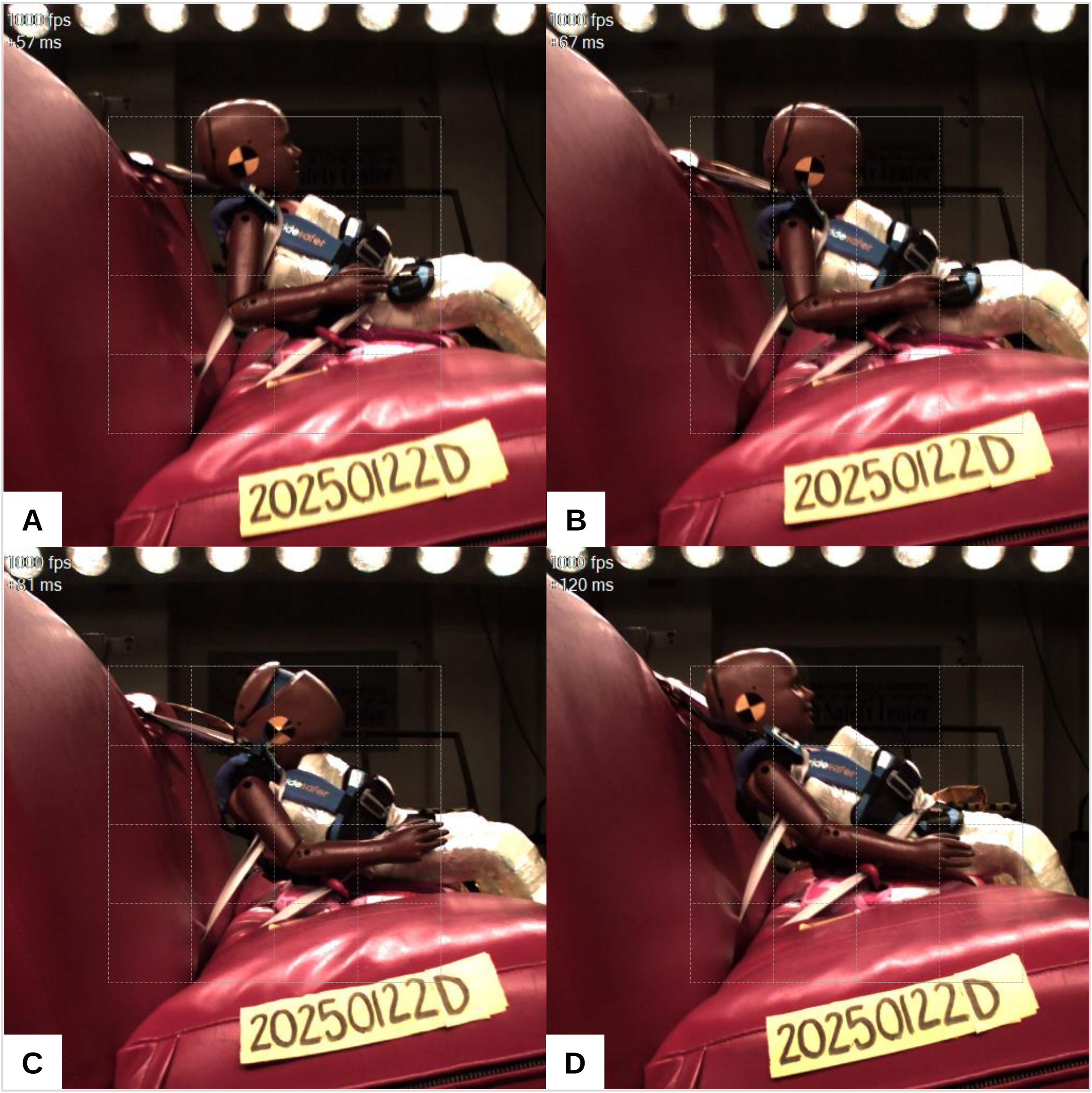

Note. (A) Peak Chest Acceleration at time = 0.057 seconds. (B) Increased Head Acceleration due restrained chest at time = 0.067 seconds. (C) Peak Head Acceleration due to head impact with cast at time = 0.081 seconds. (D) Head Deceleration shown at time = 0.120 seconds.

Figure 27

Sled Trial D Head Acceleration vs. Time

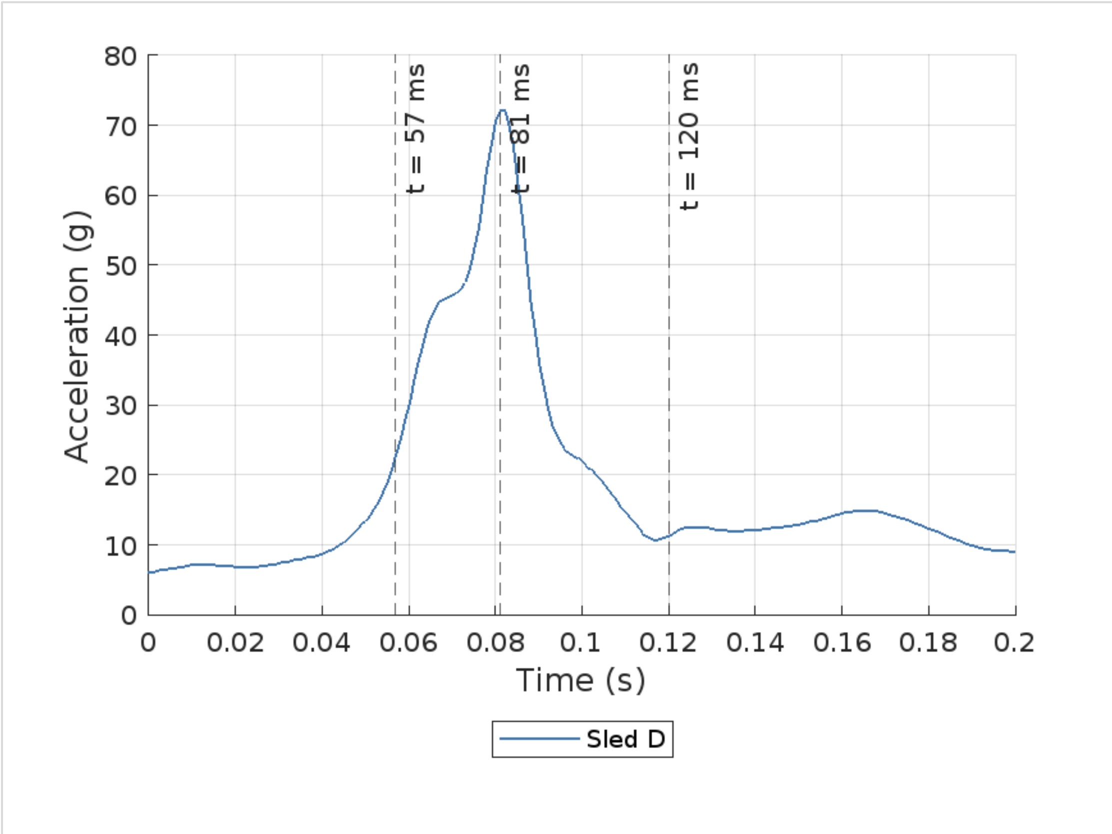

Note. Peak Chest Acceleration at time = 0.057 seconds. Increased Head Acceleration due restrained chest at time = 0.067 seconds. Peak Head Acceleration due to head impact with cast at time = 0.081 seconds. Head Deceleration trough at approximately 0.120 seconds.

Chest Acceleration values are only considered to exceed the regulatory threshold if they remain above the limiting value for a continuous duration of at least 0.003 seconds (NHTSA, 2024b). Both Trials A and B performed well below the federal limiting value of 60 g as shown in Figure 28 and 29. As well as, in Trial C and Trial D, the peak chest acceleration did not exceed the threshold for the required duration, also signifying both trials' compliance with the federal injury criteria (Figure 30, Figure 31).

An analysis of chest acceleration across test trials reveals a time delay of approximately 0.007 seconds in the chest acceleration response for casted trials when compared to the uncasted trials (Figure 32). This delay is attributed to the casting method employed during test preparation by the surgeons. As outlined in Section 1.3, the casting process involved the placement of approximately 50 mm of cotton padding over the chest and abdomen to replicate the breathing space typically accommodated for in clinical applications. After the cast cured, this padding was removed, leaving a circumferential gap of approximately 50 mm around the ATD's torso within the rigid cast structure. This intentional gap is designed to accommodate pulmonary function.

Although the ATD was restrained using the RideSafer Travel Vest and secured to the standard seat assembly by the vehicle's seat belt system, the torso was permitted to translate within the cast by up to ±50 mm before contacting the inner surface of the rigid cast. This internal translation accounts for the observed delay in the chest acceleration response.

Following this initial delay, the casted trials exhibited a more rapid increase in acceleration, as indicated by a steeper slope leading to peak values. The cast introduces an abrupt deceleration to the chest, when compared to the vehicle's seat belts, contributing to these observed peak values. Once the torso collided with the cast's interior surface, the restraint sequence initiated by the CSS progressed rapidly, producing a sharp impulse and rapid rise in chest acceleration to the peak value.

Figure 28

Sled Trial A Chest Acceleration vs. Time

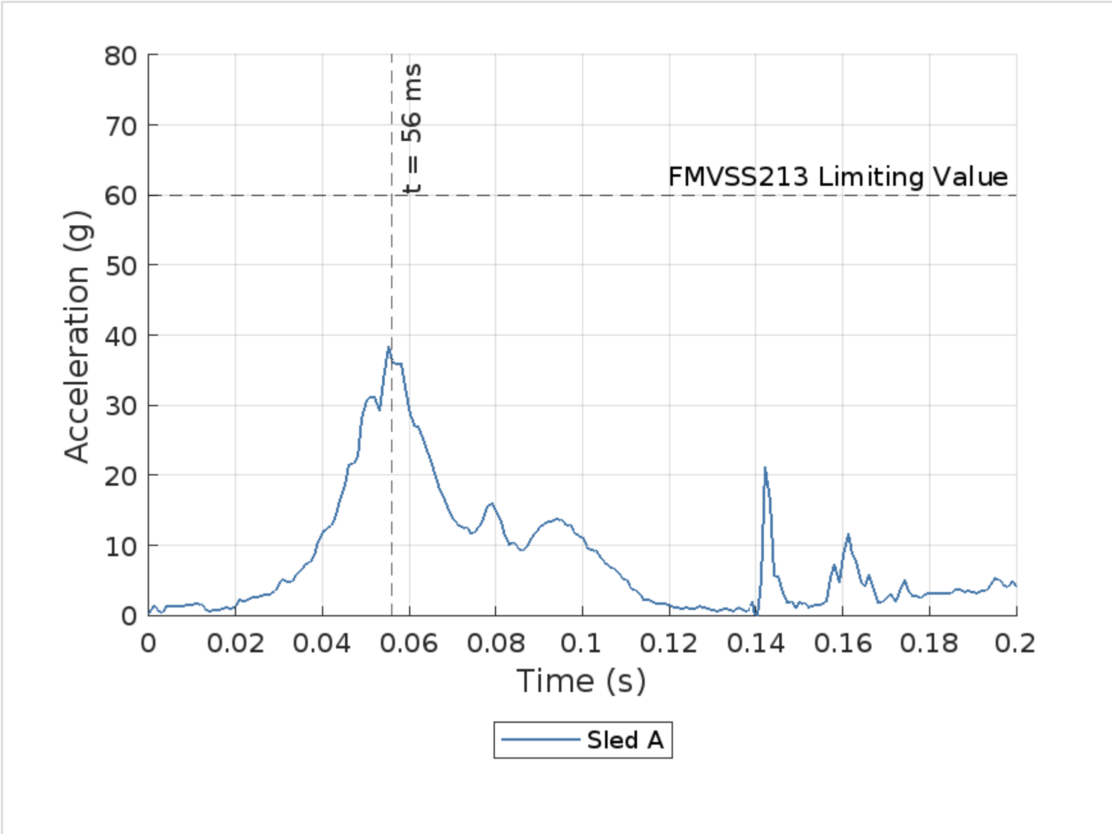

Note. Peak Chest Acceleration of 36.2 g at 0.056 seconds; however, the Chest Acceleration, 3 ms clip, is 35.22 g during the 0.054-0.57 second time range.

Figure 29

Sled Trial B Chest Acceleration vs. Time

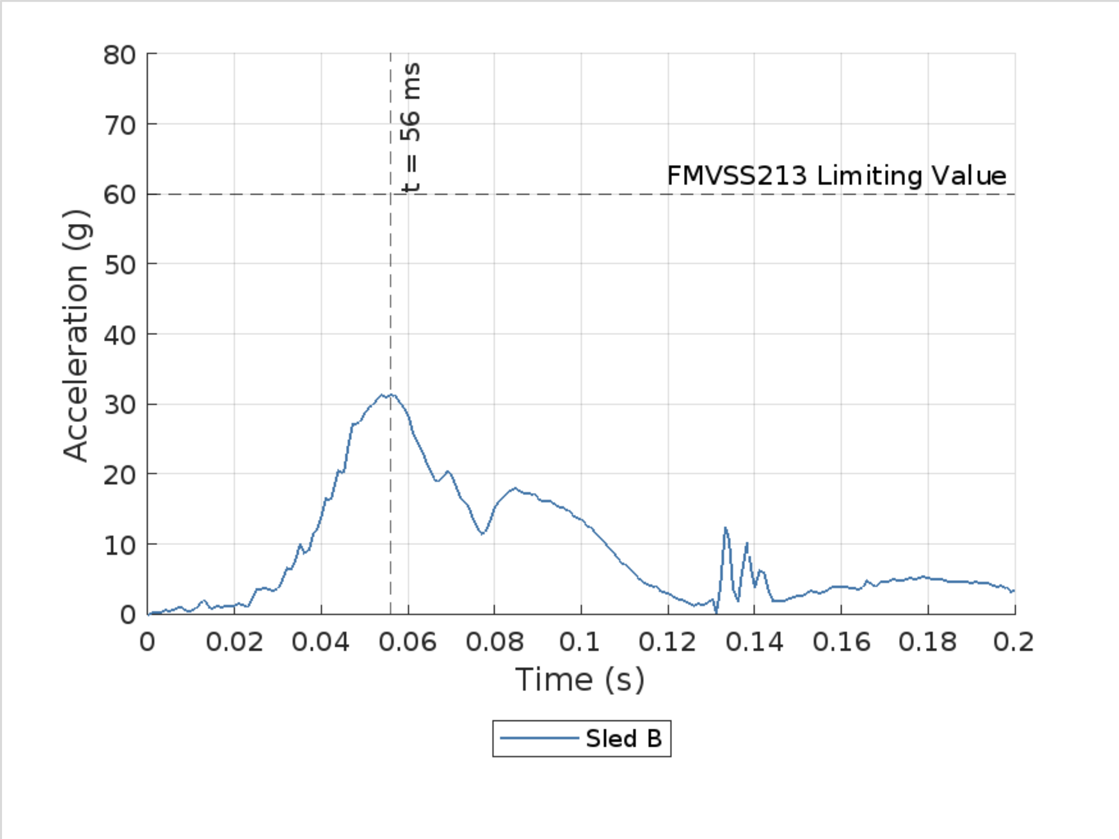

Note. Peak Chest Acceleration of 31.5 g at 0.056 seconds; however, the Chest Acceleration, 3 ms clip, is 31.28 g during the 0.054 - 0.57 second time range.

Figure 30

Sled Trial C Chest Acceleration vs. Time

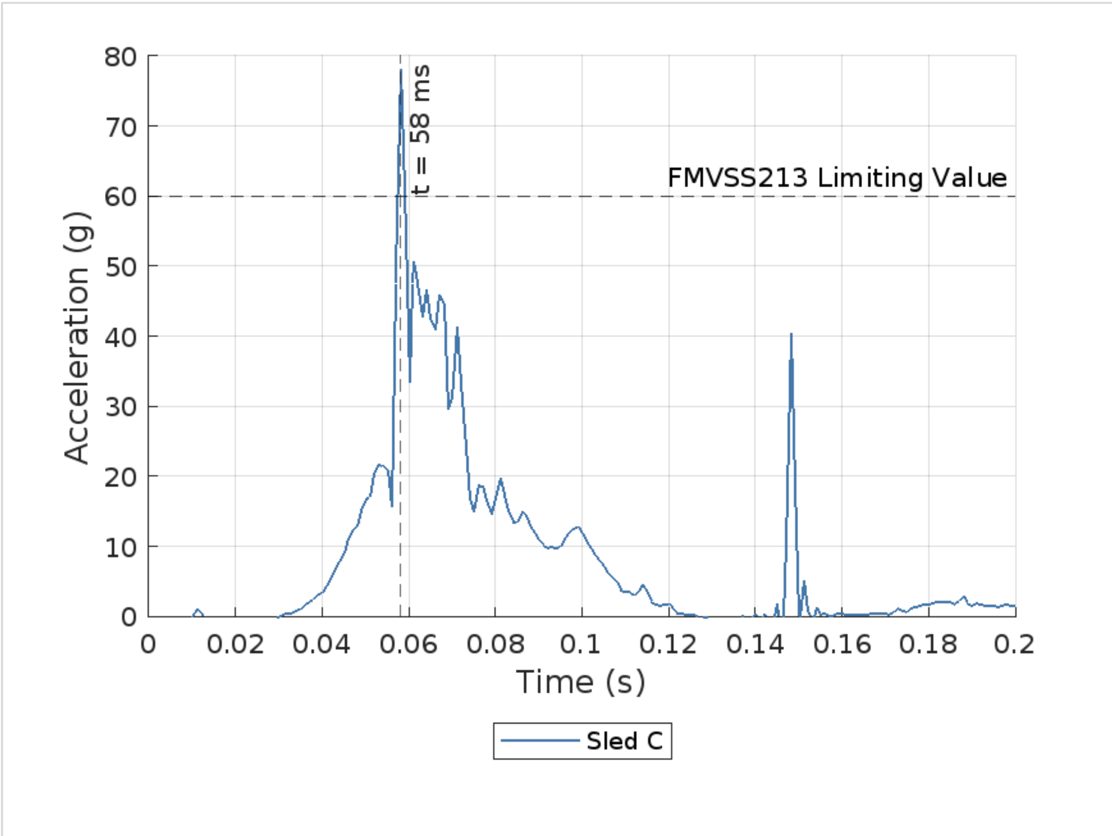

Note. Peak Chest Acceleration of 78.0 g at 0.058 seconds; however, the Chest Acceleration, 3 ms clip, is 45.096 g during the 0.062-0.065 second time range.

Figure 31

Sled Trial D Chest Acceleration vs. Time

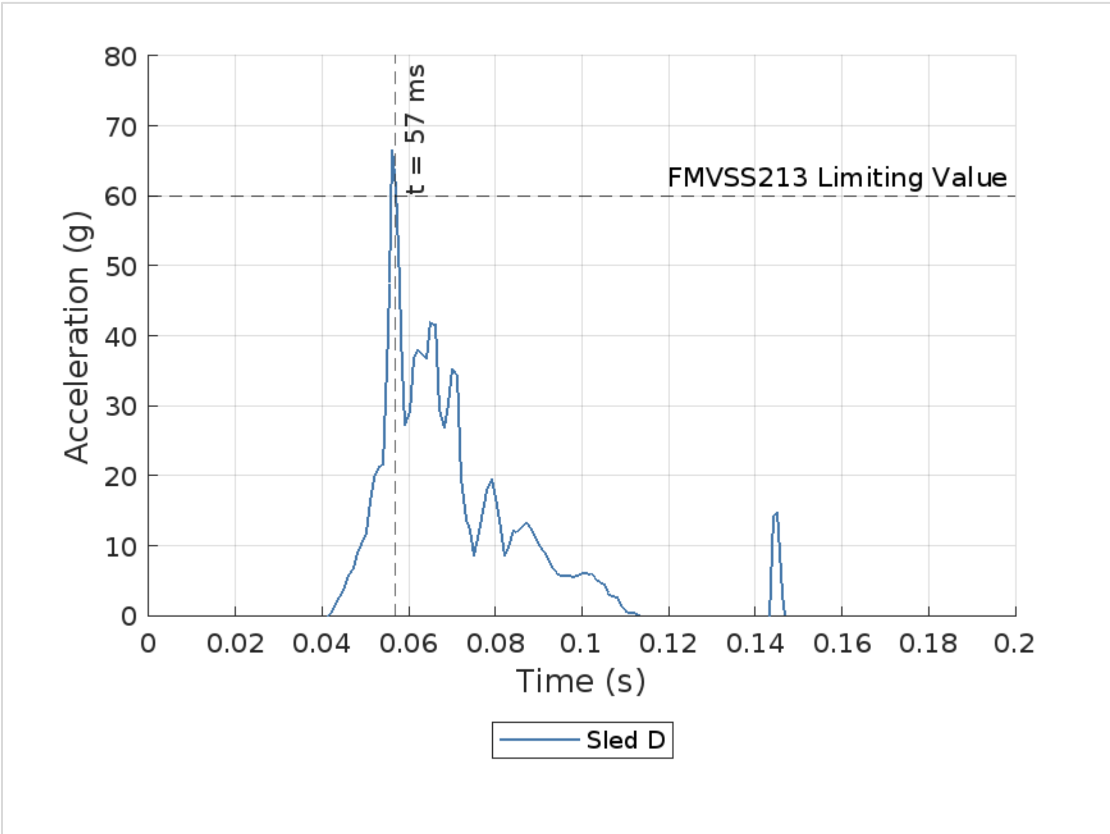

Note. Peak Chest Acceleration of 61.2 g at 0.057 seconds; however, the Chest Acceleration, 3 ms clip, is 42.638 g during the 0.061-0.64 second time range.

Figure 32

Sled Trials A-D Chest Acceleration vs. Time Comparison

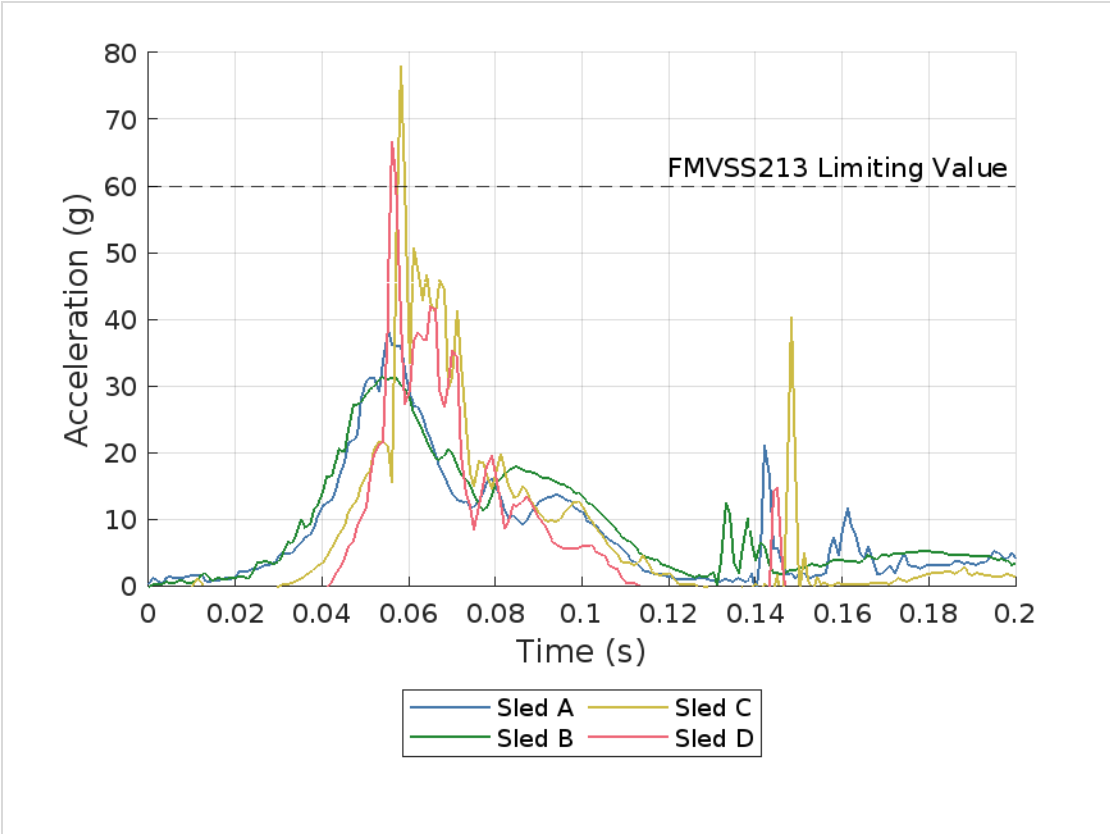

Note. Peak Chest Acceleration for C and D did not exceed the Limiting Value for 0.003 seconds.

1.5 Validation

The purpose of validation testing in product development is to determine whether the product meets the needs and expectations of the end user in real-life scenarios. To validate that the hypothesized Vest and Booster combination concept is a potential solution that not only passes federal testing requirements, but also meets the transportation needs of caregivers to spica-casted children, an in-vehicle study was performed. The expectations for end user use of a CSS established by Durbin et al.

(2018b) are that the CSS fits the child, the CSS fits the vehicle, and the CSS is used properly every single time. Therefore, a physical installation test series of CSS with casted child surrogates was evaluated and is described in the following sections.

1.5.1 Materials and Methods: In-Vehicle Study

This in-vehicle validation study was designed to examine the safe restraint of child surrogates fitted with hip spica casts and restrained in a variety of modern vehicles. Durbin et al. stated "Pediatricians should consider child passenger safety technicians as sources of information when atypical circumstances may be encountered that are not adequately managed by the algorithm" (2018b, pp13). Both ATDs shown in Figure 1 and the six casts shown in Figures 5 and 6 were used as the proxies for spica-casted children during the in-vehicle Study. Current child safety standards were followed by a Child Passenger Safety Technician (CPST) to attempt to safely restrain forward-facing and rear-facing child surrogates fitted with DDH and fracture-type casts. The ATDs were restrained in CSS which were designed with features that were likely to accommodate the fixed position of the hip spica cast. *Hypothesis 2* from Section 1.2 anticipates that caregivers are able to successfully transport a spica-casted child using a low-cost, commercially available CSS option installed independently in their personal vehicle. This validation study was formulated to determine if the child's age/size, CSS direction, cast type, and/or vehicle type would influence the ability of a caregiver to safely position and restrain the spica-casted child.

To ensure appropriate and safe transportation of the casted child surrogate, two requirements were initially used to identify candidate CSS for the installation study: first, the CSS had to be approved for use with the age, size, and weight of the casted child; and secondly, the CSS design was known to likely accommodate the shape of the casted child. Challenges with safely restraining a casted child has been observed in prior studies. Zielinski et al. (2009) studied the crash performance of casted 1- and 3-year-old ATDs using a DDH-type cast. Zielinski et al. found that the CSS seat-side bolsters adjacent to the thighs create an installation constraint. Therefore, two CSS shown in Figure 33 were ultimately selected for use in the current study with both ATDs: the Merritt Wallenberg Hip Cast Car Seat (Merritt Manufacturing, Inc., n.d.) and the Diono Radian R100 (Diono US, n.d.).

Figure 33

CSS Selected for In-Vehicle Study

Note. (A) Merritt Wallenberg Hip Cast Car Seat. (B) Diono Radian R100.

These specific CSS were chosen for several reasons: (a) both CSS have been previously crash tested with children fitted with a hip spica cast so the findings from the current study can be linked with crash safety testing data; (b) the Wallenberg is designed specifically for use with children fitted with a hip spica cast (Merritt, 2024; Collins, Adams, et al., 2022); (c) the Radian R100 is designed without seat-side bolsters on either side of the child's hips and thighs, and as such, this design allows the hip abduction common to hip spica casts used to treat developmental dysplasia of the hip (Collins et al., 2020; Zielinski et al., 2009); and (d) the Radian R100 also offers an extended length groin buckle strap which is anchored to the plastic seat shell sufficiently forward to accommodate the larger size of a casted child (Diono, 2016; Collins et al., 2020).

Both of the selected CSS are of the convertible type, meaning they are designed to function rear-facing in the vehicle or convert to function forward-facing in the vehicle. This functionality feature is important because children under two years of age are recommended to be rear-facing (Durbin et al., 2018b) to protect the head and cervical spine from the whiplash common to forward-facing car occupants in a vehicle crash. Since spica casts are typically used with children aged 6 months to 5 years, the 1-year-old ATD represented younger children and was restrained in the rear-facing direction. On the other hand, the 3-year-old ATD was only restrained in the forward-facing configuration for the Wallenberg and Radian R100 seats; this scenario was intended to represent older children greater than or equal to age 2. The third restraint investigated was the CSS combination concept presented in Section 1.3 and was studied for the forward-facing 3-year-old only. The RideSafer Travel Vest, shown in Figure 7, is designed for vehicle forward-facing children aged 2-years and older (Safe Traffic System, 2023), and the BubbleBum Booster, shown in Figure 8, is only for children who weigh between 18 and 45 kg (BubbleBum, 2013). Consequently, the combination was not employed for the 1-

year-old ATD; however, it was deemed appropriate for use with the 3-year-old ATD, as the total mass of the casted ATD wearing the RideSafer Travel Vest met or exceeded 18 kg.

The RideSafer Travel Vest manual allows for combined use with the TravelSmarter Booster Seat (Safe Traffic System, 2023). However, this study was to determine if novel installation methods could be performed using off the shelf components due to the constraints provided by the casted children. Also, the TravelSmarter Booster Seat has arm rests and small seat-side bolters which would have prevented a casted child from its use; therefore, the BubbleBum Booster was used due to its aforementioned characteristics.

A suite of vehicles was identified that would represent vehicles currently on U.S. roadways. This was done by analyzing four distinct passenger vehicle categories: Compact, Sport Utility Vehicle (SUV), Minivan, and 2-row full-size Light Truck. Selection of a given vehicle was based on United States' market share of light vehicle retail sales from 2003-2023 (GoodCarBadCar, 2024) and local availability for the research study. To determine local availability of the vehicles, the questionnaire shown in Figure 34 was sent to all students, staff, and faculty at Kettering University during the Spring 2024 semester. Based on the market share rankings and availability, the following vehicles, Figure 35, were ultimately selected for inclusion in the current study: 1) Compact, 2021 Toyota Corolla; 2) SUV, 2019 Toyota RAV4; 3) Minivan, 2017 Toyota Sienna; 4) Truck, 2018 Ford F-150 Crew Cab.

Figure 34

Test Vehicle Questionnaire

Compact Car

- [ ] 2010 or newer Toyota Corolla
- [ ] 2010 or newer Honda Civic

SUV

- [ ] 2010 or newer Toyota RAV4
- [ ] 2010 or newer Honda CRV

Truck

- [ ] 2010 or newer Ford F-150 Quad Cab
- [ ] 2010 or newer Ford F-150 Crew Cab

Minivan

- [ ] 2010 or newer Honda Odyssey
- [ ] 2010 or newer Toyota Sienna

Which days/times would your vehicle(s) be available for 3 hours? Select all timeslots that work for you.

	8th Thursday, May 23	8th Friday, May 24
9am - 12noon	☐	☐
12noon - 3pm	☐	☐
3pm - 6pm	☐	☐

Your Name *

Your phone number *

Your exact vehicle(s) Year/Make/Model *

Thank you.

We will be in contact with you very soon!

Figure 35

Selected Vehicles for Validation Study

Note. From left to right: 2021 Toyota Corolla, 2019 Toyota RAV4, 2017 Toyota Sienna, and 2018 Ford F-150 Crew Cab.

Now that all possible variables had been identified for investigation, a design of experiments (DOE) was developed to conduct 180 different installation trials. Itemization of the specific configuration for all 180 installation trials can be found in Appendix G. Figure 36 presents the structure of different levels within each factor and the three possible outcomes for each trial.

Figure 36

Verification Study Design of Experiments

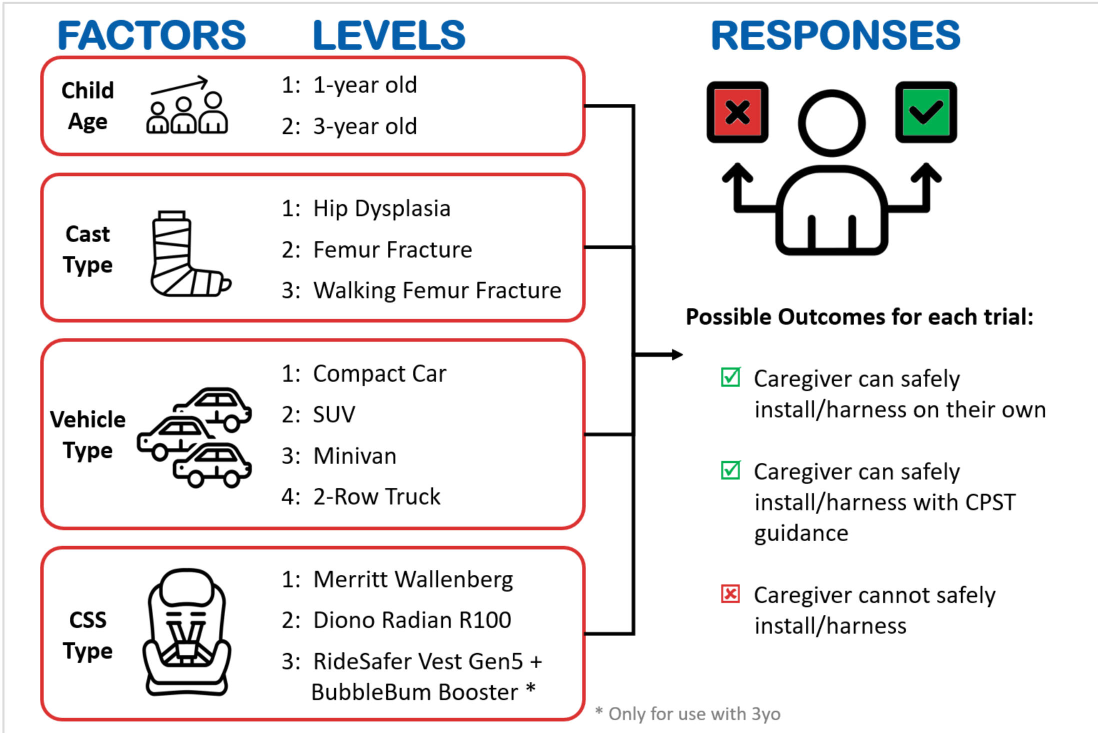

Both uncasted and casted ATDs were restrained in vehicles using the three CSS options previously outlined. A certified CPST trained through Safe Kids Worldwide (SKW) conducted the first 60 installation trials to assess whether each unique child–CSS–vehicle configuration was even physically achievable. Each installation was guided by a comprehensive, multi-criteria checklist incorporating the CSS manufacturer’s instruction manuals (Merritt, 2024; Diono, 2016; Safe Travel Systems, 2023; BubbleBum, 2013), the respective vehicle owner’s manuals (Toyota, 2019, 2020a, 2020b; Ford, 2018), NHTSA’s car seat installation guidelines, and SKW’s “Right Fit” best practice recommendations. If the ATD and CSS could be properly installed in accordance with all checklist criteria, the configuration was recorded as a *PASS*.

Otherwise, it was marked as a *FAIL* and documentation was made noting the reasons for installation failure. Key attributes of a passing installation included:

1. Unobstructed harnessing of the casted body within the vehicle-installed CSS.
2. Proper alignment of the cervical and thoracic spine in the neutral position.
3. For rear-facing configurations, the top of the ATD's head must be at least 25.4 mm below the top surface edge of the CSS.
4. Maintenance of an anterior chest-abdomen gap within the cast to support pulmonary function of the child.
5. No contact between the cast or CSS and the adjacent vehicle door in the outboard seating position.

The 25.4 mm head clearance prevents upward migration of the head during a crash, thereby reducing the risk of cervical spine hyperextension. Similarly, ensuring neutral spine alignment helps prevent preloading of the vertebral column, which could otherwise negatively alter the kinematics during impact.

For each installation attempt, a study-specific "Child Passenger Ease-of-Use Checklist" was completed, CPST installation photos we taken, and installation outcomes were documented for further analysis using the standardized forms shown in Figures 37 and 38.

Figure 37

Child Passenger Ease of Use Checklist, page 1

Child Passenger Ease Of Use Checklist

Preliminary Questions

Date of Test:
Installer:
Test Number:

Crash Dummy Type:
- One Year Old
- Three Year Old

Cast Type:
- Hip Spica
- Femur Fracture
- Walking Cast

Vehicle Type:
Toyota Corolla
Toyota RAV4
Ford F-150
Toyota Sienna

CSS Type:
- Diono Radian
- Ride Safe Vest with Bubblebum Booster Seat
- Merritt Wallenberg

CSS Location in Vehicle:

D __ __ Front Row
__ __ __ Back Row
__ __ __ Third Row

Crash Dummy Casted Height/Inches:
__ __

Crash Dummy Casted Weight/lbs:
__ __ __

Installation Details

Angle of Test Area Floor:
__ __degrees from horizontal

Child Ht/Wt correct for CSS:
- Yes
- No

CSS Correct Direction:
- Yes
- No
- N/A

Recline Angle Correct:
- Yes
- No

Upper Tether Correct:
- Yes
- No
- N/A

RF Base Angle Merritt only:
__ __degrees from horizontal

Lap/Shoulder Belt Correct:
- Yes
- No
- N/A

CSS Setup Harness Correct:
- Yes
- No
- N/A

Shoulder Harness Position
- 6 (highest - Merritt)
- 5 (highest - Diono)
- 4
- 3
- 2
- 1 (lowest)

RF Recline Angle of CSS:
__ __degrees from horizontal

Crotch Strap Position
- d (largest - Merritt)
- c (largest - Diono)
- b
- a (smallest)

Additional Pieces Used
- Merritt Wedge
- Merritt Riser
- Merritt Hammock, ____
- Pool Noodle
- N/A

Comments:

Page 1 of 2

Figure 38

Child Passenger Ease of Use Checklist, page 2

After Installation Ratings

Level of Difficulty for Harness Adjustment:

- 1 - Not possible
- 2 - Needed full CPST/3rd party assistance
- 3 - Able to do it with help
- 4 - Takes some time, minor issues on own but completed installation
- 5 - No assistance needed, no issues during installation
- N/A

Level of Difficulty for Crotch Adjustment:

- 1 - Not possible
- 2 - Needed full CPST/3rd party assistance
- 3 - Able to do it with help
- 4 - Takes some time, minor issues on own but completed installation
- 5 - No assistance needed, no issues during installation
- N/A

Level of Difficulty for Additional Pieces Adjustment:

- 1 - Not possible
- 2 - Needed full CPST/3rd party assistance
- 3 - Able to do it with help
- 4 - Takes some time, minor issues on own but completed installation
- 5 - No assistance needed, no issues during installation
- N/A

Comments/ Notes

Number of People to Harness:

Vehicle Space/ Height Issues:

Issues with Proper Fit/Ease of Use for this scenario:

PASS or FAIL

Page 2 of 2

All 60 child-cast-vehicle-CSS configurations underwent an initial fit assessment conducted by a certified CPST to evaluate the feasibility of proper vehicle installation and secure harnessing of the spica-casted ATD and the assessment was documented on a Child Passenger Ease of Use Checklist for each trial. If the CPST successfully installed the CSS and appropriately secured the ATD, the configuration was designated as a *PASS* and the configuration advanced to the caregiver installation phase for independent evaluation. Conversely, if the CPST was unable to achieve appropriate installation and harnessing, the configuration was assigned a *FAIL* status. In such cases, the scenario was excluded from further caregiver testing within the DOE, under the assumption that the caregiver would likewise be unable to achieve a successful installation and the scenario was catalogued as *CANCEL*.

During the independent installation phase, caregivers were instructed to install and secure the ATD without assistance. If the caregiver successfully achieved the installation and harnessing, the scenario was rated as a *PASS*. If unsuccessful, the caregiver was provided with support from a hospital-employed CPST with STAC training, simulating the discharge process of spica-casted children from medical facilities.

Finally, if following the provided CPST-STAC guidance the caregiver successfully completed the installation and harnessing, the scenario was reclassified as a *PASS*. If the caregiver remained unable to achieve the correct installation despite the provided support, the scenario retained a *FAIL* designation.

During the initial installations conducted by the CPST, it was determined that the bilateral femur fracture cast and the 1½ Leg walking cast produced equivalent outcomes due to identical hip and knee casting angles. Accordingly, all trials involving the walking cast were assigned a rating of *Conditionally Pass* or *Conditionally Fail*, corresponding to the *PASS* or *FAIL* outcome of the bilateral femur fracture cast within the same child–vehicle–CSS configuration.

1.5.2 Results: In-Vehicle Study

Installations meeting all installation criteria were cataloged as achievable by a CPST professional. The next phase of the study assessed whether untrained caregivers could perform the same installations across four vehicle types, both independently and if necessary with the support of a CPST with additional Safe Travel for All Children (STAC) Training. Installation assessments from the CPST trials are summarized in Tables 5 and 6 below.

Table 5

CPST Installation Assessments for Casted 3-year-old

CSS	Cast	Compact	SUV	Minivan	Truck	Pass Rate (%)
Wallenberg	DDH	Pass	Pass	Pass	Pass	100
	Fracture	Pass	Pass	Pass	Pass	100
	1½ Leg	Pass	Pass	Pass	Pass	100
Radian	DDH	Pass	Pass	Pass	Pass	100
	Fracture	Pass	Pass	Pass	Pass	100
	1½ Leg	Pass	Pass	Pass	Pass	100
RideSafer &	DDH	Pass	Pass	Pass	Pass	100
BubbleBum	Fracture	Fail	Fail	Pass	Fail	25
	1½ Leg	Fail	Fail	Pass	Fail	25
Pass Rate (%)	—	83	83	100	83	—

Note. The 3-year-old crash test ATD was positioned forward-facing in the four vehicles in the different casts and three restraint options. The CPST then attempted to safely restrain the casted ATD; either a successful restraint condition was achieved (*PASS*) or not (*FAIL*). Any trial assigned a rating of *Conditionally Pass* or *Conditionally Fail* is listed simply as either *PASS* or *FAIL* for clarity in the table above.

Table 6

CPST Installation Assessments for Casted 1-year-old

CSS	Cast	Compact	SUV	Minivan	Truck	Pass Rate (%)
Wallenberg	DDH	Pass	Pass	Pass	Fail	75
	Fracture	Fail	Pass	Fail	Fail	25
	1½ Leg	Pass	Pass	Pass	Fail	75
Radian	DDH	Pass	Pass	Pass	Pass	100
	Fracture	Fail	Fail	Fail	Fail	0
	1½ Leg	Fail	Fail	Fail	Fail	0
Pass Rate (%)	—	50	67	50	17	—

Note. The 1-year-old crash test ATD, in three different casts, was positioned rear-facing in both CSS in all four test vehicles. As with the 3-year-old tests, the casted ATD was safely restrained (*PASS*) or not (*FAIL*) by a CPST. Any trial assigned a rating of *Conditionally Pass* or *Conditionally Fail* is listed simply as either *PASS* or *FAIL* for clarity in the table above.

1.5.3 Discussion: In-Vehicle Study

This study sought to evaluate different options to position children treated with different hip spica designs in a range of typical, recent vehicles. More specifically, DDH and fracture-type casts were applied to crash test ATDs that served as surrogates for 1- and 3-year-old children. A CPST then attempted to safely restrain the casted surrogates in child seats and harnesses in different vehicles. It should be noted that every control installation with the 1- and 3-year-old uncasted ATDs, in all CSS and vehicle scenarios, conformed to each of the guidelines and were thus deemed a *PASS*. This includes the control installation of the 3-year-old ATD in the new CSS concept of the RideSafer Travel Vest and BubbleBum Booster (Figure 39).

Figure 39

Control Installation of the 3-Year-Old ATD in the New CSS Concept

Note. (A) Installation in Compact Vehicle Type. (B) Installation in SUV Vehicle Type. (C) Installation in Truck Vehicle Type.

The cast type, child age, and vehicle type all appeared to affect the likelihood that the child could be safely restrained. Based on Federal and AAP requirements, the 1-year-old surrogate must be rear-facing in the vehicle while the 3-year-old can be forward-facing (NHTSA, 2024b; Durbin et al., 2018b). In general, the forward-facing 3-year-old was safely restrained in 83% of cases while the 1-year-old was safely restrained in 50% of cases. The cast influenced the likelihood of a *PASS* condition for the two child surrogates.

As shown in Table 5, the 3-year-old forward-facing ATD was safely restrained in an average of 87% of installations for the four vehicles (range 83-100%). For the DDH casted 3-year-old, hip abduction led to the feet being spread apart such that positioning the ATD in the vehicle outboard seating position caused potential impingement with the door panel. In all DDH trials, the vehicle door was closed and the foot always happened to fit into the door panel pocket typically used to store drink bottles and other items. As such, no impingement ultimately occurred.

For the RideSafer and BubbleBum concept, safe restraint was achieved in all DDH trials, but varied with the Femur and Walking cast trials. For the failed cases, due to the posterior tibia portion of the cast restricting seat positioning, the child slumped in the vehicle seat such that the proper positioning of the vehicle shoulder belt could not be achieved. This space constraint prevented proper seating of the ATD within the CSS and resulted in an unacceptable gap between the ATD and the CSS (Figure 40) that caused the cervical-thoracic spine to be misaligned and the vehicle shoulder belt to come in contact with the ATD’s neck. Durbin et al. (2018b) states that correct belt fit is achieved when “the shoulder belt lies across the middle of the chest and shoulder, not the neck or face” (p. 6).

Figure 40

Example of Failure Due to Femur Cast Leg Constraint on 3-year-old

Note. (A) Magenta star locates the interference between the cast and the vehicle seat resulting in an unacceptable gap between ATD and vehicle seat back (dashed white line) and causing the cervical-thoracic spine to be misaligned (dashed green line). (B) Cyan arrow points to vehicle shoulder belt in contact with ATD anterior neck.

The study identified that the Merritt Wallenberg could not be safely installed in a rear-facing configuration in any second-row seating position within the large 2-row truck vehicle type. This *FAIL* rating was attributed to vehicle–CSS incompatibility, rather than issues related to harnessing a casted ATD. This outcome was unexpected by the CPST, given that the 2-row truck features a comparatively larger interior occupant compartment than Compact or SUV vehicle types. The incompatibility was traced to the interaction between the truck's 70/30 split bench seat and the design of the Wallenberg's aluminum base. Specifically, the base legs of the Wallenberg positioned into the actual bench split as shown in Figure 41, preventing installation in accordance with the manufacturer's instructions for use (Merritt, 2024).

Figure 41

Truck-Wallenberg Incompatibility

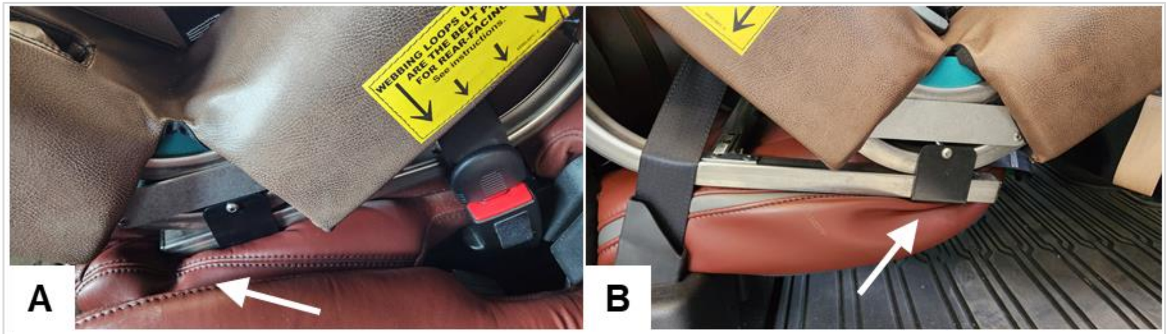

Note. (A) 70/30 split in second-row bench seat. (B) When the rear-facing Wallenberg is positioned out of the bench split as shown in 30A, the CSS base overhangs the edge of the vehicle seat which is unacceptable.

The DDH casted 1-year-old was successfully installed in each vehicle trial except for the Merritt Wallenberg in the Truck due to the aforementioned CSS-vehicle incompatibility. The CPST observed that had the CSS-vehicle been compatible, then the DDH casted 1-year-old installation trial would have been classified as a *PASS* as well. The primary challenge observed with the 1-year-old ATD seated rear-facing in both the femur fracture and walking cast configurations was the fixed leg extension imposed by the cast, which exceeded the available clearance between the CSS seat back and the vehicle seat back. This space constraint prevented proper seating of the ATD within the CSS and resulted in an unacceptable gap between the ATD and the CSS (Figure 42) that caused the cervical-thoracic spine to be misaligned. Durbin et al. (2018b) states "proper installation results in a semi-reclined angle of approximately 45°, which enables the infant's head to lie against the back of the CSS, as opposed to potentially falling forward, compromising the infant's airway if the seat is angled too upright" (p. 4). Therefore, it is important that correct cervical-thoracic spine alignment be verified to ensure proper pulmonary function during transportation.

Figure 42

Example of Failure Due to Walking Cast Leg Constraint on 1-year-old

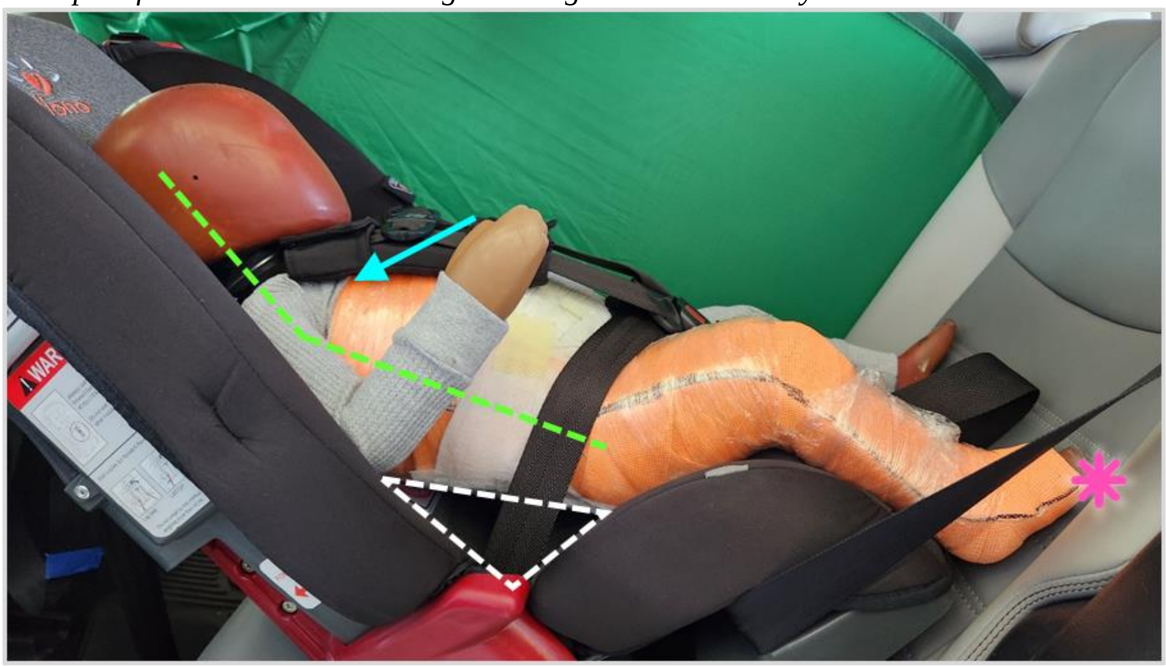

Note. Magenta star locates the interference between the cast and the vehicle seat back resulting in an unacceptable gap between ATD and CSS (dashed white line) causing the cervical-thoracic spine to be misaligned (dashed green line). Cyan arrow points to anterior chest hard-pressed to the interior of the antero-superior cast.

The 1-year-old rear facing ATD was safely restrained in an average of 46% of the installations in the four vehicles (range for the test vehicles of 17%-67%) with the lowest pass rate was for the pickup truck as shown in Table 3. The use of the Wallenberg and Radian CSSs also influenced the rate of safe installations: a safe installation was achieved in 58% of cases with the Wallenberg CSS (7 of 12) but only 33% (4 of 12) with the Radian CSS. While all but one installation with the DDH cast were safely installed (7 of 8 or 88%) with CSS, the fracture cast and 1½ Leg fracture cast were only safely restrained in 25% of the installations (4 of 16). Typical reasons for a *FAIL* included: the crown of the ATD's head being less than 25.4 mm from the top of the CSS; impingement of the 5-point CSS harness on the cast, misalignment of the cervico-thoracic spine which is associated with anterior tilt of the child's body in the cast. While an optional head rest is provided by the manufacturer of the Wallenberg, for extended use in rear-facing scenarios only, the head rest could only be attached in the minivan vehicle. In the other three vehicles of the current study, there was insufficient room to accommodate the size of the head rest.

1.6 Analysis

Further analysis of injury values using simulation was performed in Working Model (MSC, 2004). Working Model (WM) is a 2-dimensional (2D), dynamic motion simulation tool able to measure position, velocity, acceleration, force, torque, momentum, and kinetic energy of a mechanical system. By developing a validated WM simulation of the sled tests described in Section 1.4, additional untested configurations, such as a 3-year-old ATD in a DDH cast, can be evaluated to predict their compliance with the performance requirements specified in FMVSS No. 213.

1.6.1 Simulation Methods

The Kettering University Crash Safety Center maintains an existing validated FMVSS No. 213 simulation model of a 3-year-old child in a CSS developed in the WM software, as shown in Figure 43. Each body segment within the model was constructed to reflect the corresponding size and mass of the associated anatomical region of the ATD. Connections between body segments, including shoulder, elbow, wrist, hip, knee, and ankle, were modeled using pin joint representations. For pin joints on the ATD that do not permit full 360° rotation, massless rigid blocks were incorporated to act as rotational end stops, effectively replicating the real constraints a joint in the body experiences. Vehicle seat belts and the CSS harness were simulated as tunable spring-damper components to capture their dynamic response to rapid acceleration and deceleration. Similarly, the viscoelastic behavior of the vehicle seat cushion assembly was represented using spring-damper systems, optimized using displacement data obtained from physical sled testing. This model served as the initial baseline configuration for the simulations conducted in this study.

Figure 43

Validated 3-year-old in a CSS WM Simulation

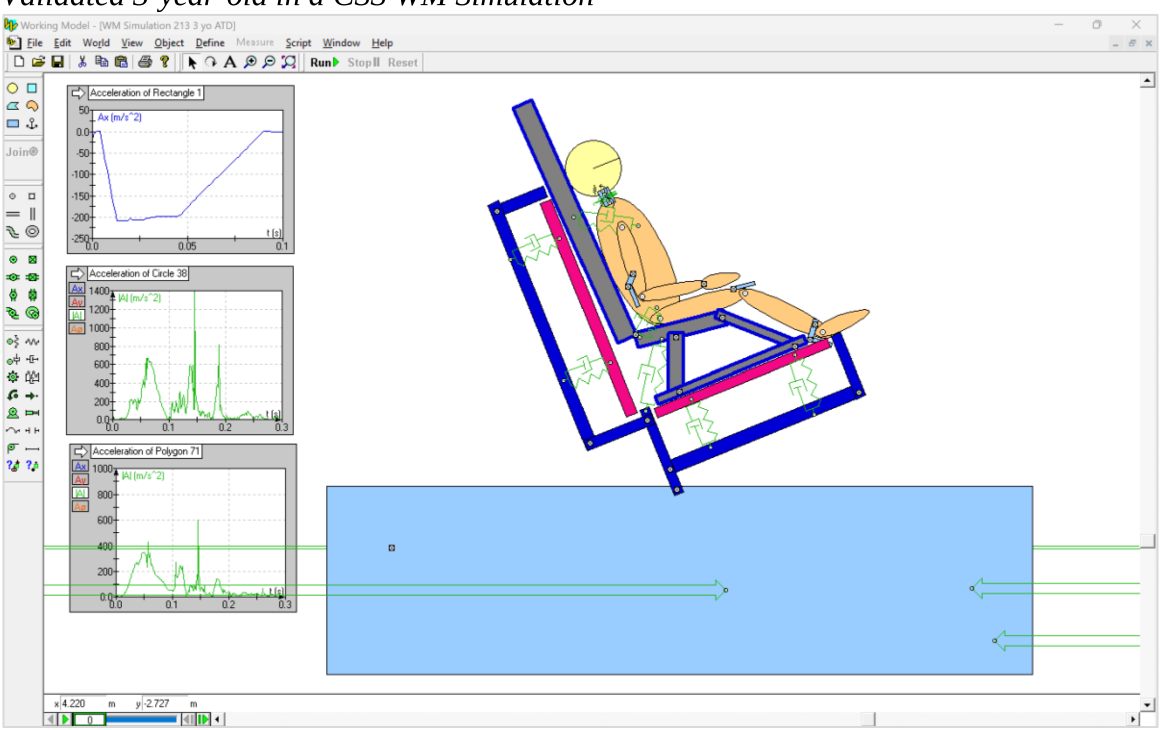

The baseline model was revised to replicate the test set up of Trial A in Section 1.4 by removing the CSS, translating the ATD to contact the seat back and seat pan surfaces of the bench seat, adjustment of seat back height to accurately match the height in Trials A-D, and fixation of the two spring-dampers from the ATD's torso to the bench mount to replicate the dynamic response of the Travel Vest secured by a vehicle's 3-point seat belt during a crash event. WM Trial A, version 1 (Figure 44).

Figure 44

WM Trial A, version 1

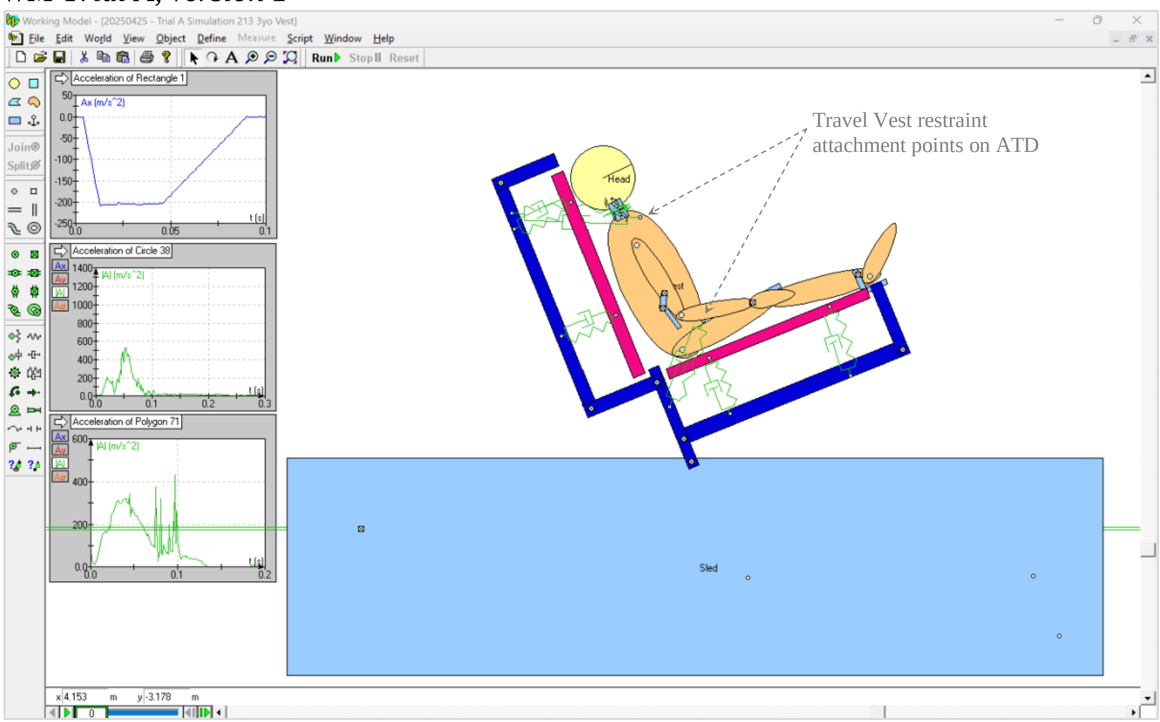

To determine the performance metrics of a Working Model simulation, the model was first employed to visualize the kinematic motion of the modeled ATD to ensure the motion is similar to the recorded side videos captured during the physical sled testing and also that the objects in the model are set up to collide properly. Next, the model is reset and the data sets collected, at a frequency of 1000 Hz, during the simulation run are exported to a Meter Data file, in .dta format, for analysis. Meter Data files can be opened in Microsoft Excel using the embedded Text Import Wizard to tab delimiters to create columns of the data sets collected. An example of a raw data set opened in Excel that was exported from Working Model is shown in Figure 45.

Figure 45

Working Model Exported Raw Data Set Example

	A	B	C	D	E	F	G	H	I	J	K	L	M	N
1	20250530 - A - Trial A 3yo Vest_v46													
2	5/30/2025 12:20													
3	Sled Acceleration		Head Acceleration					Chest Acceleration					Velocity of Sled 1	
4	t	Ax	t	|A|				t	|A|				t	Vx
5	0	-0.032	0	9.807	-	-	-	0	12.205	-	-	-	0	0
6	0.001	-0.026	0.001	9.825	-	-	-	0.001	9.828	-	-	-	0.001	-2.93E-05
7	0.002	-0.021	0.002	9.804	-	-	-	0.002	9.656	-	-	-	0.002	-5.32E-05
8	0.003	-0.018	0.003	9.769	-	-	-	0.003	9.328	-	-	-	0.003	-7.27E-05
9	0.004	-0.061	0.004	9.713	-	-	-	0.004	8.915	-	-	-	0.004	-9.67E-05
10	0.005	-21.289	0.005	9.626	-	-	-	0.005	8.517	-	-	-	0.005	-0.011
11	0.006	-42.485	0.006	9.507	-	-	-	0.006	8.293	-	-	-	0.006	-0.043
12	0.007	-63.642	0.007	9.38	-	-	-	0.007	8.419	-	-	-	0.007	-0.096
13	0.008	-84.76	0.008	9.272	-	-	-	0.008	9.192	-	-	-	0.008	-0.17
14	0.009	-105.846	0.009	9.209	-	-	-	0.009	11.107	-	-	-	0.009	-0.265
15	0.01	-126.909	0.01	9.218	-	-	-	0.01	14.604	-	-	-	0.01	-0.382
16	0.011	-147.959	0.011	9.347	-	-	-	0.011	19.862	-	-	-	0.011	-0.519
17	0.012	-169.006	0.012	9.668	-	-	-	0.012	27.006	-	-	-	0.012	-0.678
18	0.013	-190.01	0.013	10.299	-	-	-	0.013	36.168	-	-	-	0.013	-0.857
19	0.014	-189.838	0.014	11.453	-	-	-	0.014	47.204	-	-	-	0.014	-1.047
300	0.295	0.221	0.295	31.797	-	-	-	0.295	17.841	-	-	-	0.295	-11.06
301	0.296	0.17	0.296	33.735	-	-	-	0.296	13.607	-	-	-	0.296	-11.06
302	0.297	0.113	0.297	35.059	-	-	-	0.297	9.526	-	-	-	0.297	-11.06
303	0.298	0.042	0.298	35.449	-	-	-	0.298	6.04	-	-	-	0.298	-11.06
304	0.299	-0.03	0.299	34.962	-	-	-	0.299	4.075	-	-	-	0.299	-11.06
305	0.3	-0.098	0.3	33.779	-	-	-	0.3	4.834	-	-	-	0.3	-11.06
306	0.3	-0.054	0.3	13.814	-	-	-	0.3	1.79	-	-	-	0.3	-11.06

Columns A through N were extracted and imported into a dedicated Microsoft Excel workbook titled *Chest G and HIC Calculator.xls*, developed specifically for this study to compute simulation performance metrics. The calculator is programmed to filter the data sets to remove noise according to filtering process described in SAE J211-1 (1995). The calculator then automatically computes and highlights three key values from the simulation data: (a) chest acceleration using a 3 ms clip (g), (b) HIC36, and (c) velocity (mph). These key values are calculated using embedded Excel formulas implementing Equations 1 and 2 from Section 1.4.1, including a conversion of velocity from meters per second to miles per hour. Examples of the formulas in each cell of the workbook for Chest Acceleration and HIC36 calculation are shown in Appendix E.

A Butterworth 4-Pole Phase-less Digital Filter from SAE J211-1 (SAE, 1995) is used to smooth the data sets from impact tests within a frequency range without attenuating the overall amplitudes prior to calculating the HIC36 and Chest Acceleration, 3 ms clip, values reported in this study. The sample period for all calculations is 0.001 seconds for a time array of 0.0-0.3 seconds. The filtering calculations also use a specific Channel Frequency Class (CFC) dependent on the test measurement (Table 7). Examples of the filter formulas in each cell of the workbook are shown in Appendix E.

Table 7

Channel Frequency Classes

Test Measurement	Channel Frequency Class (CFC)
ATD, Head Accelerations	1000
ATD, Spine Accelerations	180
Sled Acceleration	60

The Butterworth digital filter used in this study first passed the data, from time steps 0.0 to 0.3 seconds, through the following equation and through the equation a second time in reverse, from time steps 0.3 to 0.0 seconds, to eliminate any phase shift in the filtered data (SAE, 1995). Equation 3 shown below is the Butterworth digital filter difference equation:

$$\boldsymbol{y(t) = a_0x(t) + a_1x(t-1T) + b_1y(t-1T) + b_2y(t-2T)} \tag{3}$$

where,

$\boldsymbol{y(t)}$ = filtered data in the time domain;

$\boldsymbol{x(t)}$ = raw data in the time domain;

$\boldsymbol{t}$ = time in seconds;

$\boldsymbol{T}$ = sample period in seconds;

$(\boldsymbol{t-1T})$ = time at one less sample period in seconds;

$(\boldsymbol{t-2T})$ = time at one less sample period in seconds;

$\boldsymbol{a_0, a_1, a_2, b_1, b_2} =$ equation constants that are dependent on the specific test measurement CFC.

The constants in Equation 3 are determined using the subsequent equations (SAE, 1995):

$$\boldsymbol{w_d = 2\pi \cdot \mathrm{CFC} \cdot 2.0775} \tag{4}$$

$$\boldsymbol{w_a = \frac{\sin\left(w_d \cdot \frac{T}{2}\right)}{\cos\left(w_d \cdot \frac{T}{2}\right)}} \tag{5}$$

$$\boldsymbol{a_0 = \frac{w_a{}^2}{1 + \sqrt{2}w_a + w_a{}^2}} \tag{6}$$

$$a_1 = 2a_0 \tag{7}$$

$$a_2 = a_0 \tag{8}$$

$$b_1 = \frac{-2({w_a}^2 - 1)}{1 + \sqrt{2}w_a + {w_a}^2} \tag{9}$$

$$b_2 = \frac{-1 + \sqrt{2}w_a - {w_a}^2}{1 + \sqrt{2}w_a + {w_a}^2} \tag{10}$$

The “run-analyze-refine” iterative method was employed to optimize the simulation model for alignment with the performance metrics obtained from physical testing. For Model A, a total of 46 model iterations were developed, with version history summarized in Table D1 shown in Appendix D. Ultimately, WM Trial A, Version 46 (Figure 46), was identified as the configuration that most accurately replicated the results of physical sled Test Trial A.

Figure 46

WM Trial A, version 46

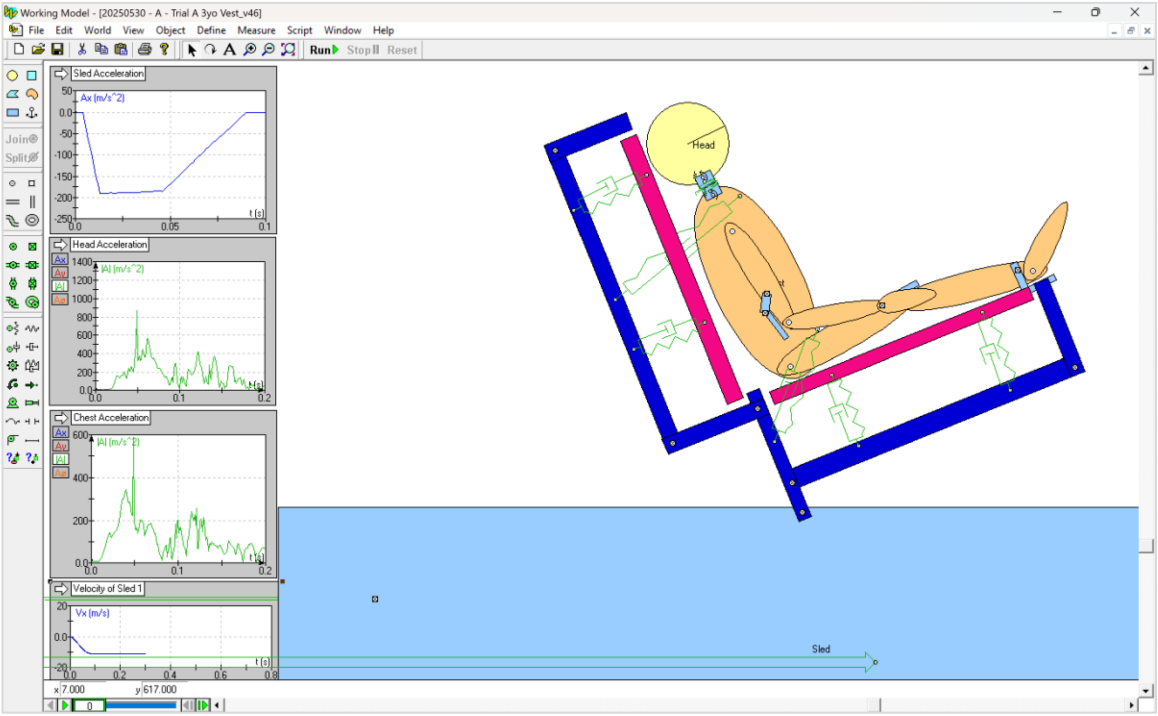

For Model B, a total of 56 model iterations were developed, with version history summarized in Table D2 shown in Appendix D. Ultimately, WM Trial B, Version 56 (Figure 47), was identified as the configuration that most accurately replicated the results of physical sled Test Trial B.

Figure 47

WM Trial B, version 56

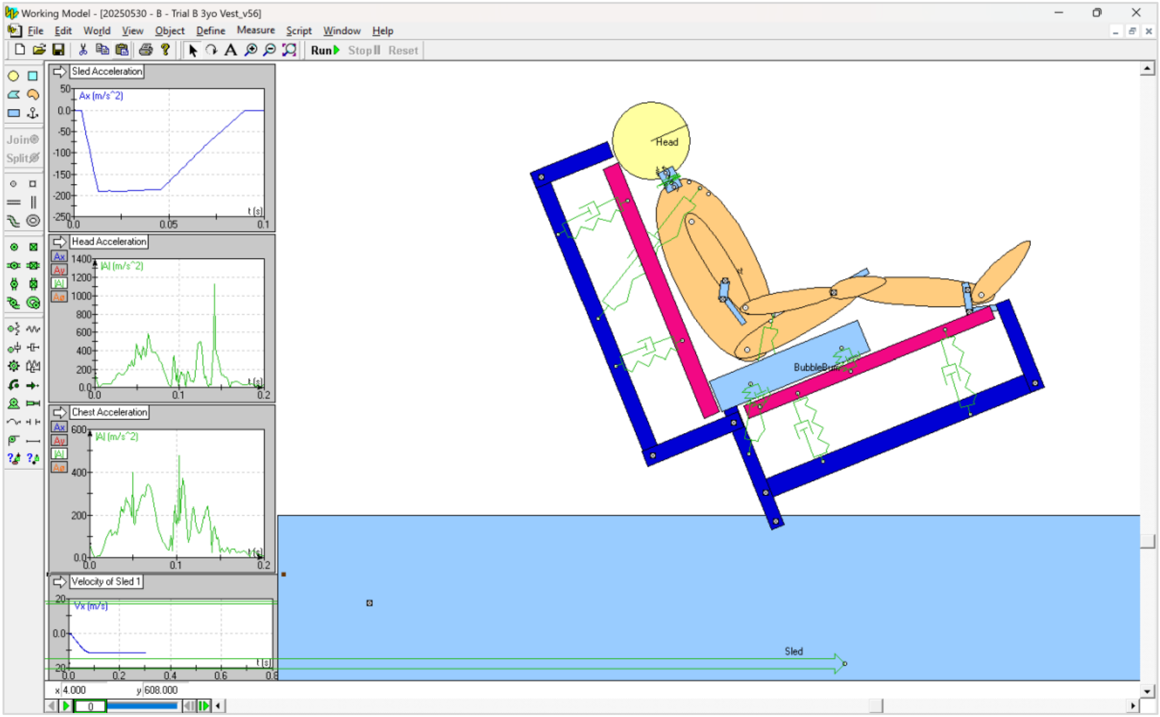

For Model CD, a total of 30 model iterations were developed, with version history summarized in Table D3 shown in Appendix D. Since Sled Test D was a repeated of Sled Test C for confirmation of results, only one model was created to simulate the results representative of both sled tests. Ultimately, WM Trial CD, Version 30 (Figure 48), was identified as the configuration that most accurately replicated the averaged results of physical sled Test Trials C and D.

Figure 48

WM Trial C/D, version 30

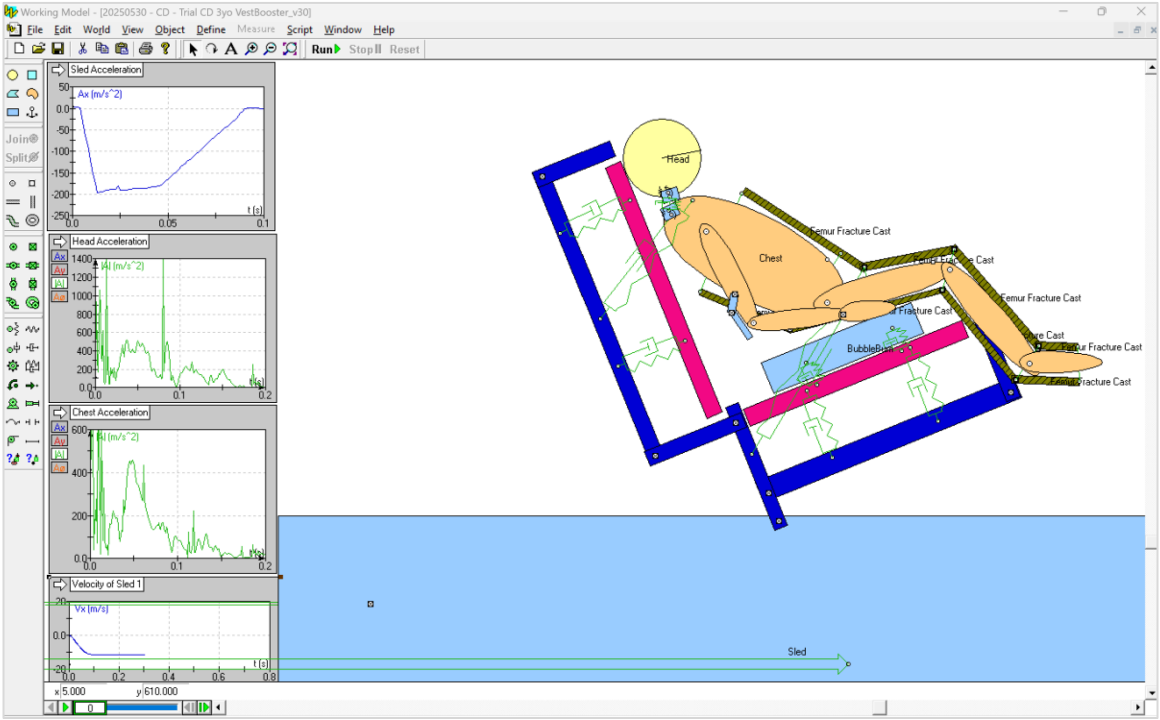

Since the DDH cast was not tested in Section 1.4, a simulation model was created to predict the injury criterion values of this cast type. The DDH model was based off of Model B, version 47, and the ATD was manipulated to the correct hip and knee angles for a DDH casting scenario. The length of the femur and foot objects had to be reduced, while keeping the mass constant, to reflect an accurate side view of the ATD with increased hip abduction. Once the ATD was in position, the DDH cast constraining object was added to the model. For a complete list of all 13 model iterations developed, refer to Table D4 in Appendix D. Ultimately, WM Trial DDH, Version 13 (Figure 49), was identified as the representative configuration for a 3-year-old ATD in a DDH cast.

Figure 49

WM DDH Cast, version 13

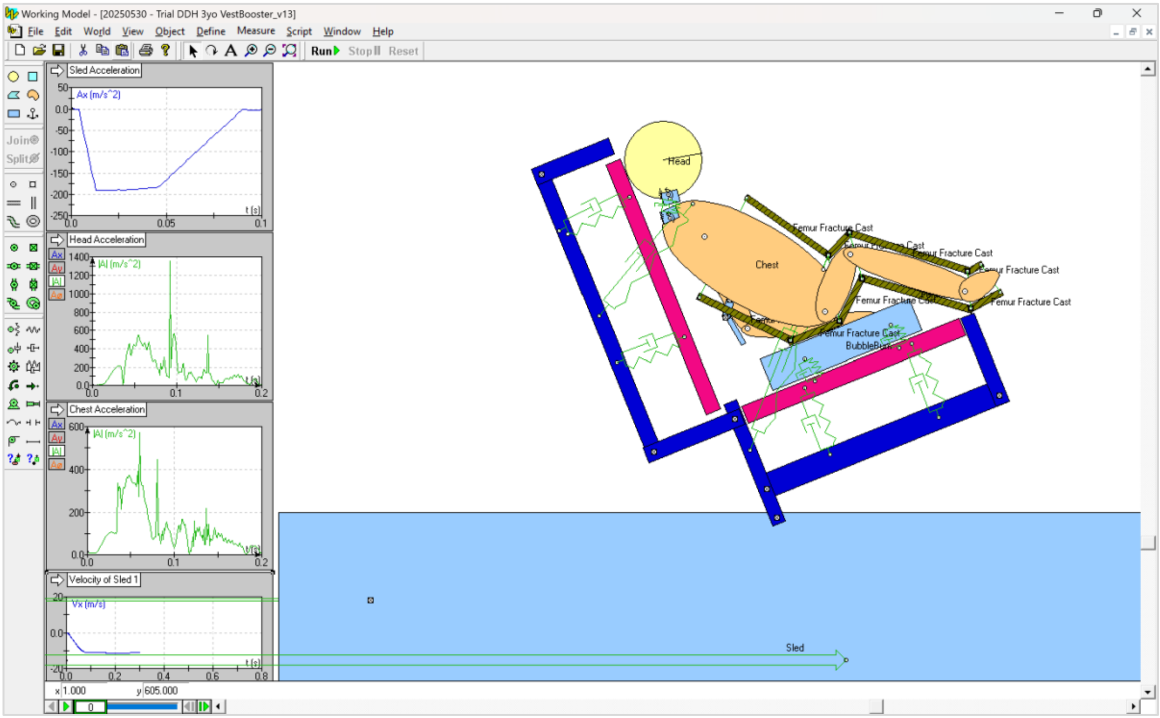

1.6.2 Simulation Results

Injury values for each model were calculated using the method presented in Section 1.6.1 and are reported in Table 8. Excursion data metrics were excluded from this analysis due to all testing trials satisfying the excursion criteria during physical testing in Section 1.4. Subsequently, excursion performance was not further investigated within the scope of the simulation analysis. Included in the forthcoming summary of results is a comparison to the injury values found for each corresponding sled test scenario and the percent error between the theoretical (simulation) and actual (sled test) values.

Table 8

Working Model Simulation Results

Trial	Injury Criterion	Simulation	Sled Test	Percent Error
A	Chest Accel (g)	31.67	35.22	11.2%
	HIC36	302.2	289	4.4%
B	Chest Accel (g)	35.00	31.50	10%
	HIC36	320.8	312	2.7%
C/D	Chest Accel (g)	49.96	46.35	7.2%
	HIC36	427.9	421	1.6%
DDH Cast	Chest Accel (g)	37.71	—	—
	HIC36	382.6	—	—

Note. Sled Test Injury Criterion values shown for Trial C/D are the average of the actual values from Trial C and Trial D. DDH Cast was not sled tested.

In a previously published study that validated simulation models against physical crash testing (Wang et al., 2022), percent errors below 15% were considered acceptable to confirm both the model validity and the effectiveness of the optimization methods used to create the models. Consistent with these guidelines, the four models developed in this study to represent a spica-casted 3-year-old ATD all exhibited percent error values below 15%, thereby confirming the simulation results' reliability and accuracy.

1.6.3 Simulation Discussion

While simulation models are not exact replicas of physical testing, they serve as valuable tools for predicting unknown outcomes with increased time efficiency and reduced cost. In this study, simulation analyses were conducted in Working Model 2D modeling software for the previously sled tested scenarios. The resulting model that was developed was utilized to predict injury criteria for an additional casting type, the 3-year-old in the DDH Cast. Figure 50 presents a comparison of all sled acceleration profiles over time, for both the physical tests and the models, illustrating the consistent repeatability of the model parameters applied across all tested configurations.

Figure 50

Sled Acceleration Over Time Comparison

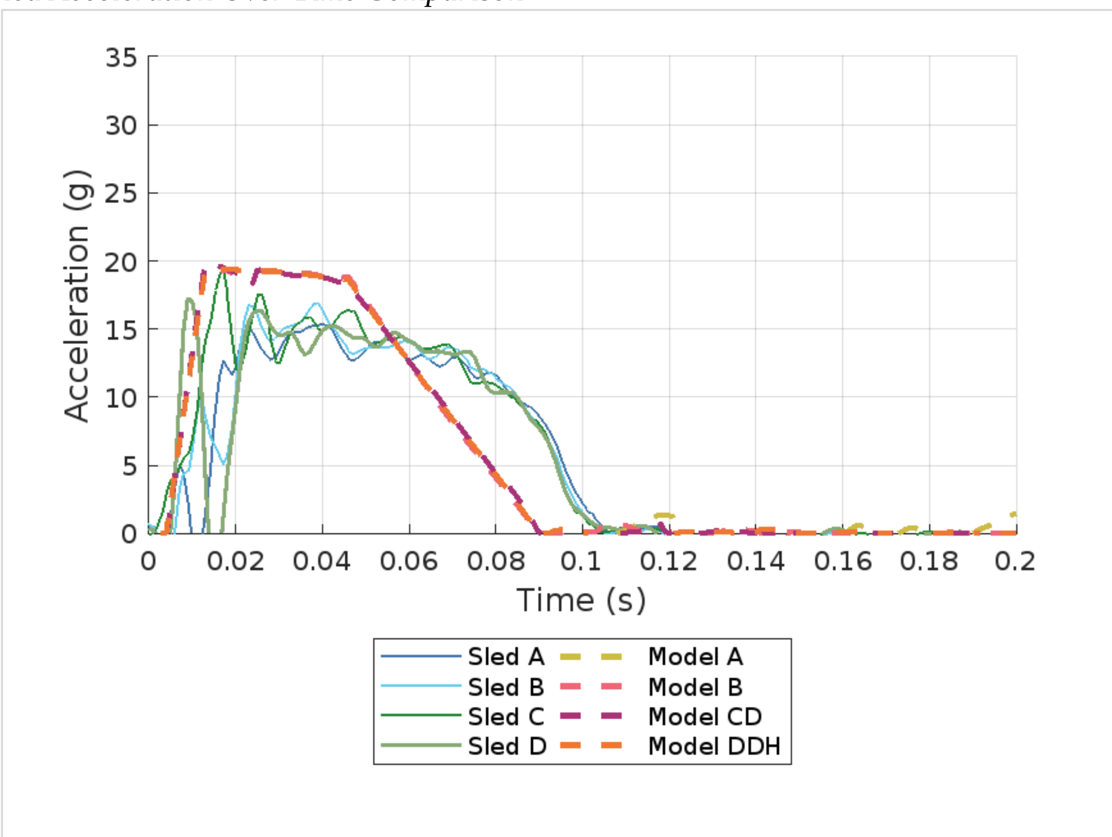

For Model A, chest acceleration as a function of time was compared to the corresponding data from Sled Trial A (Figures 51 and 52). While the two overall acceleration profiles exhibited similar shapes, the model's response was quicker by approximately 10 ms, indicating that the model replicated the dynamic behavior of the physical test but with a faster onset. Likewise, the Head Acceleration profiles and side-view images (Figures 53 and 54) confirm a faster yet similar response with the model. The percent errors for the Chest Acceleration, 3 ms clip, was calculated to be 11.2%, and the HIC36 was at 4.4%, which both fall within an acceptable range for model validation.

Figure 51

Chest Acceleration Profiles for Sled A and Model A

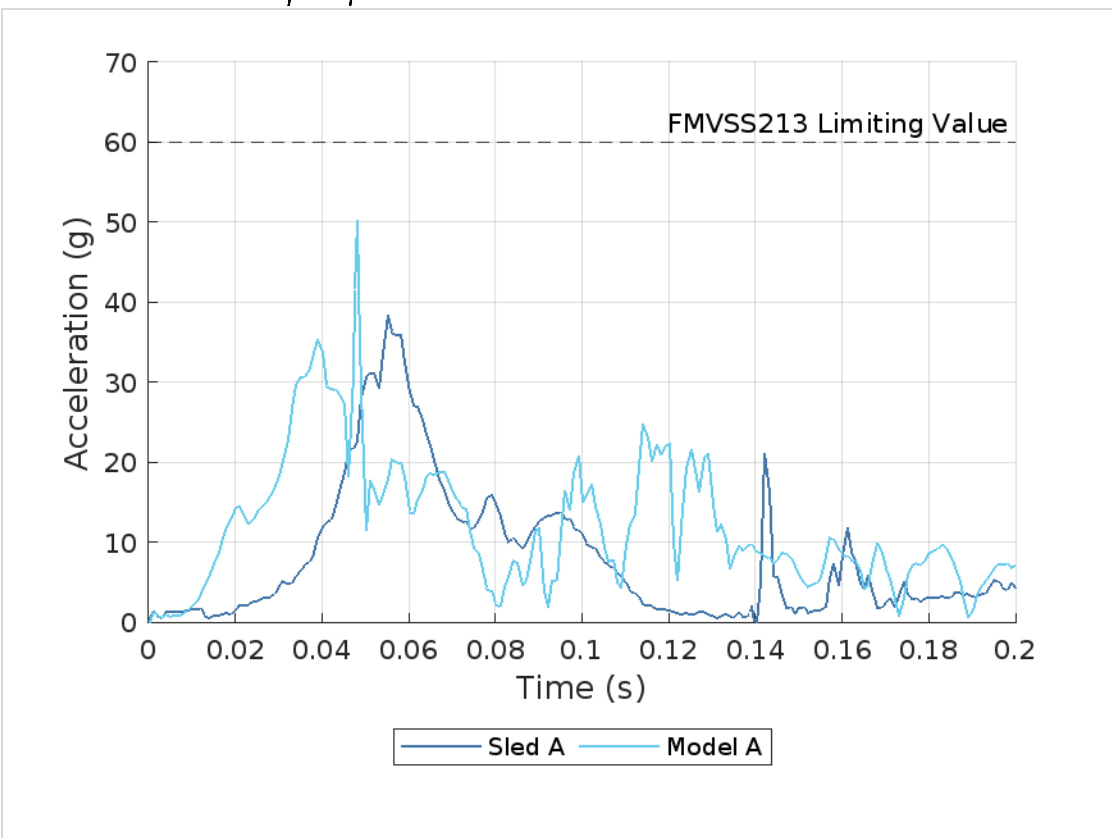

Note. Sled A Peak Chest Acceleration at time = 0.056 seconds. Model A Peak Chest Acceleration at time = 0.049 seconds.

Figure 52

Chest Acceleration Peaks for Sled A and Model A

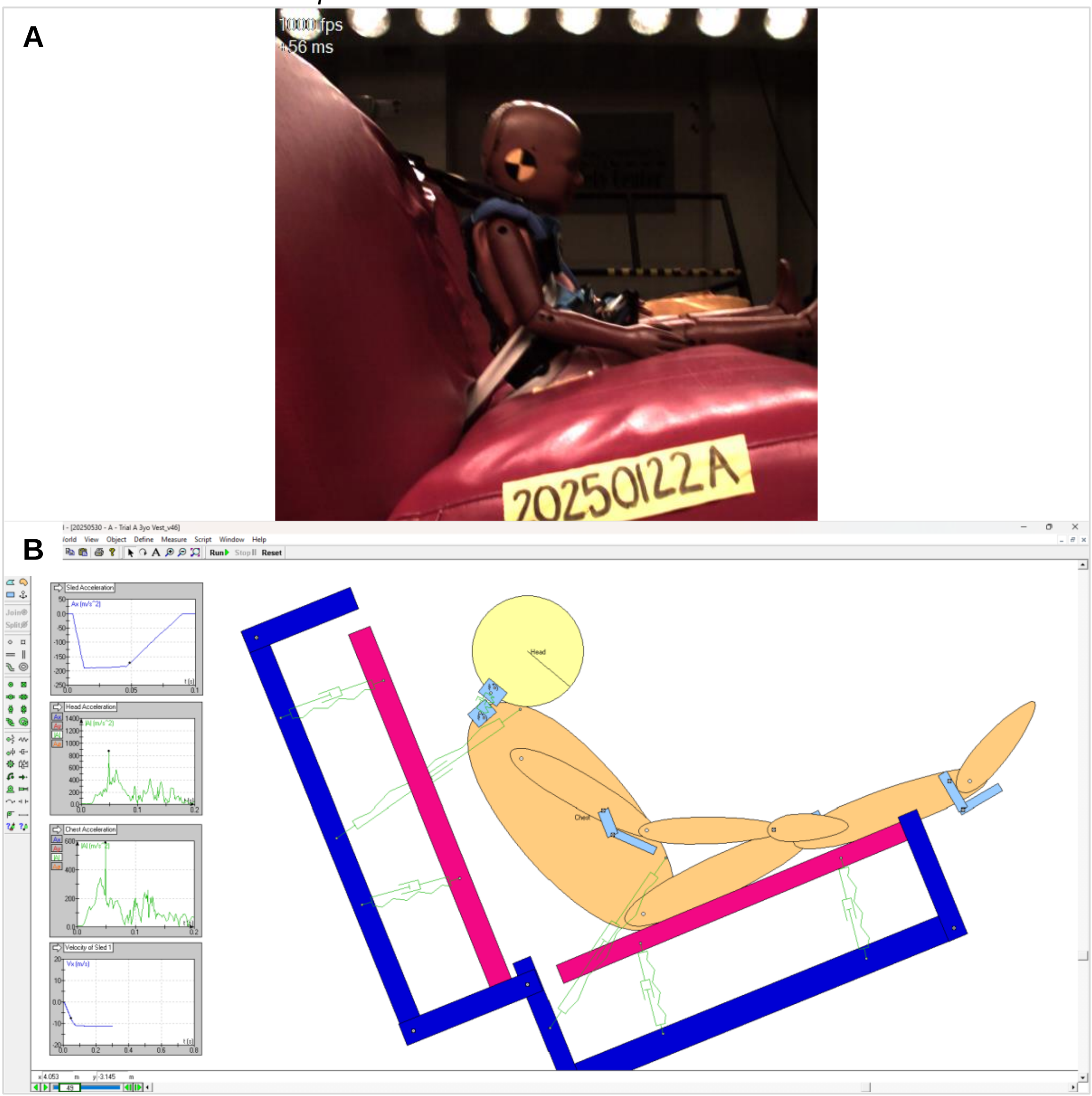

Note. (A) Sled Trial A at 0.056 seconds. (B) Model A at 0.049 seconds.

Figure 53

Head Acceleration Profiles for Sled A and Model A

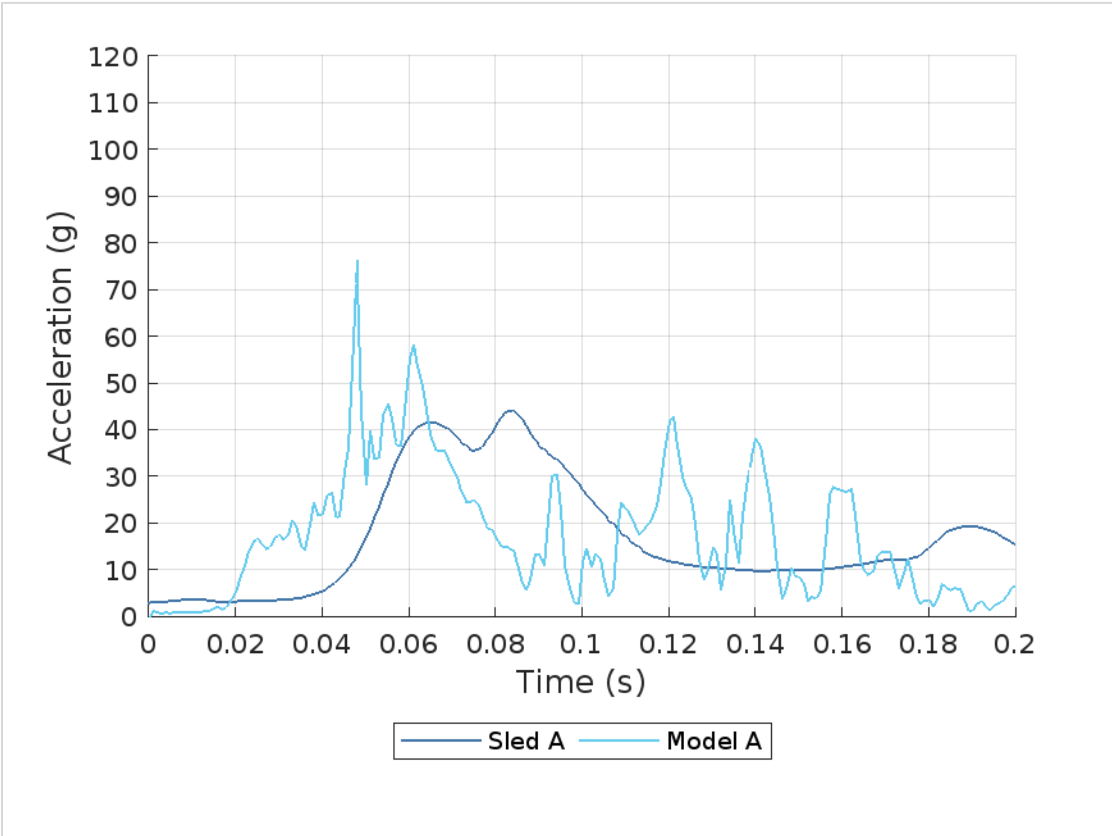

Note. Sled A Peak Head Acceleration at time = 0.083 seconds. Model A Peak Head Acceleration at time = 0.062 seconds.

Figure 54

Head Acceleration Peaks for Sled A and Model A

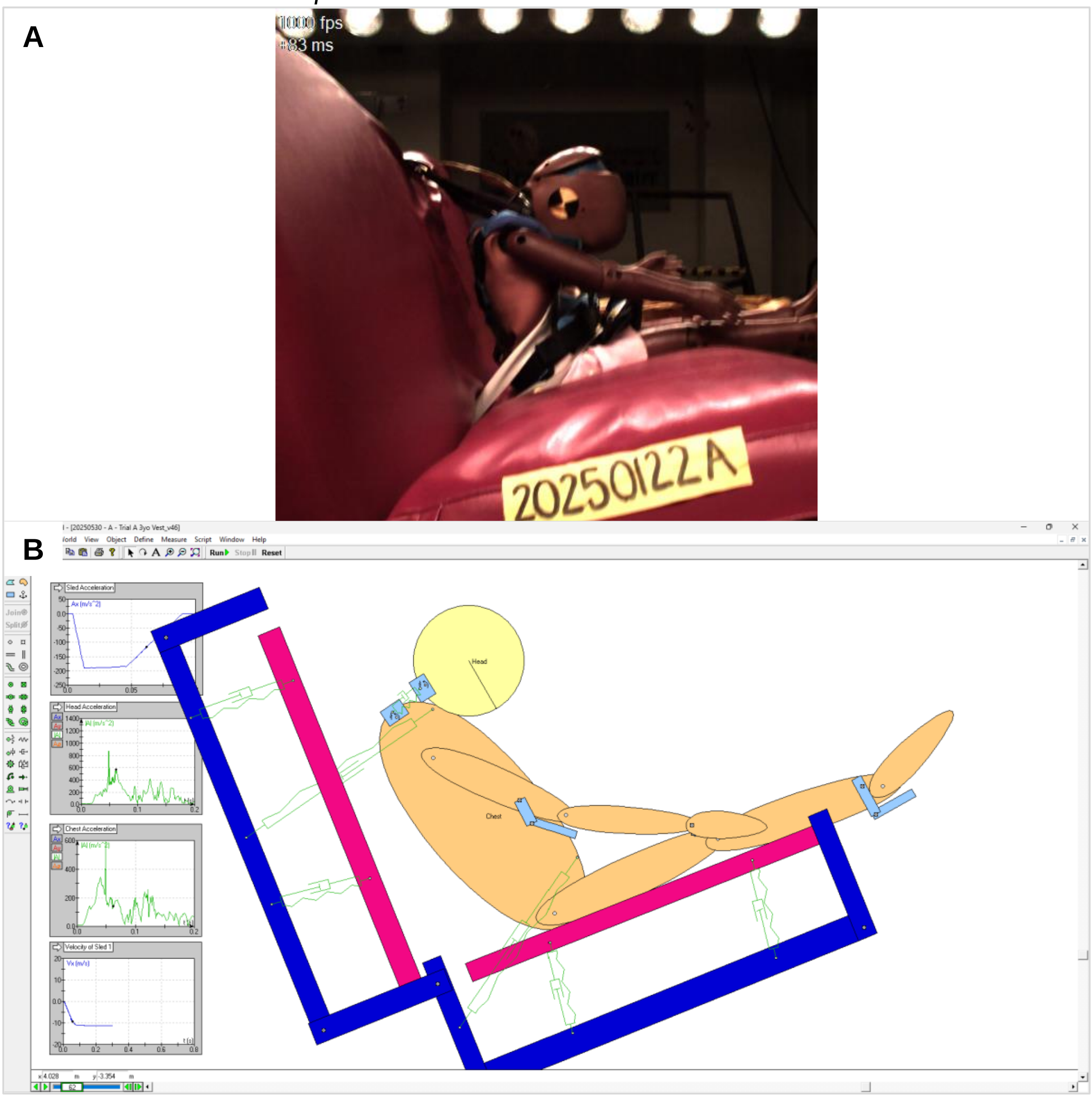

Note. (A) Sled Trial A at 0.083 seconds. (B) Model A at 0.062 seconds.

The chest acceleration over time for Model B was compared to the corresponding data from Sled Trial B (Figures 55 and 56). The acceleration profiles demonstrated similar overall shapes, indicating that the model effectively replicated the dynamic behavior of the physical test but with an earlier rise time. Similarly, the head acceleration profiles and supporting side-view images (Figures 57 and 58) confirmed a comparable response with the model exhibiting a slightly faster response. The percent error for the Chest Acceleration, 3 ms clip, was calculated at 10%, while the HIC36 error was 2.7%; both values fall within acceptable thresholds for model validation.

Figure 55

Chest Acceleration Profiles for Sled B and Model B

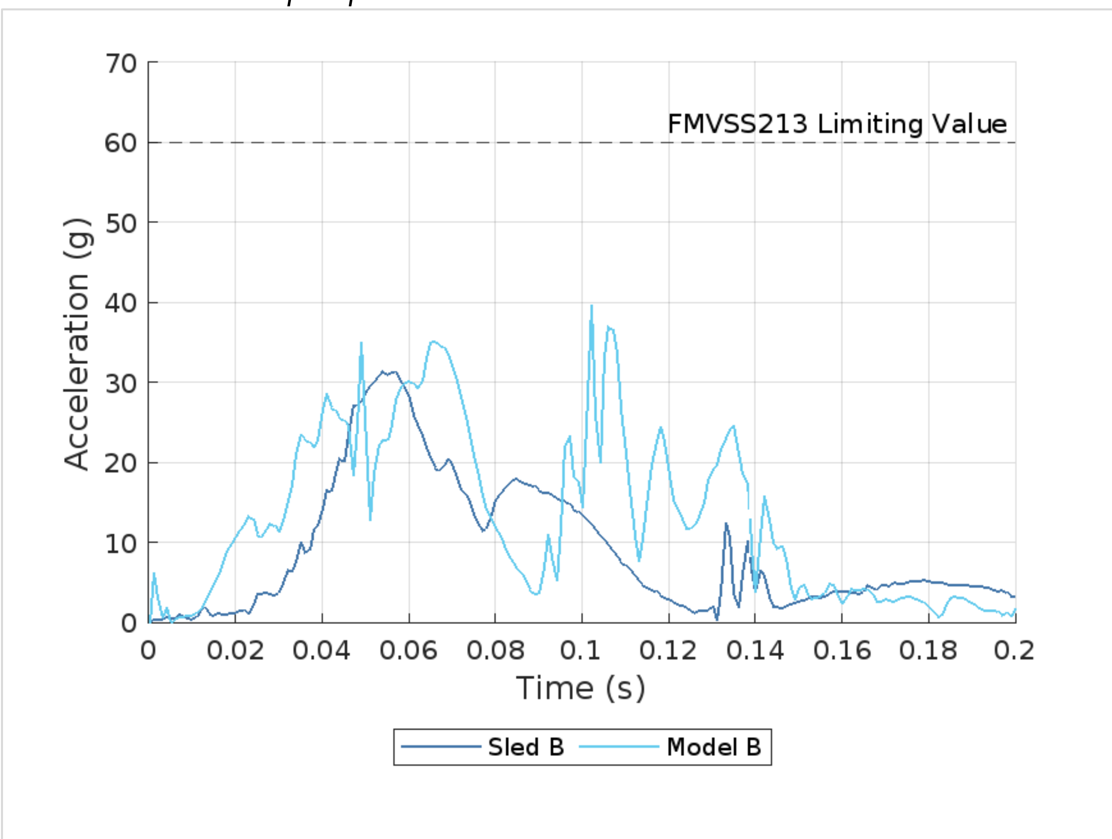

Note. Sled B Peak Chest Acceleration at time = 0.056 seconds. Model B Peak Chest Acceleration at time = 0.063 seconds.

Figure 56

Chest Acceleration Peaks for Sled B and Model B

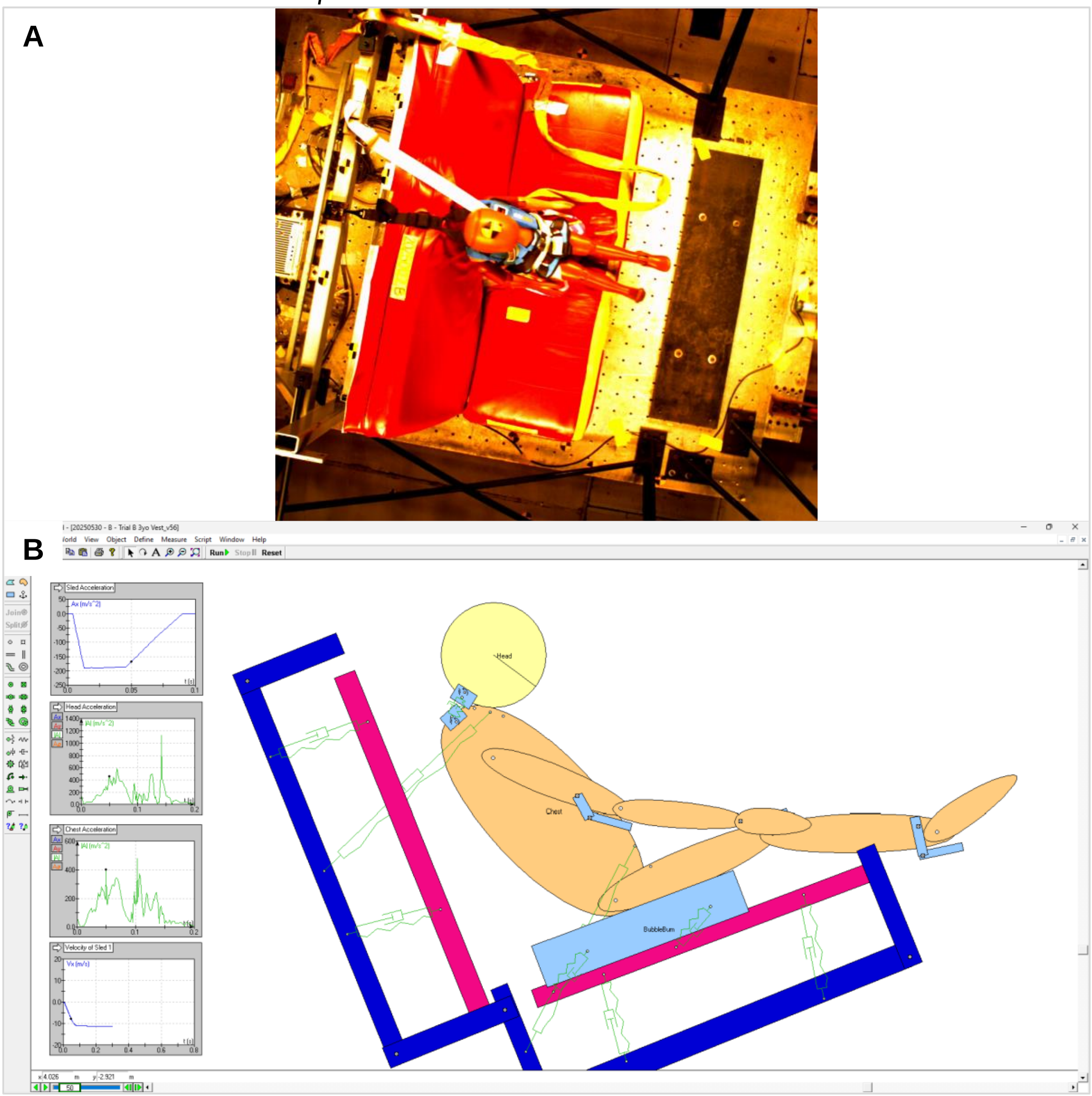

Note. (A) Sled Trial B at 0.056 seconds. (B) Model B at 0.063 seconds.

Figure 57

Head Acceleration Profiles for Sled B and Model B

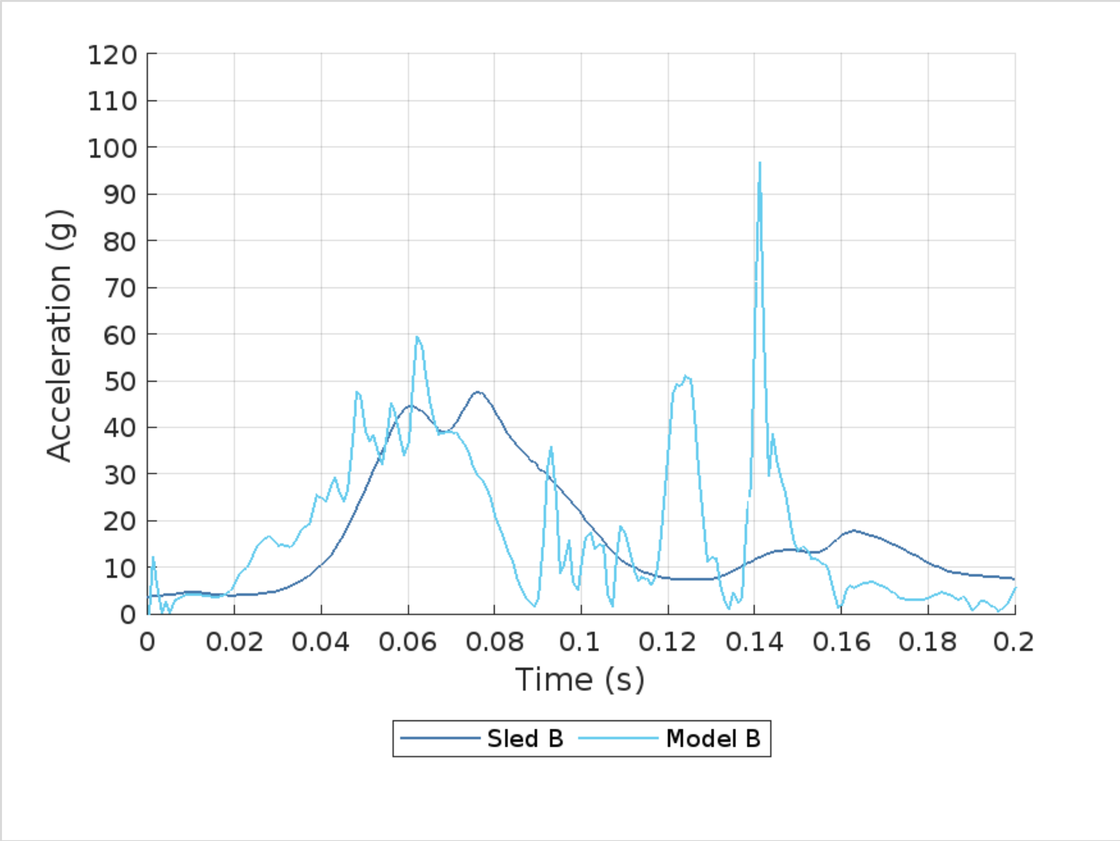

Note. Sled B Peak Head Acceleration at time = 0.076 seconds. Model B Peak Head Acceleration at time = 0.063 seconds. Model B maximum peak at 0.142 seconds is due to head collision with seat back which yielded artificially elevated acceleration values not observed in the corresponding physical testing, Trial B.

Figure 58

Head Acceleration Peaks for Sled B and Model B

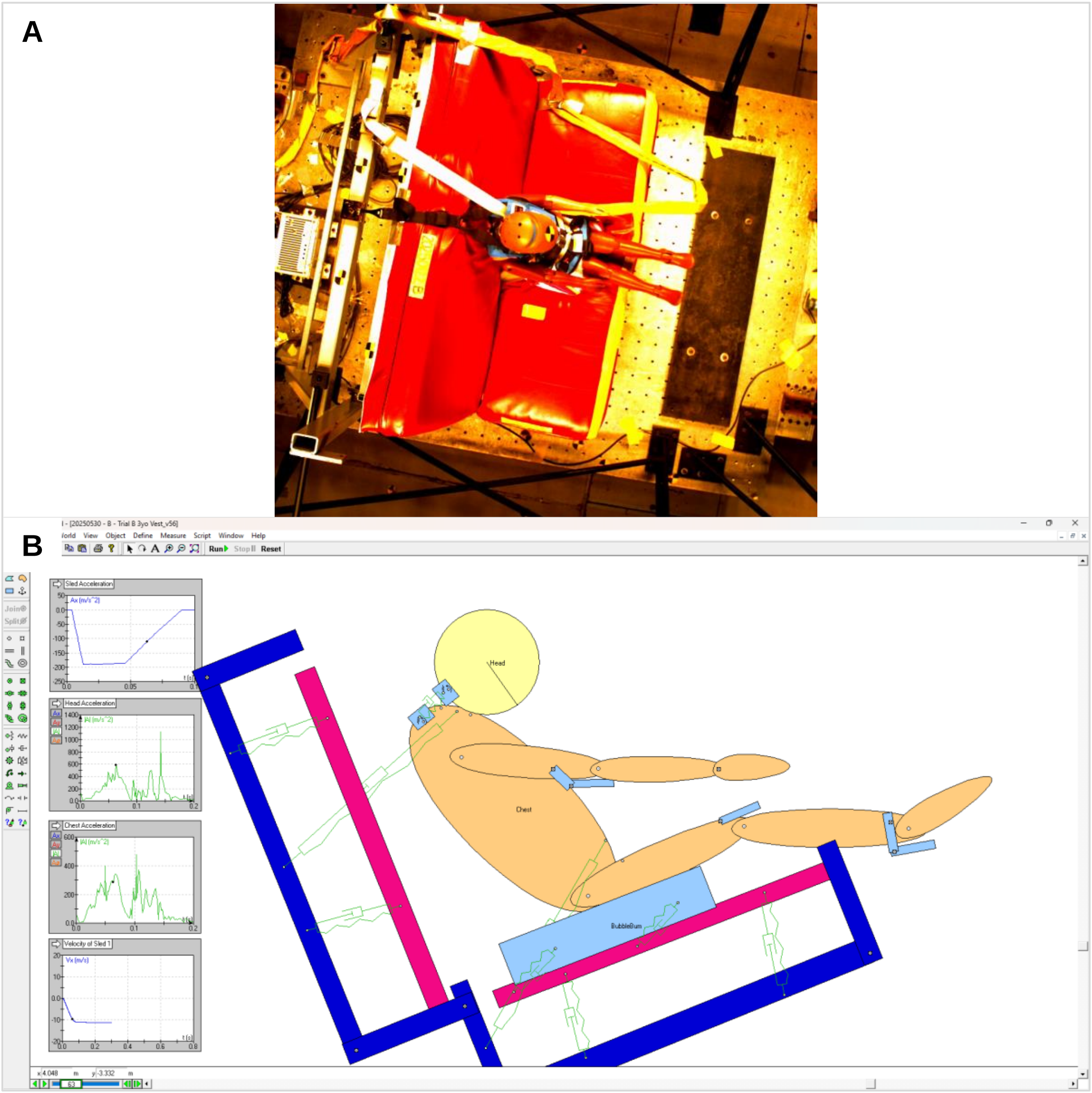

Note. (A) Sled Trial B at 0.076 seconds. (B) Model B at 0.063 seconds.

Consistent with the previously validated models, chest acceleration over time for Model CD was compared to the corresponding data from Sled Trials C and D (Figures 59 and 60). The acceleration profiles exhibited similar overall shapes, indicating that the model accurately captured the dynamic response of the physical tests, with an onset approximately 10 ms earlier. The percent error for the Chest Acceleration, 3 ms clip, was calculated within acceptable thresholds for model validation at 7.2%.

Figure 59

Chest Acceleration Profiles for Sled C, Sled D, and Model CD

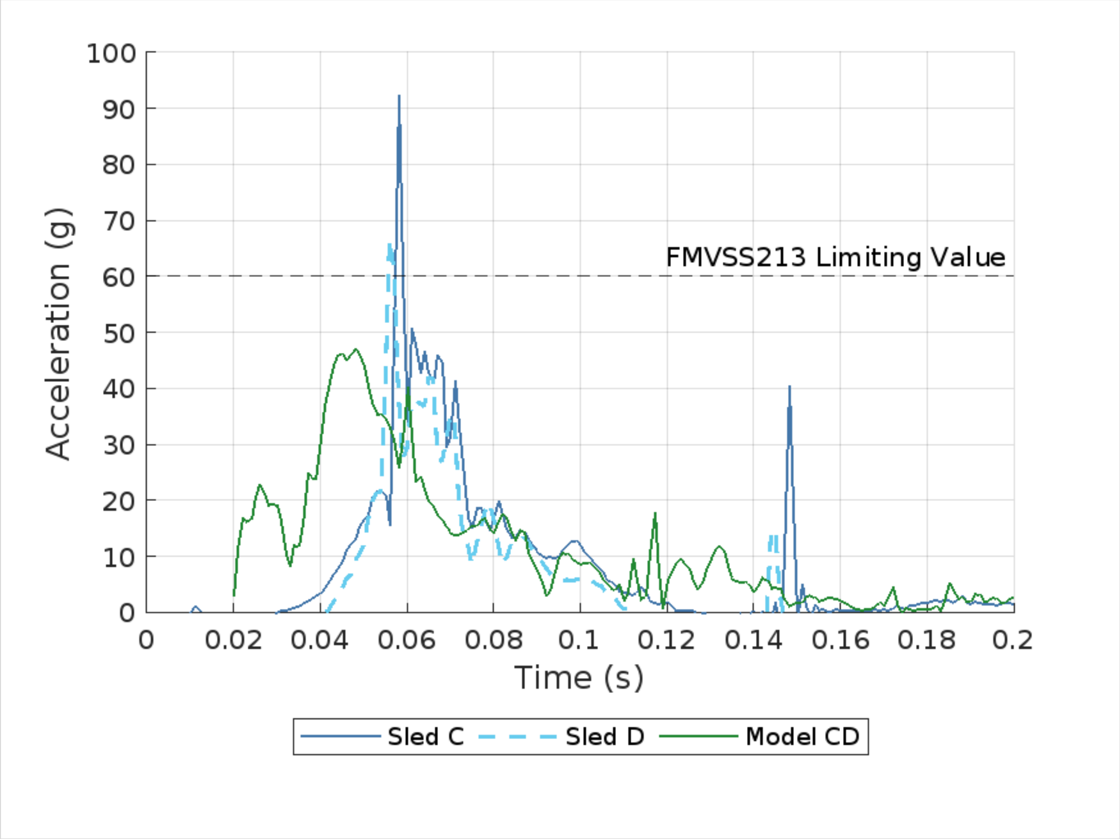

Note. Sled C Peak Chest Acceleration at time = 0.058 seconds. Sled D Peak Chest Acceleration at time = 0.057 seconds. Model CD Peak Chest Acceleration at time = 0.049 seconds. Model CD data was trimmed at times <0.02 seconds to exclude initial ATD position settling which yielded artificially elevated acceleration values not observed in the corresponding physical testing, Trials C & D.

Figure 60

Chest Acceleration Peaks for Sled C, Sled D, and Model CD

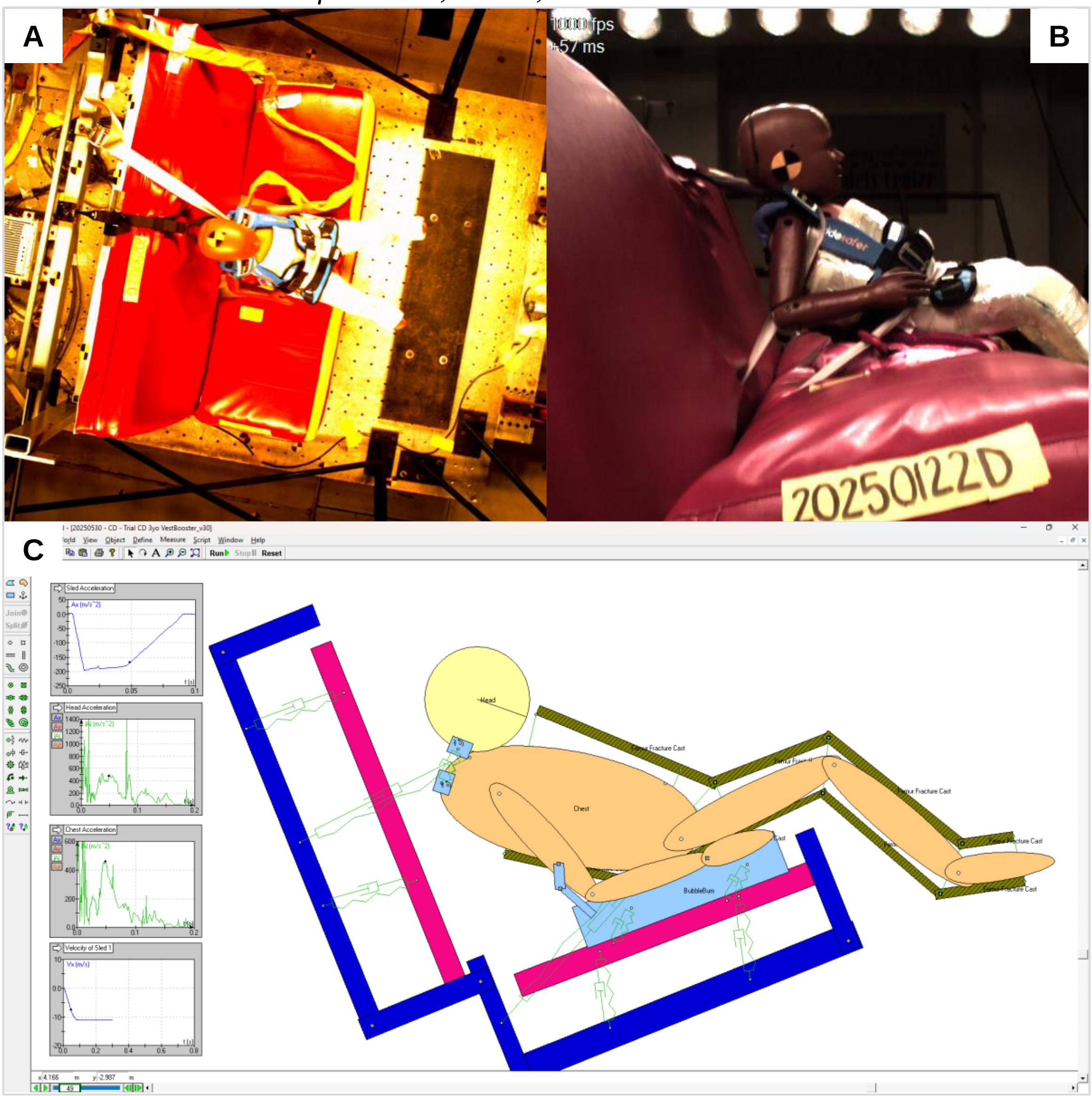

Note. (A) Sled Trial C at 0.058 seconds. (B) Sled Trial D at 0.057 seconds. (C) Model CD at 0.049 seconds.

Notably, the model accurately predicted that the ATD head would contact the anterio-superior edge of the cast, resulting in an instant peak in head acceleration, consistent with observations from Sled Trials C and D. This finding aligns with observations by Oliver et al. (2009), who reported that, during sled testing of a forward-facing 3-year-old configuration, facial impact with the anterior edge of the casted torso contributed to elevated HIC and Nij values. The head acceleration profiles and corresponding side-view images (Figures 61 and 62) demonstrated a comparable response, with the model exhibiting an earlier onset relative to the physical tests. Despite this time shift, the calculated HIC36 percent error was only 1.6%, further supporting the model's validity in replicating the physical test conditions.

Figure 61

Head Acceleration Profiles for Sled C, Sled D, and Model CD

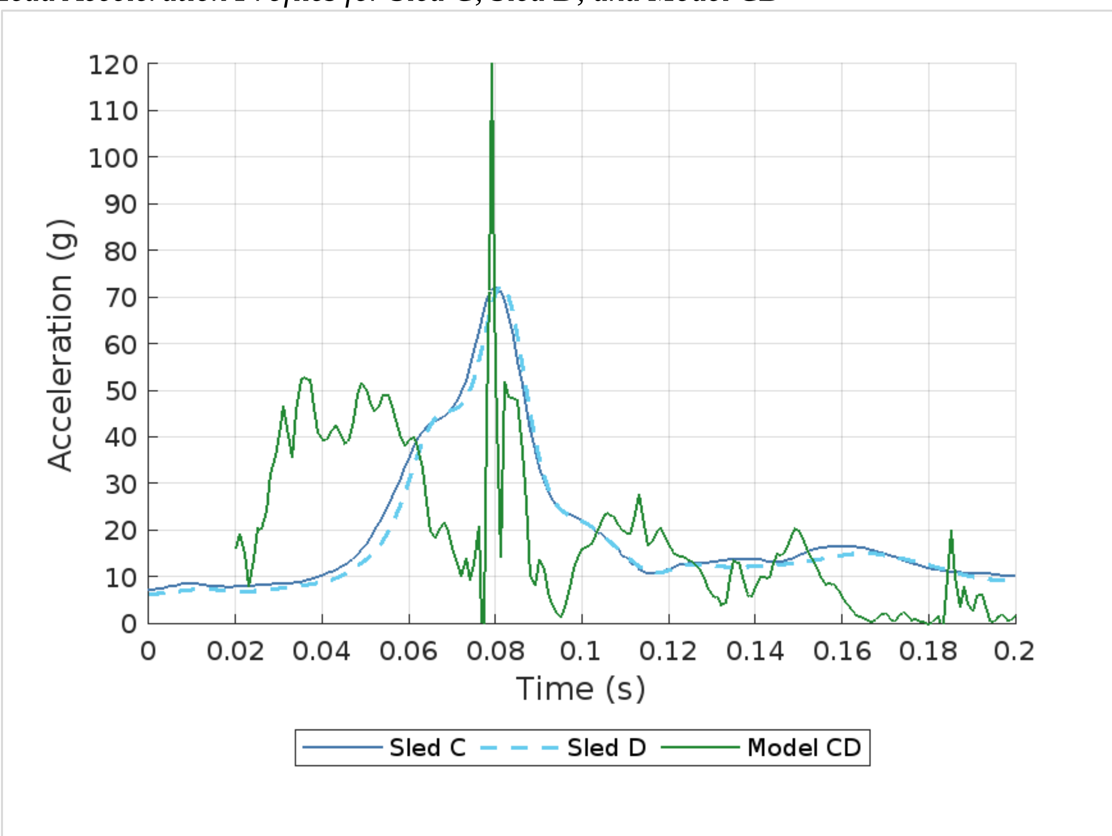

Note. Sled C Peak Head Acceleration at time = 0.080 seconds. Sled D Peak Head Acceleration at time = 0.081 seconds. Model CD Peak Head Acceleration due to head-cast collision at 0.057 seconds. Model CD maximum peak at 0.080 seconds is due to head collision with seat back which yielded artificially elevated acceleration values not observed in physical testing, Trial C & D. Model CD data was trimmed at times <0.02 seconds to exclude initial ATD position settling which yielded artificially elevated acceleration values not observed in the corresponding physical testing, Trials C & D.

Figure 62

Head Impacts with Anterior Edge of Cast for Sled C, Sled D, and Model CD

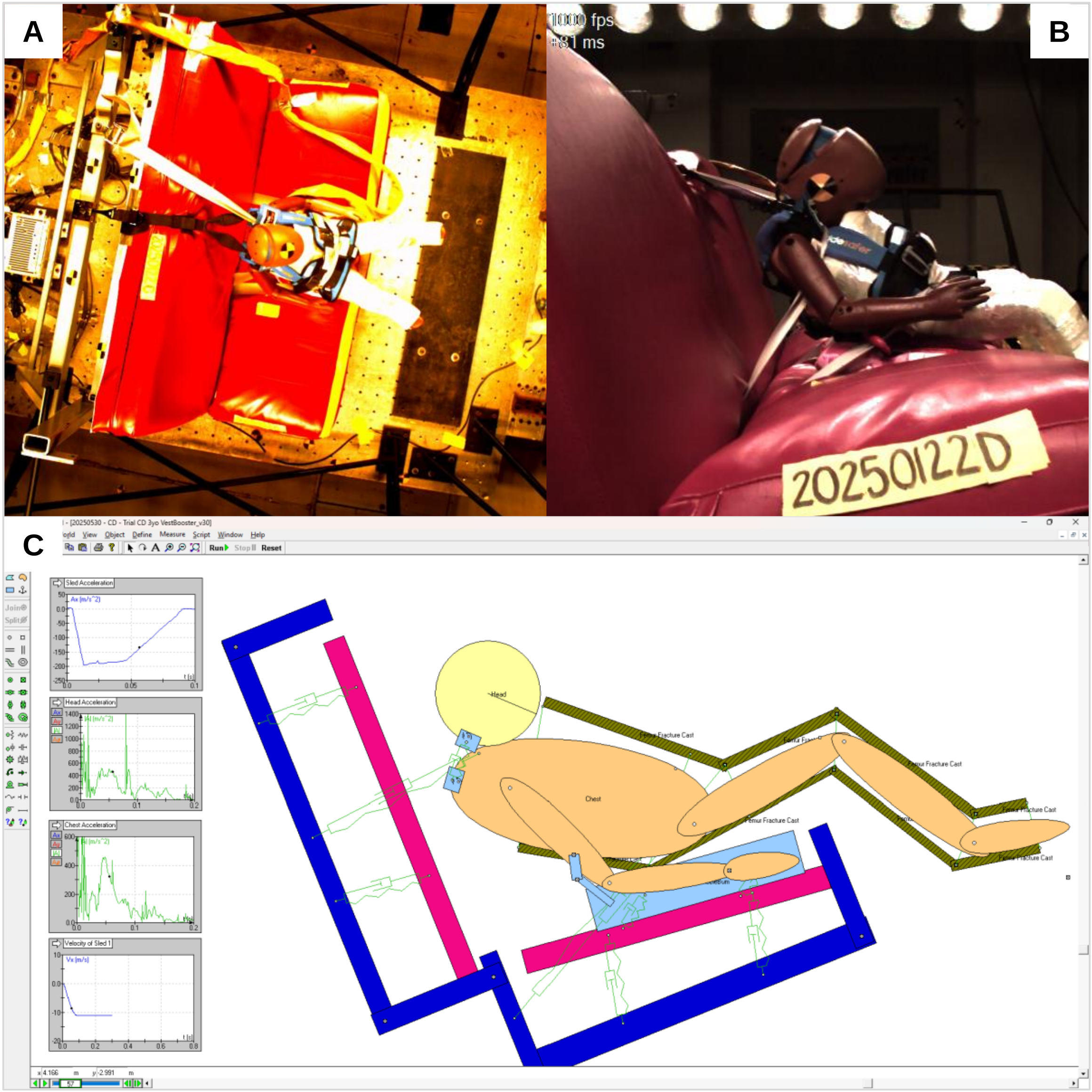

Note. (A) Sled Trial C with head-cast collision at 0.080 seconds. (B) Sled Trial D with head-cast collision at 0.081 seconds. (C) Model CD at 0.057 seconds when head impacts cast.

Building upon the validated Model CD, a new simulation, Model DDH, was developed to predict injury metrics for a 3-year-old ATD in a DDH cast configuration. The chest and head acceleration profiles generated by Model DDH closely aligned with those from the previously validated models, as illustrated in Figures 63 and 64. This consistency supports confidence in Model DDH's ability to produce accurate injury predictions under comparable test conditions.

Figure 63

Chest Acceleration Profiles for All Models

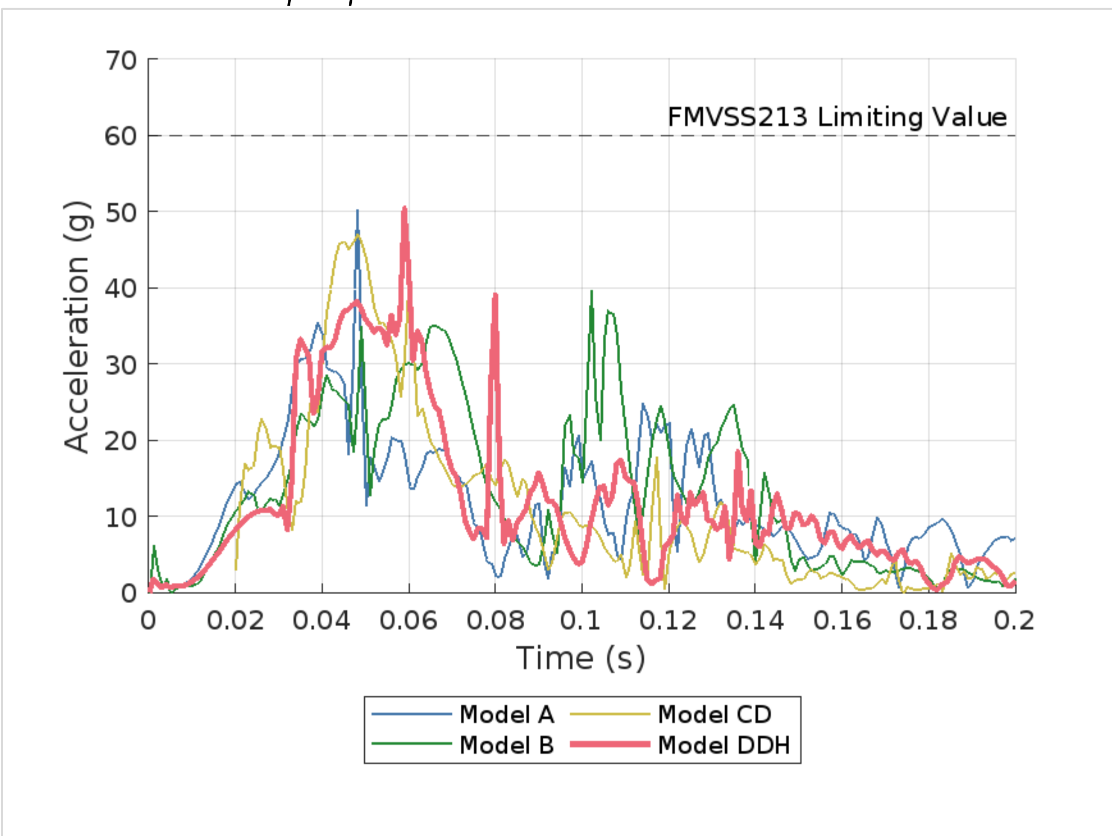

Note. Model CD data was trimmed at times <0.02 seconds to exclude initial ATD position settling which yielded artificially elevated acceleration values not observed in the corresponding physical testing, Trials C & D.

Figure 64

Head Acceleration Profiles for All Models

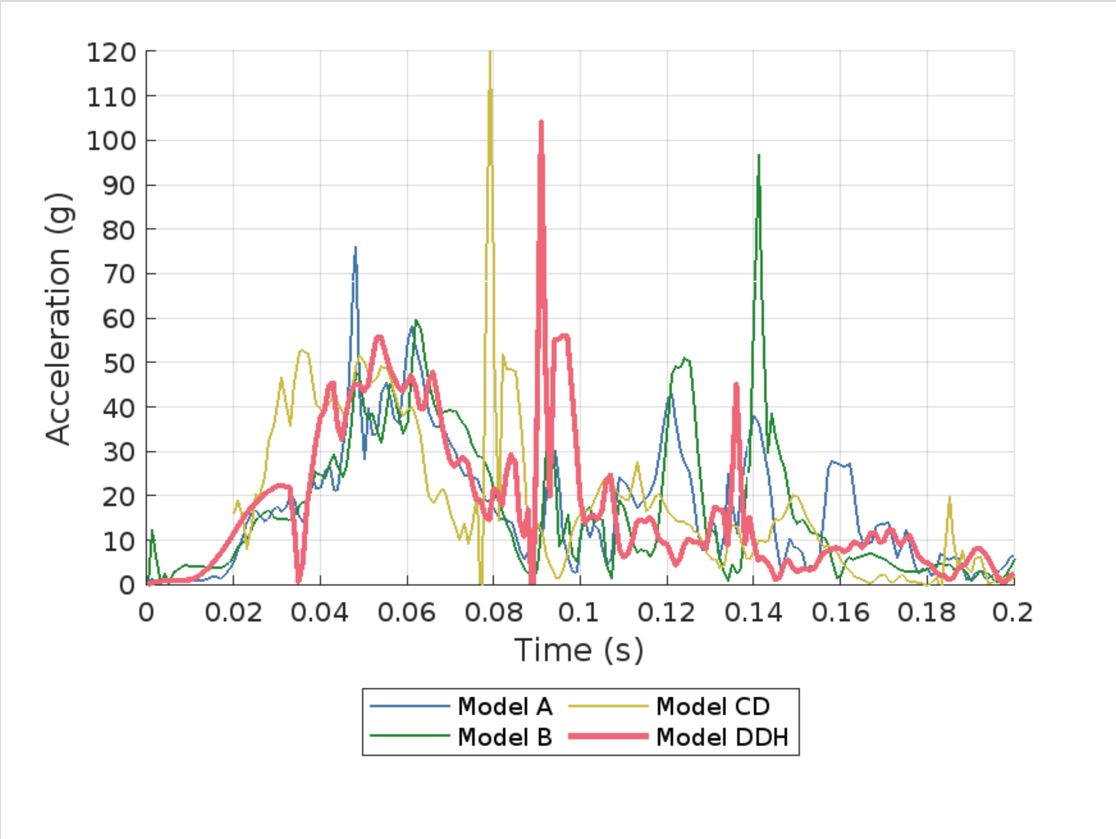

Note. Model B peak at 0.142 seconds is due to head collision with seat back which yielded artificially elevated acceleration values not observed in the corresponding physical testing, Trial B. Model CD peak at 0.080 seconds is due to head collision with seat back which yielded artificially elevated acceleration values not observed in the corresponding physical testing, Trial C & D. Model DDH peak at 0.092 seconds is due to head collision with seat back which yielded artificially elevated acceleration values not observed in similar physical testing. Model CD data was trimmed at times <0.02 seconds to exclude initial ATD position settling which yielded artificially elevated acceleration values not observed in the corresponding physical testing, Trials C & D.

Simulation analysis predicts that the peak chest acceleration for Model DDH occurs at 0.060 seconds, with a calculated Chest Acceleration, 3 ms clip, value of 37.71 g. This result is 37% below the FMVSS No. 213 limit, as illustrated in Figure 65.

Figure 65

Chest Acceleration Peak for Model DDH

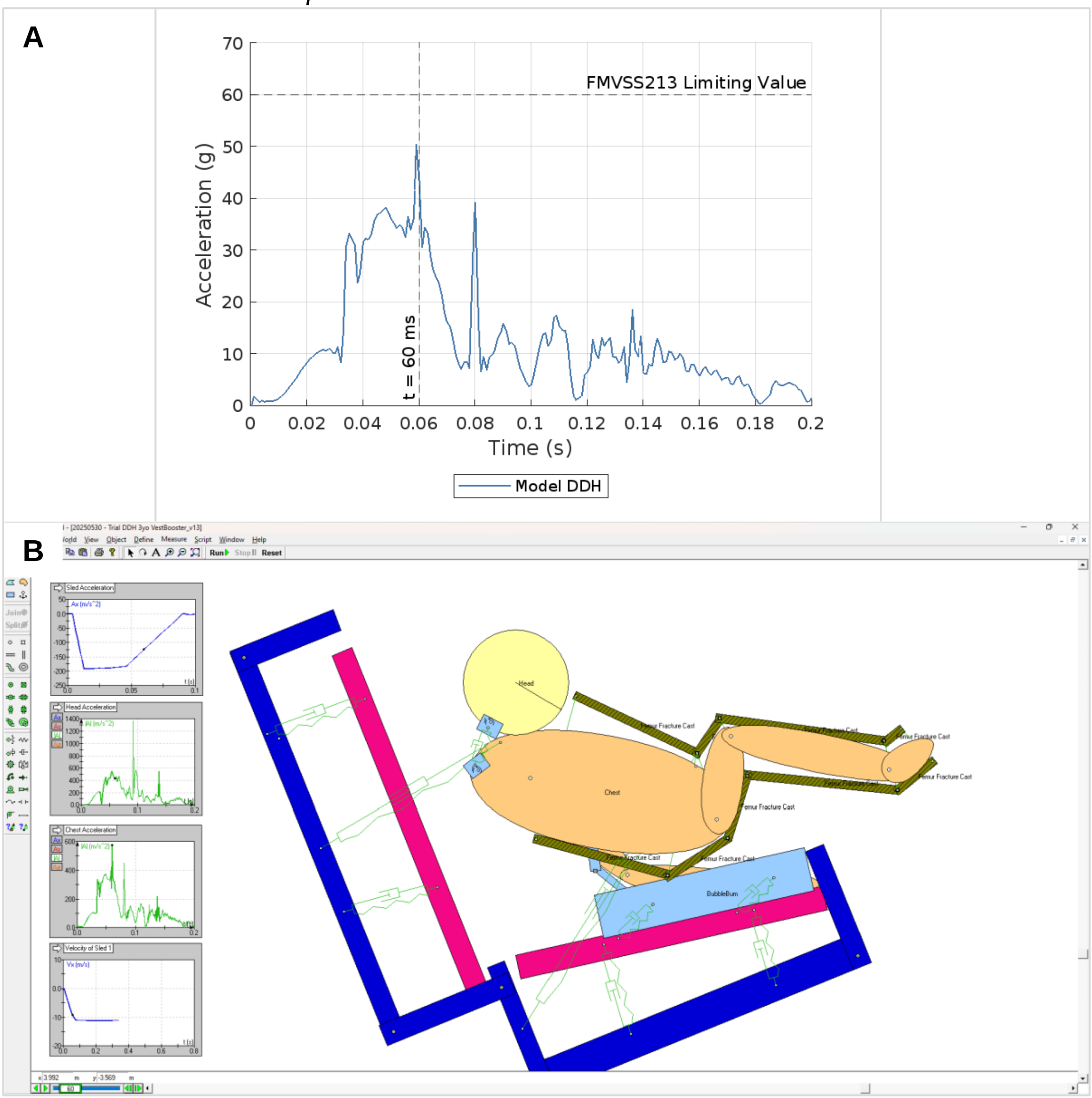

Note. (A) Chest Acceleration profile for Model DDH with peak value at 0.060 seconds. (B) Model DDH at 0.060 seconds.

Consistent with the behavior observed in Model CD, Model DDH also predicted head contact with the cast at 0.067 seconds, as shown in Figure 66. The calculated HIC36 value for Model DDH was 382.6, which is 62% below the FMVSS No. 213 threshold. Given that both predicted injury metrics fall significantly below the regulatory limits, it can be concluded that this configuration would also meet the performance criteria required for sled test verification.

Figure 66

Head Impact with Anterior Edge of Cast for Model DDH

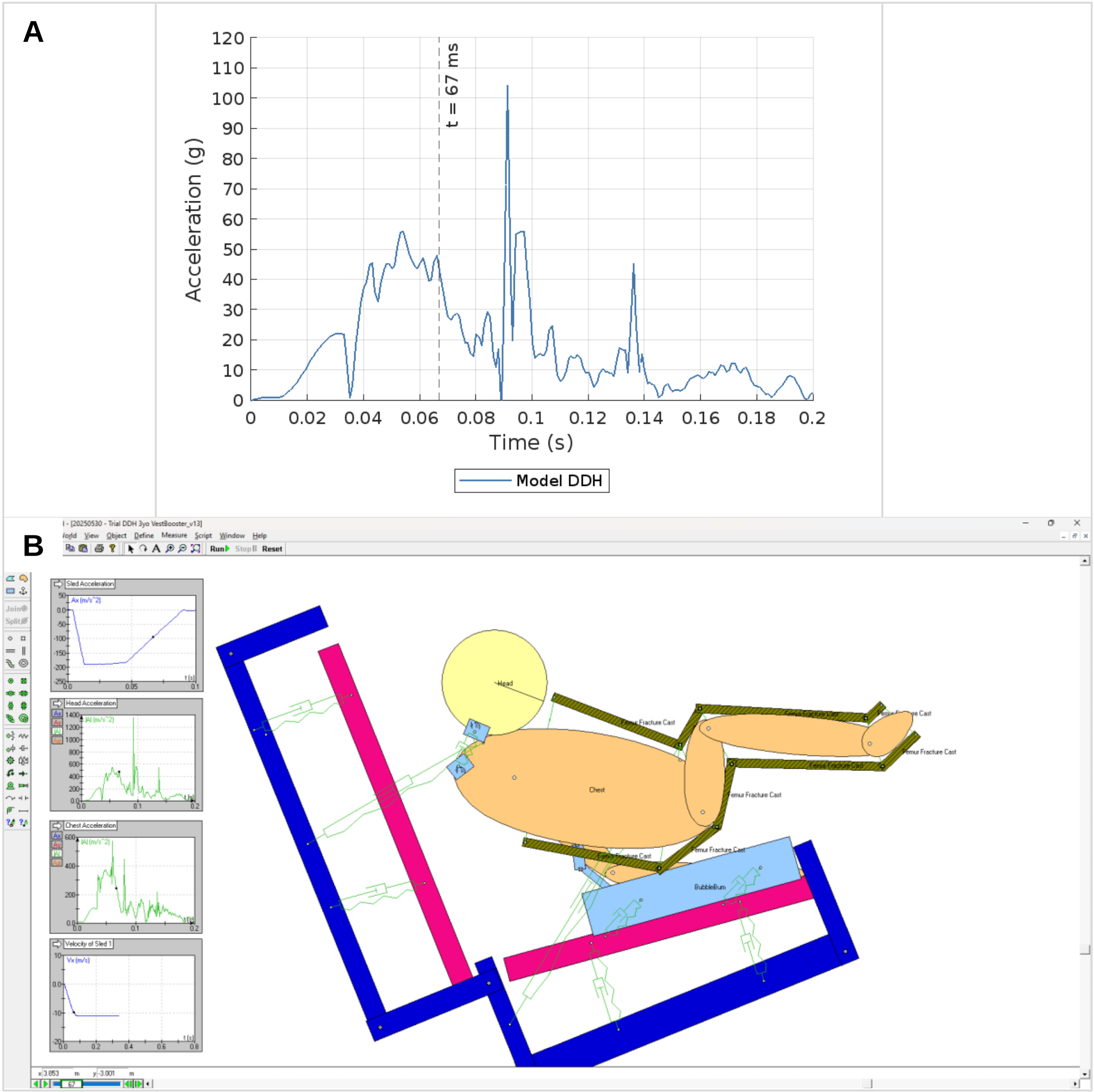

Note. (A) Head Acceleration profile for Model DDH with head-cast collision at 0.067 seconds. Model DDH maximum peak at 0.092 seconds is due to head collision with seat back which yielded artificially elevated acceleration values not observed in similar physical testing. (B) Model DDH at 0.067 seconds when head impacts cast.

1.7 Conclusions

Prior research has identified significant challenges faced by caregivers transporting children in hip spica casts during the post-operative period. These challenges arise from factors such as cast type, child age, CSS installation orientation requirements, the cost of specialized CSS, and compatibility issues with typical personal vehicle types. This study sought to evaluate two hypotheses: (1) that a low-cost, commercially available CSS solution can meet FMVSS No. 213 crash safety criteria for spica-casted children, and (2) that caregivers can independently achieve proper CSS installation for these casted children in their personal vehicles.

Sled testing presented in Section 1.4 confirmed *Hypothesis 1*, as all measured injury criteria remained well below FMVSS No. 213 thresholds across all trials. Specifically, the RideSafer Travel Vest combined with the BubbleBum Booster demonstrated a HIC36 of 312 in uncasted conditions and only 10% higher in casted configurations, still safely below the 1000 threshold limit. Simulation analysis in Section 1.6 for Model DDH further validated these findings, with predicted chest and head accelerations well within acceptable ranges and consistent with the other validated models presented.

Caregiver installation trials provided partial support for *Hypothesis 2*. The 3-year-old ATD in the forward-facing configuration was successfully and safely restrained in 83% of tested scenarios. The high success rate observed for the DDH cast configuration was attributed to the cast's geometry, which facilitated appropriate positioning and effective harnessing within various vehicle environments. For all three casted 3-year-old configurations, at least one low-cost, commercially available CSS was identified as a viable solution.

In contrast, the rear-facing 1-year-old ATD exhibited a lower overall installation success rate of 46%. This reduced performance was primarily attributed to cast-imposed constraints, misalignment of the cervical-thoracic spine, and CSS-vehicle incompatibility between the Merritt Wallenberg CSS and truck configurations. Among all evaluated scenarios, the rear-facing 1-year-old in either a femur or walking cast presented the greatest challenges, with no low-cost, commercially available CSS solution identified as suitable across any tested vehicle type.

These findings highlight that while a commercially available, low-cost CSS options can meet safety standards for crash protection, successful real-world implementation is influenced by multiple variables including cast type, child orientation, vehicle geometry, and CSS design. Therefore, both engineering validation and real-world usability assessments are essential for identifying viable transportation solutions for spica-casted children.

1.8 Acknowledgements

This research study was a collaborative effort of many labs and resources. Casting support was provided by Laith Hasan MD, Jonathan Sheu MD, Maxwell Phillips MD, and Matthew Coon MD of McLaren-Flint Hospital. Scott LaForest facilitated the use of Kettering University’s Mobility Research Center. Expert guidance was provided by Patrick Atkinson PhD, Theresa Atkinson PhD, and Clint Lee in the Kettering University’s Crash Safety Center. Casted measurements used for Working Model simulations were completed by Sabrina York BS of Kettering University. In-vehicle

installation trials were completed by Morgan Freshney BS, and Isabella Weingartz BS of Kettering University, as well as, Nicole Matthews Papelain BSN, RN, CPST, of Henry Ford Health.

PART TWO

SCENARIO 2: NON-TRANSPORTATION RELATED CHILD SAFETY SEAT INJURIES

2.1 Literature Review

Car Safety Seats (CSS) have been shown to reduce child mortality in motor vehicle collisions in the past several decades (Goldstick et al., 2022; Ames et al., 2024). CSS have become the standard restraint practice in child automobile safety and are legislated by state. Individual statewide child passenger safety laws vary greatly across the United States and require CSS usage dependent on the child's age, weight, height, seating rows in the vehicle, and/or CSS manufacturer instructions, which is typically 57 inches tall (Durbin et al., 2018a; Weaver et al., 2013). This height is typically achieved by the age of 8 at which time the child can safely use the vehicle seat and seat belt (Durbin et al., 2018a). Since the 1990s, state-specific CSS requirements were implemented in the United States to reduce pediatric morbidity and mortality in motor vehicle collisions (Bae et al., 2014). Federally, the National Highway Traffic Safety Administration (NHTSA) has established Federal Motor Vehicle Safety Standard No. 213 (NHTSA, 2024b) for CSS performance criteria in a vehicle collision. This federal standard dictates that child crash test ATDs, representing infants (birth to <2 years of age) and children (2 to <8 years), must be adequately protected from injury when subjected to frontal crash tests, as well as, with a recent addition of a side impact crash test FMVSS No. 213 (NHTSA, 2024b). In addition to the FMVSS No. 213 crash tests, the American Academy of Pediatrics (AAP) provide recommendations as to what type of

CSS should be used as the child ages from infant to older child and ultimately when able to use the vehicle seat belt similar to an adult passenger (Durbin et al., 2018a, 2018b; Weaver et al., 2013). The recommendations from the AAP involves progressing through the following CSS designs for growing children: infant-only rear-facing, rear- and forward-facing convertible, and forward-facing booster. While the AAP provides guidance discouraging the use of a CSS outside of the vehicle (Durbin et al., 2018b), no federal guidelines discuss the use of CSS for non-transportation purposes.

Even with guidance provided by AAP and CSS user manual instructions, some form of misuse was observed in 72.6% cases of an observational study conducted by Decina and Lococo (2005). The same study found that the most common misuse cases were due to the CSS being placed on an elevated surface and/or improper 5-point harness management by the caregivers. Sadly, injury due to misuse is 100% preventable with proper caregiver education and consistent messaging from pediatricians, CPSTs, and CSS manufacturers.

Prior studies have investigated infants sleeping or resting in the IC outside of the vehicle (Singhal et al., 2012). This is readily possible for infants since, as noted above, many CSS designed for infants are easily detached from a base that remains secured inside the vehicle. As such, a child may be carried in the IC into a variety of settings such as the home or a shopping cart (Smith et al., 2006). If the CSS is placed on an elevated surface, there is the potential for a fall-related injury (Batra et al., 2015). Partial or non-use of the CSS harness can lead to additional injuries as the infant can tumble out of the IC when falling to the floor (Parikh & Wilson, 2010). Parikh and Wilson (2010) used the United States' National Electronic Surveillance System (NEISS) for the years

2003-07 to investigate injuries to infants <1 year of age when an IC is used outside of a vehicle. This large case series represented a weighted population of nearly 44,000 infants over a 5-year time frame. The majority of the injured infants were younger than 4 months old with 84% of the subjects suffering a fall-related head injury. In a similar study using a smaller case series of 87 infants, aged <1-year-old, from a single children's hospital Emergency Department (ED), Desapriya et al. (2008) report similar findings using data from the years 1997-2002.

Somewhat surprisingly, there have not been recent analyses of non-transportation -related CSS injuries. Parikh and Wilson had the most recent student 15 years ago in 2010. This is relevant since CSS designs continue to evolve to meet or exceed updates to federal safety requirements and customer feedback. In addition, new CSS models have become available which represent updated CSS geometry (size and shape), to new designs with sensor technology that pairs wirelessly with caregivers (Jiang et al., 2022; Babyark, 2025). Analysis of more recent data from a large database would be helpful in determining if injuries suffered during non-transportation use of a CSS has changed with more recent CSS designs. In addition, previous studies focused on infants aged <1 year (Parikh & Wilson, 2010; Desapriya et al., 2008); subjects aged over 1 year were excluded from analysis. Including subjects >1-year-old would prove useful in determining if injuries associated with CSS interaction while not engaged in transportation are also prevalent. Increasing subject age exceeding 1 year might be expected to lead to altered injury characteristics since CSS designs typically change as subjects become older (Durbin et al., 2018b; Weaver et al., 2013). Since CSS models with detachable IC are typically not designed for children >2 years, it might be expected that the frequency and types of injury may differ with increasing subject age.

2.2 Hypothesis Development

The current study analyzed recent data from the NEISS database to document non-transportation-related CSS injury trends in the US with a focus on subjects aged <8 years of age. More specifically, all cases in the data set involve non-intentional injuries occurring outside of motor vehicle crashes. There were three hypotheses: 1) falls would be the most common injury event for infants <6 months with the head being the most frequently injured body region, 2) CSS harness misuse would be common for injured infants, 3) injury to older subjects would likely differ due to differences in CSS designs.

2.3 Materials and Methods

Nine years of data spanning 2015 through 2023 were obtained from the United States' National Electronic Injury Surveillance System (NEISS) website maintained by the Consumer Products Safety Commission. This dataset documents emergency department visits in the United States for injuries associated with a broad range of consumer products. The NEISS is a stratified sample with the strata corresponding to hospital size. It provides national weighting for each case to allow researchers to estimate yearly events across the entire United States. The injury data from this source were screened to identify cases involving CSS, Product Code 1519. As the data set focuses on injuries related to consumer products, the injuries that were identified corresponded to non-crash events involving a CSS, with the exception of a single case. This study was reviewed and approved by both McLaren's Institutional Review Board (IRB) and Scholarly Activity Review Committee (SARC) committees; see Appendices A and B for full signed documentation. The McLaren IRB conducts approval determination for all non-human research and the McLaren SARC reviews and approves proposed study designs to be conducted.

The injured persons' age, sex, and codes for diagnosis, injured body part, location of event (e.g. home or school), and disposition (e.g. treated and released or admitted) were extracted from the data set. Data was further sub-grouped by age into infant (<2 years) and child (2 to <8 years) groups. The narrative descriptions for the NEISS cases were searched for keywords to identify terms describing the injury event. This process used the text search and logic tools embedded within Microsoft Excel. For the infant and child groups, these terms included text such as the use of a stroller or shopping cart, terms suggesting the restraint fell or was dropped, and terms describing the surface the seat may have been set upon. For some queries, the narratives included word choice and spelling variants. All queries were reviewed via random sampling of cases to confirm that the search algorithm properly classified the cases. All analysis was performed using the sampling weights in order to provide estimates for national yearly incidence frequencies.

2.4 Results

The database included a total of 2,538 cases with a total weighted estimate of 57,596 cases of non-transportation related CSS injuries in the United States over the 9-year time period of 2015-2023 shown in Figure 67.

Figure 67

Yearly Non-Transportation Related CSS Injuries Reported in the United States

Note. The United States NEISS (National Electronic Injury Surveillance System) database was queried to document all non-transportation injuries associated with Car Safety Seats (CSS) for subjects <8 years of age. For the 9-year analysis period, this represented a total of 57,596 weighted cases (2,538 raw cases).

Trends in the yearly totals were similar between the raw and weighted nationalized counts of cases. Infants (all subjects from 1-23 months of age) represented 48,527 cases while children (from 2 to <8 years of age) represented 9,069 cases for a total of 57,596 cases of infants and children. Similar rates of appearance for each sex were noted in the groups (50.70% male for infants and 49.85% for children). Two cases involved a fatality; both involving infants who experienced cardiac arrest while sleeping in the CSS. A minority of case narratives indicated a sleeping, napping or resting child (7.96% of cases in the infant group and 0.90% in the child group). The majority of cases were treated and released accounting for 91.62% of infants and 95.97% of children, however 6.71% of infants were either admitted, transferred, and/or observed compared to 1.80% of children. Cases involving children more frequently left the ED without being seen (2.23% vs. 1.63% for infants). Falls were the most frequent injury event and represented 41,068 cases or 71.30% of all infants and children <8 years of age. Displayed in Figure 68, the frequency of falls associated with non-transportation CSS use was observed to decrease with increasing age: 60.70% (or 24,925 cases) of these falls occurred to infants aged 1-6 months of age, 22.47% (9,226 cases) for infants 7-12 months, 5.14% (2,112 cases) for infants 13-18 months, 1.69% (693 cases) at age 19-23 months, 5.79% (2,377 cases) at 2 years, 3.69% (1,517 cases) at 3-4 years, and 0.53% (219) at 5-7 years old.

Figure 68

Yearly Prediction for CSS Fall Related Injuries in the United States

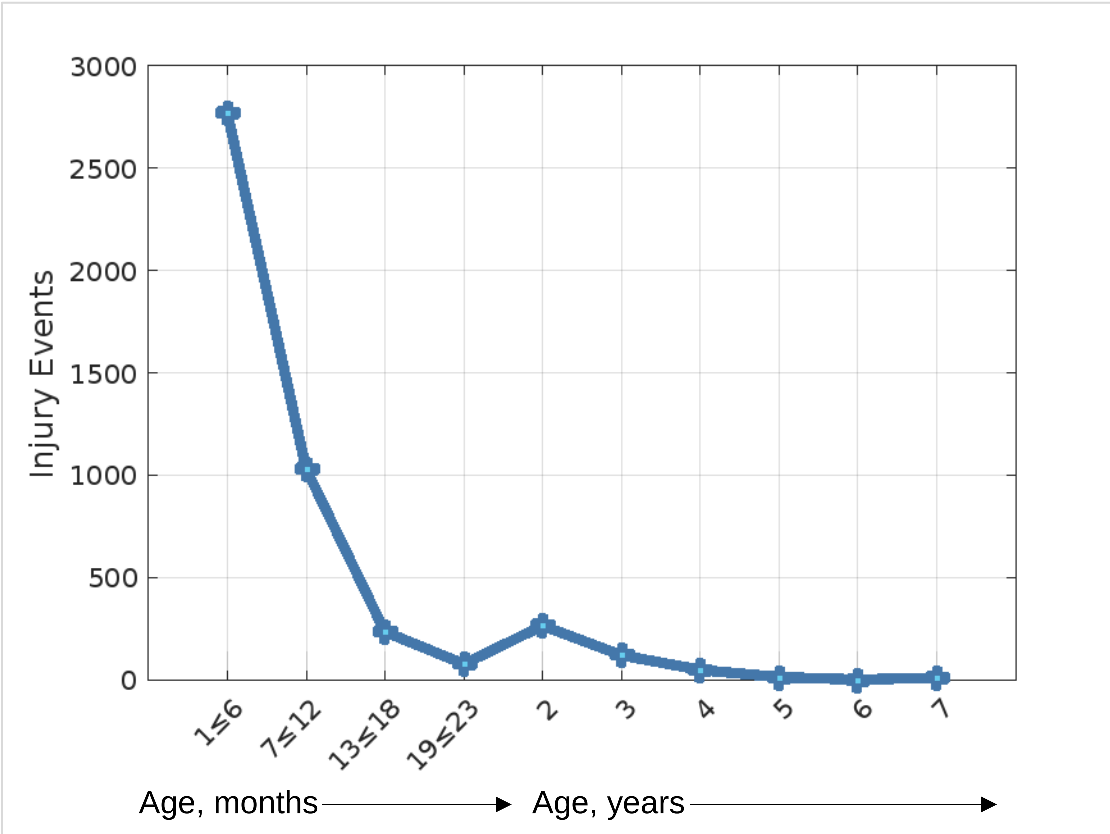

Note. Falls were the most frequent injury event associated with a CSS affecting subjects <8 years of age. The majority of the fall injury cases involved infants aged 1≤6 months (projected yearly rate of 2,769) and 7≤12 months (projected yearly rate of 1,025 cases) with declining frequencies as age increased.

Considering infants, injury to the head was the most frequent (60.66% of injuries) with a projected yearly event rate that decreased with age as shown in Figure 69. The majority of these were internal head injury (frequently described as Closed Head Injury (CHI) in the narrative), reported in 78.92% of head injury cases. Head injuries were also the most frequent injury for admitted/transferred/observed cases. Other common injuries were face contusions, head contusions, and elbow dislocations at 9.53%, 6.66%, and 4.72% of cases, respectively. For infants, falls were the most common mechanism, with CHI related to the infant falling out of the CSS. Harness non-use cases 33.93% (16,465 cases) had narrative descriptions documenting either lack of harness use or stated that the infant fell out of the seat implying improper use since CSS manufacturer instructions state that the harness must be properly positioned, clipped, and tightened at all times. Another common injury contributor, described in 27.40% (13,296 cases) involved placement of the IC on an elevated surface including couch, table, counter, bench, dryer, sofa, bed, or chair. Less common factors were shopping cart use (4.77% or 2,315 cases) and stroller use (4.59% or 2,226 cases).

Figure 69

Yearly Prediction for CSS Non-Crash Event Head Injuries in the United States

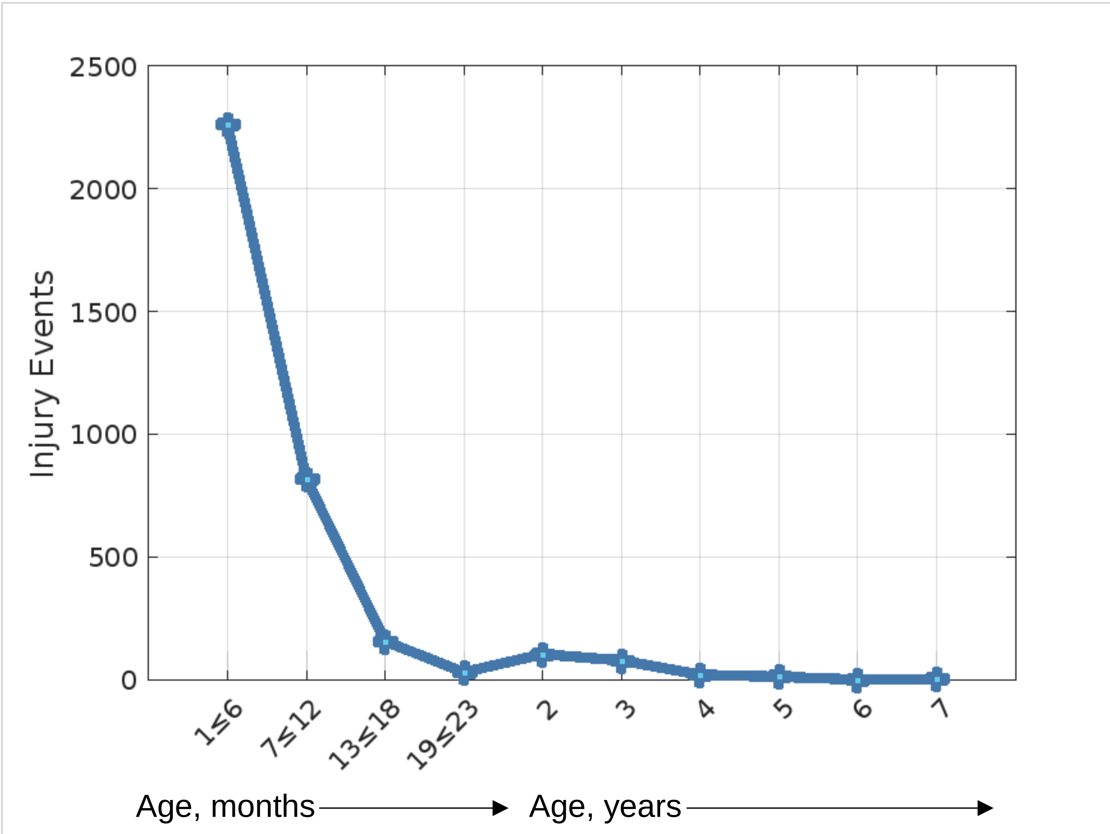

Note. Similar to falls, the majority, 88.47%, of head injury cases involved infants aged 12 months and under. The highest frequency of head injuries occurred to infants aged 1≤6 months (projected yearly rate of 2,264), followed by infants aged 7≤12 months (projected yearly rate of 819 cases) with declining frequencies as age increased.

When considering injuries involving all children in the age group 2 to <8 years, the most common body regions for injuries were elbow (2,638 cases, 29.09%), head (1,935 cases, 21.34%), face (1,827 cases, 20.15%), and mouth (413 cases, 4.56%). Among the elbow injury cases, “elbow dislocations” were the most common injury code representing 2,188 cases, 82.95%. While admissions for injuries in this age group were rare (12 cases raw count) they were most frequently due to head injury (35.09% of projected admissions, or 3 cases raw count) or femur fracture (22.52%, or 4 cases raw count). In the femur fracture cases, two indicated osteogenesis imperfecta, one indicated spina bifida, and the fourth was reported as due to a high-speed motor vehicle event. Note that this motor vehicle event was one of two cases in the data set involving a vehicle, with the other being a case of an infant in a stroller struck by a vehicle.

Further narrative analysis of all elbow dislocation cases for infants and children reveals nursemaid elbow as the most common diagnosis. This injury accounted for 91.11% (2,087 cases) of elbow injuries in infants and 85.21% (1,865 cases) in children. Narrative accounts describe the injury as occurring while removing the infant or child from the CSS. The incidence of nursemaid's elbow increases with age until the majority occur at the age 2 (40.20% of 3,952 cases) and then decreases at ages 3 and 4, with no cases for the ages 5 to <8 illustrated in Figure 70. Significantly, there are other elbow dislocation cases in the database occurring more frequently in children than in infants (14.79% of child cases) that were confirmed via individual narrative review to be dislocations and not nursemaid elbow injuries, further demonstrating the influence of subject age on injury patterns.

Figure 70

Yearly Prediction of Nursemaid's Elbow Cases in the United States

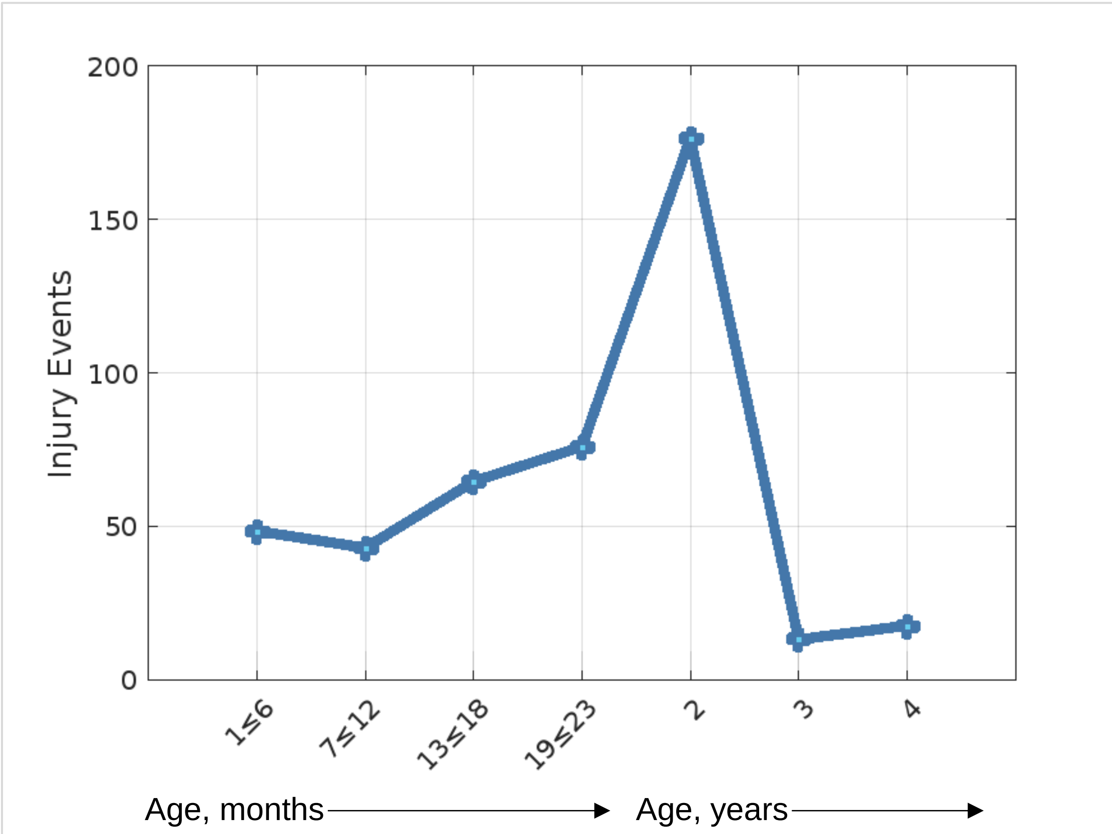

Note. Predicted yearly frequency for nurse-maid's elbow cases associated with CSS non-crash event shows a majority occur to children aged 2 years and no cases for ages above 4.

2.5 Discussion

The objective of the current study was to use the NEISS database to document recent, CSS-related injuries when the seat is not being used for transportation for infants (0 to<2 years) and children (2 to <8 years). It was hypothesized that a frequent injury scenario would be to infants who suffer head injury secondary to falls and associated harness misuse. It was further hypothesized that older subjects would suffer different injuries as they typically utilize different seating designs.

A total of 57,594 weighted cases of non-transportation-associated CSS injuries in the United States were documented in the NEISS database from 2015-2023, the most recent years that are available. These subjects primarily suffered non-fatal injuries that required an ED visit, with the largest proportion of cases (84.25%) involving infants of age less than 2 years. Falls were the most common injury event for infants and children with the majority of these cases involved CSS harness non-use/misuse. Head injuries were frequent in infants, when considering all causes, with a frequency that decreased with subject age. Somewhat surprisingly, the elbow was the most common injured body region in children, with the majority of these cases documented with the injury code of "dislocation". While the terms "elbow" and "dislocation" are specifically coded in the database, additional detail was identified by reviewing 100% of the narratives for all "elbow" and "dislocation" cases. This analysis identified terminology such as "nursemaid", "radial head subluxation", as well as, spelling variants of these terms. Collectively, the current study refers to these injuries as "nursemaid's elbow" and represented 88.23% of all elbow dislocations.

The current study confirms data from prior studies analyzing injuries associated with CSS use outside of a motor vehicle. Parikh and Wilson (2010) analyzed data from 2003-2007 from the same NEISS database used in the current study, however they limited their analysis to subjects aged <1 year. The study documented that the majority (62.4%) of injuries were to infants aged 1-4 months who suffered a fall from an elevated surface, with 84.3% sustaining a head injury. This data is also reflected in a smaller study of 87 infants aged <1 year at a single children's hospital (Despriya et al., 2008). In regard to injuries in children over the age of 2, no previous study was identified which analyzed non-transportation-associated CSS injury patterns in this age group. This renders comparison with previous data difficult. It should also be noted that Parikh and Wilson (2010), and Desapriya et al. (2008) only studied CSS-associated injury outside of the vehicle while the current study investigated all non-transportation injuries related to a CSS. Per information contained in the narratives in the current study, it was observed that some of the injuries were incurred while the child was entering a CSS in the vehicle before travel or exiting a CSS in the vehicle after travel. Some of these narratives, for example, revealed that some of the nursemaid injuries were associated with an infant or child being lifted by a caregiver into the CSS via the subject's arm(s) or being helped out of the seat in the same manner. This loading may have subjected the arm to traction which might explain the nursemaid's elbow injury. It is worth noting that a nursemaid's injury is not typically categorized as a frank dislocation, but is actually classified as a soft tissue injury to the annular ligament. The nursemaid's elbow injury identified in this study had a frequency that increased with age until age 2, and decreases at ages 3 and 4 with no documentation for children 5-7 years old with this specific injury type. This is not surprising since nursemaid's elbow injury has been noted in the clinical literature to be limited to subjects aged under 4 years (Nardi & Schaefer, 2023). This age limit is attributed to progressive strengthening of the annular ligament and other restraining structures with age that tether the radius in place by approximately the age of 4.

This study is limited by the availability and consistency of injury coding and narration provided in the NEISS database. While relatively detailed codes exist for some data, more granular information was identified by analysis of the short narratives that accompany each case. These short narrations of the injury event are reported by the ED but are prone to grammatical and spelling errors, with a variety of synonymous terms sometimes used. In the current study, electronic query tools were used to identify the relevant wording, including various word choices and typical spelling variants. In some cases, 100% of the narrations were reviewed to ensure all relevant data was captured. These steps were intended to make use of the narratives to gather as much of the available data as possible.

In summary, the current study documents that falls resulting in head injuries are common for harness misuse cases for infants aged 1-6 months for the recent 9-year study period. A similar trend was noted in an earlier study of the same database during the 5-year period from 2003 to 2007. This is despite messaging from the AAP discouraging the use of CSS for non-travel purposes (Durbin et al., 2018b). Since fall-related head injuries persist with IC outside of a vehicle, it suggests that improvements in monitoring education for caregivers may be warranted. It is encouraging that hands-on, in-person, educational sessions with a child passenger safety technician have demonstrated improved knowledge for participants (Budziszewski et al., 2021). Surveys of caregivers reveal that there is a perception of mixed messaging regarding specifics of CSS usage. Parents often look to pediatricians as the authority on CSS use but consistent messaging can vary between providers (Weaver et al., 2013). Additionally, information consumed on social media may not be correct or current and can affect caregivers' decision-making. The recent NEISS data tabulated in the current study demonstrates that incorrect CSS use leads to preventable injuries; as such, this public health issue would benefit from clear and concise messaging that encourages proper use of the CSS at all times and discourages use outside of transportation.

In addition to improved messaging to caregivers, fail-safe mechanisms can possibly be put in place as a mechanical mitigation to inappropriate CSS use. Some newer models of CSS have implemented “smart” features including alerts for high temperature with automatic cooling and ventilation as well as a pressure sensor which can alert the caregiver if a child is left unattended in the vehicle (Jiang et al., 2022; Babyark, 2025). Similarly, timed alarms or mobile app based alert systems could be implemented to notify caregivers to remove a child from the restraint device when vehicle motion is not detected. Additional features in the restraints may focus on ease of use designs that would allow children to ingress/egress a CSS without axial traction delivered to the upper extremity.

2.6 Acknowledgments

This study was completed as a partnership between Kettering University and McLaren-Flint Hospital. I am grateful to Jasmine Kaur, MD, Ajay Srivastava, MD, Patrick Atkinson, PhD, and Theresa Atkinson, PhD for their knowledgeable contribution into these findings.

PART THREE

SCENARIO 3: DESIGNING FOR CHILD SAFETY IN CONNECTED AND AUTOMATED VEHICLES

3.1 Literature Review

The landscape of connected and automated vehicles (CAV), Advanced Driver Assistance Systems (ADAS), and Automated Driving Systems (ADS) have the potential to improve roadway safety for both the vehicle occupants and other road users. Developed in part to compensate for human driver shortfalls such as distraction, fatigue, or impairment, these systems are designed to make fewer mistakes than humans while improving performance over time based on continual data collection. Society of Automotive Engineers (SAE) Level 4 and 5 driverless vehicles are already in use in small, geo-fenced locations around the United States. In 2022, NHTSA released a final rule to update all 200-level FMVSS to further define the driver's seating position as a passenger position (NHTSA, 2024a). However, no specific U.S. Federal Regulation exists addressing this type of mobility or if they should be used venerable road users such as children.

The history of vehicle technology development teaches us that the unique safety needs of children must be considered throughout the CAV/ADAS/ADS development process to avoid outcomes that may hinder safety or create serious inadvertent hazards. The unintended consequences of past safety technology efforts justify this proactivity as CAV technology matures. Among the most tragic examples of failure to consider child safety, is when passenger air bags were first required to protect adult passengers. As they were introduced in the mid-1990s, these safety devices killed over 250 children and injured numerous others (NHTSA, 2010). Even today FMVSS No. 208 (NHTSA, 2024a) only statically tests out-of-position children in the front passenger seating position. Dynamic frontal and side impact testing with child-sized ATDs, covered in FMVSS No. 213 (NHTSA, 2024b), is completed on a sled bench that is not representative of current, real-world vehicle architecture and applications. While the potential risk to out-of-position (OOP) children had been recognized and documented as early as the 1970s, improvements such as cut-off switches, depowered air bags and ultimately Advanced Air Bag systems were not implemented until after these tragic deaths and injuries occurred. Children and other vulnerable passengers and road users deserve advance consideration as the next era of vehicle technology unfolds.

For these reasons, Safe Kids Worldwide (SKW), a globally recognized injury prevention non-profit that has led numerous child passenger safety initiatives in the United States and certifies Child Passenger Safety Technicians (CPST), convened a "Blue Ribbon Panel on Children in Autonomous Vehicles" in 2018. The group began by identifying potential child safety concerns, expanded to provide safety recommendations for policymakers and industry, and most recently developed a child-focused Design Failure Modes and Effects Analysis (DFMEA) for CAV. The DFMEA is a widely-used industry analysis process that focuses on the end user, typically an adult, making the child focus of this initiative relatively unique and significantly vital. This study lays out the process and considerations for the development of a child-focused DFMEA for CAV.

3.2 Hypothesis Development

For decades, children have not been the priority end-user in automotive design, but rather an afterthought. Children's bodies have different safety restraint needs and cannot be considered small adults. This failure of child-focused safety design considerations resulted in hundreds of child deaths caused by airbags of the past. To prevent history from repeating itself, the current study hypothesized that a child-focus DFMEA created by experts in the fields of child passenger safety, vehicle design and testing, and CSS design, would prevent unintended consequences and possible potential safety concerns for children in and around autonomous ride-share vehicles.

3.3 Method

3.3.1 Selection of Experts

In developing this DFMEA, the aptly named Safe Kids in Advancing Vehicles Alliance (SKAVA) has leveraged the cumulative expertise of researchers, vehicle and child restraint manufacturers, pediatricians, law enforcement, emergency medical service, fire safety, and highway safety professionals, consumer advocates, communications experts, an attorney and public health organizations representing 17 U.S. states and three additional countries.

A Blue-Ribbon Panel of top-level safety and transportation experts was organized by Safe Kids Worldwide to begin the process (SKW, 2018a). The 17-member panel released a report in October 2018, outlining a call to action and specific recommendations, including seeking the input of child safety experts throughout the CAV development and design phases, in an effort to ensure that the safety needs of children under 13 were adequately addressed in future vehicle designs (SKW, 2018b).

The evolving Children in Autonomous Vehicles Consortium was then structured into two working groups. The first focused on policy, legislation, and enforcement needs, while the second worked on public information and education (SKW, 2019). Combined, this phase of the program created public information and education tools designed to guide draft legislation, policy, enforcement and best practices for child safety in and around CAV. These tools were then expanded and amplified by expert teams in the forms of a position paper, educational programming for child safety advocates, and a white paper for consideration by industry, regulators and policymakers (SKAVA, 2024).

3.3.2 Mapping of Potential Failures

In the absence of specific regulation of these evolving technologies, industry stakeholders have been expected to include safety cases in their development processes. To facilitate the early inclusion of child safety consideration, SKAVA extended the experts' concerns into a usable and familiar format. The resulting DFMEA focuses specifically on the safety needs of children in the context of a SAE Level 4 or Level 5 CAV (SAE, 2021). It seeks to identify child safety considerations and issues that need to be included at the research and development stage to prevent child injuries in automated vehicles, including priority areas where voluntary industry standards for evaluating potential child injury can be developed, adopted, and appropriate regulation can follow. The objective of the proposed DFMEA is to formalize a process for a voluntary safety case into an accepted industry standard that can then be later incorporated into a federal-level safety regulation.

SKAVA members used a combination of online and in-person surveys to gather potential child safety risks in CAV from engineers, advocates, certified CPSTs and others. In addition, the group presented and collected potential failures and failure modes from many sources including: Society of Women Engineers (SWE), New Jersey CPS advocates, Children's Safety Network participants, attendees at road and child safety conferences such as Lifesavers and Safe Kids' PrevCon, and through its safekids.org/AVs website.

This failure modes and effects analysis breaks down potential failures across several factors: first by timing (Before Travel, During Travel, After Travel, During Crash, After Crash), then by system (Interior vs. Exterior), and ultimately by subsystem (e.g., child restraint systems). It should be noted that because this tool is specifically focused on children as a user group, risks may not be identical to those faced by adults. By its nature, a DFMEA is not a complete and perfect list, but rather, a constantly evolving document that can advance and be refined as the technology progresses. This DFMEA is no exception and provides a starting point for manufacturers to incorporate into their own already established system and subsystem DFMEA they manage and update internally.

3.3.3 Risk Analysis

Potential risk to a child often differs from potential risk to an adult, whether in a crash, a sudden maneuver, or other event. Since this analysis was targeted to one specific vulnerable user group, children under age 13, the needs of this target group must be appropriately balanced with the needs of other users and affected populations.

The most obvious starting point is differing restraint needs. While all current child restraint systems are tested for performance in frontal collisions on front-facing vehicle seats, the youngest passengers must be in rear-facing child restraints designed to support their backs, necks and heads during a frontal crash and provide lateral protection in a variety of other crash dynamics (Durbin et al., 2018b). As bi-directional vehicles are introduced, rear-facing must be more accurately defined as facing the rear of the vehicle relative to the direction of travel.

Once a child has outgrown the height or weight limits of rear-facing modes, forward-facing child restraints, typically using integrated 5-point harnesses for restraint, must be used to their maximum heights or weights (Durbin et al., 2018b). Both rear-facing and forward-facing child restraints must be securely attached to front-facing vehicle seats using either vehicle seat belt systems or dedicated lower attachments that connect to required vehicle anchor counterparts.

When children outgrow these rear-facing and forward-facing systems with integrated harnesses, they are still not large enough or developed enough to fully benefit from the adult restraint systems built into a vehicle. Instead, they must ride in booster seats that position a child to take advantage of vehicle occupant protection features while utilizing a vehicle lap and shoulder belt for direct restraint (Durbin et al., 2018b). As with other child restraints, booster seats are designed for use on front-facing vehicle seats and tested for performance in frontal crashes. Advancing vehicle technologies and features, including seating designs, active occupant restraints and air bags, must be compatible with each of these three child restraint types.

A child cannot fully benefit from vehicle systems alone until seat belts and seating designs fit correctly. Considering that safety restraints systems are designed for vehicle occupants that are 57-inches in height or taller, this benefit occurs for children between the ages of 8 and 12 and is also dependent on specific vehicle seating designs and physical characteristics of the specific child (Durbin et al., 2018b)

Beyond these clear and historically proven physical risks and interventions, the more nuanced areas of child maturity, knowledge and ability must be considered as new vehicle system designs are introduced. Evidence-based policies must be developed to determine when and how children at different developmental stages can independently and safely interact with automated systems and the vehicles themselves. Using scientific methods, developers must address appropriate child supervision, cases when that supervision is not present or could be hindered, functionality during various emergent events, and even infrastructure considerations for safely loading and unloading children and their restraints in rideshare environments.

To ensure safety, reduce injury and prevent fatality, each emerging component must be adequately tested for safety, utility, compatibility with child needs, and the likelihood of use as intended, designed and tested. Marketing of CAV must clearly represent safe and proper use, consistent with best practice recommendations, vehicle and equipment regulations, state usage legislation, and consumer education resources (Durbin et al., 2018b).

3.3.3.1 Safety Standards. Safety standards take several basic forms, and each must be respected for its intention and effect. Individual proprietary standards are important for any producer of new technologies or features, and due to the unique nature of each emerging item must be robustly developed and adhered to. Voluntary industry standards, often formalized by industry groups, such as SAE, address common technologies and provide minimum design and performance standards that supplement mandatory regulations such as SAE J1819 (SAE, 2015). The FMVSS set forth by NHTSA and other mandatory regulations prescribe minimum performance, design and reporting standards that must be adhered to and can be enforced. Federal and state legislation provide additional mandatory requirements, often focused on product usage or commerce, but may also include product regulatory requirements.

These standards each have an important role in defining the safe design and use of advancing vehicles. While premature Federal regulations may unnecessarily hinder new technology development or may not yet include adequate data on newer concepts, proprietary and industry standards are more expedient and can provide temporary or permanent guidance that matches current safety needs. In addition, state legislative requirements can be used to prepare for future needs (e.g., roadway infrastructure) and support current needs (e.g., occupant restraint requirements).

When appropriate, standards in various forms should ensure child restraint systems can be used consistently as children are transported between vehicles at various stages of automation. They can include the provision of standardized plain language or pictograms for consumers who transport child occupants using adaptive, add-on, or integrated equipment. All standards should recognize basic facts, including that changes to the vehicle cabin design and passenger positioning may significantly impact child passenger safety restraints and testing protocols currently conducted only in a forward-facing vehicle seat orientation.

3.3.3.2 Usability Testing. Stakeholders should conduct or sponsor usability testing that includes families, whether transporting a single child or multiple children, and which considers the needs of children at different ages and developmental stages in tests of all new features in CAV. It can be easily ascertained through the literature that adults are included in usability tests, including CAV pilot programs currently underway in multiple cities across the United States. However, it is not clear that children are appropriately included in this testing or that their unique needs are adequately considered.

To assure safety and consumer acceptance, developers should conduct or sponsor testing and be transparent with the public to build confidence in the fidelity of the testing process. This transparency, as part of the NHTSA's original policy framework on automated vehicles, should be considered a valuable part of the entire safety system that evokes confidence among passengers. Toward that objective, stakeholders should promote usability testing that evaluates: 1) families of young children of varying ages and various restraint needs; 2) families or caregivers that transport more than one child; 3) the more complex needs of children with developmental or physical disabilities; 4) child-specific needs regarding interaction with new features and alternative seating configurations not currently considered by FMVSS; and 5) child interactions with vehicle features in circumstances with inadequate adult supervision due to an impaired, incapacitated, or absent adult.

Testing should include communicating with adults, and specifically caregivers, in an effort to understand how children could or would interact with CAV in situations where an adult passenger has become incapacitated, e.g. due to a medical emergency.

3.3.3.3 Inclusive Design. To ensure that the full breadth of child safety needs and restraint compatibility are considered, industry leaders should seek the input of child passenger safety specialists throughout CAV product development and design. This practice will not only address accommodation of the safety needs of children at all stages and ages but will help avoid unintended adverse consequences. To ensure that child-centered best practice recommendations are considered and evolve as each new advancing automated feature is developed, having the child safety community at the table during the development and innovation stages, rather than after vehicles and features are in production, will decrease risks to child safety. Organizations like Safe Kids Worldwide, the National Safety Council (NSC), the American Academy of Pediatrics (AAP), and other child-focused expert groups are well positioned to provide input from child safety advocates and experts in this effort.

3.3.3.4 Appropriate Supervision. Stakeholders should conduct research that informs best practice and policy recommendations regarding the appropriate level of supervision for children of different ages and developmental stages in CAV, assuring enhanced safety simultaneously with innovation. While current vehicles and laws require an alert driver to operate a vehicle with child passengers, research is needed to identify the appropriate level of adult supervision to ensure the safety of children when the potential exists for no caregiver to be present or alert in the vehicle. Scenarios might include children who unbuckle themselves or other children, bored children who play unsafely with unused seat belts, children who are unintentionally or intentionally left unattended by adults, and more. Furthermore, there is a need to develop best practices around the appropriate age at which a child can safely and effectively ride alone in an CAV.

At a minimum, these research efforts should consider the possibilities of the following scenarios: 1) the caregiver is not there to meet the child at the CAV destination; 2) the CAV does not complete its route or is re-routed to an unknown location; 3) the child cannot communicate a problem with the CAV appropriately; 4) the child becomes ill or injured en route; 5) the child attempts to leave the vehicle before arriving at the final destination set for all passengers; 6) the supervising adult in the vehicle is sleeping or impaired; 7) the CAV transporting a child is involved in a crash when the responsible adult is unavailable.

3.3.3.5 Marketing Standards. Manufacturers and other stakeholders should ensure all marketing and advertising shows families riding in CAV according to already established child passenger safety best practices, accurate product intentions, and proper use of instructions. Product developers are in a unique position of communicating and modeling safe behaviors, in relation to their products, through such marketing representations. Conversely, experts have also ascertained that marketing can represent conflicting or contradictory messages that lead to unsafe product use.

3.4 Results

Drawing upon the developmental work and resulting findings detailed in Sections 3.3.1, 3.3.2, and 3.3.3, which included consultations with industry experts and significant stakeholders, as well as, the identification of potential failure modes through engagement with professional organizations and technical conferences, Table 9 presents a Design Failure Mode and Effects Analysis (DFMEA). This DFMEA is intended to formalize a structured methodology for developing a voluntary safety case framework. The objective is to establish an industry-accepted standard that could serve as the foundation for future integration into federal safety regulations.

Table 9

Potential Failure Modes for Child Passengers in SAE Level 4 & 5 CAV

No.	Subsystem	Potential Mode	Potential Failure	Potential Effect
	Timing: Before Travel System: Vehicle Interior			
1	Climate	Interior climate unsafe for child passengers (too hot / too cold)	Climate control sensor failure	Hyperthermia, Hypothermia
2	CSS	CSS incapable of restraining child properly	Seat belt / LATCH not accessible or compatible	Child injury or death
3			Top tether not accessible	Child injury or death
4			Seating position does not meet SAE J1819	Child injury or death
5			Caregiver unsure of install in vehicle	Child injury or death
6			Child not compatible for CSS provided	Child injury or death
7			CSS not available in vehicle	Child injury or death
8	CSS & Vehicle Seat Configuration Interaction	Diminished restraint provided by CSS	CSS installed in incorrect seating position	Child injury or death
9			Seat locked into incorrect direction for CSS installation	Child injury or death

Table 9 (continued)

No.	Subsystem	Potential Mode	Potential Failure	Potential Effect
	Timing: Before Travel System: Vehicle Interior			
10	CSS & Air Bags Interaction	Unintended harm caused by CSS	CSS incompatible with airbags in seating position	Child injury or death
11	CSS in Vehicle	Incompatibility between CSS and Vehicle Restraint System	Not evaluating the vehicle restraint system using SAE J1819	Child injury or death
	Timing: Before Travel System: Vehicle Exterior			
12	General Exterior	Child locked out	Loss or unintended function of locking mechanism	No access to vehicle
13		Incorrect vehicle selection	Child gains access to incorrect vehicle	Lost and unattended child
14			Stranger has access to enter vehicle	Child endangerment
15		Hazardous vehicle ingress	Child impacted by passing-by vehicle	Child injury or death
16			Child impacted by AV before / during ingress	Child injury or death

Table 9 (continued)

No.	Subsystem	Potential Mode	Potential Failure	Potential Effect
	Timing: During Travel System: Vehicle Interior			
17	General Interior	Stops / Starts / Maneuvers unsafely	Child accesses controls	Child injury or death.
				Impact with vehicles, pedestrians, surrounding area
18		Too hot / Too cold (e.g., heater too high for weather condition)	Interior climate unsafe for passengers	Hyperthermia, Hypothermia
19		Sensor system does not correctly identify child distress, child emergency and notify first responders, caregiver, emergency point of contact	Child experiences distress and / or medical / health emergency during travel	Child injury or death
	Timing: During Travel System: Vehicle Exterior			
20	General Exterior	Loss of function: Stranger has access to enter vehicle	Doors or windows do not lock as required / Passenger monitoring	Child injury or death
21	Window	Loss or partial function: Interior climate unsafe (windows down in winter / up in summer)	Interior climate control system failure / window control failure / notification system failure	Child injury or death
22		Unintended function: Child has access to be partially outside vehicle	Windows do not lock as required / Passenger monitoring	Child injury or death

Table 9 (continued)

No.	Subsystem	Potential Mode	Potential Failure	Potential Effect
	Timing: During Travel System: Vehicle Exterior			
23	Child Seat	Loss of function: Child unrestrained	Child self-unbuckles	Child injury or death
24		Loss of function: Child unrestrained	Child unbuckled by another passenger	Child injury or death
25	CSS & Vehicle Seat Configuration Interaction	Loss of function: Child unrestrained	Seat unlocked during travel	Child injury or death
26		Loss or partial function: Child improperly restrained	Direction of travel not compatible with CSS	Child injury or death
27		Loss or partial function: Child insufficiently restrained	Switched CSS mode of use	Child injury or death
28	Unexpected Stop	Unintended function: Child exits vehicle prior to destination	Passenger monitoring and notification on travel status	Child injury or death
29		Unintended function: Stranger has access to enter vehicle	Passenger monitoring and notification on travel status	Child injury or death

Table 9 (continued)

No.	Subsystem	Potential Mode	Potential Failure	Potential Effect
	Timing: During Travel System: Vehicle Exterior			
30	Planned Route	Loss of function: Undesired rout change authorized	Route planning and approval system failure	Child injury or death
31		Partial function: Desired route change not authorized	Route planning and approval system failure	Child injury or death
32		Loss or partial function: Child in distress requires stop or route change	Passenger monitoring system failure / interactive controls	Child injury or death
33	Emergency Maneuvering	Loss of function	Vehicle does not apply emergency maneuvers	Child injury or death
34		Partial function	Vehicle emergency maneuvers insufficient	Child injury or death
35		Exceeding function	Vehicle applies emergency maneuvers when not required	Child injury or death
	Timing: After Travel System: Vehicle Interior			
36	General Interior	Child remains in AV on purpose	Misunderstood / ignored exit signal	Heat Stroke, Lost Child
37		Child remains in AV on accident	Misunderstood exit signal	Heat Stroke, Lost Child
38		Child exits AV at incorrect stop	Misunderstood exit signal	Lost and unattended child

Table 9 (continued)

No.	Subsystem	Potential Mode	Potential Failure	Potential Effect
	Timing: After Travel System: Vehicle Interior			
39	Door	Child locked in, no egress	Doors do not unlock as required	No access to Street / Sidewalk, Heat Stroke, Lost Child
40	Climate	Too hot / Too cold	Interior climate unsafe for child passengers	Hyperthermia, Hypothermia
41	Child Seat	Ease of uninstallation	Infrastructure not set up for Drop off zones	Child injury or death
	Timing: After Travel System: Vehicle Interior			
42	Door	Stranger has access to enter vehicle	Doors unlock before safe exit is verified	Child endangerment
43	Unloading Zone Infrastructure	Safe Drop off location	Infrastructure not set up for unloading zones	Child pedestrian struck by traffic
44		Child user / bystander hit by AV	Insufficient surrounding awareness by the AV	Child Injury or Death
45		Child user hit by other traffic	Infrastructure not set up for unloading zones	Child Injury or Death

Table 9 (continued)

No.	Subsystem	Potential Mode	Potential Failure	Potential Effect
	Timing: During Crash System: Vehicle Interior			
46	CSS & Vehicle Seat Configuration Interaction	Insufficient restraint provided by CSS	Unique vehicle seating configuration affects CSS intended performance in vehicle environment	Child Injury or Death
47		Insufficient restraint provided by CSS	Vehicle travel direction and CSS installation orientation incompatibility (e.g.: rearward-facing CSS in vehicle travelling rearward)	Child Injury or Death
48		Excessive restraint provided by CSS	Unique vehicle seating configuration affects CSS performance in vehicle environment (intended performance)	Child Injury or Death
49			Vehicle travel direction and CSS installation orientation incompatibility (e.g.: rearward-facing CSS in vehicle travelling rearward)	Child Injury or Death

Table 9 (continued)

No.	Subsystem	Potential Mode	Potential Failure	Potential Effect
	Timing: During Crash System: Vehicle Interior			
50	CSS & Vehicle Restraint Interaction	Insufficient restraint provided by vehicle (LATCH, seat belt, pre-tensioning, load-limiting)	Unique crash dynamics affect standard vehicle restraint performance and effectiveness (intended performance)	Child Injury or Death
51	CSS & Airbags Interaction (primarily vehicle)	Unintended Child / CSS interaction with airbag (OOP testing included)	CSS incompatible with airbags in seating position	Child Injury or Death
52	CSS & Airbags Interaction (primarily CSS design)	Unintended Child / CSS interaction with airbag (OOP testing included)	CSS incompatible with airbags in seating position	Child Injury or Death
	Timing: During Crash System: Vehicle Exterior			
53	Child Pedestrian and Vehicle Interaction	Insufficient impact protection provided by vehicle	Direction of vehicle travel affects interacting structures during impact (hood vs. trunk)	Child Injury or Death

Table 9 (continued)

No.	Subsystem	Potential Mode	Potential Failure	Potential Effect
	Timing: After Crash System: Vehicle Interior			
54	Door	Child locked in, no egress	Doors do not unlock / open as required	Child injury or complications of injury
55			First responders cannot safely access vehicle interior (First responders' access to vehicle interior/occupants delayed)	Child injury or complications of injury
	Timing: After Crash System: Vehicle Exterior			
56	Vehicle & Roadway Interaction	Vehicle inoperable due to crash	Vehicle fully or partially on roadway. Vehicle cannot be moved to safe location	Potential for second crash
57		Vehicle inoperable due to crash	Vehicle fully or partially on roadway. Vehicle unable to stop or move to in safe location	Child exits into roadway
58	CSS & Vehicle Seat Interaction	CSS difficult or impossible to be released from vehicle anchorage by first responders	Damage to car seat or car seat anchorage	Potential complications to spinal / other child injury
59			Missing or unclear removal instructions	Child Injury

Table 9 (continued)

No.	Subsystem	Potential Mode	Potential Failure	Potential Effect
	Timing: After Crash System: Vehicle Exterior			
60	Emergency Notification System	First responders not aware a child is in the vehicle	Child obscured from occupant sensor or visibility	Child does not receive immediate attention
61		First responders not aware a child was in the vehicle	Child ejected from vehicle	Ejected child not accounted for. Child injury or death.
62		Sensor system does not correctly identify a crash and notify EMS	No automated assurance that help is on the way	Panic. Complications of injury. Injury due to attempted egress.
63		Caregiver, Guardian, Emergency Point of Contact not notified of crash	Vehicle Manufacturer does not have a notification system, or it is not working	Child does not receive immediate attention. Panic.

Note. EMS refers to Emergency Medical Services

3.5 Discussion

The overarching goal was to prepare a child-focused DFMEA line items that CAV software and vehicle manufacturers should incorporate into their own internal system DFMEA. The line items listed in Table 9 above can and should be used as new CAV products and features are developed, and as states, counties and municipalities provide for their real-world use and expansion. Although this DFMEA is primarily intended for CAV developers, designers, manufacturers, and policymakers, its insights may also be useful to others who are considering the implications of CAV implementation on road safety at the child, family, community, roadway system, and societal levels. By identifying hazards that may be overlooked when primarily contemplating adult vehicle users, this tool can help engineers and designers prepare for, prevent, and mitigate the potential for child injuries and fatalities.

The recommendations to the CAV industry are as follows:

1. Utilize the child-focused DFMEA throughout the development process of advancing vehicles and features.
2. Seek the input of child safety experts throughout the CAV development and design phases to ensure the safety needs of children at all stages and ages are accommodated.
3. Conduct research that helps inform appropriate levels of supervision of children in CAV.
4. Recommend that marketing and advertising for CAV shows families with children riding according to best practices and instructions.
5. Conduct testing that considers the needs of children and be transparent about such testing to instill consumer confidence that child safety is a priority.
6. Support appropriate modifications to proprietary, industry, regulatory and legislative safety standards to ensure child safety systems are incorporated into vehicles with emergent features and novel seating configurations.
7. Develop evidence-based model legislation for states that maintains protection for children of all ages.

3.6 Acknowledgements

The analysis provided in Part Four was truly an ensemble effort since it relied on the input of global experts across many industries. Valuable guidance and insights were provided by Joseph Colella, Shane Simenstad, J.T. Griffin, and Torine Creppy of Safe Kids Worldwide, as well as, expert analysis from everyone involved in the Safe Kids in Advanced Vehicles Alliance.

PART FOUR

CONTRIBUTION TO THE FIELD AND FUTURE WORK

As transportation systems and mobility technologies continue to evolve, it remains essential to address and advocate for the safety and accommodation of child occupants. The future work outlined in the following three sections identifies key areas for continued investigation, analysis, and discussion. These topics are intended to guide subsequent research efforts and also highlight the meaningful contributions this work has generated to the advancement of knowledge within the field of child injury prevention.

4.1 Contribution to the Field and Future Work for Scenario 1

The Scenario 1 study contributes meaningfully to child occupant protection by identifying, validating, and promoting a low-cost, accessible CSS configuration for transporting spica-casted children. A major outcome was the positive performance of the RideSafer Travel Vest used in combination with the BubbleBum Booster concept, which met the required FMVSS No. 213 injury thresholds. Following the presentation of these results at the 2025 Lifesavers Conference, Safe Traffic Systems, Inc., the manufacturer of the RideSafer Travel Vest, confirmed they would revise their Owner's Manual to include allowable use with spica-casted children under Safe Travel for All Children conditions. This marks a pivotal advancement in expanding commercially available solutions for special needs transportation. Future work will involve formally requesting Special Needs Use approval from the manufacturer of the BubbleBum Booster based on the findings presented in this study. If approved for use, this will help address a long-standing gap in child passenger safety by offering caregivers a validated, safe, and affordable alternative for forward-facing, spica-casted children. In addition, testing with the newer Q-series ATD is recommended due to its enhanced biofidelity relative to the earlier surrogate models from Humanetics. Future efforts should also include evaluations under side-impact loading conditions. With potential industry support, a broader test matrix could be executed to assess the effects of occupant position variability on restraint performance.

Another key contribution from this work lies in the development and validation of cast-specific dynamic simulation models that accurately replicate injury metrics observed during physical sled testing. This modeling framework opens the door for future work that includes expanding the validated models to other cast geometries. Simulations would predict injury criteria for a broader range of spica cast configurations, reducing the need for repeated physical sled tests and allowing for evaluation of other potential CSS solutions during discharge planning.

Based on the results from the verification, validation, and analysis sections of this study, a practical, decision-support tool was designed for use by hospital discharge professionals. This decision tree, presented in Appendix I, facilitates collaborative planning between Pediatric Surgeons, CPSTs with STAC training, and caregivers regarding appropriate CSS selection and installation feasibility prior to surgery. The initial presentation of the decision tree at the 2025 Lifesavers Conference received positive feedback and multiple requests for access, indicating strong practitioner interest. The tool enables tailored planning based on vehicle type, child age, and cast configuration, thus reducing transportation uncertainties post-discharge. Future planned work includes disseminating the finalized decision tree and corresponding educational materials through professional conferences, peer-reviewed publications, and digital resource libraries. Additionally, an online, interactive decision-making tool is envisioned. An interactive tool would allow its users to input parameters such as vehicle type and cast configuration to receive real-time CSS recommendations and measurement guidance. Immediate online updates would ensure medical professionals and caregivers have access to the most current evidence-based guidance and latest CSS options, potentially eliminating reliance on outdated hard-copy handouts and reducing the likelihood of defaulting to costly ambulance transport when not necessary.

In summary, this research provides data-driven solutions to a critical medical transportation challenge, sets a foundation for scalable simulation modeling for spica cast injury prediction, and introduces a novel, actionable approach for hospital-based CSS decision-making with the ultimate goal of improving safety, accessibility, and caregiver autonomy in transporting spica-casted children.

4.2 Contribution to the Field and Future Work for Scenario 2

This study advances the field of child injury prevention by providing a comprehensive, updated analysis of non-transportation injuries related to CSS use utilizing data from the NEISS database. The findings confirm that improper and/or unintended CSS use outside of the vehicle remains a significant cause of injury particularly to infants. While previous published works provided preliminary findings for infants under one year of age, the current study is the first to comprehensively report injury patterns in children aged 2 to <8 years, filling a critical gap in the literature.

The patterns identified have multiple implications for future work. First, they emphasize the need for enhanced and consistent messaging to caregivers regarding proper CSS use and discouraging use of the CSS outside of its intended purpose in the vehicle. Second, design innovations to CSS to mitigate potential injuries specifically for the injury modalities found in this study. Scenario 2 lays the groundwork for injury prevention through caregiver education and design innovation to enhance child occupant protection and reduce injury risk associated with misuse of child restraint systems.

4.3 Contribution to the Field and Future Work for Scenario 3

The study in Scenario 3 produced an innovative contribution to the field of automated vehicles and child passenger safety by developing a child-focused DFMEA intended to guide CAV manufacturers in addressing child-specific safety concerns and mitigate potential risks. By emphasizing risk assessment from a child passenger perspective, this DFMEA promotes proactive design strategies that can prevent or reduce the likelihood of injuries and fatalities among child occupants in automated vehicles.

In conclusion, future work should include the development of federal regulations that ensures children of all ages remain protected in evolving transportation modes. By incorporating child safety considerations into technical and regulatory frameworks, the CAV industry can more effectively support the safe and equitable integration of automated vehicles into roadways.

APPENDIX A

Institutional Review Board (IRB) Approvals

Figure A1

IRB Approval for Spica Casted Studies

McLaren
HEALTH CARE

Division of Scholarly Inquiry
Department of Academic Affairs
McLaren Health Care

March 9, 2024

Dear Dr. Atkinson:

Thank you for your Predetermination Request for Subject Research for your project entitled:

Spica Casted Clild Crash Dummies in Different Car Seats and Vehicle Types

Based on the information you have provided, the MHC SARC has determined that this project

☑ **DOES NOT** qualify as human subject research as outlined in 45 CFR 46.102(d) and (f) or 21 CRF56.102(c)and (e) and is not subject to oversight by the MHC IRB.

You must submit your project to the Scholarly Activity Review Committee (SARC) for further review and full approval by emailing sarc@mclarenmeded.org and carlos.rios@mclaren.org. **MHC SARC full approval is required prior to the commencement of any non-human subject research.** Although this project does not fall under the oversight of the MHC IRB, you still need to follow other institutional policies. It is also recommended that you consult with any departments that may be impacted by your project to ensure any departmental requirements are met." **Please be advised, it is your responsibility to consult with the SARC, in writing, if any changes are made in the project's current design, procedures, etc. Such changes may necessitate a new complete pre-determination submission. It may change it to human subject research. Do not implement changes until approved.**

☐ **DOES** fit the definition of human subjects research requiring MHC IRB approval / oversight (45 CFR 46).

Activities that meet the federal definitions for both "research" and "human subjects" must be submitted to the MHC IRB for review via the iRIS electronic submission system. Additionally, interventional studies must be reviewed and approved by the McLaren Center for Research and Innovation Protocol Review Committee (MCRI PRC). **MHC IRB approval is required prior to the commencement of any human subject research.**

If needed, please contact the IRB at (248) 484-4950, or via e-mail at hrpp@mclaren.org, to learn how to proceed with a formal submission to the MHC IRB using iRIS. **Please be advised, it is your responsibility to consult with the IRB, in writing, if any changes are made in the project's current design, procedures, etc. Such changes may necessitate a new complete IRB submission. Do not implement changes until approved.**

This letter also confirms the soundness of the research design and the ability of the research to achieve its aims.

IMPORTANT: This pre-determination expires after SIX months from the date the letter is issued. After SIX months without a submission to the SARC, a new pre-determination application must be submitted.

Sincerely,

HSR Predetermination Committee
Carlos F. Rios-Bedoya, M.P.H., Sc.D.
Robert F Flora, MD, MBA, MPH

Scholarly Activity Review Committee
MHC Division of Scholarly Inquiry

One McLaren Parkway .Grand Blanc, Michigan 48439 • email: mhc.sarc@mclarenmeded.org

Version 3. Updated 2/9/24

APPENDIX B

Scholarly Activity Review Committee (SARC) Approvals

Figure B1

SARC Approval for Spica Casted Studies

McLaren HEALTH CARE

APPROVED
By SARC at 5:00 pm, May 03, 2024

McLaren Health Care Scholarly Activity Review Committee (SARC) Review

RE: Spica Casted Child Crash Dummies in Different Car Seats and Vehicle Types (Protocol 202403-09).

Dear Dr. Atkinson,

Thank you for submitting the application for the above-referenced project. The SARC committee determined that the protocol meets the criteria for SARC Review and approved it without stipulations. The MHC SARC will be notified of this action at the next scheduled meeting. Reviewers' comments are attached for your consideration.

All research must be conducted in accordance with the Health Insurance Portability and Accountability Act (HIPAA), as well as McLaren Health Care Policies, Guidelines, and Procedures.

ALL INVESTIGATORS MUST COMPLY WITH THE FOLLOWING:

1. Use only current SARC approved tools (questionnaires, letters, advertisements, etc.) and data collection forms.
2. Submit any changes to your project that might impact the SARC determination immediately.
3. Approval will be for a period of twelve months.
    - At the end of the twelve-month period, if your project has been completed, abandoned, discontinued, or not completed for any reason, you must submit a final report to MHC SARC.
    - At the end of the twelve-month period, if you intend to continue the project you should submit an email notification to sarc@mclarenmeded.org. **If no notification is sent it will be considered to be administratively closed.**
4. Notify the MHC SARC office immediately in the event of any unforeseen incidents that might affect your project or the privacy or confidentiality of the data.

IMPORTANT REMINDERS:

1. This approval may be revoked at any time if any of the SARC requirements as outlined in the most updated version of the MHC Graduate Medical Education Policy and Procedure Manual are not followed.
2. The PI is responsible for ensuring that all personnel comply with institutional policies and have current **CITI training prior to and during participation in this project**.
3. Investigators are expected to adhere to ethical principles for non-human subject research and QI projects:
    - Acting in accordance with relevant professional standards and codes of conduct as generally accepted in the relevant academic and/or professional disciplines(s).
    - Ensuring that information is collected in an ethical manner.
    - Protecting the Privacy and Confidentiality of participants by taking appropriate safeguards for security and confidentiality.
4. All projects may be subject to be audited as determined by the MHC SARC Committee /Chair.

If you have questions, contact the SARC via e-mail at sarc@mclarenmeded.org

We wish you luck with your project.

Jacek Cholewicki, PhD
McLaren Health Care SARC Chair

April 30, 2024
Date

This approval is independent of the McLaren Health Care Institutional Review Board.

Figure B2

SARC Approval for Non-Vehicle Use of CSS Studies

McLaren
HEALTH CARE

APPROVED
By SARC at 10:28 am, Jan 12, 2024

NOTICE OF MHC SARC REVIEW

RE: Injuries due to Non-Vehicle Use of Infant Car Seats (Protocol 202312-06).

Dear Dr. Srivastava:

Thank you for submitting the application for the above-referenced project. The SARC committee determined that the protocol meets the criteria for SARC Review and approved it without stipulations. The MHC SARC will be notified of this action at the next regularly scheduled meeting. Reviewers' comments are attached for your consideration.

All research must be conducted in accordance with all applicable Department of Health and Human Services regulations 45 CFR 46, Food and Drug Administration regulations 21CFR 50, 21CFR 56, 21 CFR 312, 21 CFR 812, 21 CFR 814 Subpart H (when applicable), and the Health Insurance Portability and Accountability Act (HIPAA).

ALL INVESTIGATORS MUST COMPLY WITH THE FOLLOWING:

1. Use only current SARC approved tools (questionnaires, letters, advertisements, etc.) and data collection forms.
2. Submit a Continuing Review application at least one-month prior to the study expiration dateto continue research activities.
3. Submit a Final Report to the SARC when the study is completed.
4. Submit a Modification and obtain pre-approval from MHC SARC for any changes in research.
5. Notify the MHC SARC office immediately if any problems / issues occur during the conduct of research that may increase the risk to subjects.

IMPORTANT REMINDERS:

1. This approval may be recalled at any time if SARC Policies and Procedures are not followed.
2. The PI is responsible for ensuring that all personnel comply with institutional policies and have current McLaren-required training prior to and during participation in this project.
3. All research studies are expected to conform to Good Clinical Practice (GCP) guidelines.
4. All studies are subject to audit by the Office of Research Compliance and/or Institutional Review Board to confirm adherence to institutional, state, and federal regulations.

If you have questions, contact the SARC via e-mail at sarc@mclarenmeded.org

Good luck with your project.

Jacek Cholewicki, PhD
McLaren Health Care SARC Chair

January 10, 2024
Date

Reviewers' comments:

1. This is an interesting study. Such information has not been presented over 10 years.
2. Considering the length of time the data represents, there may be some opportunity to describe the injury rates over the COVID-19 pandemic (if applicable).

APPENDIX C

Kistler CrashDesigner Test Analysis Reports for Trials A-D

Figure C1

Trial A, Sled Acceleration, 010000

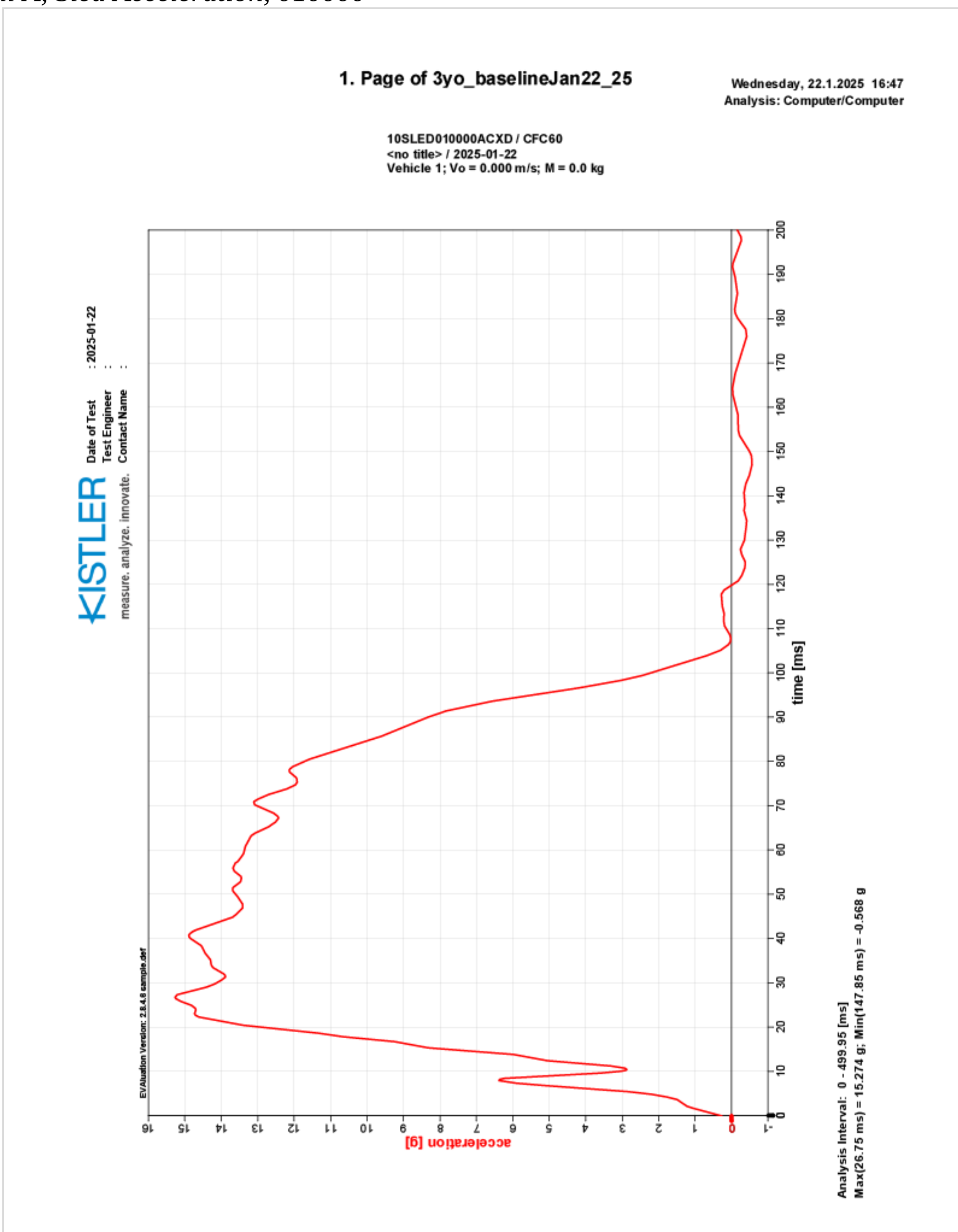

Figure C2

Trial A, Velocity and Displacement Integration, 010000

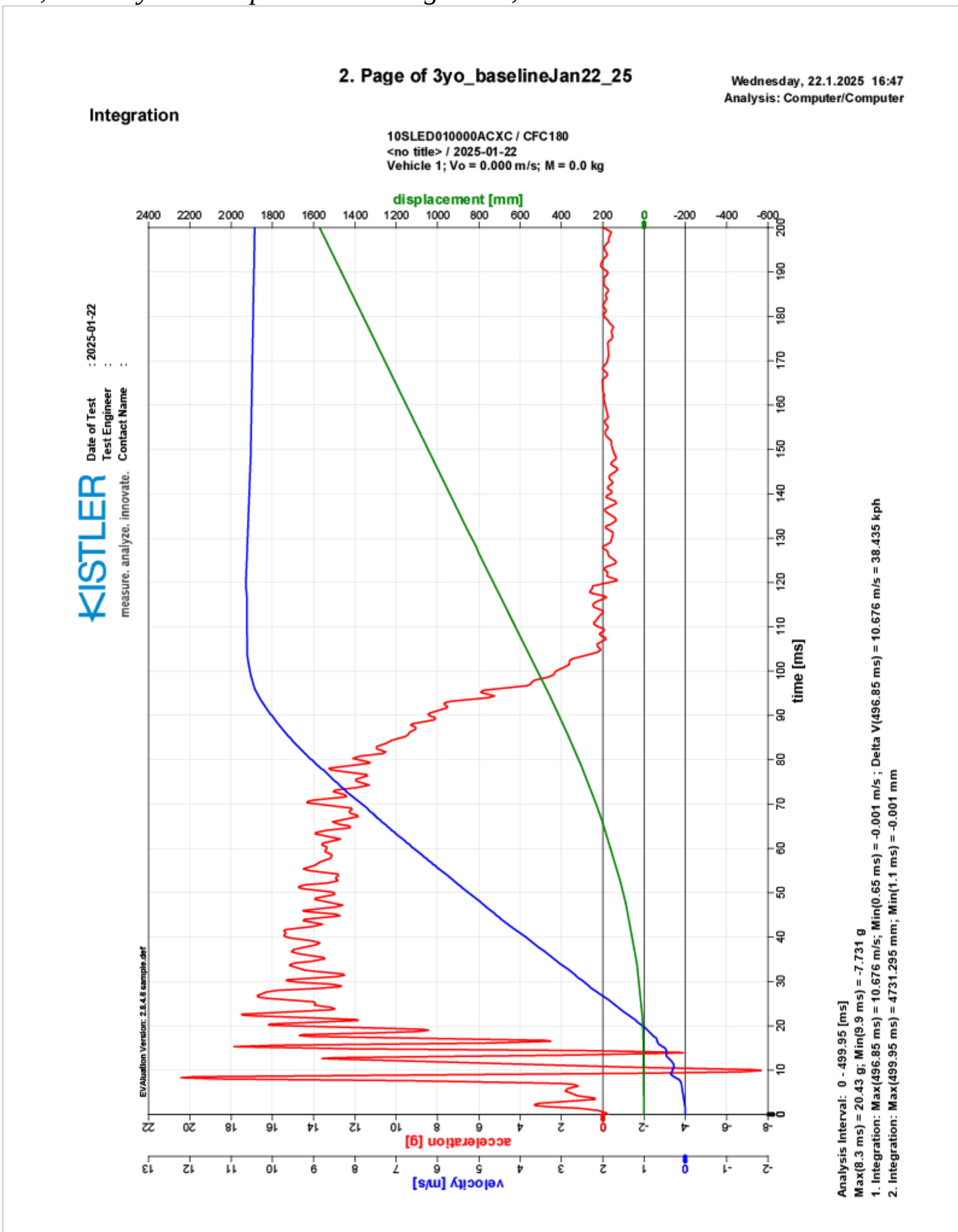

Figure C3

Trial A, Sled Acceleration, 020000

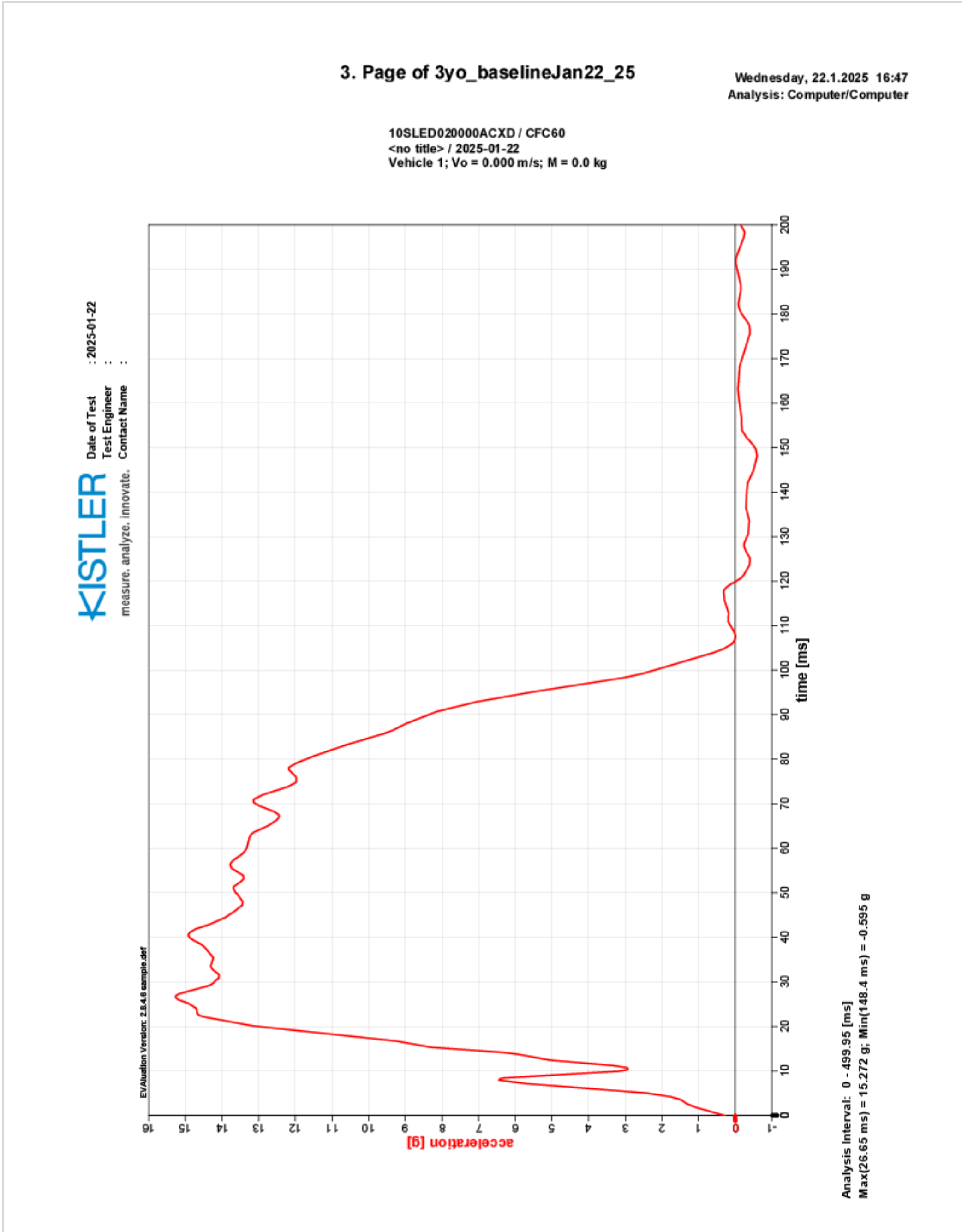

Figure C4

Trial A, Velocity and Displacement Integration, 020000

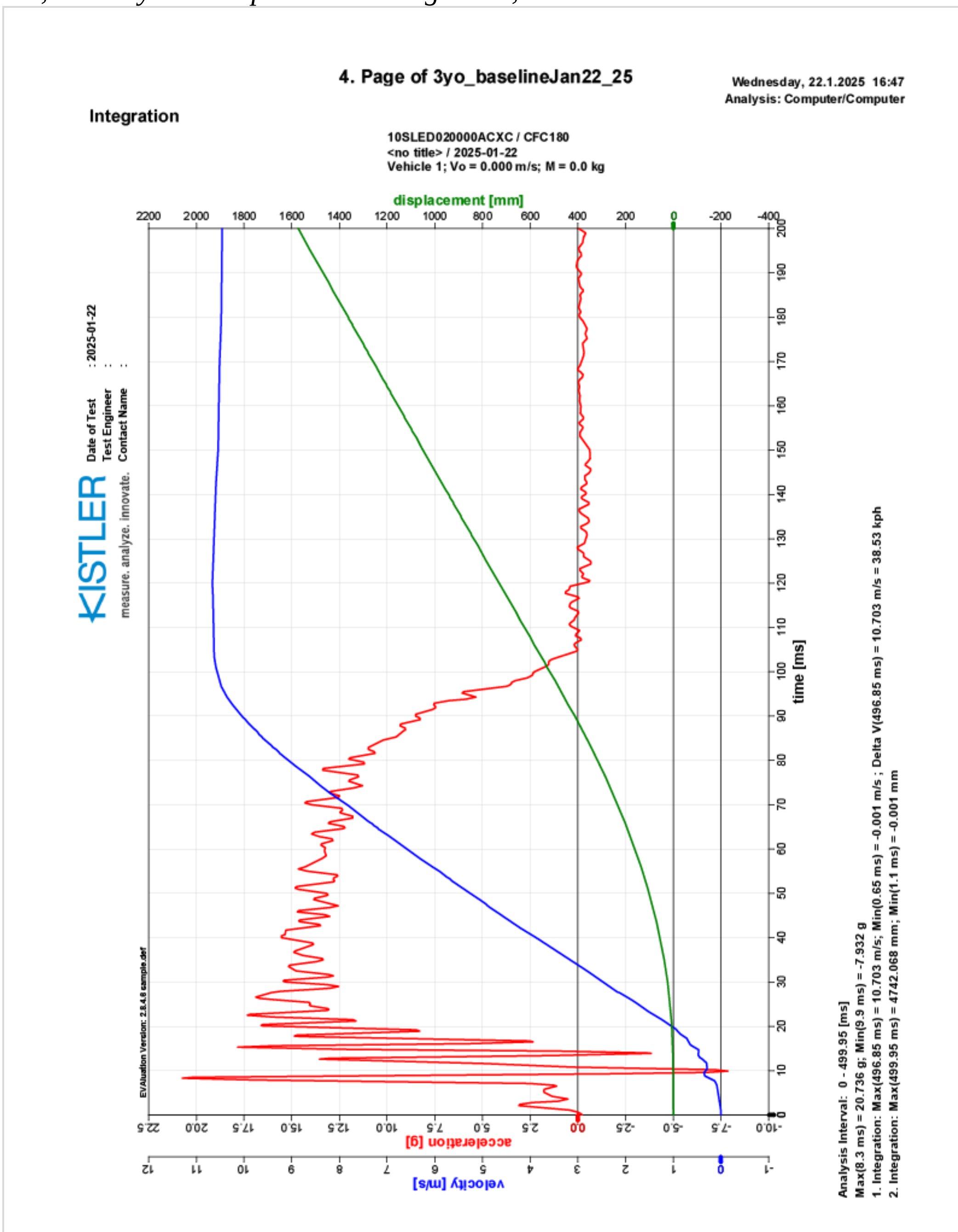

Figure C5

Trial A, Head Acceleration Resultant

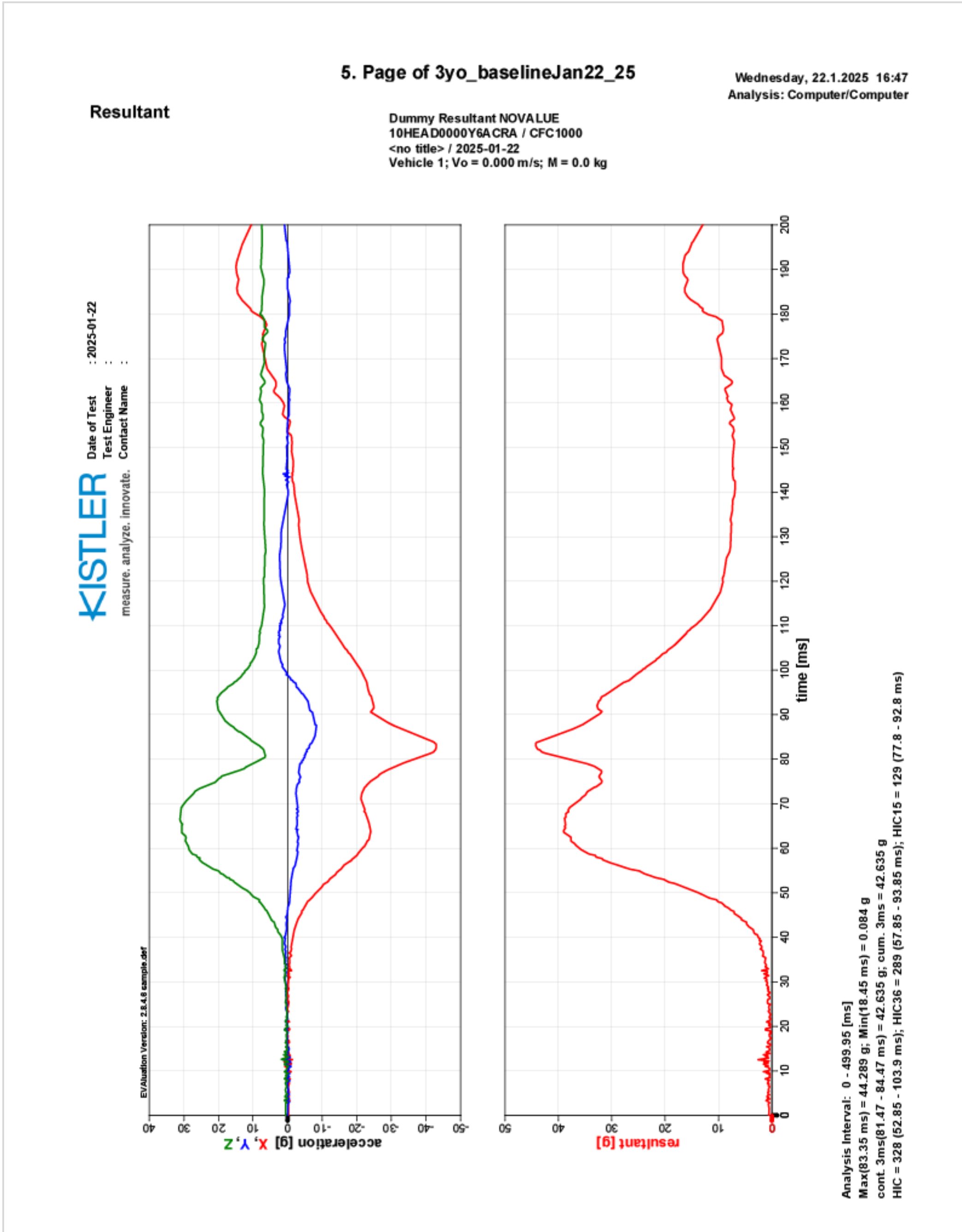

Figure C6

Trial A, Head Acceleration, X-axis

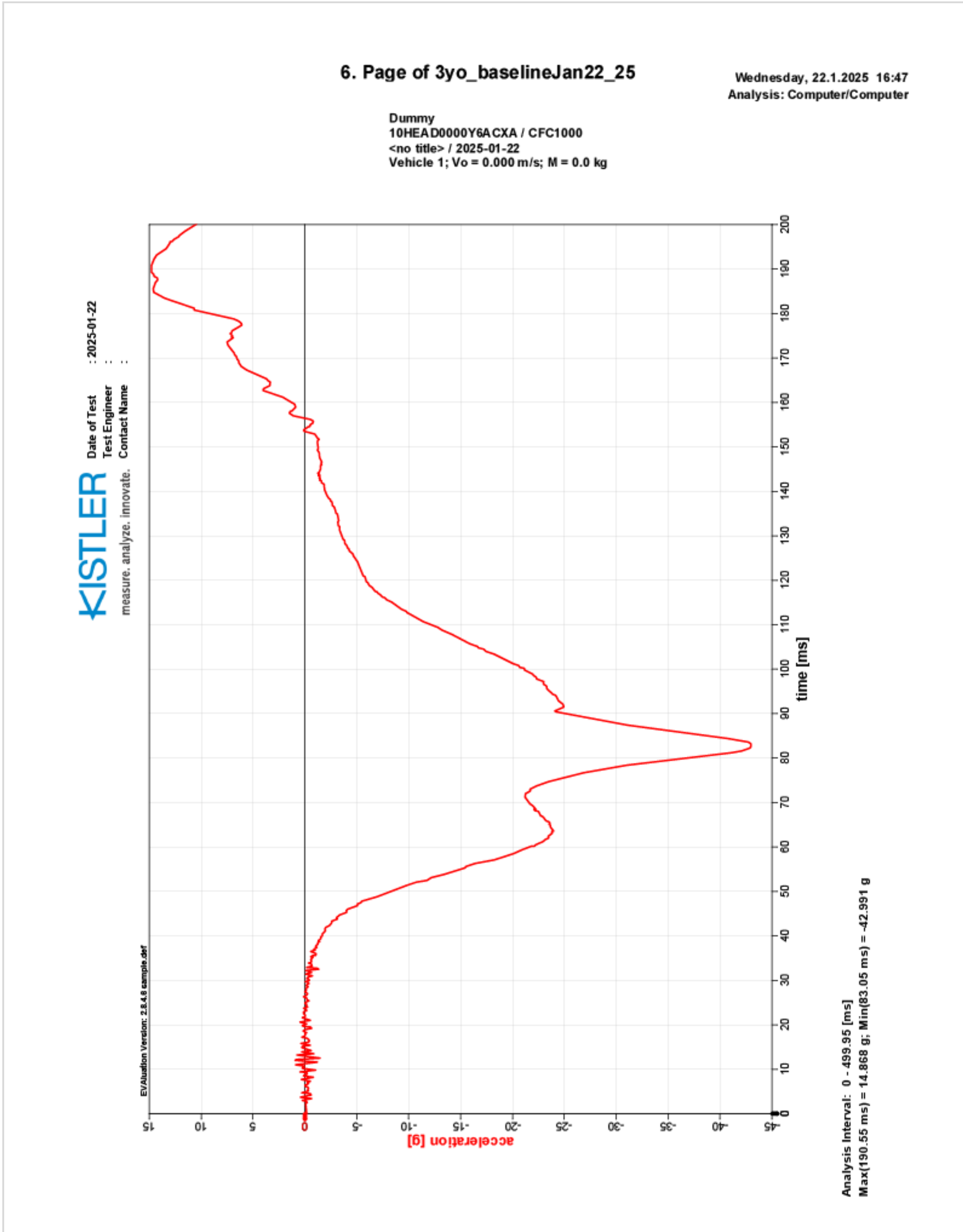

Figure C7

Trial A, Head Acceleration, Y-axis

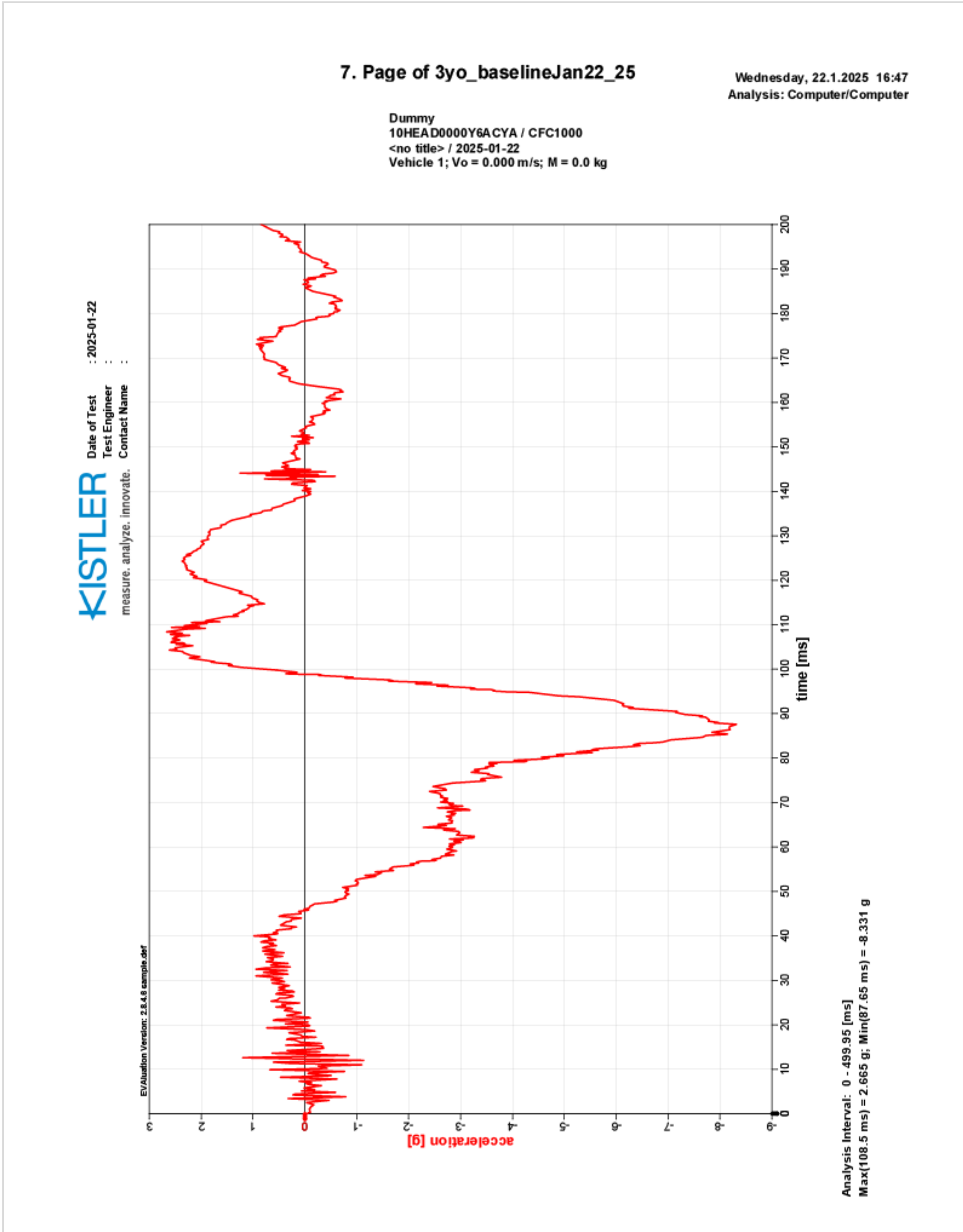

Figure C8

Trial A, Head Acceleration, Z-axis

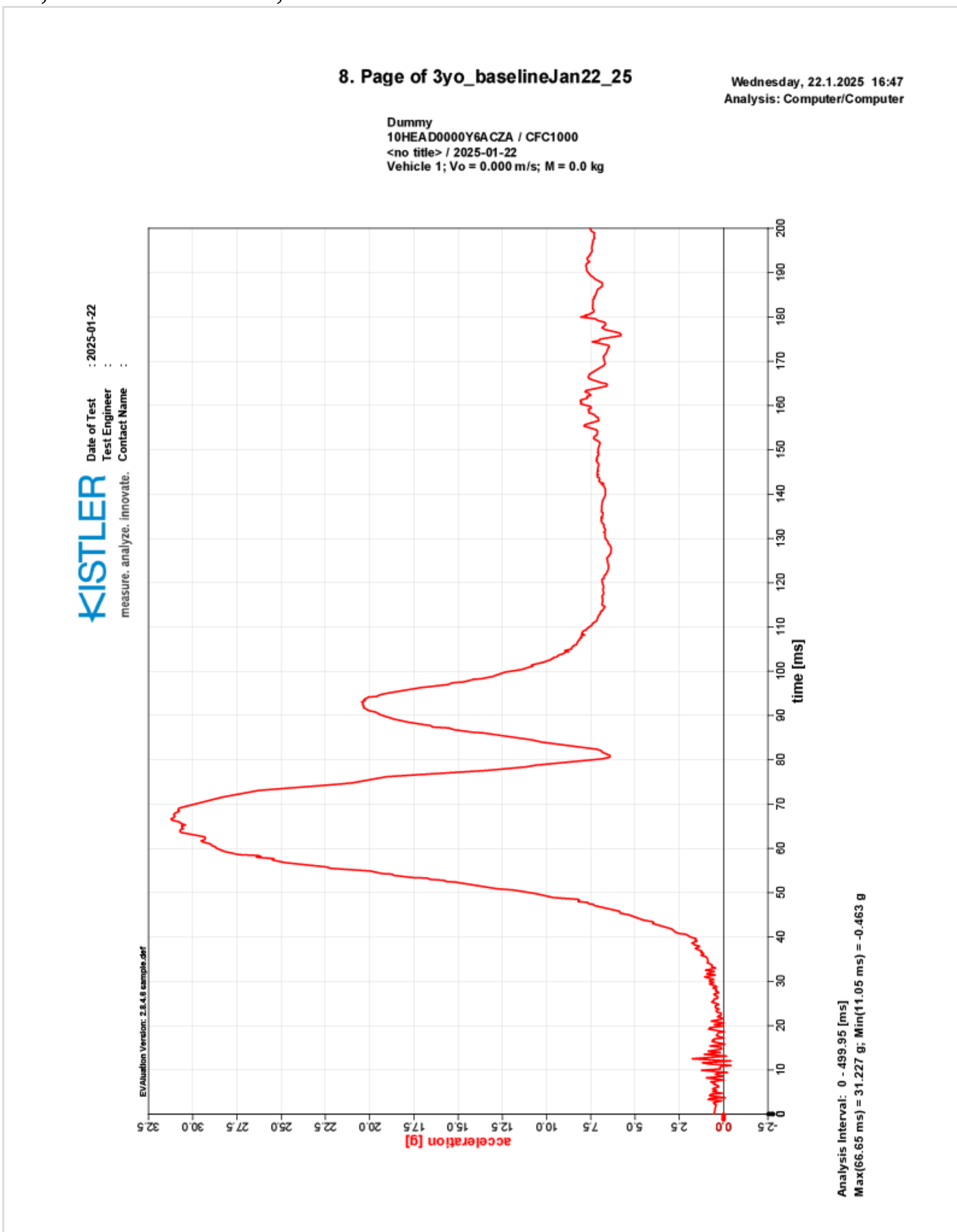

Figure C9

Trial A, Chest Acceleration Resultant

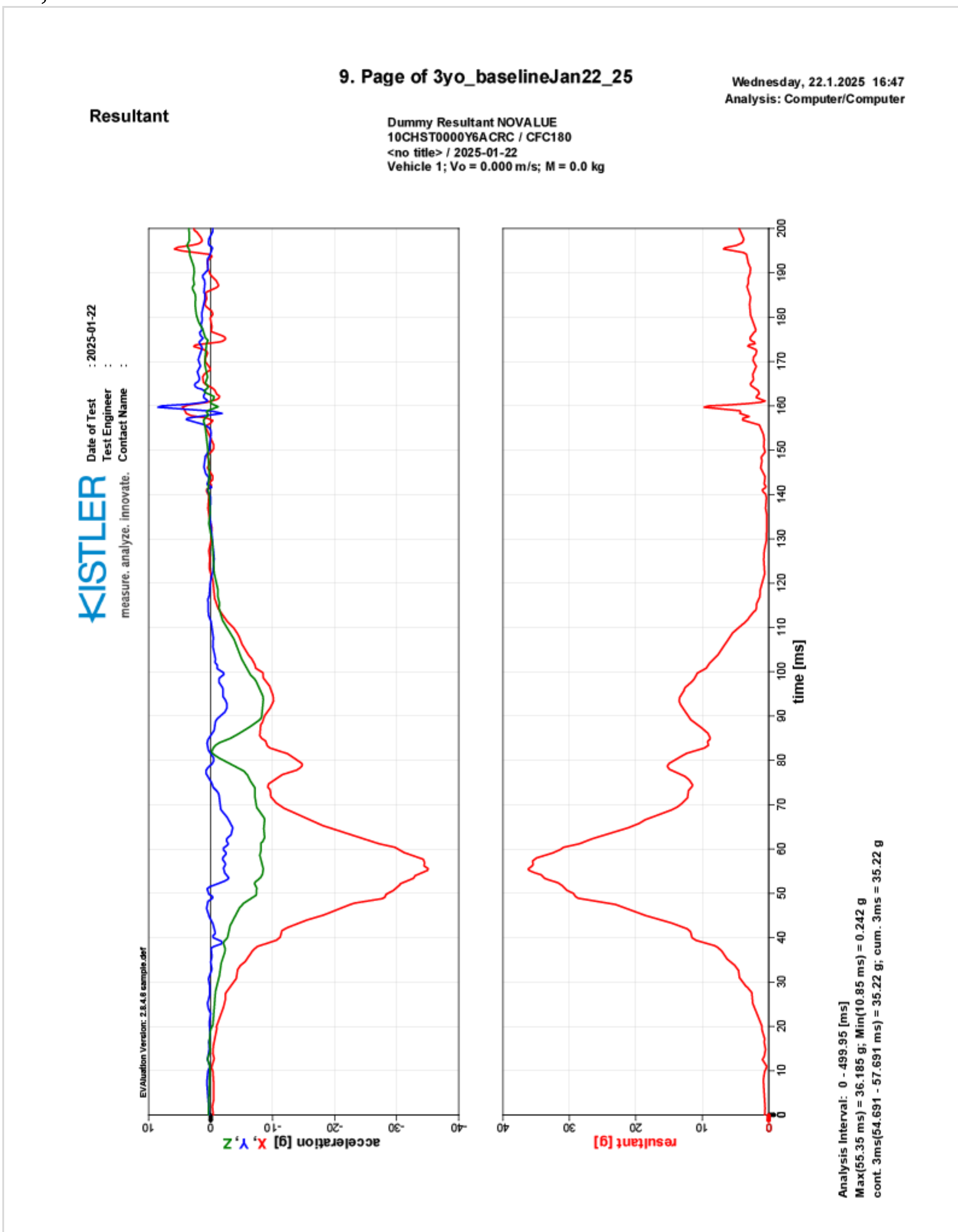

Figure C10

Trial A, Chest Acceleration, X-axis

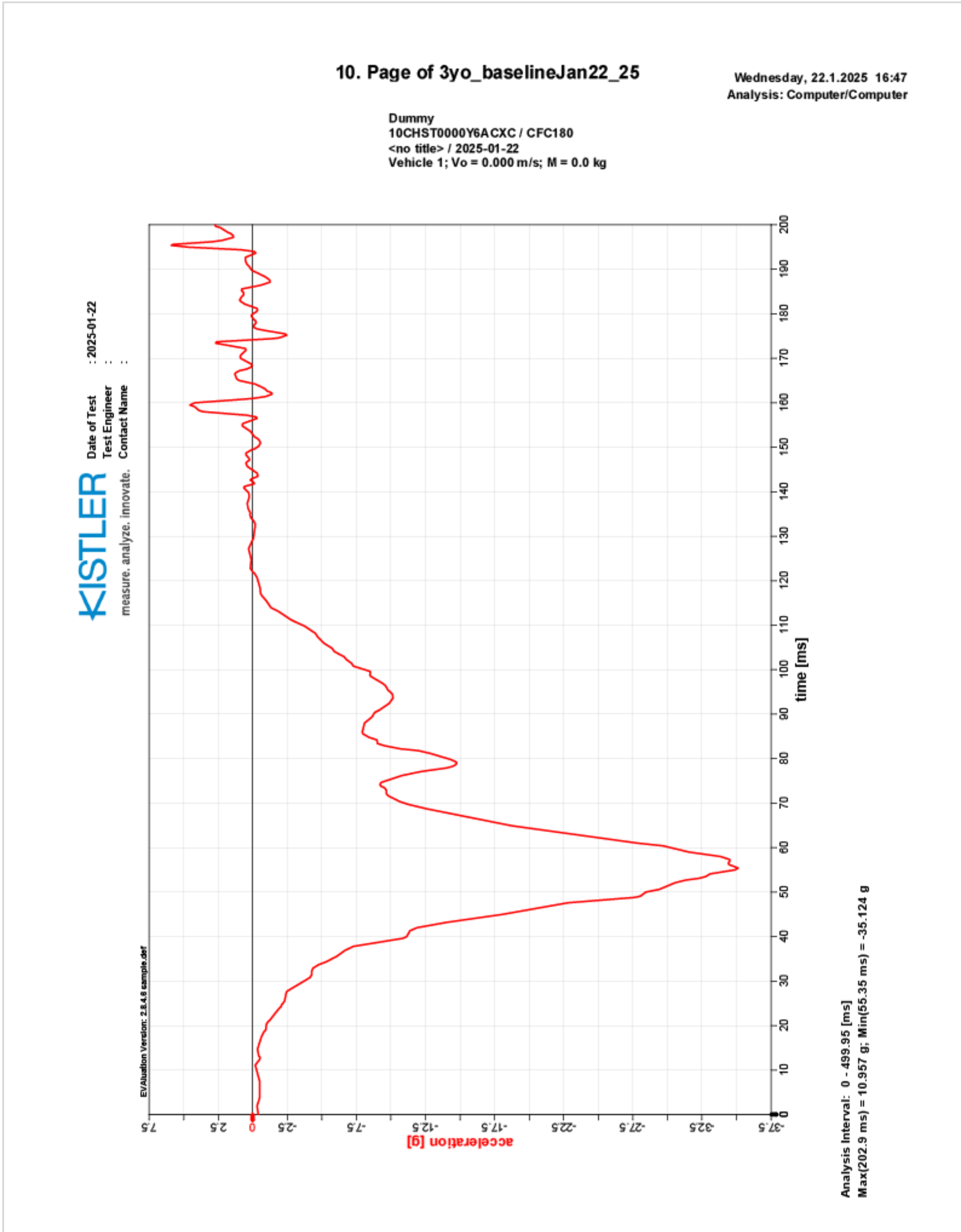

Figure C11

Trial A, Chest Acceleration, Y-axis

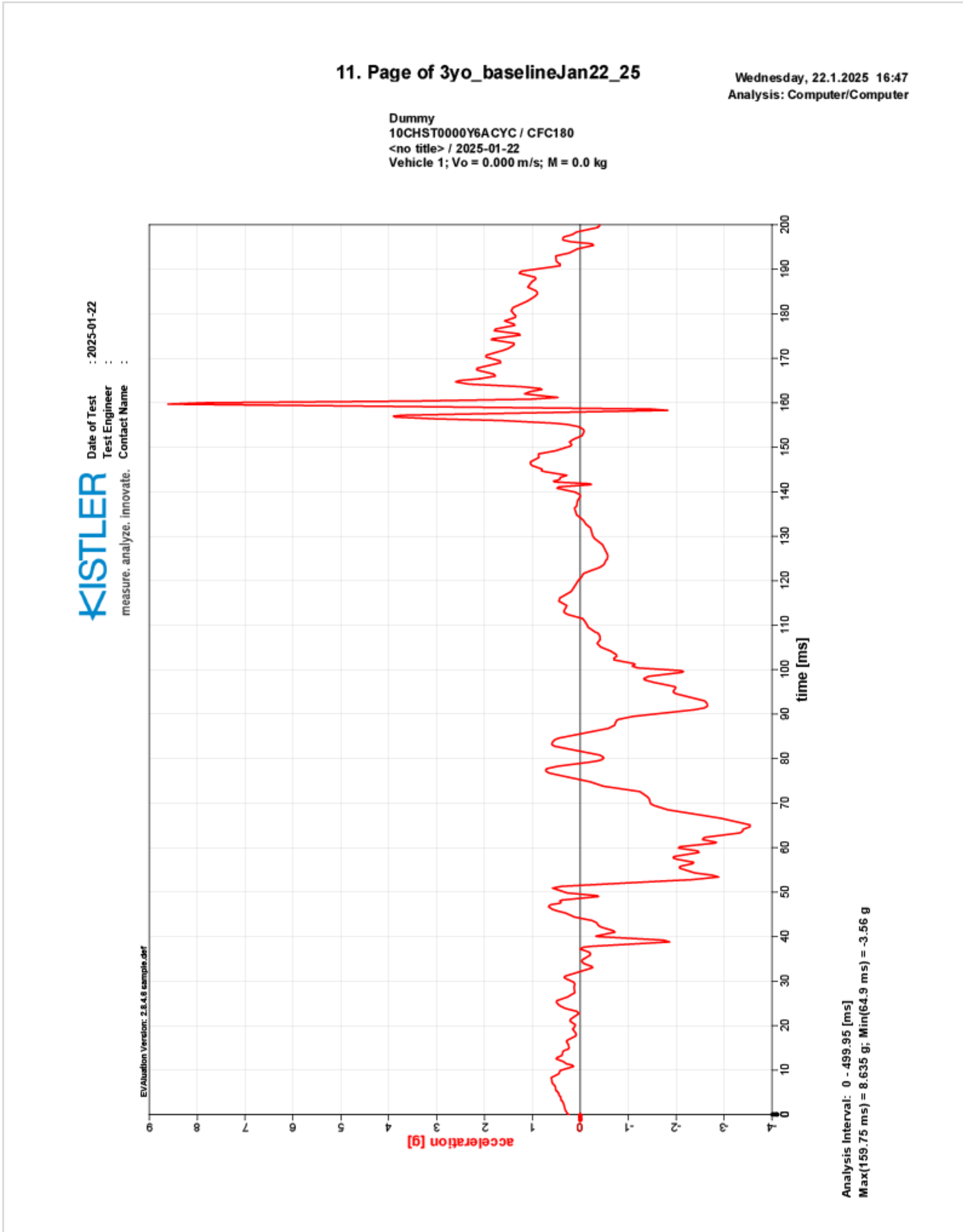

Figure C12

Trial A, Chest Acceleration, Z-axis

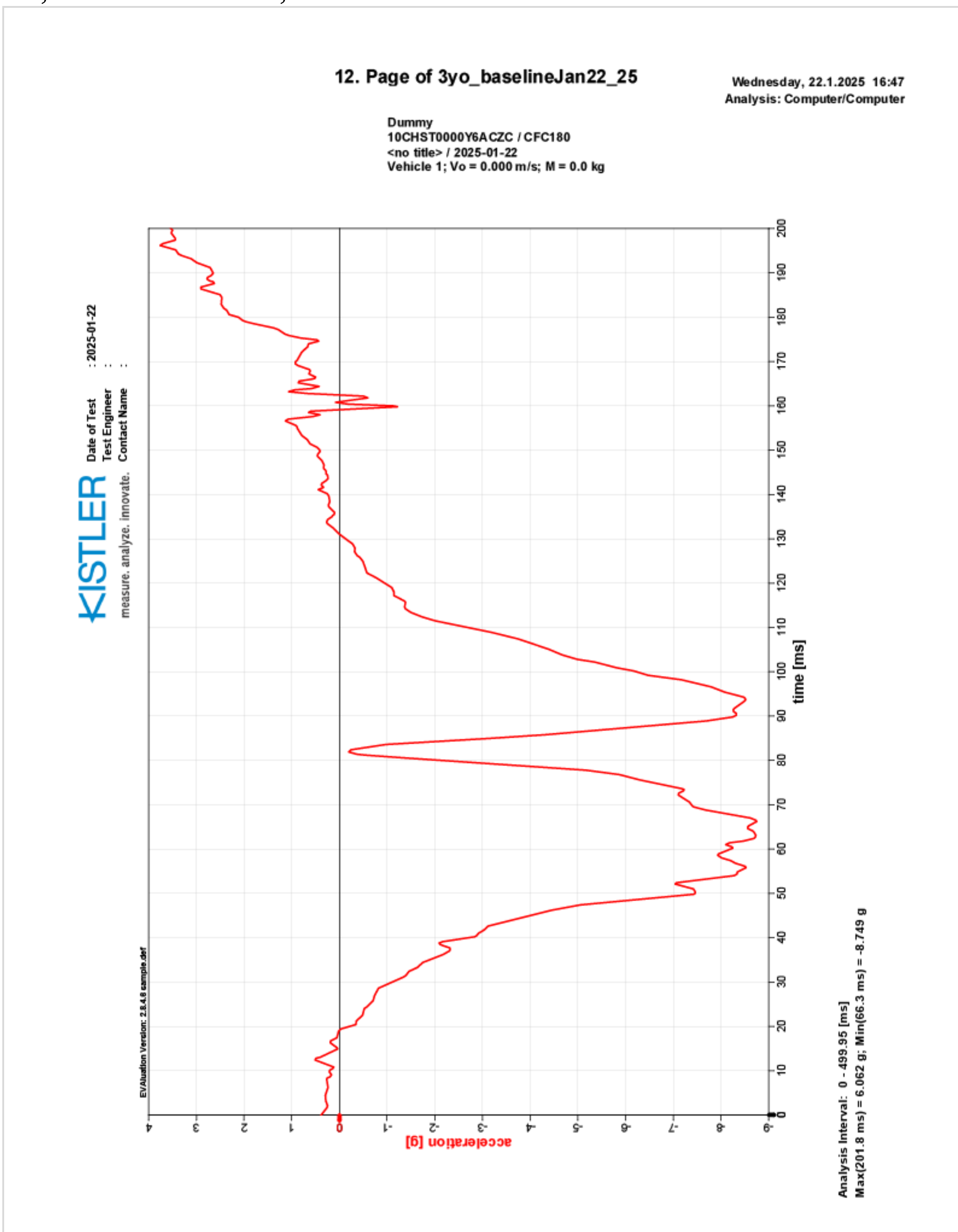

Figure C13

Trial B, Sled Acceleration, 010000

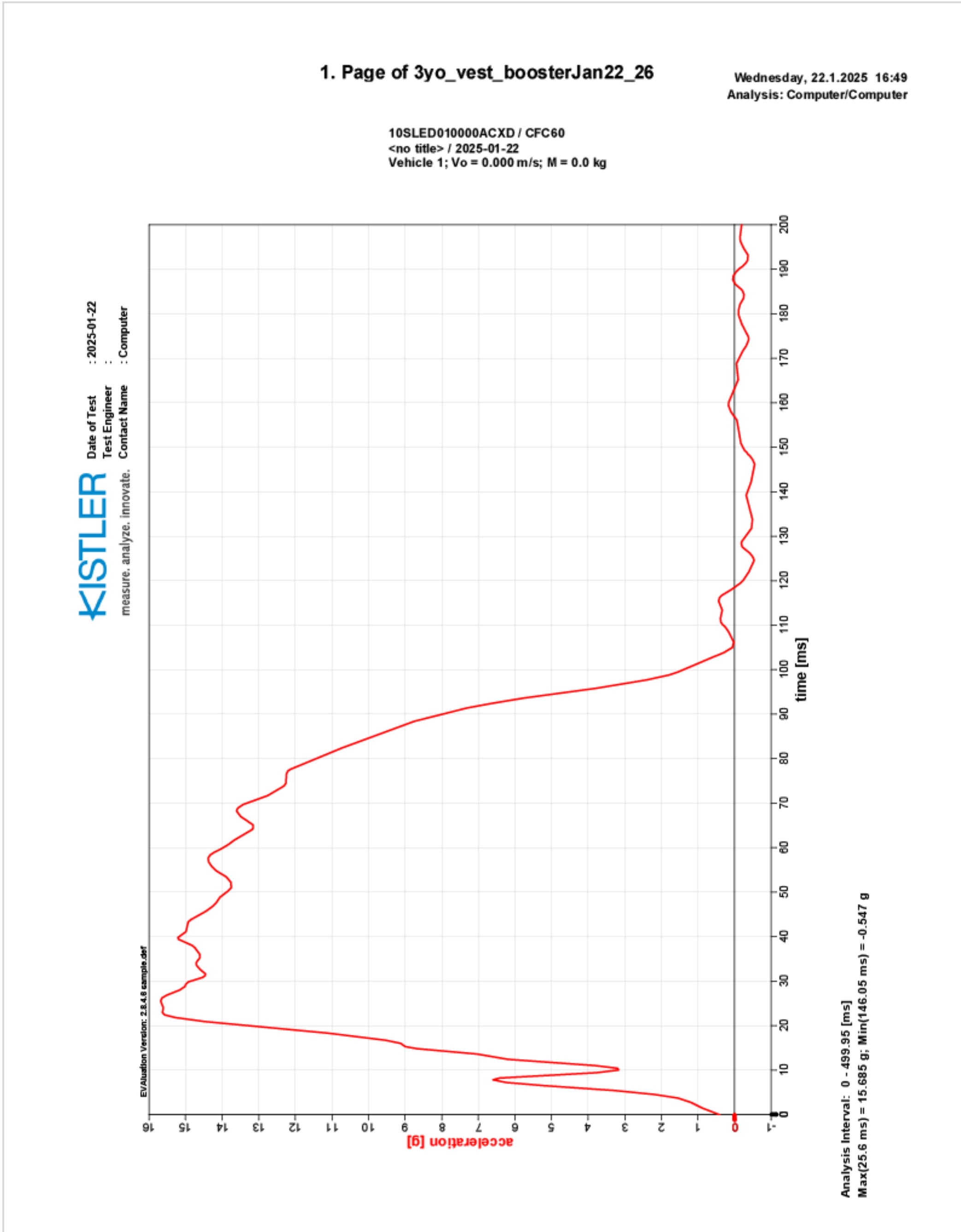

Figure C14

Trial B, Velocity and Displacement Integration, 010000

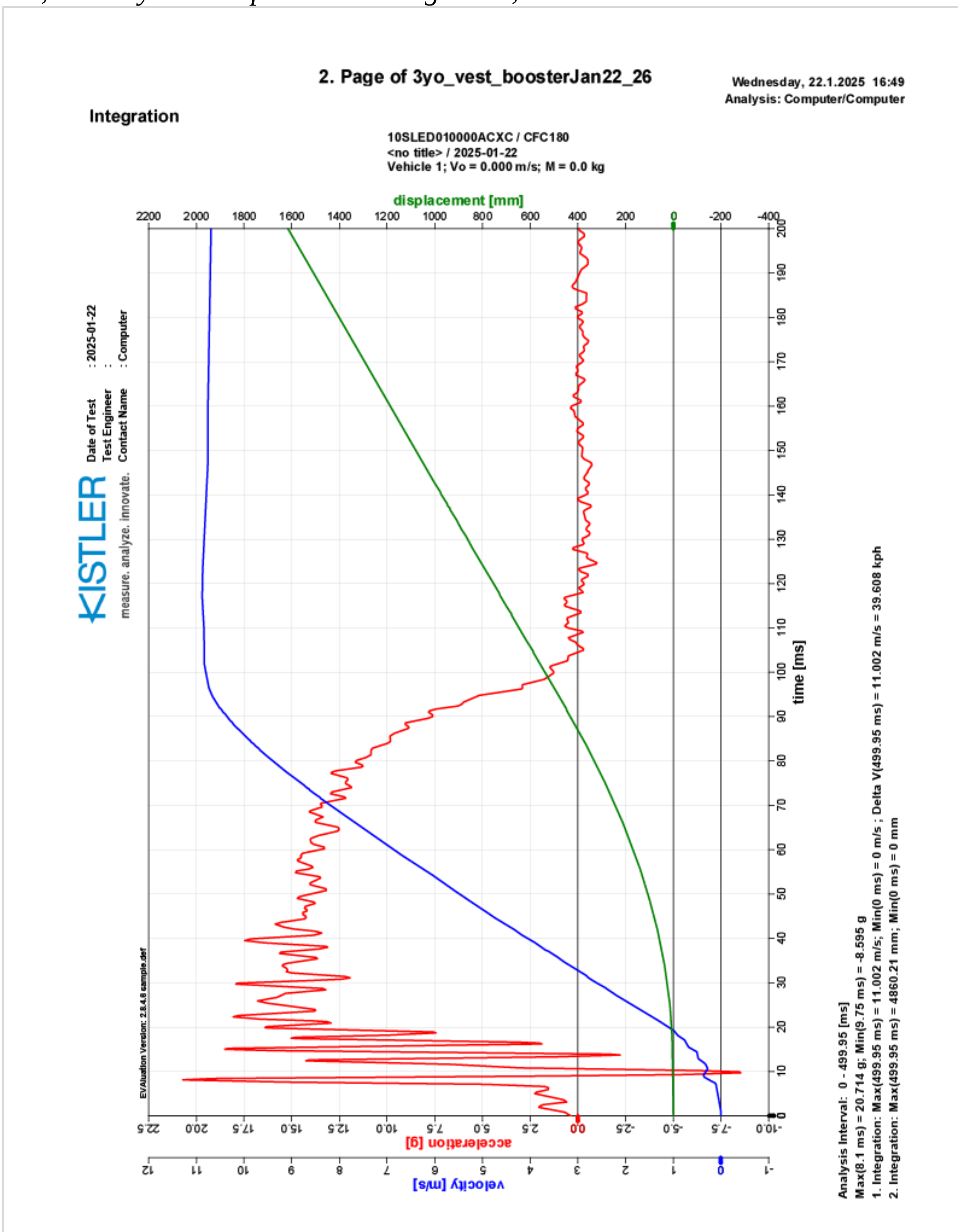

Figure C15

Trial B, Sled Acceleration, 020000

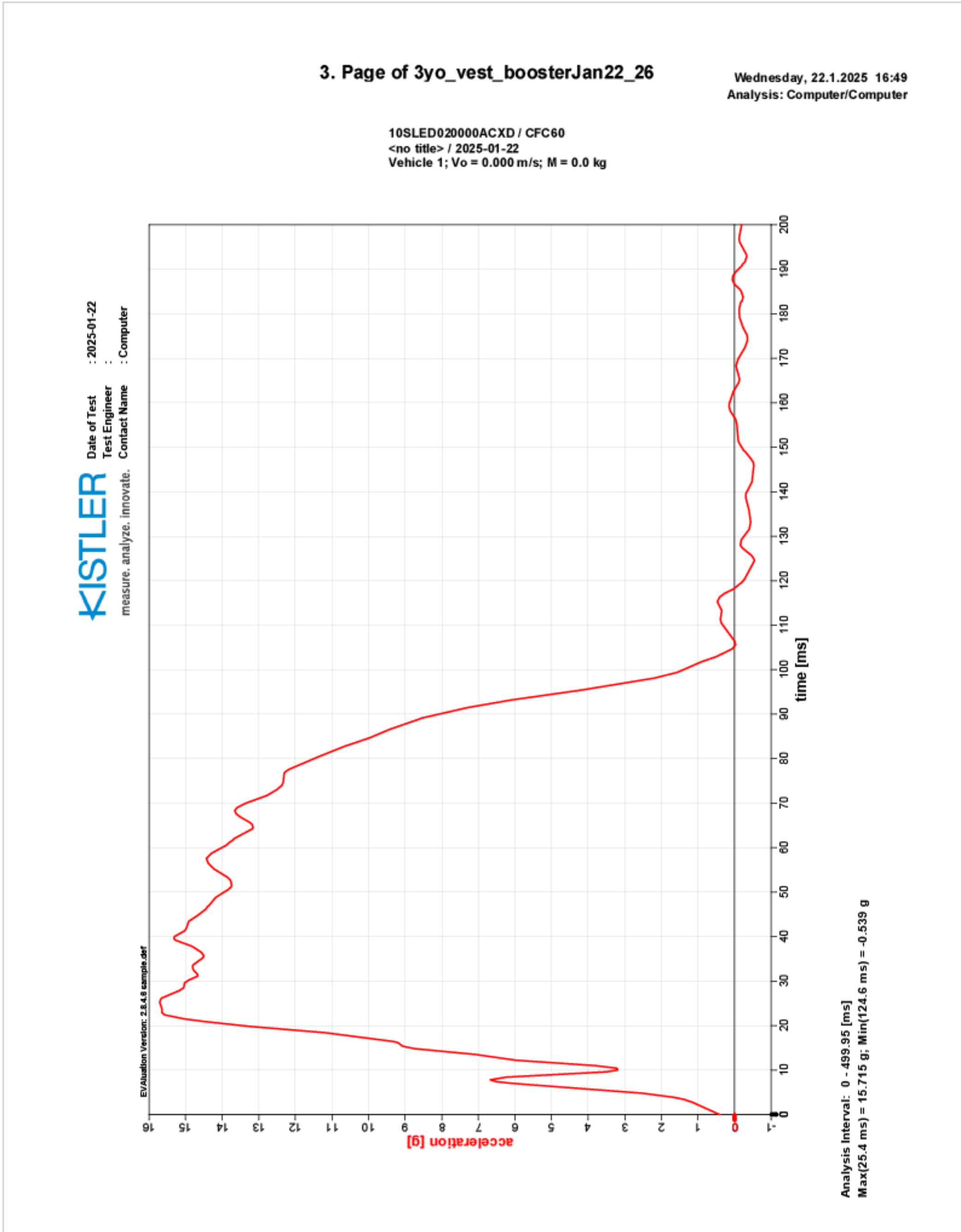

Figure C16

Trial B, Velocity and Displacement Integration, 020000

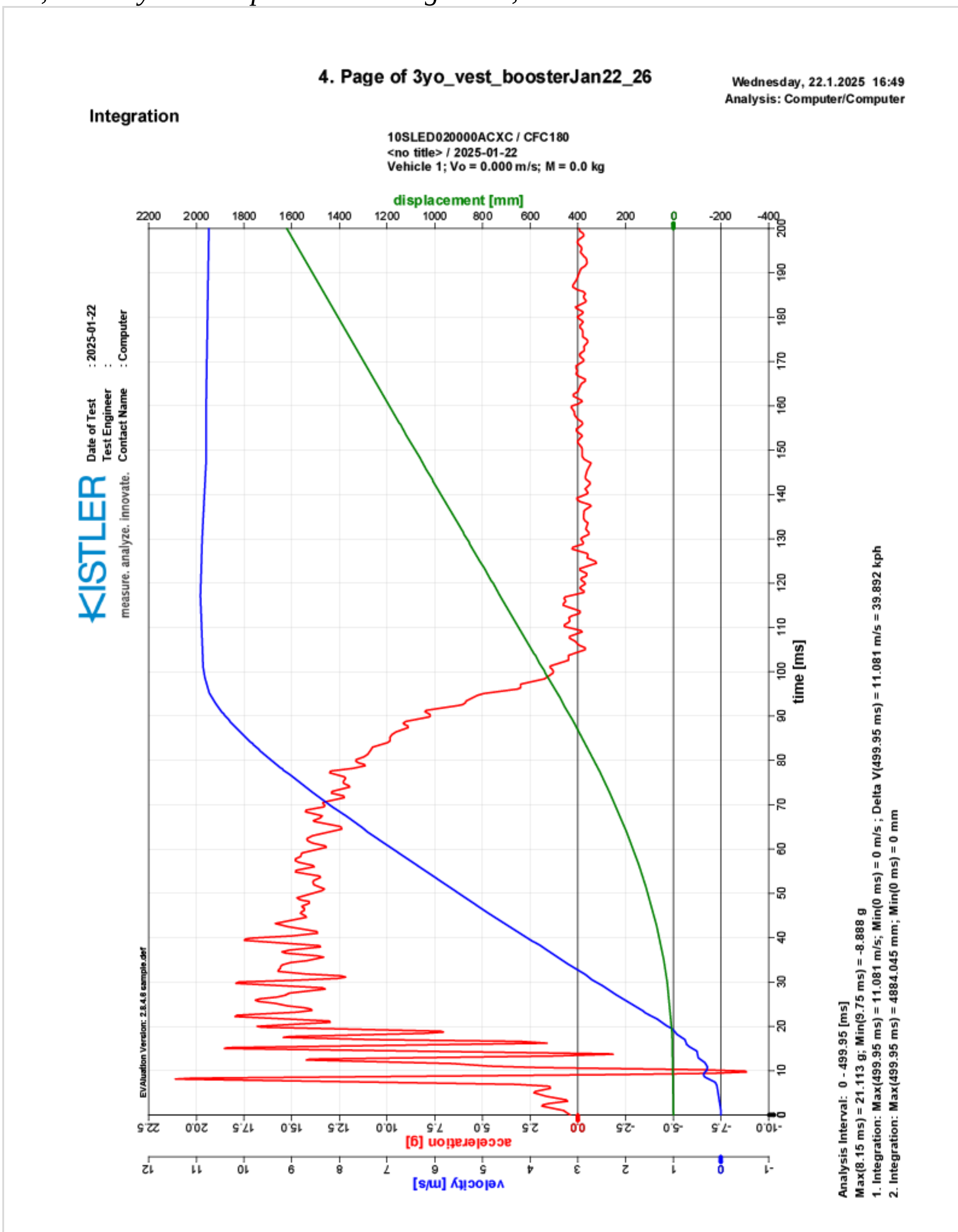

Figure C17

Trial B, Head Acceleration Resultant

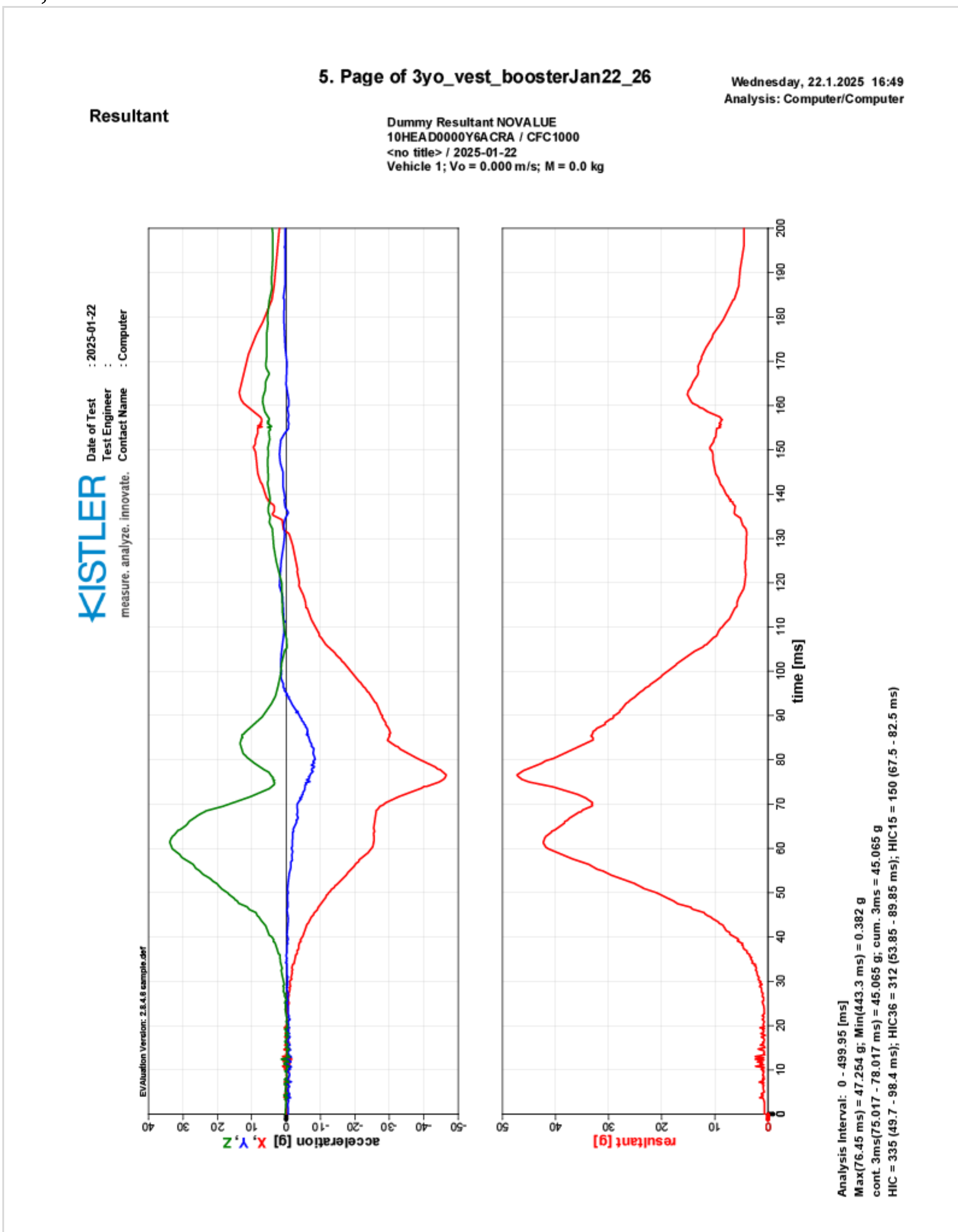

Figure C18

Trial B, Head Acceleration, X-axis

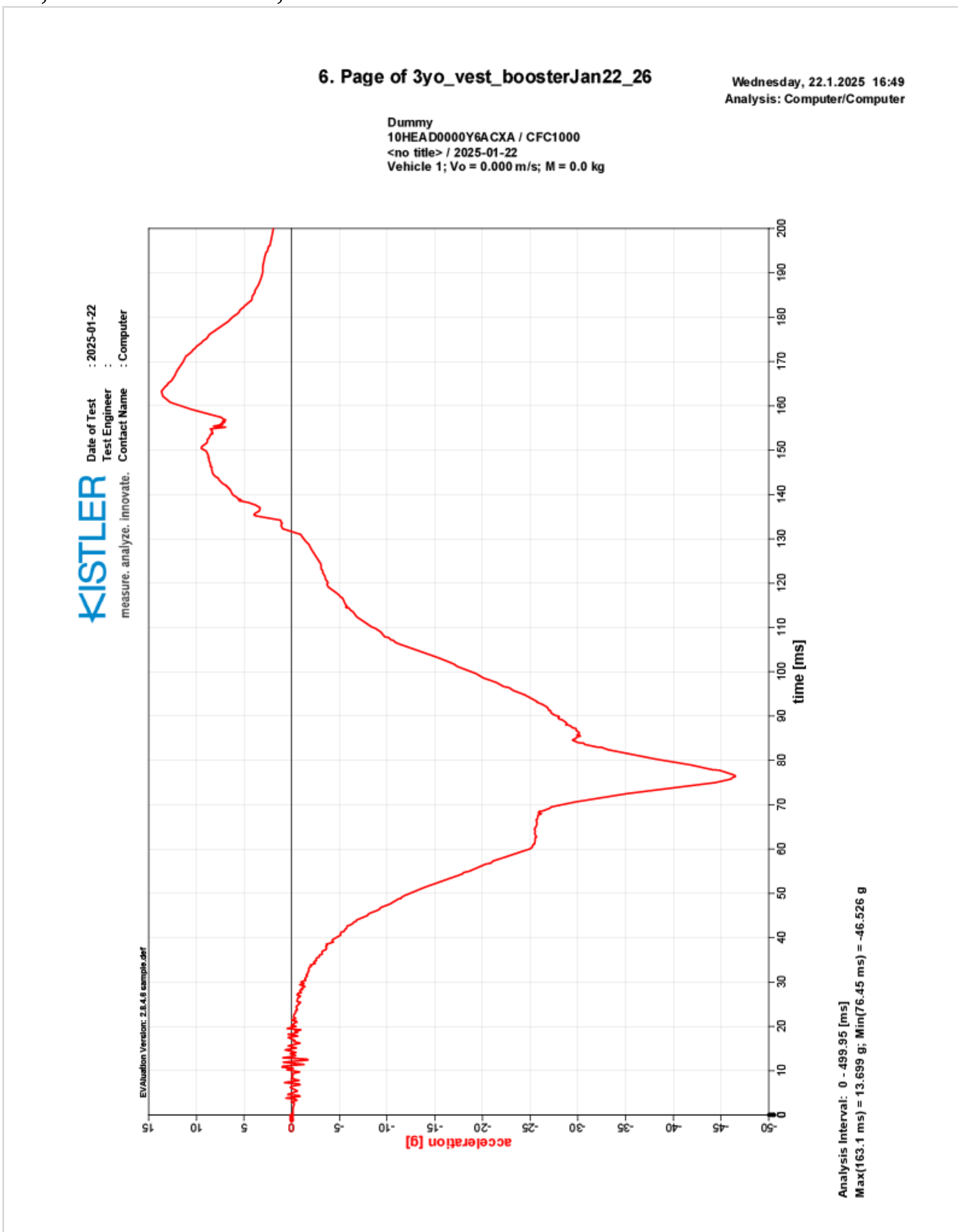

Figure C19

Trial B, Head Acceleration, Y-axis

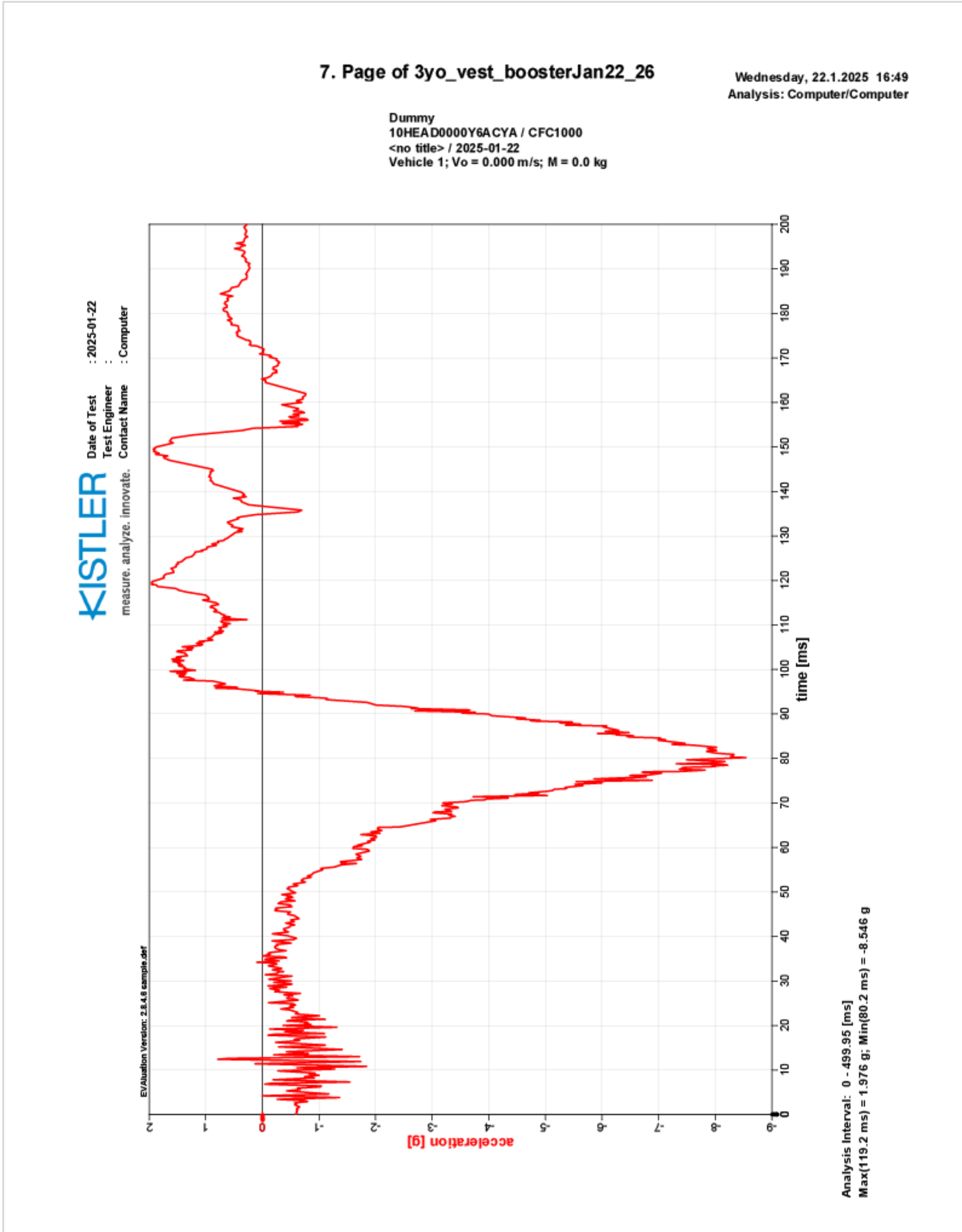

Figure C20

Trial B, Head Acceleration, Z-axis

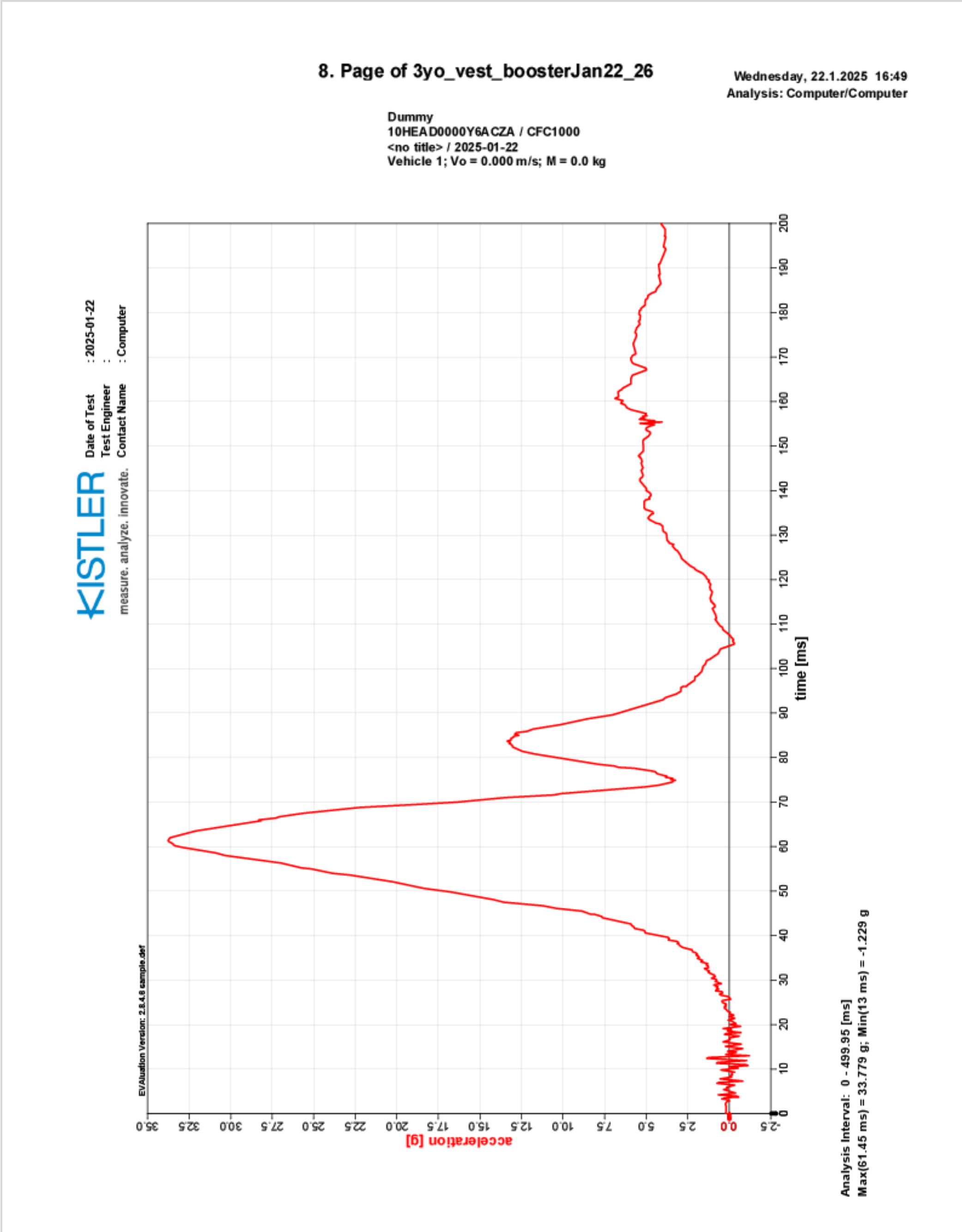

Figure C21

Trial B, Chest Acceleration Resultant

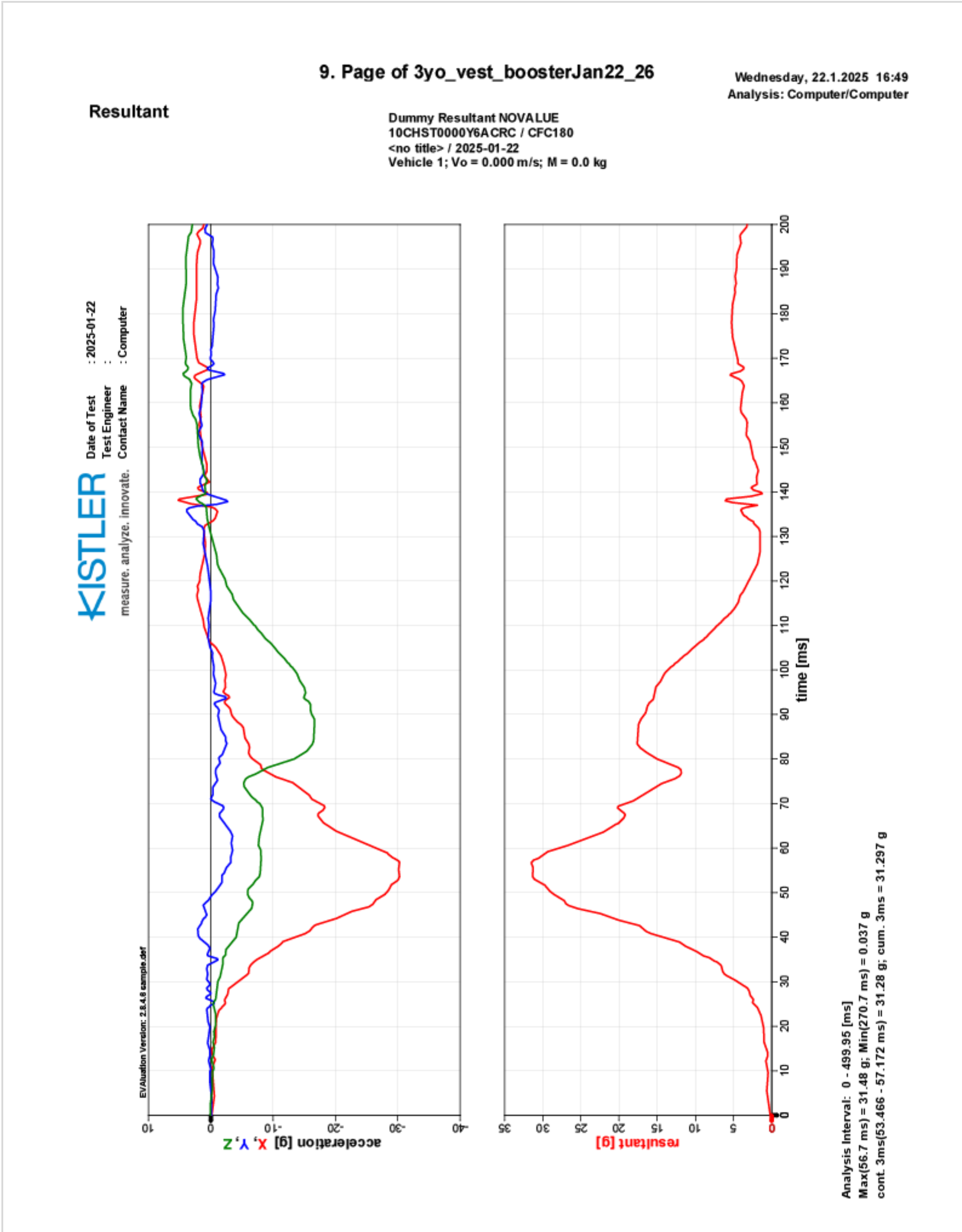

Figure C22

Trial B, Chest Acceleration, X-axis

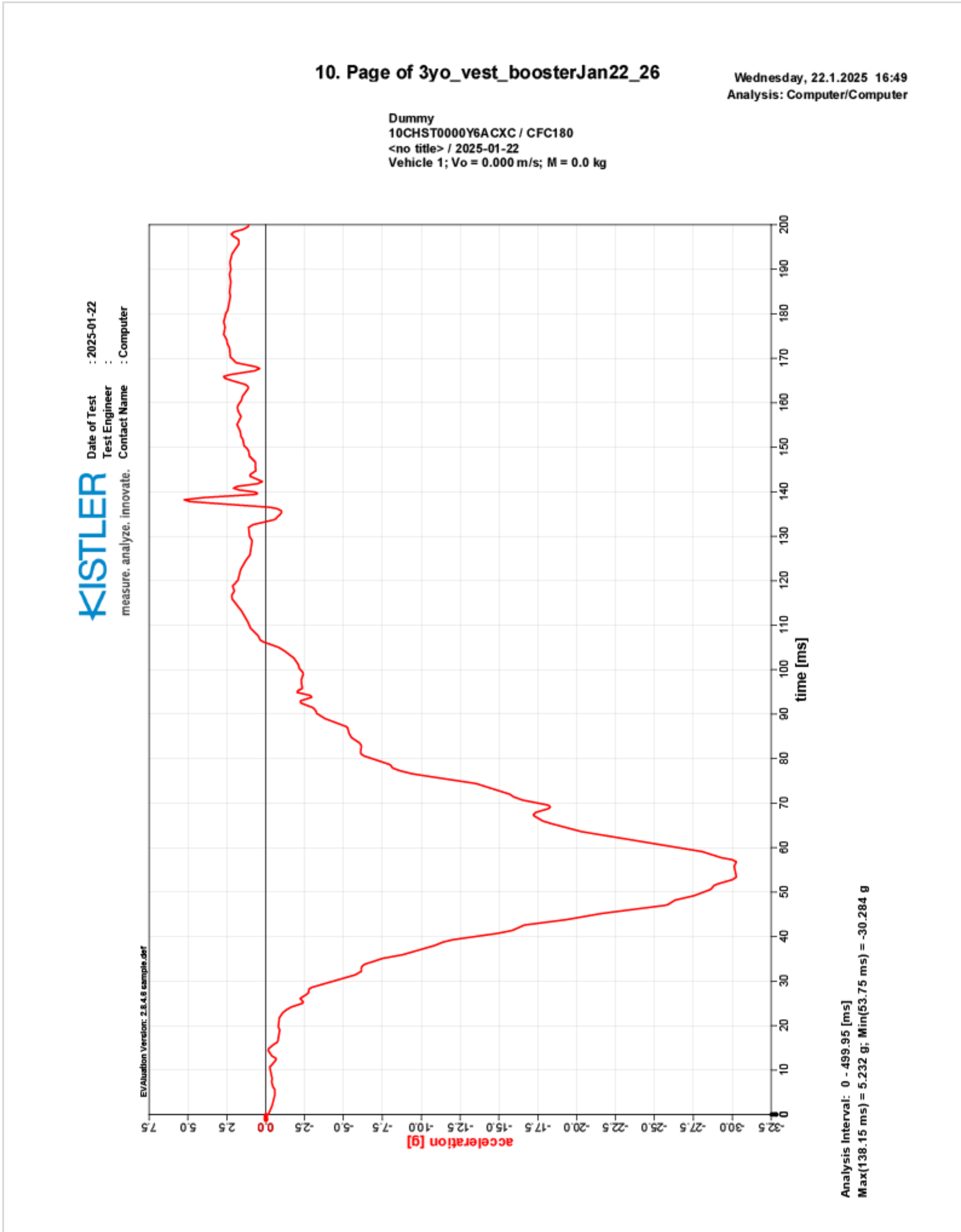

Figure C23

Trial B, Chest Acceleration, Y-axis

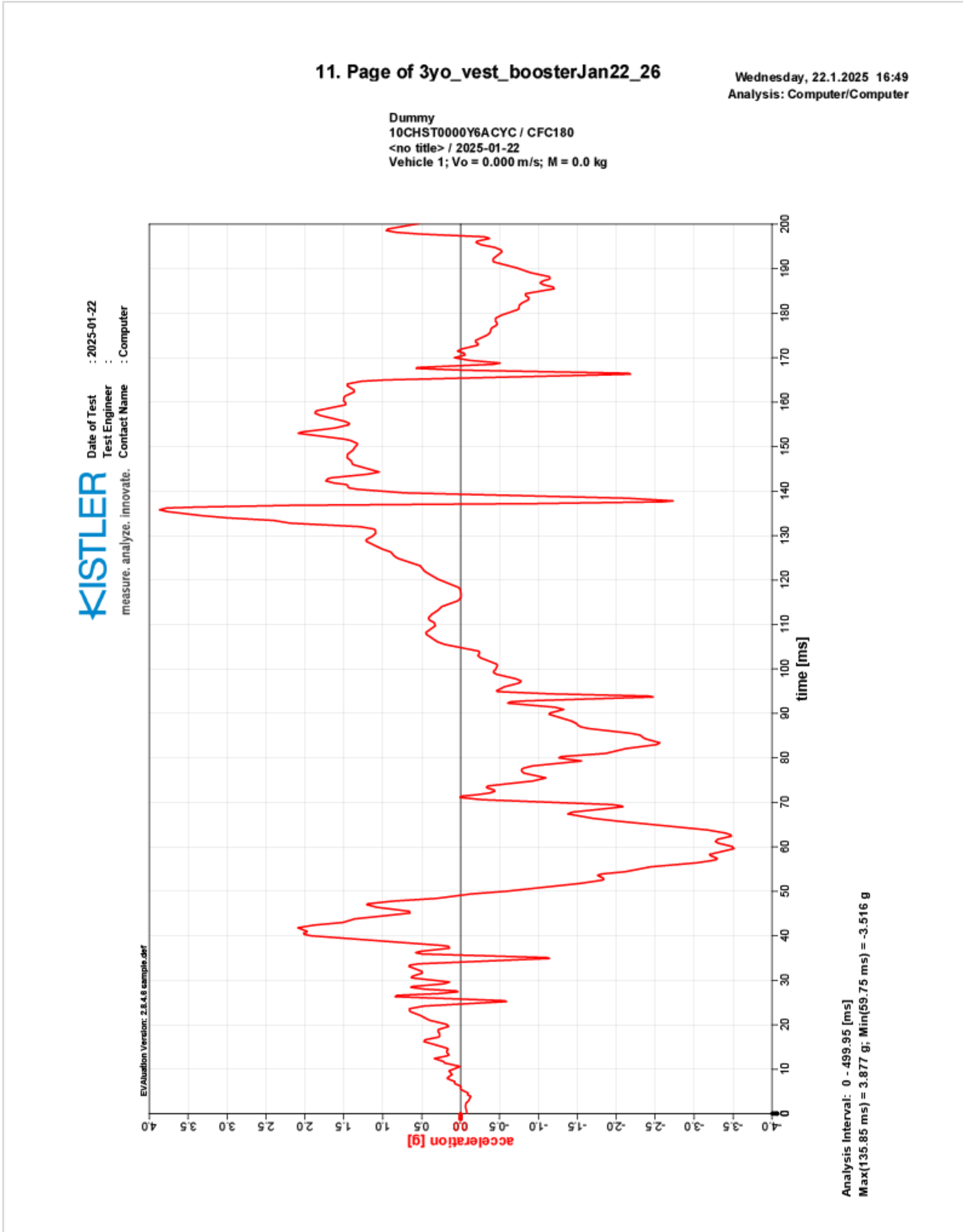

Figure C24

Trial B, Chest Acceleration, Z-axis

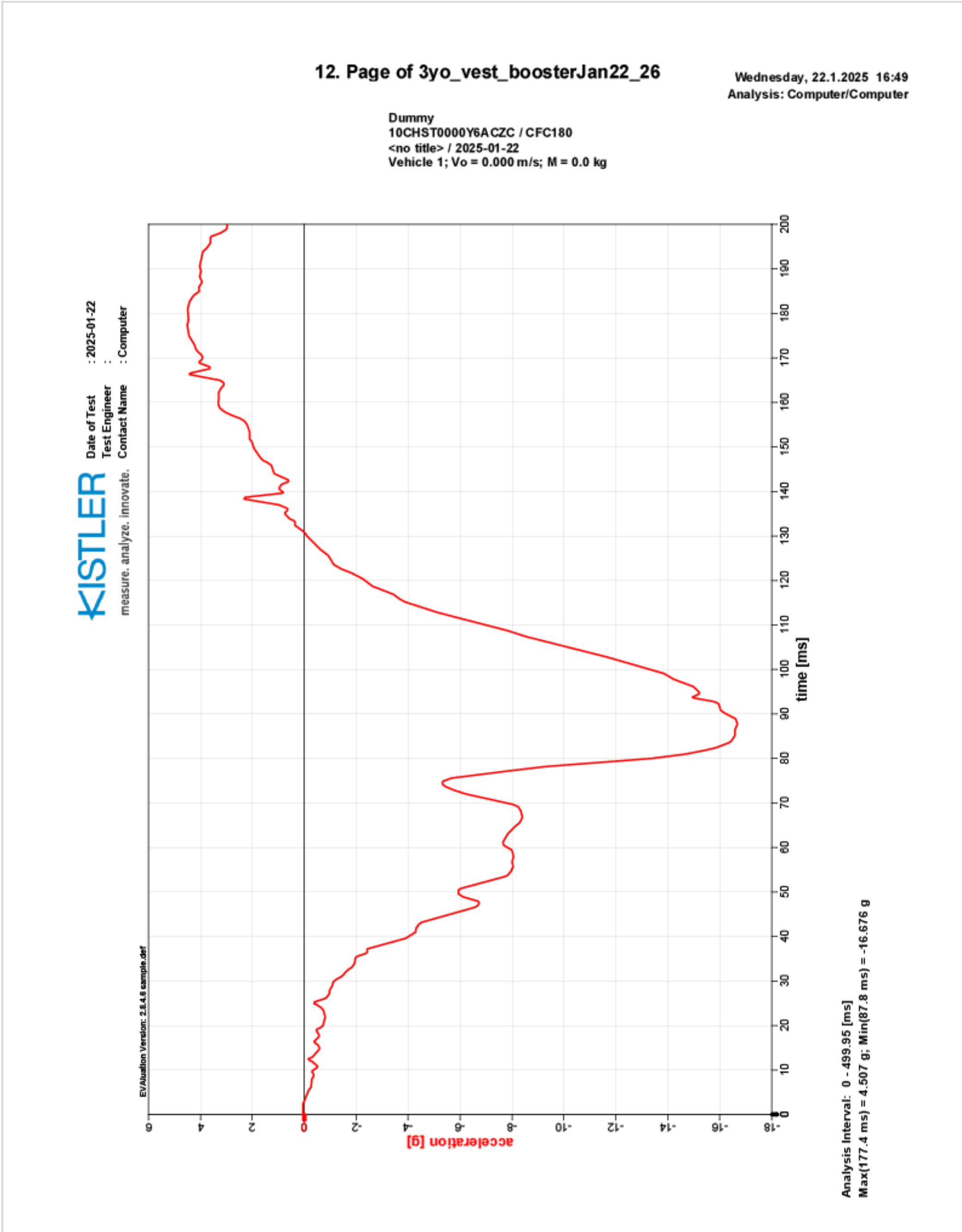

Figure C25

Trial C, Sled Acceleration, 010000

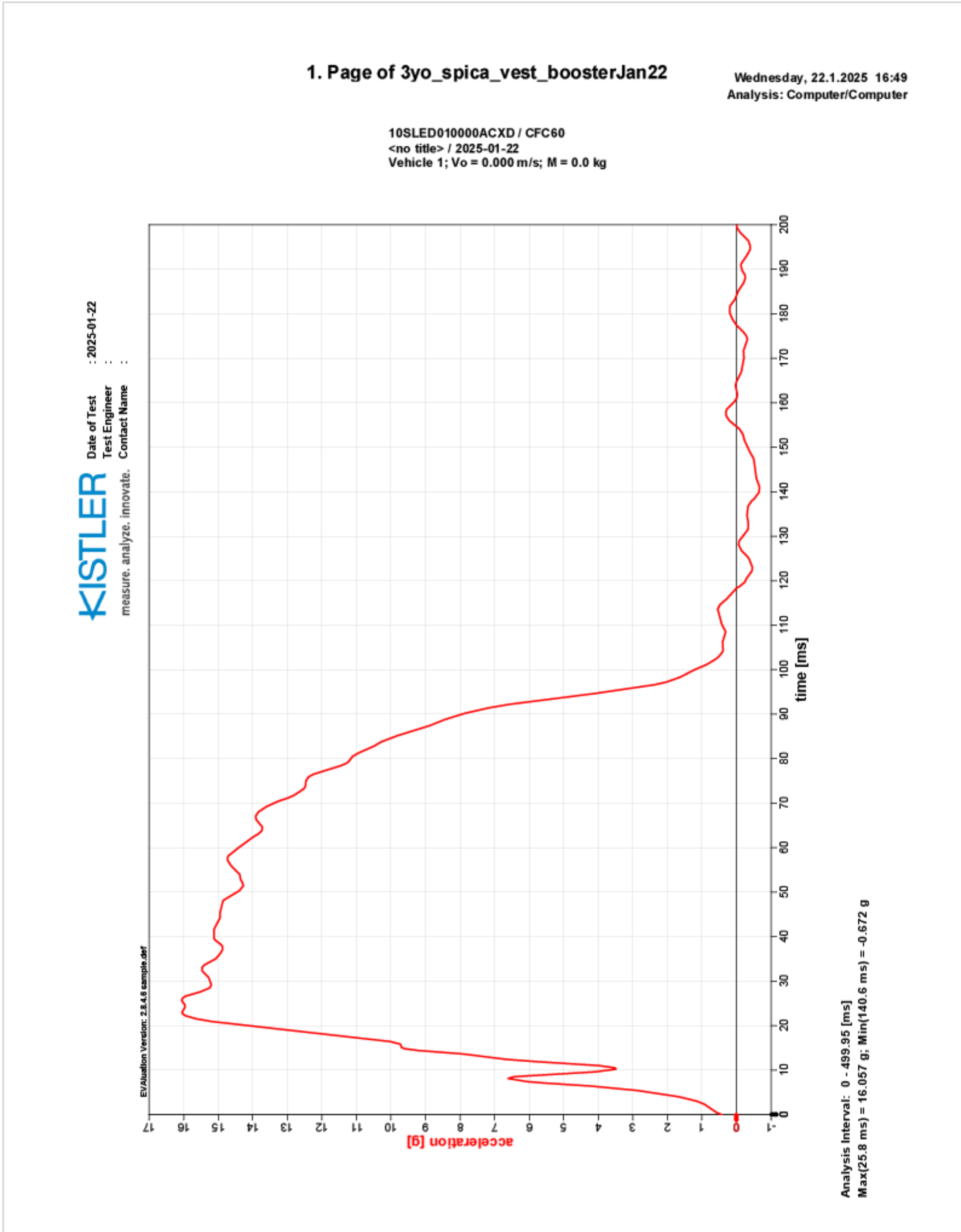

Figure C26

Trial C, Velocity and Displacement Integration, 010000

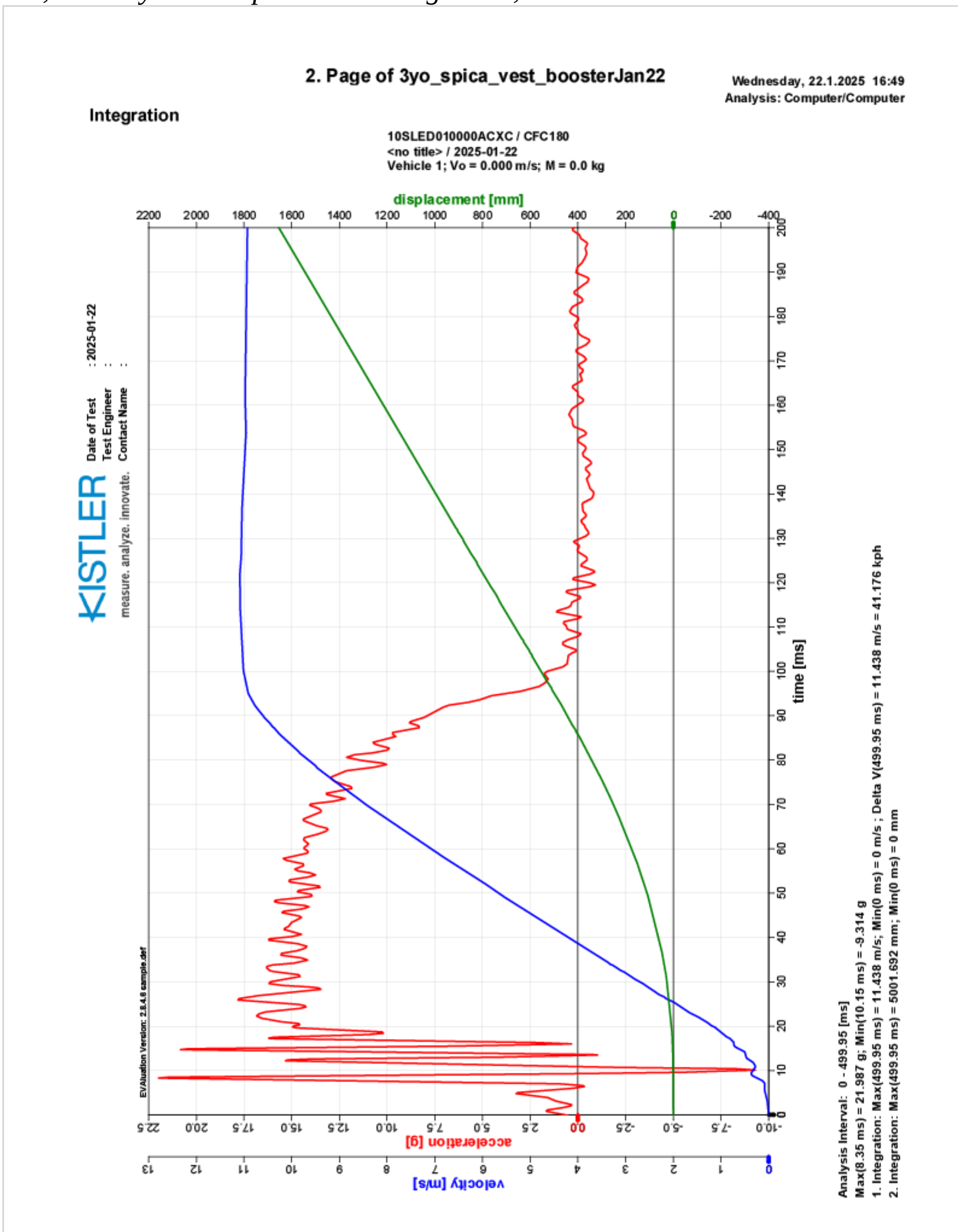

Figure C27

Trial C, Sled Acceleration, 020000

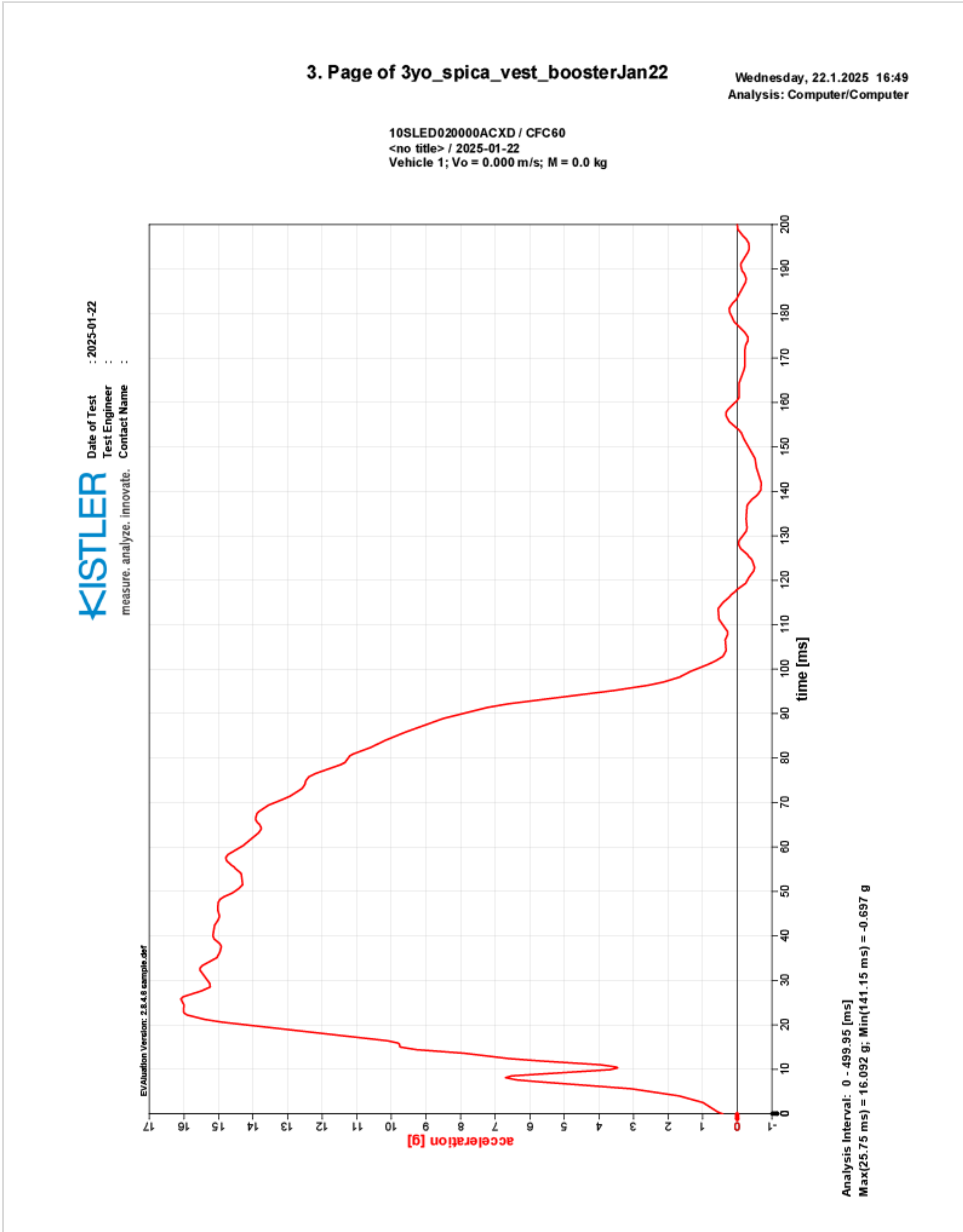

Figure C28

Trial C, Velocity and Displacement Integration, 020000

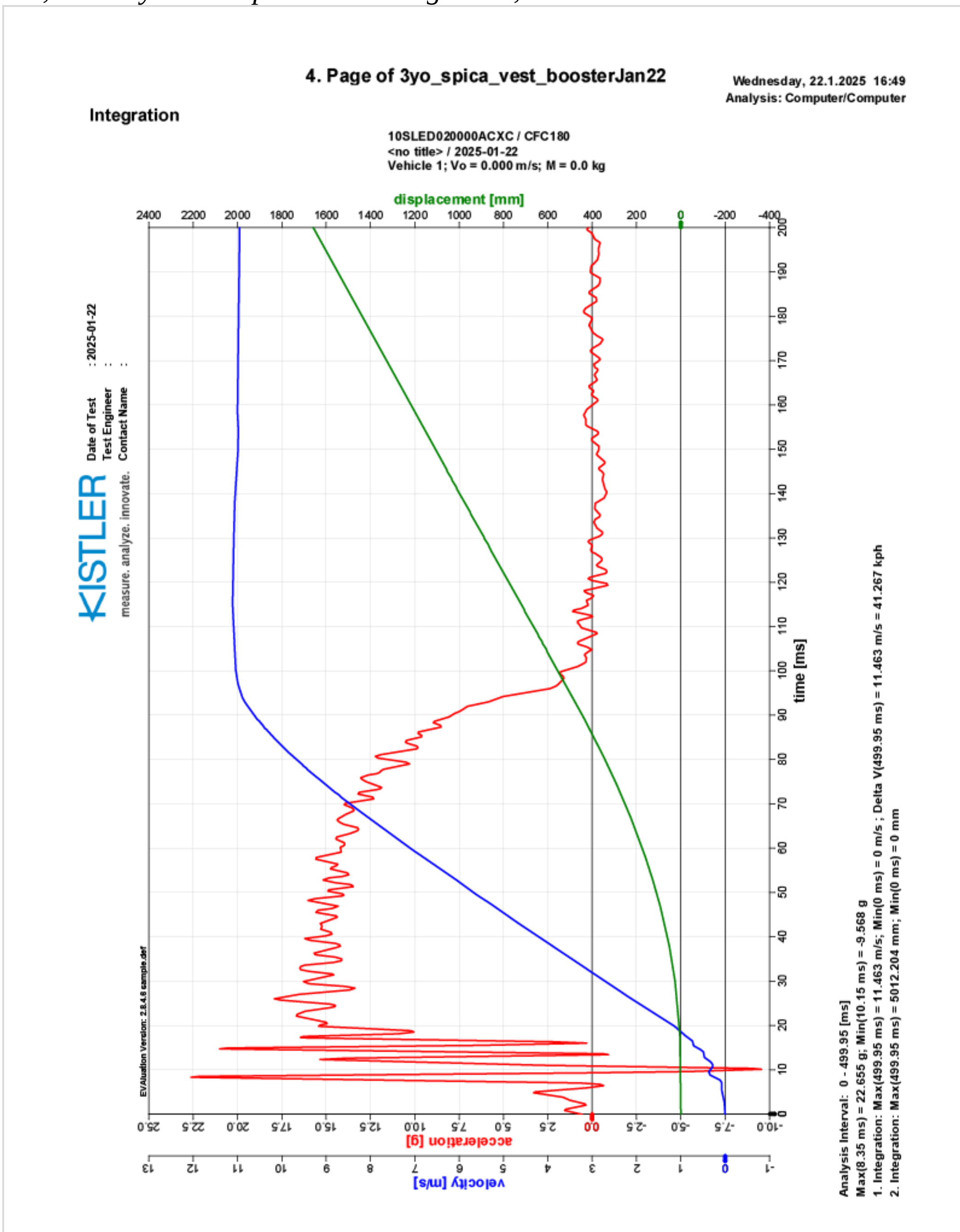

Figure C29

Trial C, Head Acceleration Resultant

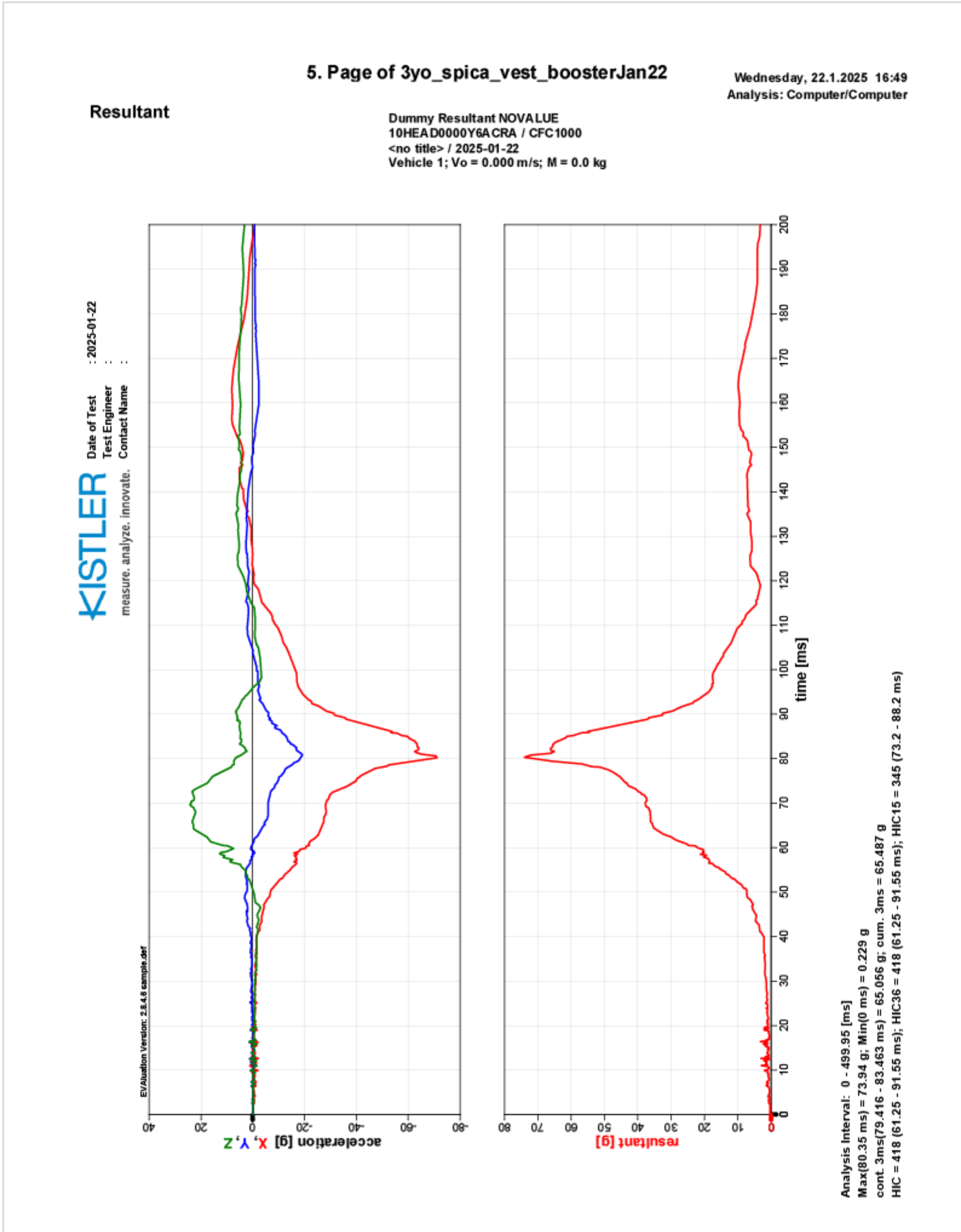

Figure C30

Trial C, Head Acceleration, X-axis

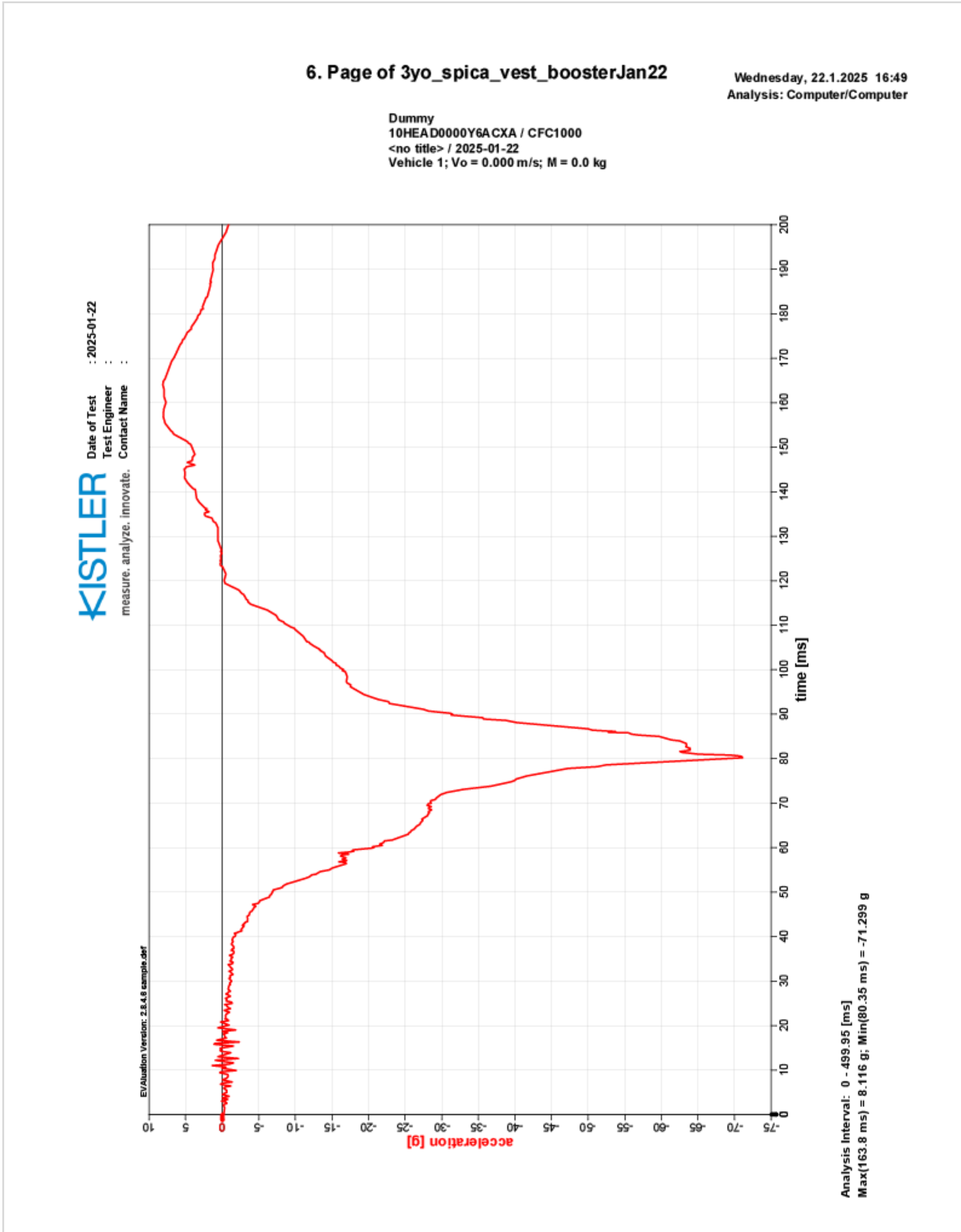

Figure C31

Trial C, Head Acceleration, Y-axis

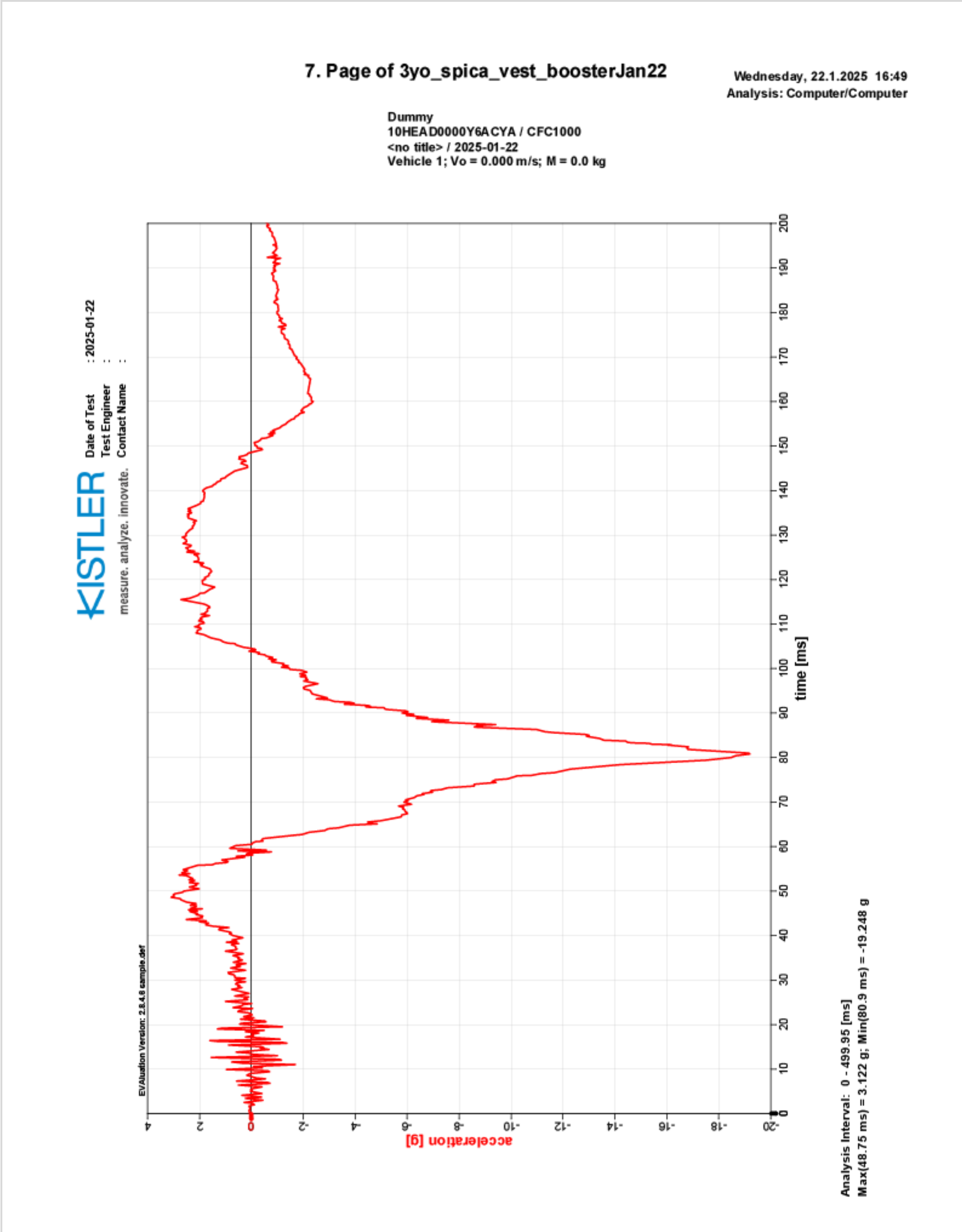

Figure C32

Trial C, Head Acceleration, Z-axis

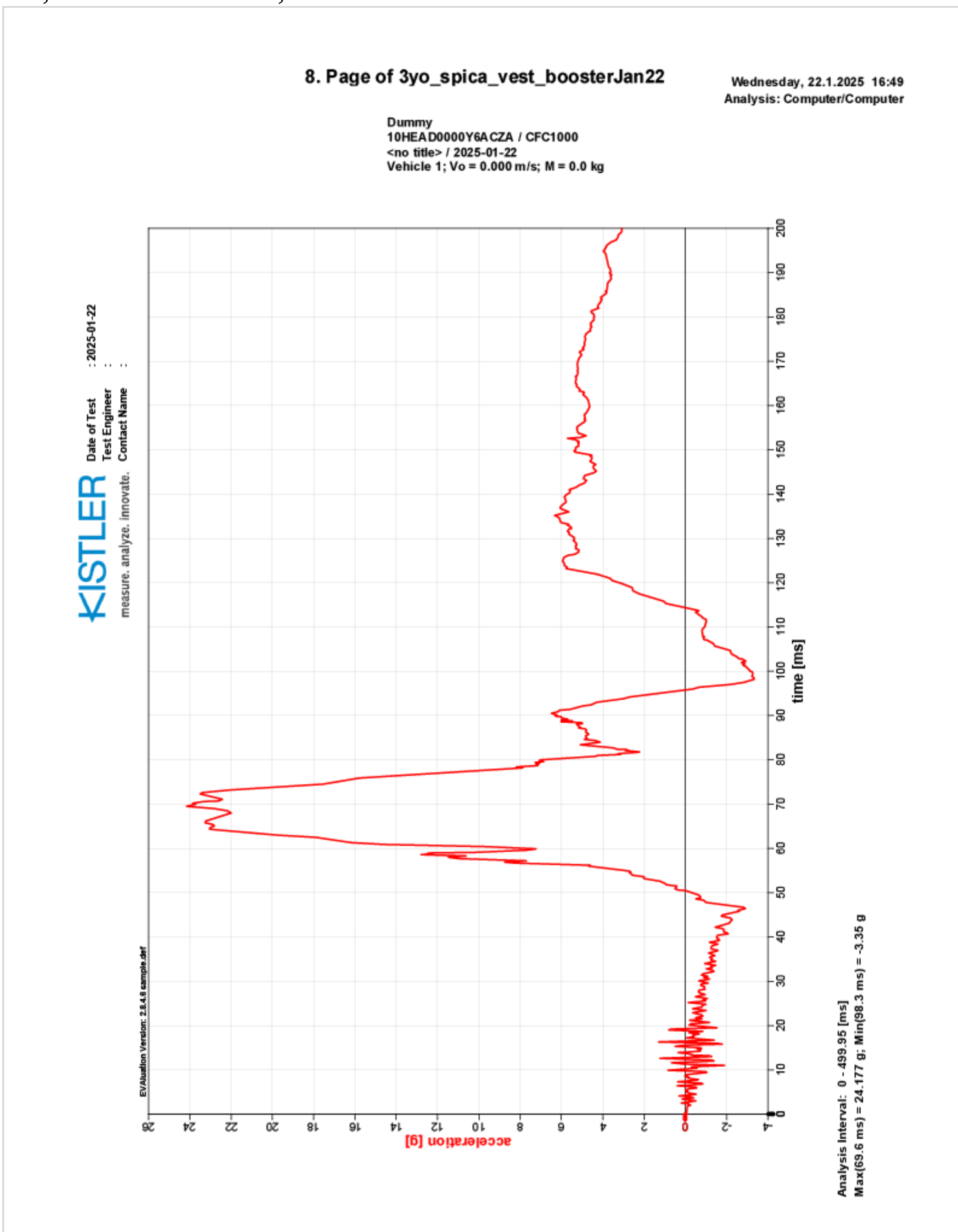

Figure C33

Trial C, Chest Acceleration Resultant

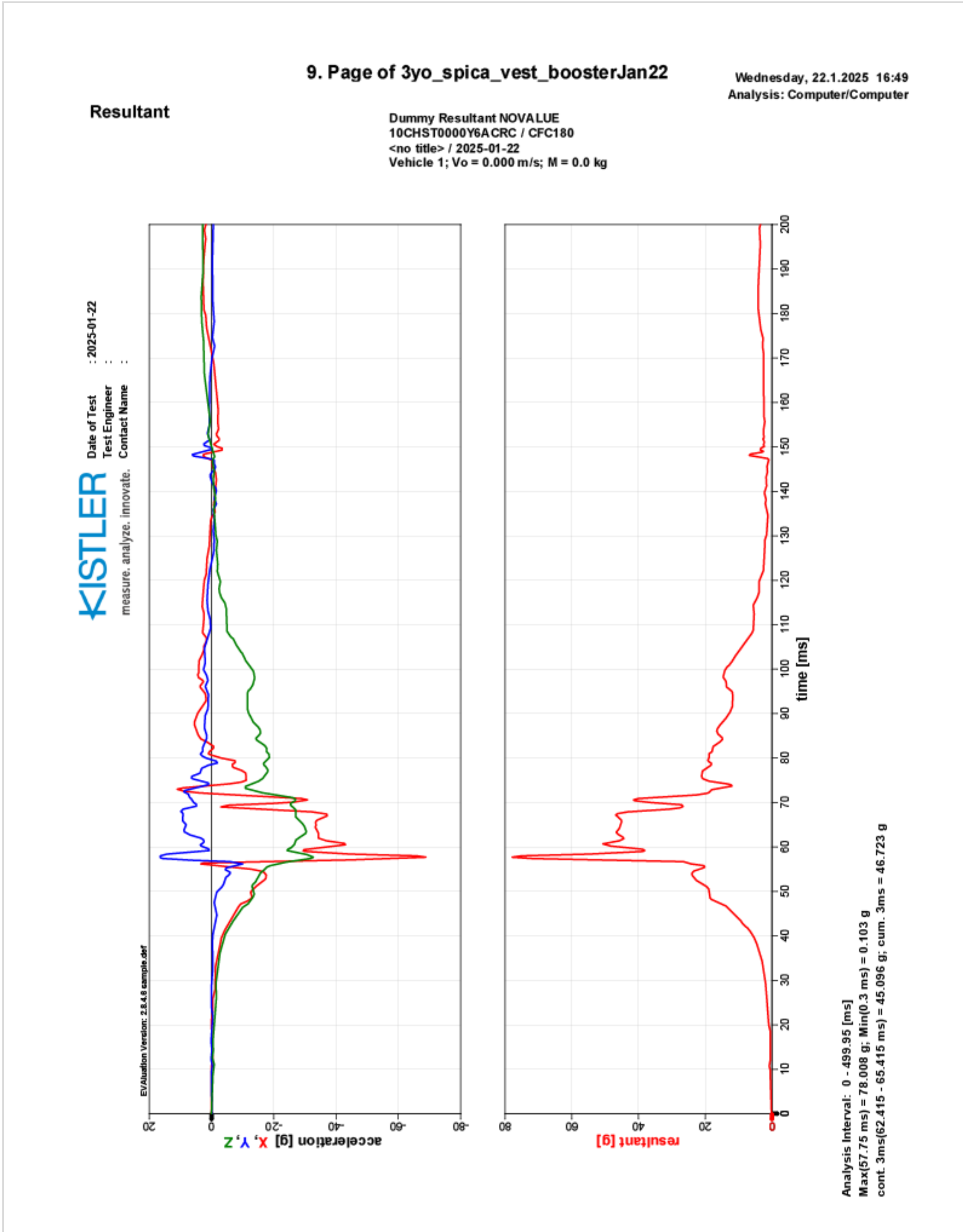

Figure C34

Trial C, Chest Acceleration, X-axis

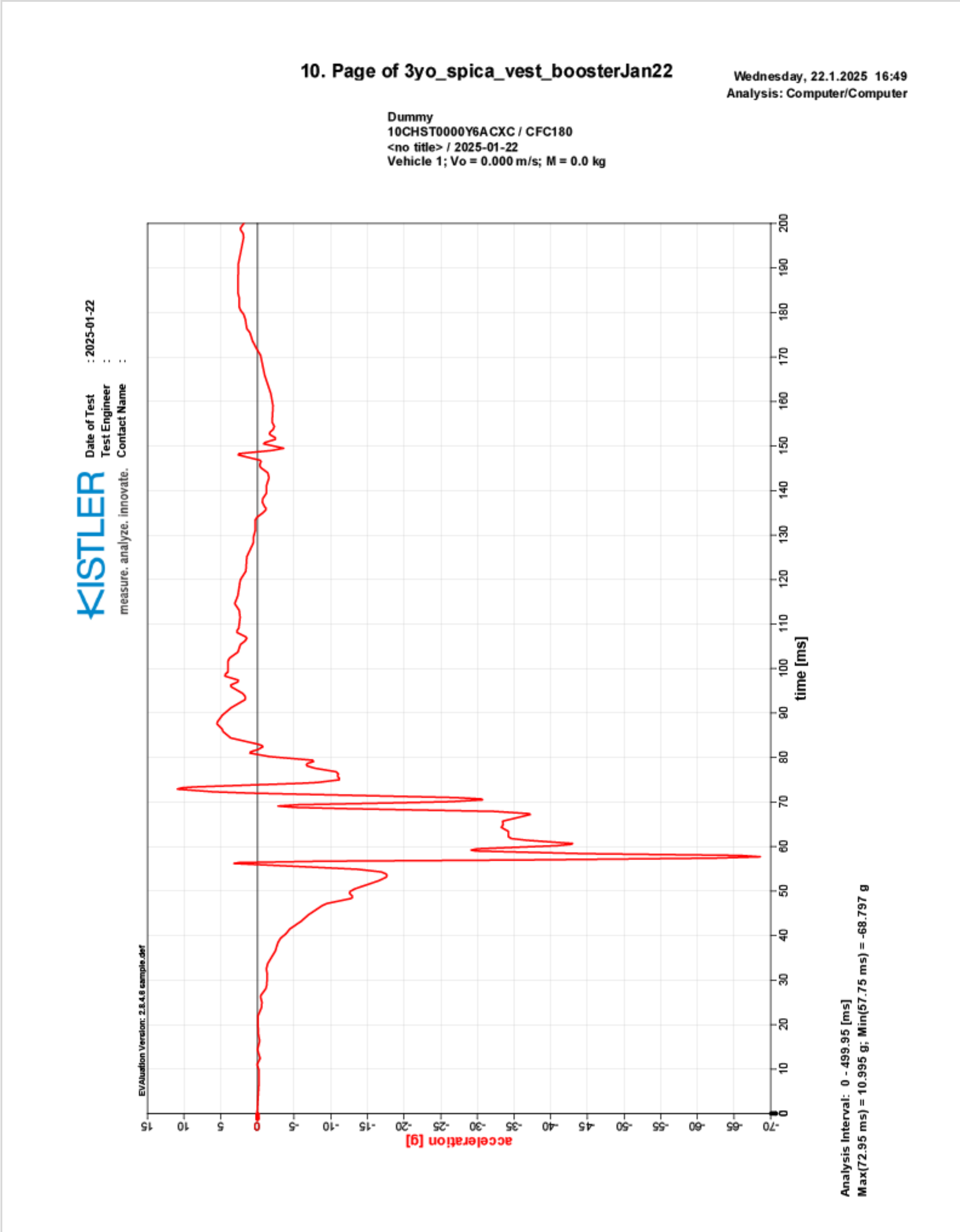

Figure C35

Trial C, Chest Acceleration, Y-axis

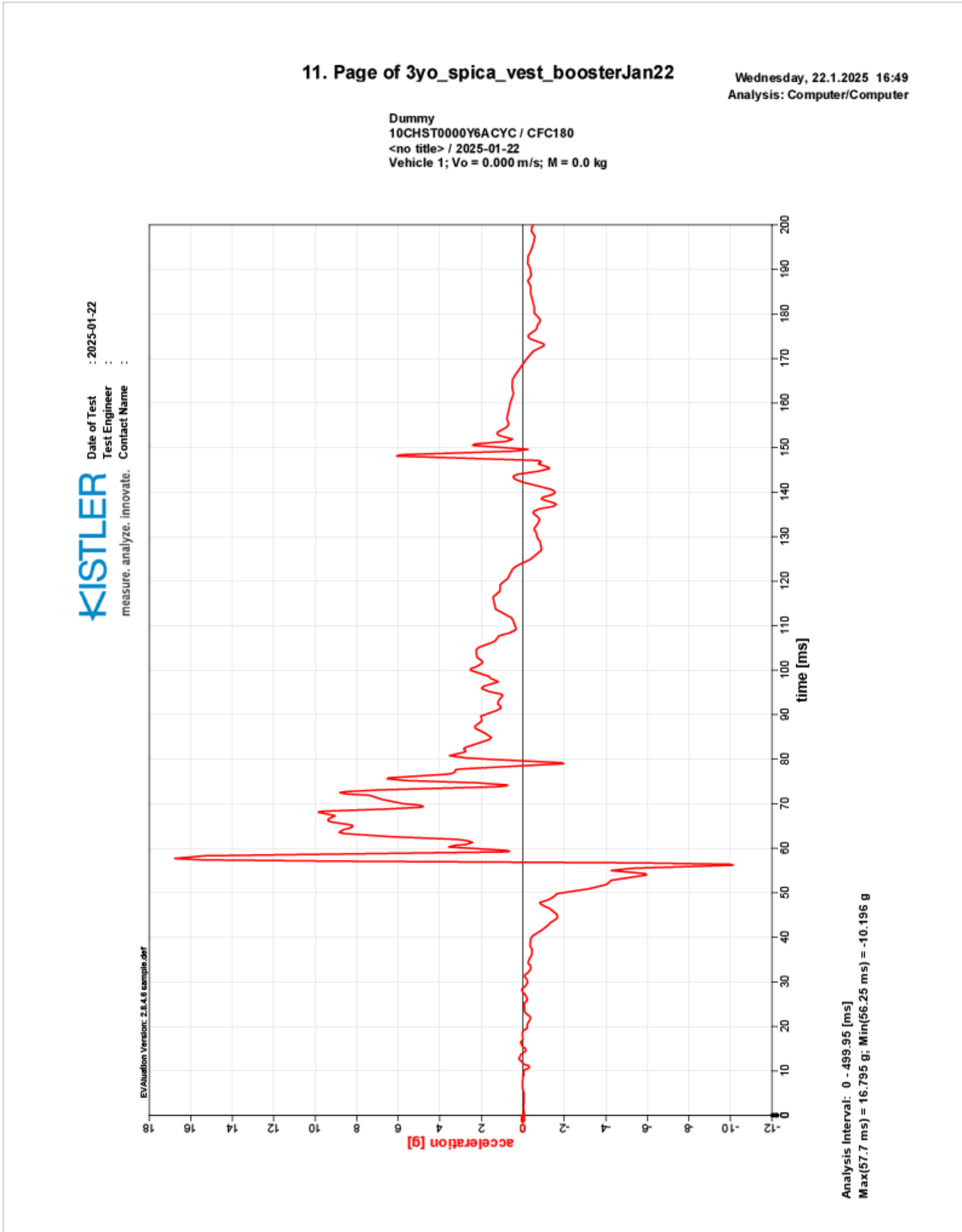

Figure C36

Trial C, Chest Acceleration, Z-axis

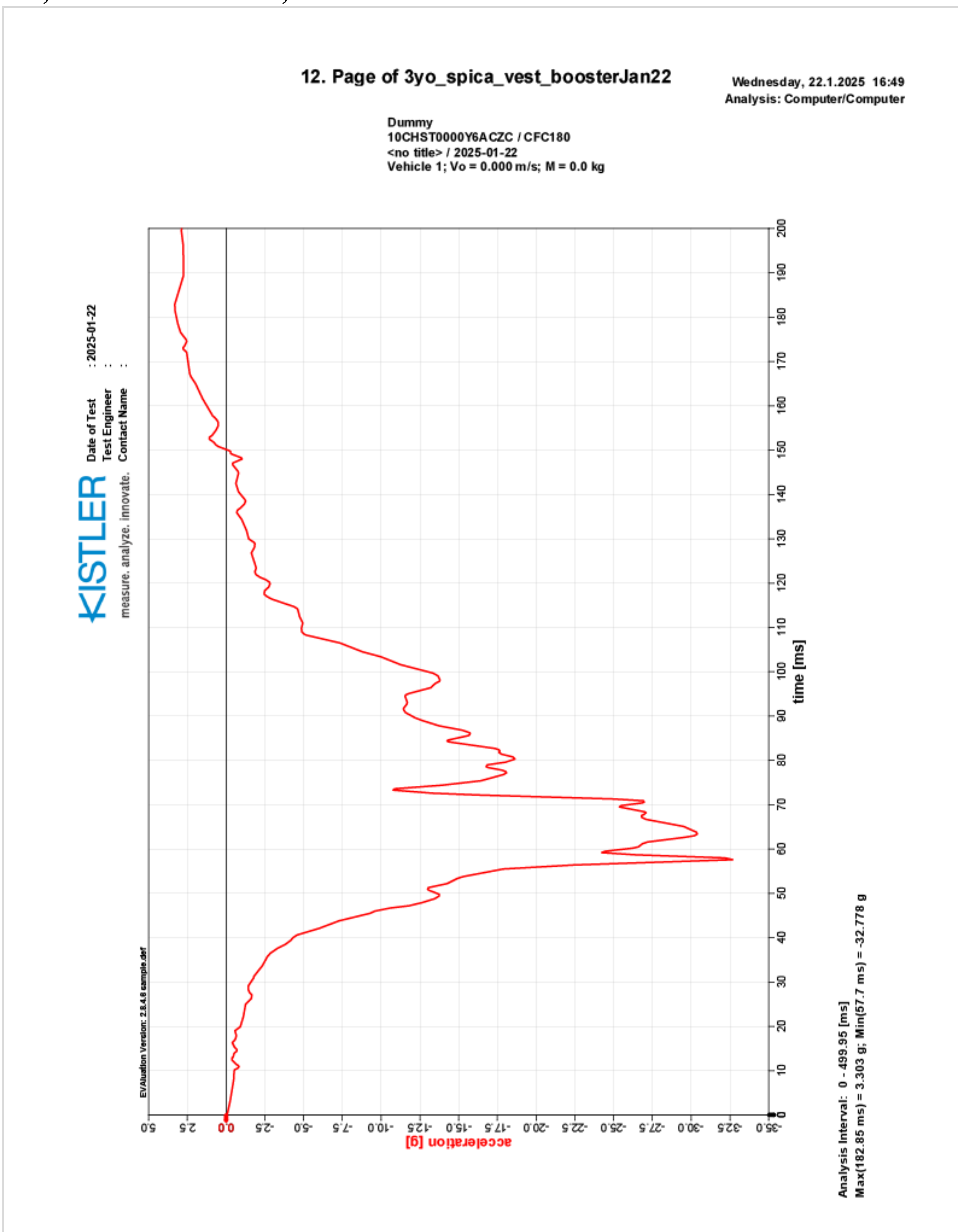

Figure C37

Trial D, Sled Acceleration, 010000

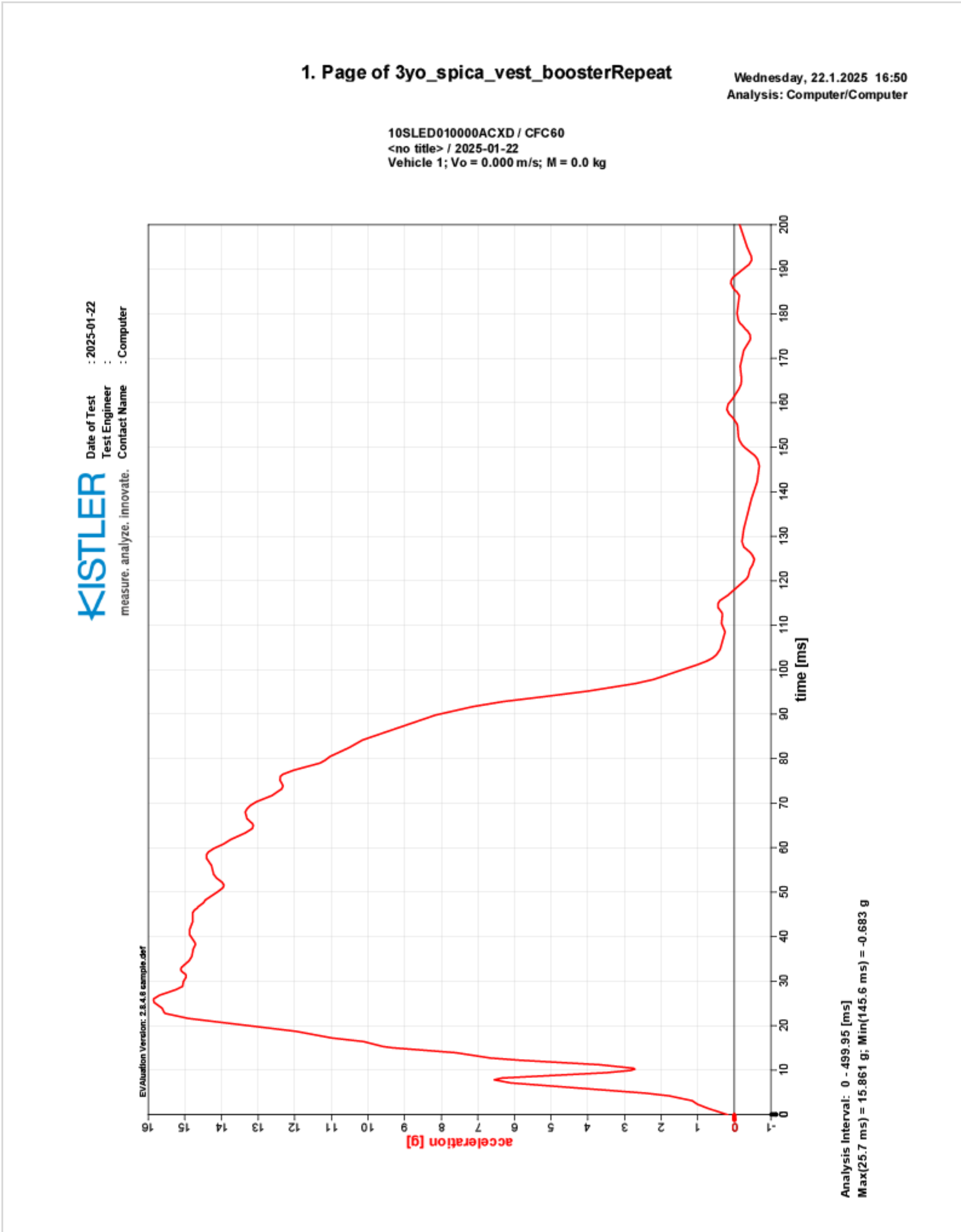

Figure C38

Trial D, Velocity and Displacement Integration, 010000

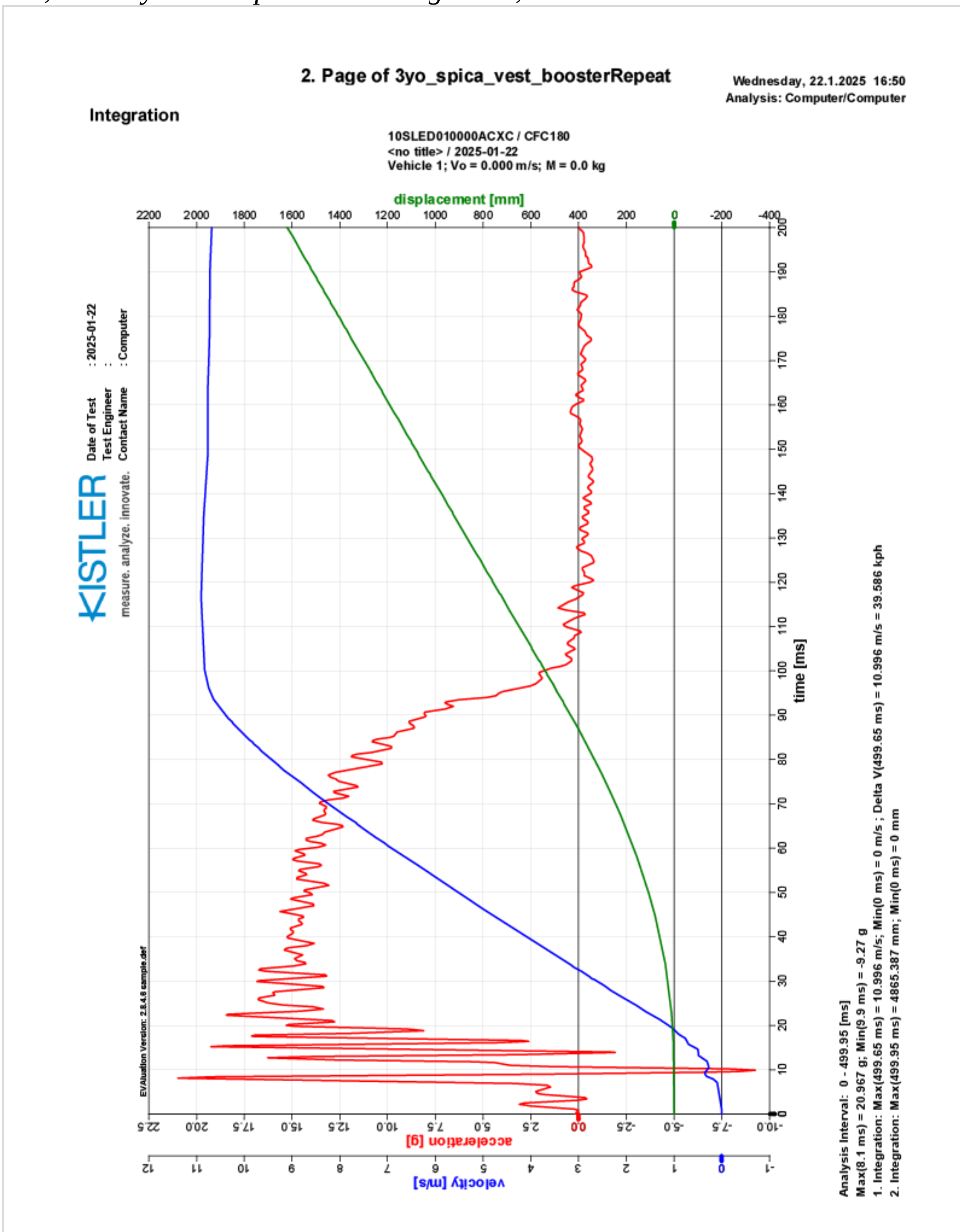

Figure C39

Trial D, Sled Acceleration, 020000

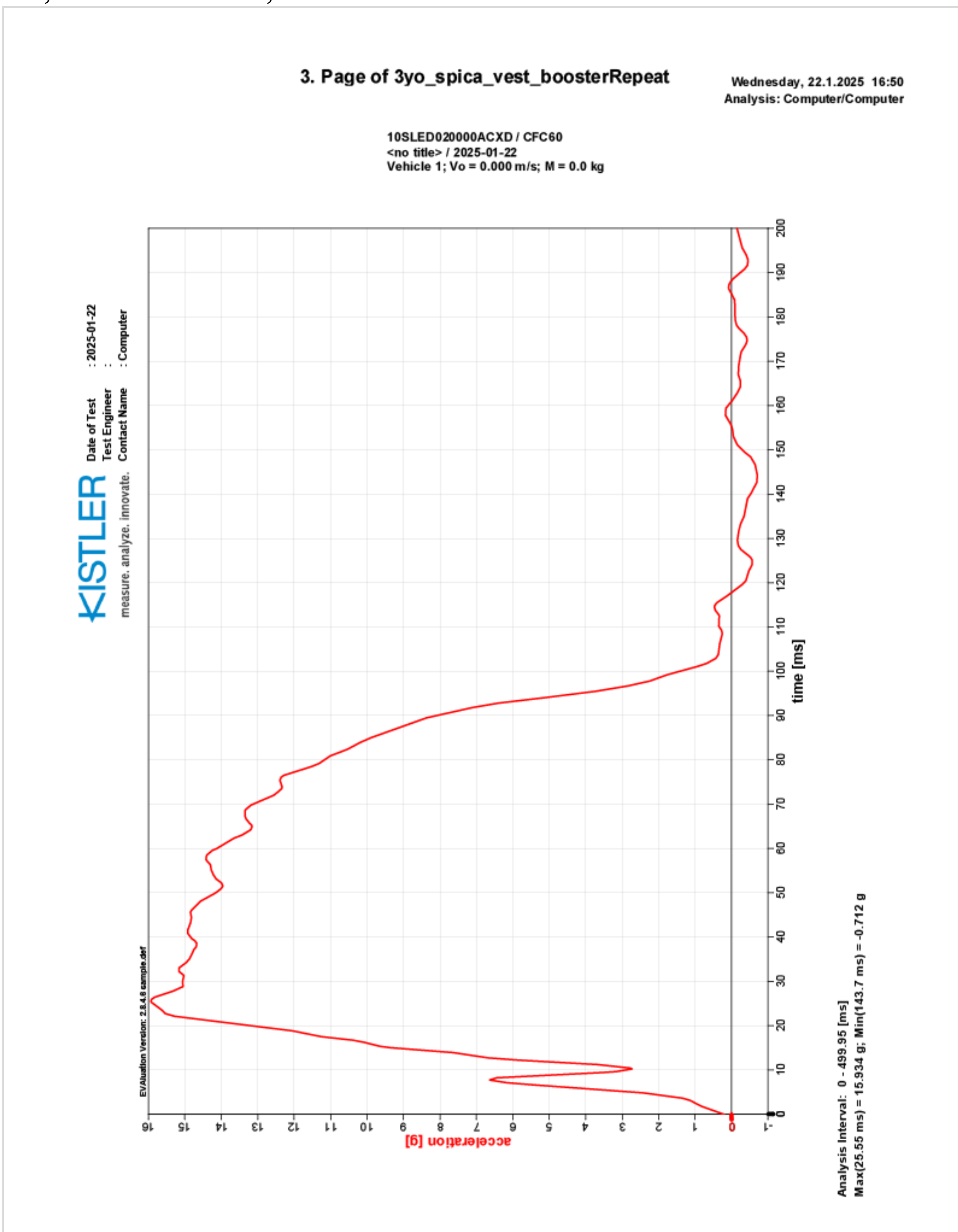

Figure C40

Trial D, Velocity and Displacement Integration, 020000

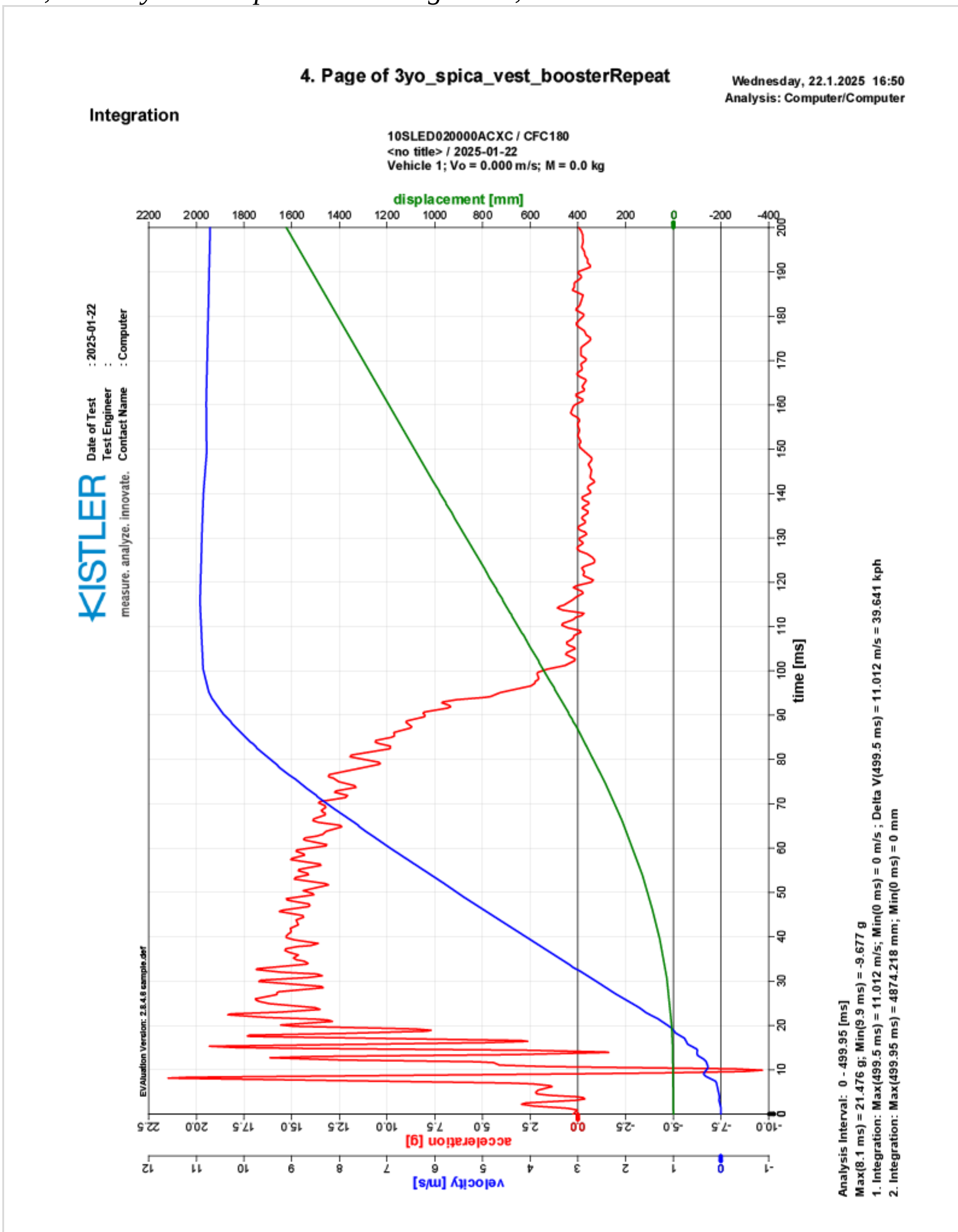

Figure C41

Trial D, Head Acceleration Resultant

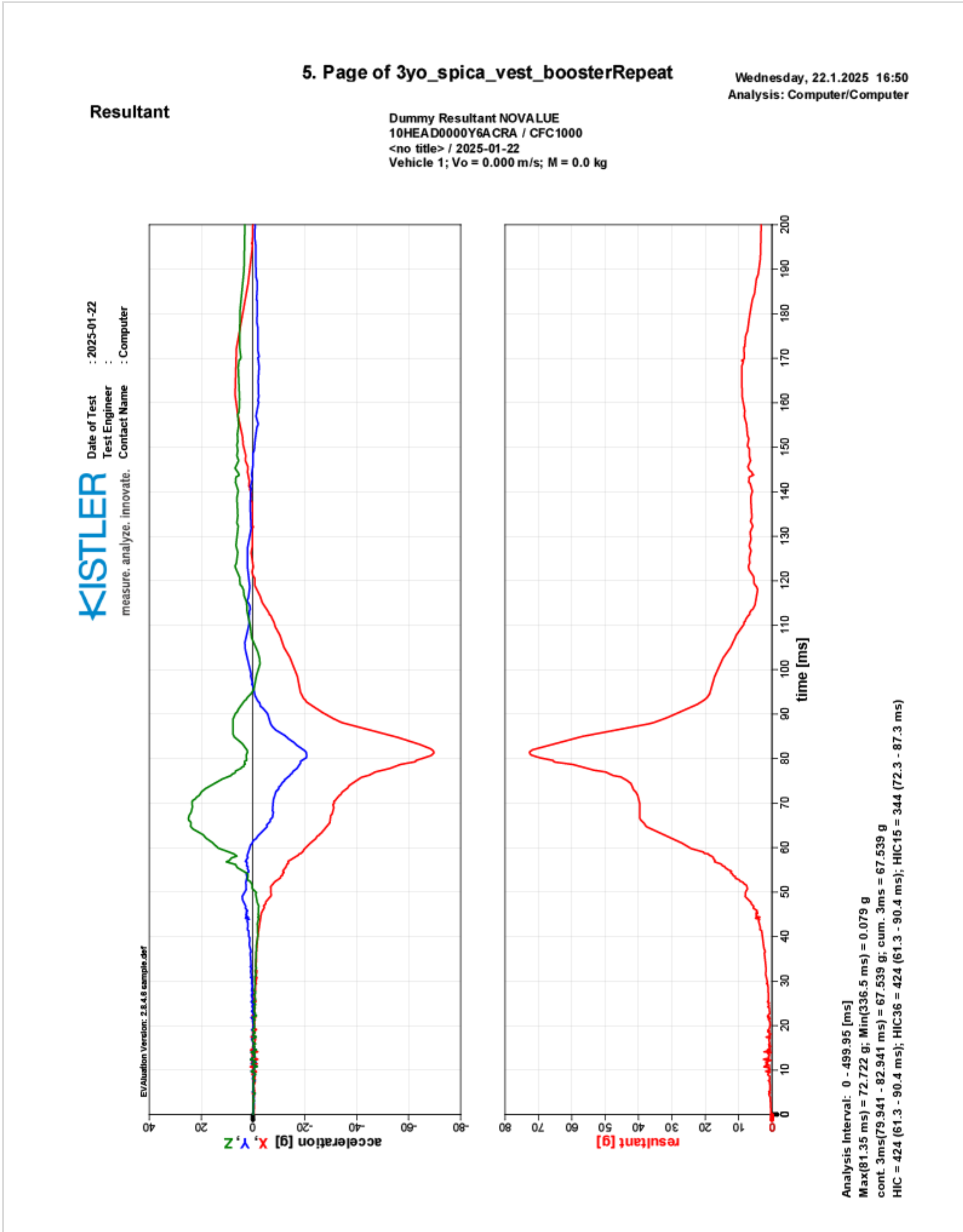

Figure C42

Trial D, Head Acceleration, X-axis

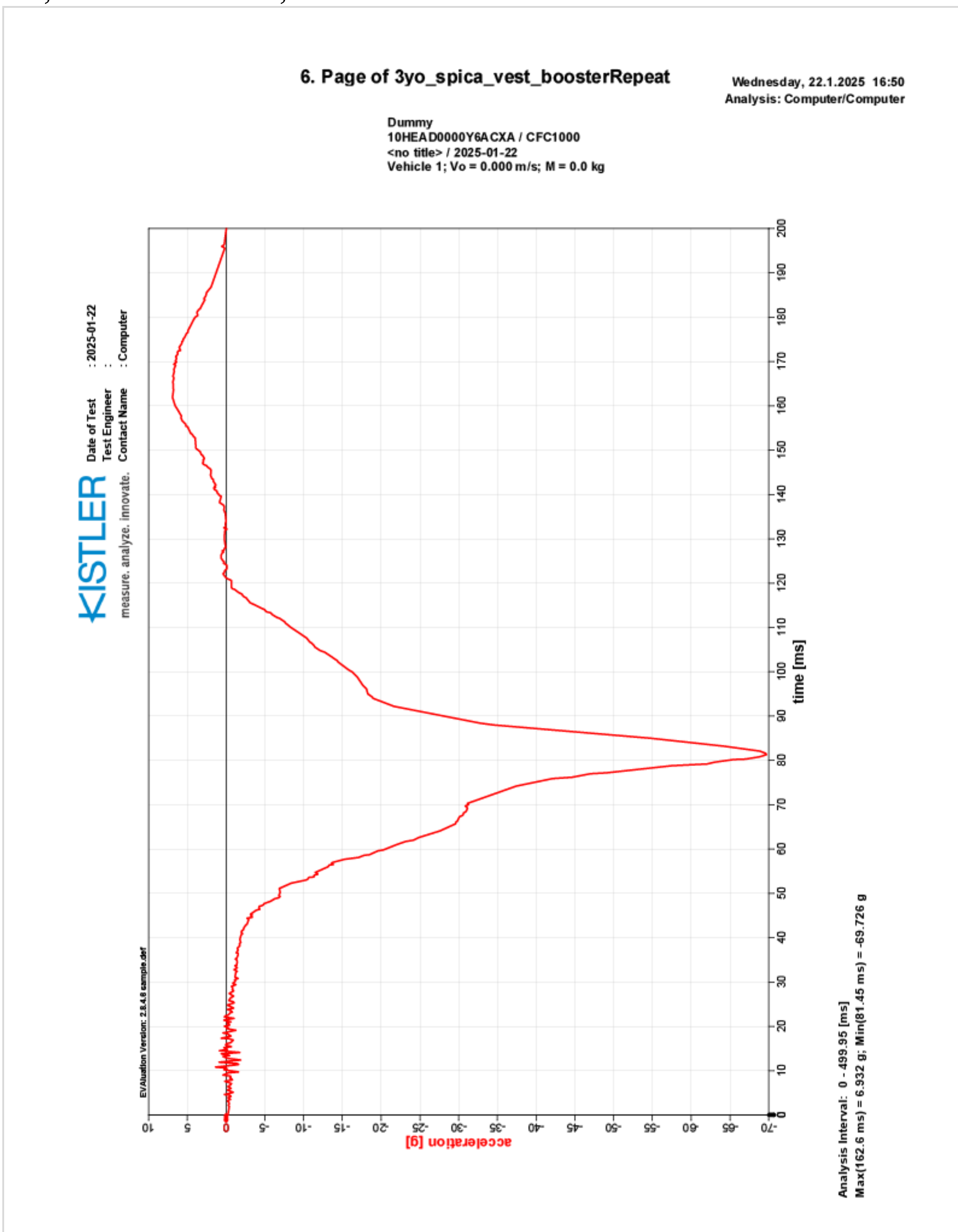

Figure C43

Trial D, Head Acceleration, Y-axis

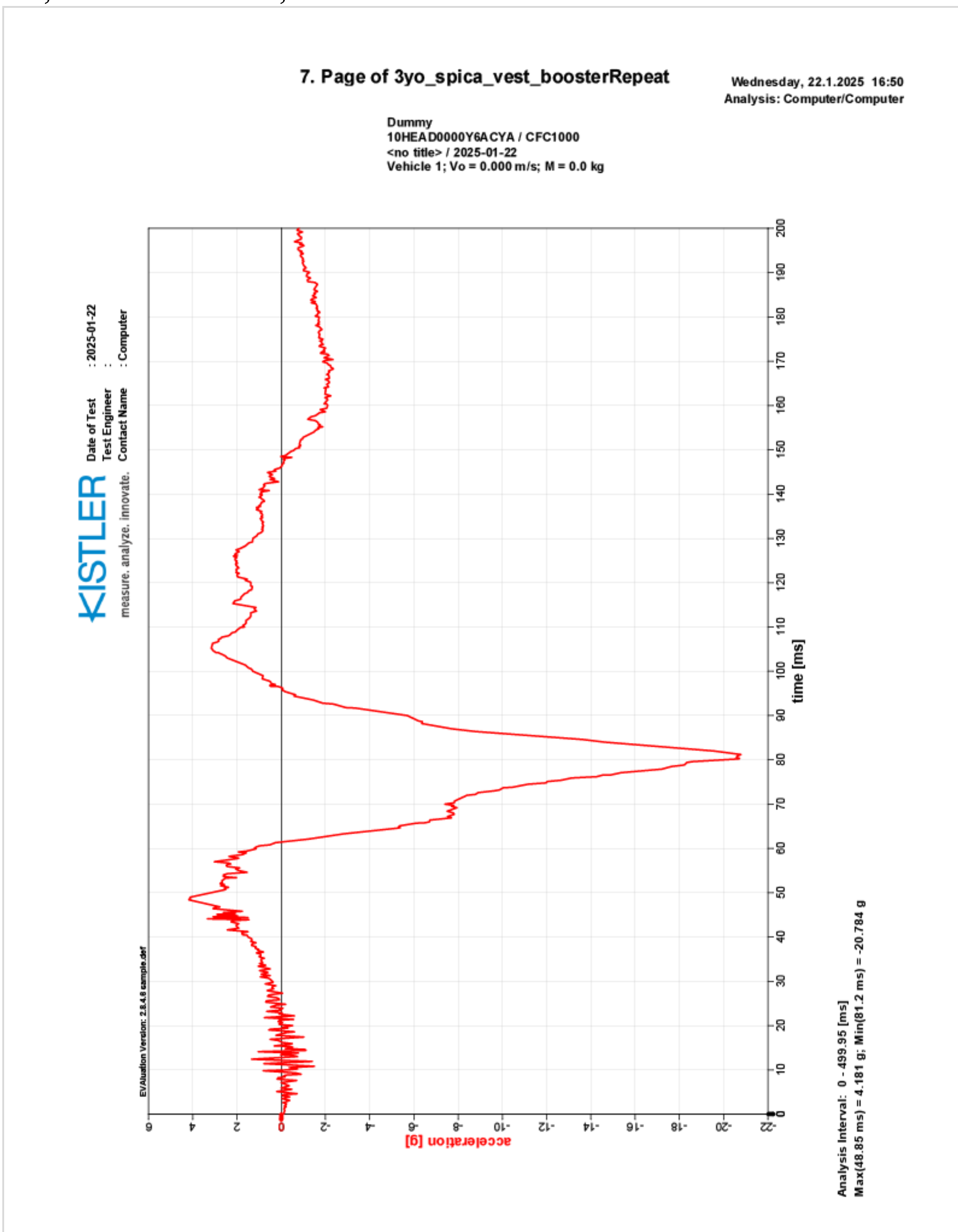

Figure C44

Trial D, Head Acceleration, Z-axis

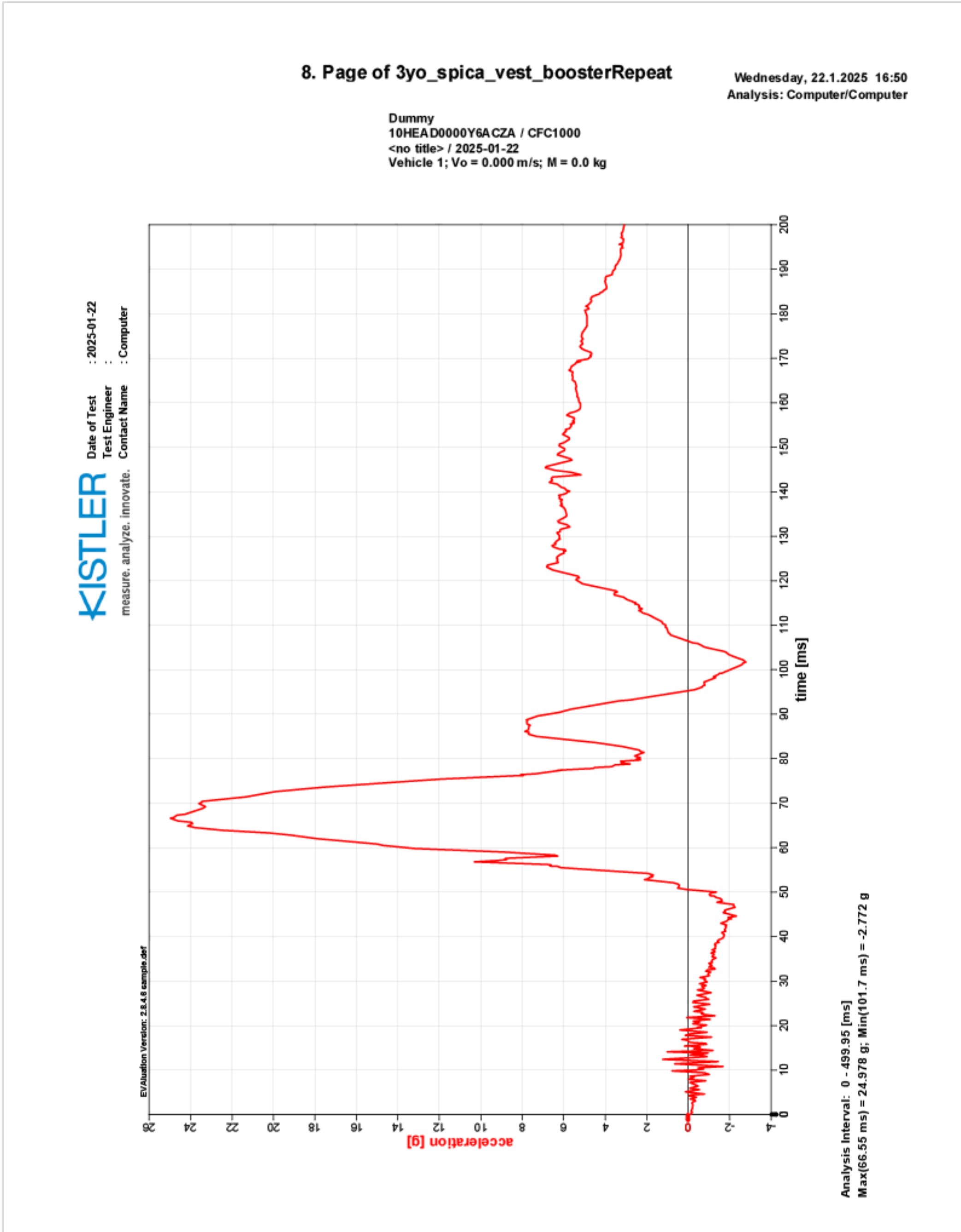

Figure C45

Trial D, Chest Acceleration Resultant

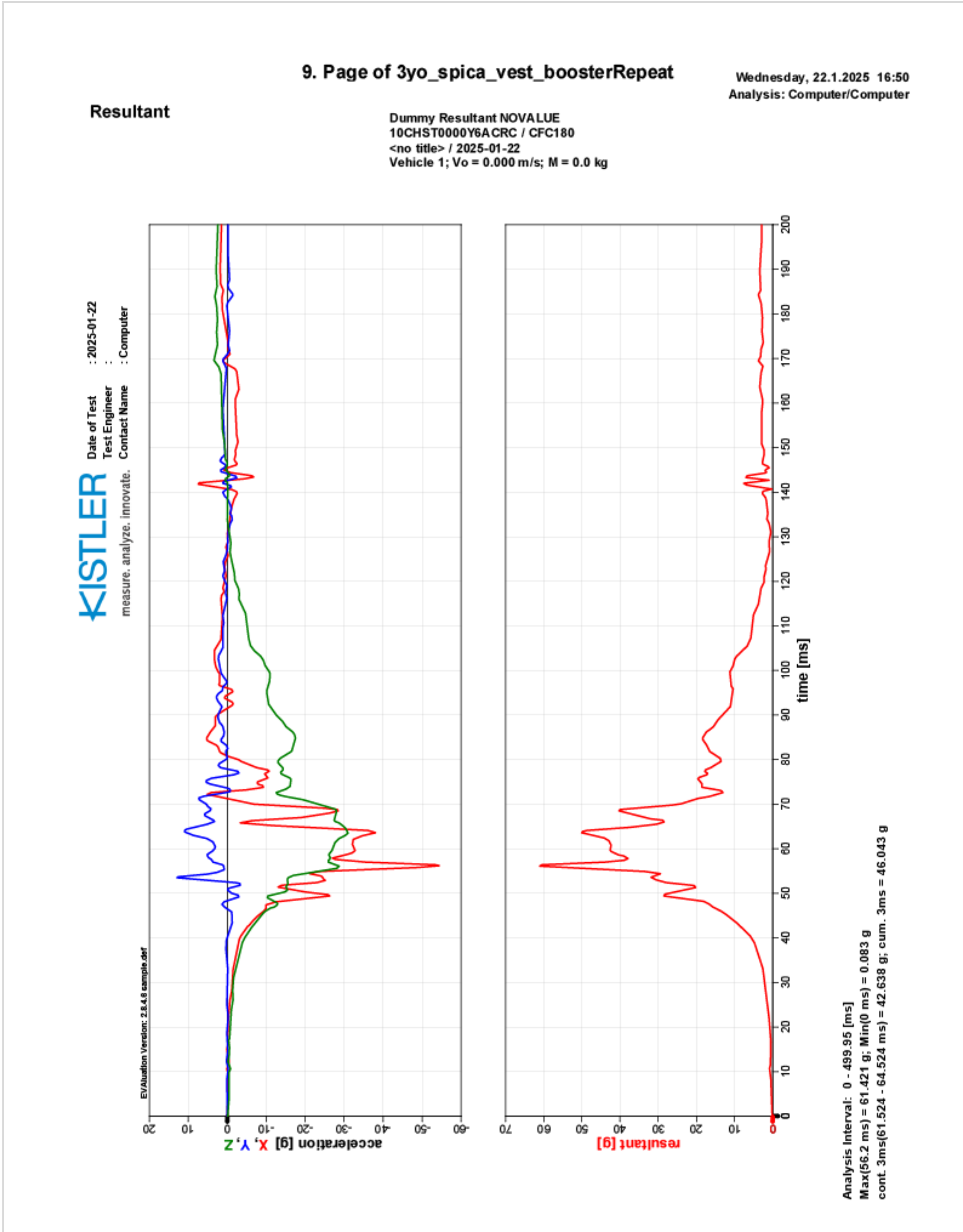

Figure C46

Trial D, Chest Acceleration, X-axis

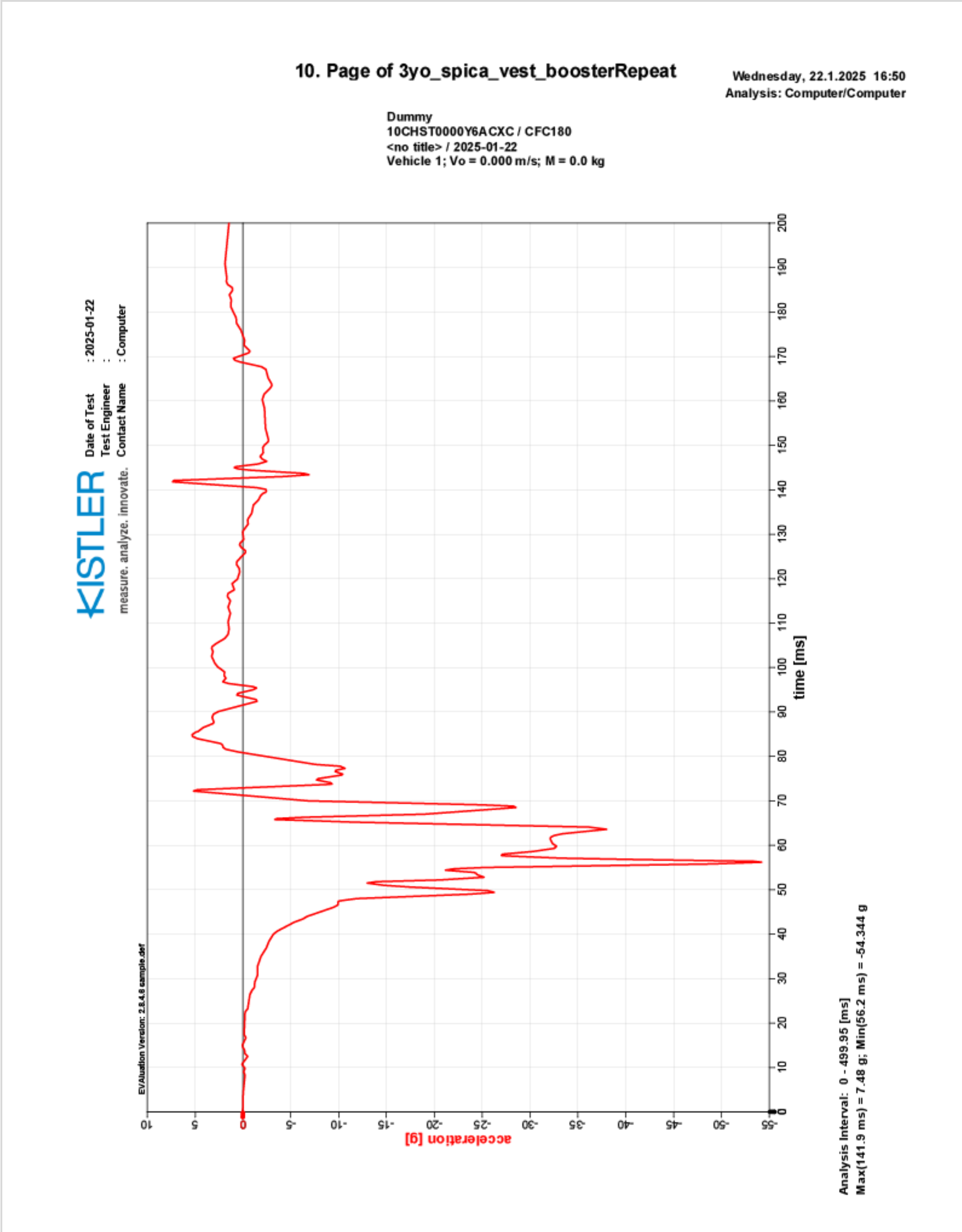

Figure C47

Trial D, Chest Acceleration, Y-axis

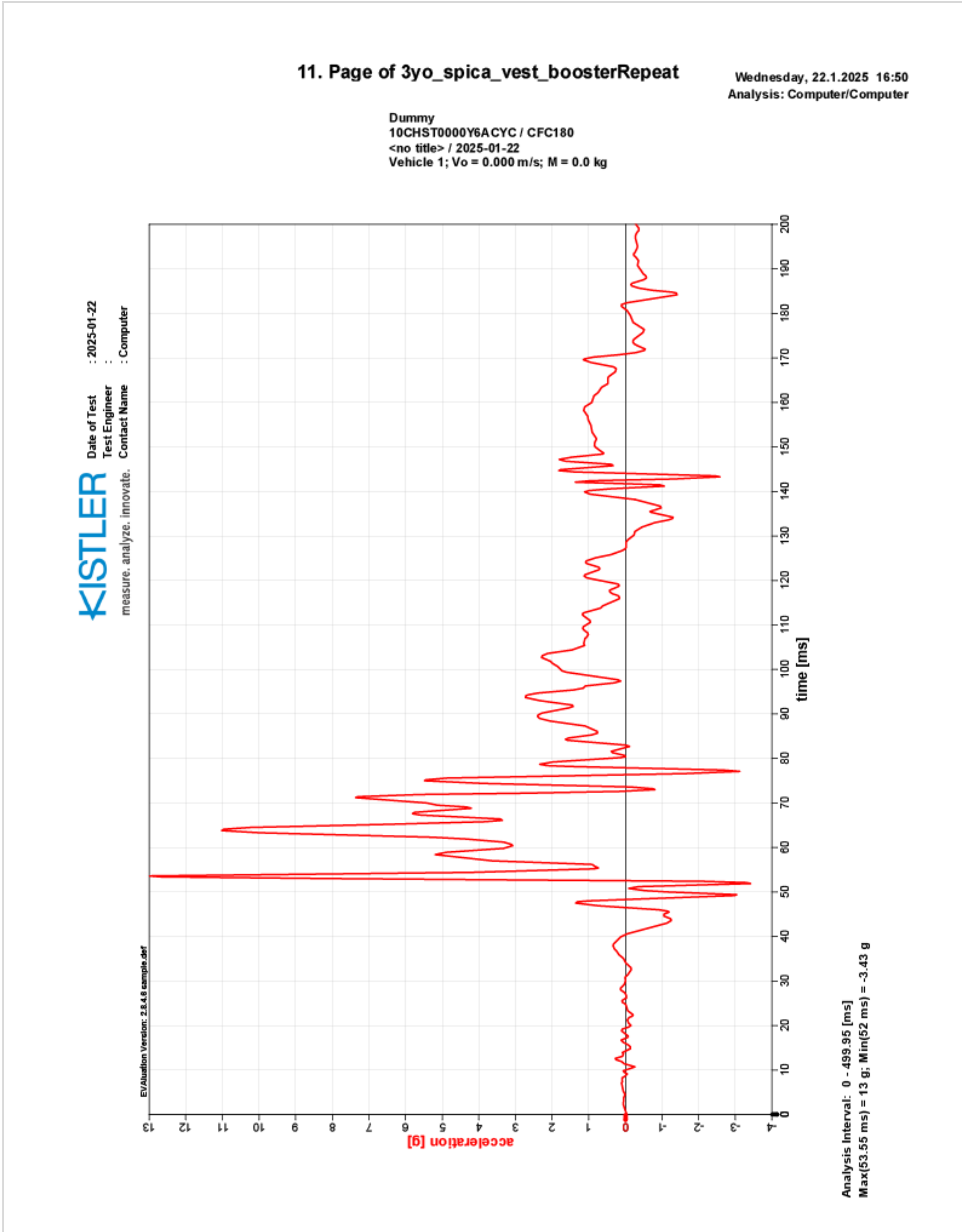

Figure C48

Trial D, Chest Acceleration, Z-axis

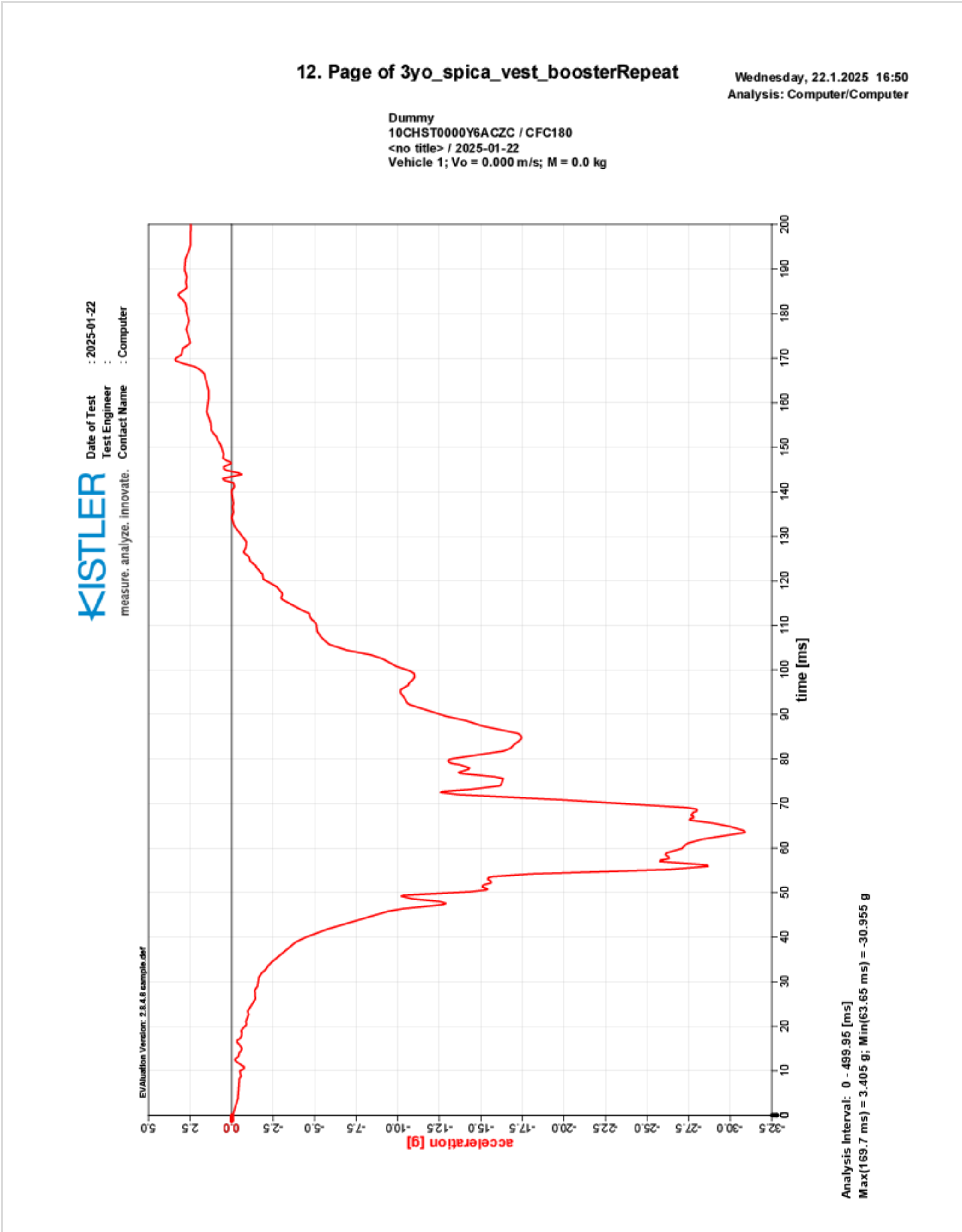

APPENDIX D

Working Model Simulation Model Version Histories

Table D1

Working Model Trial A Model Versions

Version	HIC36	Chest Accel (g)	Version History
1	204.6	32.88	Started with WM_Simulation_213_3_yo_ATD.wm2d Removed CSS and its SD constraint Translated ATD to contact seat back and seat pan SBSD anchors on seat back mount at Gx=4.419, Gy=-3.126, and on torso at Gx=4.693, Gy=-3.135 LBSD anchors on seat back mount at Gx=4.756, Gy=-3.540, and on torso at Gx=4.827, Gy=-3.356 SBSD: k=7e4, b=6000, Length=0.274 m, Current=0.274 m LCSD: k-7e4, b=4000, Length=0.197 m, Current=0.197 m
2	204.6	32.75	SBSD: k=7e4, b=6000 LCSD: k-7e4, b=4000
3	209.5	32.60	SBSD: k=7e4, b=6000 LCSD: k-7e4, b=4000
4	217.5	34.16	SBSD: k=7e4, b=6000 LCSD: k-7e4, b=4000

Table D1 (continued)

Version	HIC36	Chest Accel (g)	Version History
5	208.9	32.57	SBSD: k=7e4, b=6000 LCSD: k-7e4, b=4000
6	225.9	36.44	Translated SBSD anchor on seat back mount to Gx=4.443, Gy=-3.186
7	218.6	35.23	Translated SBSD anchor on seat back mount to Gx=4.433, Gy=-3.168
8	224.6	35.17	SBSD: k=11e4, b=6000
9	235.3	35.08	SBSD: k=15e4, b=6000
10	191.7	35.48	Sled Mass=945 kg
11	214.1	32.76	Head Mass=3.5 kg NSD: k=1e5, b=1500
12	307.7	32.32	Head Mass=2.72 kg NSD: k=1e5, b=500
13	261.7	32.31	NSD: k=1e5, b=750
14	269.0	32.41	NSD: k=1e5, b=700
15	289.3	32.54	NSD: k=1e5, b=600
16	317.2	32.56	Translated SBSD anchor on seat back mount to Gx=4.435, Gy=-3.182
17	304.8	32.57	Started with _v15 SBSD: k=15e4, b=5000 LCSD: k=7e4, b=4000 NSD: k=1e5, b=600

Table D1 (continued)

Version	HIC36	Chest Accel (g)	Version History
18	283.2	32.15	SBSD: k=7e4, b=4000
19	289.0	32.54	SBSD: k=15e4, b=6000
20	292.0	32.31	Translated SBSD anchor on seat back mount to Gx=4.433, Gy=-3.168
21	228.4	32.27	NSD: k=15e4, b=900
22	n/a	n/a	No changes from _v21
23	210.1	31.33	Started with _v19 SBSD: Length=0.1 m, Current=0.269 m
24	419.0	176.00	SBSD: Length=0.4 m, Current=0.269 m
25	353.0	34.63	SBSD: Length=0.3 m, Current=0.269 m
26	315.0	32.74	SBSD: Length=0.285 m, Current=0.269 m
27	275.6	35.36	Started with _v25 NSD: k=1e5, b=1000
28	276.4	35.26	NSD: k=1e5, b=1100
29	282.3	35.23	NSD: k=1e5, b=1200
30	256.5	35.20	NSD: k=1e5, b=1250
31	246.8	34.88	NSD: k=1e5, b=1200, Length=0.019 m, Current=0.018 m
32	263.2	35.23	NSD: k=1e5, b=1210, Length=0.018 m, Current=0.018 m

Table D1 (continued)

Version	HIC36	Chest Accel (g)	Version History
33	275.7	35.96	NSD: k=1e5, b=1150
34	268.9	35.14	Stared with _v29 Head Mass=2.8 kg
35	264.3	35.31	Head Mass=2.65 kg
36	261.8	33.47	NSD: k=1e5, b=1205
37	273.9	36.65	NSD: k=1e5, b=1190
38	258.3	34.44	NSD: k=1e5, b=1200, Length=0.02 m, Current=0.018 m
39	282.3	33.47	Seat: μ_s=μ_k=0.5
40	255.7	34.58	Translating seat pan spring-dampers to match attachment locations on B_v51
41	261.4	35.47	Seat: μ_s=μ_k=0.5 SBSD: k=15e4, b=6000, Length=0.3 m, Current=0.269 m
42	326.4	49.37	SBSD: k=15e4, b=20 LCSD: k=7e4, b=20
43	214.9	33.36	Translated SBSD anchor on seat back mount to Gx=4.494, Gy=-3.307
44	255.7	34.50	Started with _v41 Seat: μ_s=μ_k=0.3 SBSD: k=15e4, b=6000, Length=0.3 m, Current=0.269 m

Table D1 (continued)

Version	HIC36	Chest Accel (g)	Version History
45	254.5	28.74	NSD: b=600
46	302.2	31.67	Translated SBSD anchor on seat back mount to Gx=4.494, Gy=-3.307

Note. Chest Accel refers to the Chest Acceleration, 3 ms clip. SD refers to spring-damper. SBSD refers to the shoulder belt spring-damper. LBSD refers to the lap belt spring-damper. k refers to the spring constant in N/m. b refers to the damping coefficient in N-s/m. Gx refers to the Global x position in m. Gy refers to the Global y position in m. NSD refers to the neck spring-damper. _v refers to the model version number. μ_s refers to the coefficient of static friction. μ_k refers to the coefficient of kinetic friction.

Table D2

Working Model Trial B Model Versions

Version	HIC36	Chest Accel (g)	Version History
1	n/a	n/a	Started with A_v29 Added Booster: h=0.057, w=0.264, Mass=0.015, μ_s=μ_k=0.3, BSD: k=50, b=1, Length=0.098 m, Current=0.098 m
2	210.4	31.84	Translated ATD to contact the Booster BSD: k=50, b=1, Length=0.098 m, Current=0.043 m
3	322.4	41.56	Booster: h=0.029, w=0.264 BSD: k=50, b=1, Length=0.058 m, Current=0.029 m
4	317.6	42.44	BSD: k=50, b=10
5	317.0	40.77	BSD: k=1000, b=10
6	327.9	44.87	BSD: k=10,000, b=10
7	322.3	43.31	Started with _v5 BSD: k=1000, b=100
8	319.7	43.64	BSD: k=50, b=100
9	325.5	44.35	BSD: k=5000, b=100
10	n/a	n/a	BSD: k=5e5, b=25e4
11	330.1	47.30	Started with _v5 BSD: k=1000, b=50
12	329.2	46.24	BSD: k=500, b=500

Table D2 (continued)

Version	HIC36	Chest Accel (g)	Version History
13	314.5	43.26	BSD: k=10, b=10
14	308.5	41.74	BSD: k=20, b=10
15	316.9	44.57	BSD: k=10, b=5
16	303.9	41.34	BSD: k=50, b=25
17	313.6	43.04	BSD: k=50, b=20
18	319.8	40.52	BSD: k=50, b=2
19	236.4	35.53	Started with _v2 Booster: h=0.08, w=0.279, Mass=0.425 kg, μ_s=0.9, μ_k=0.8, E=0.95, ρ=19.041 BSD: k=50, b=1, Length=0.029 m, Current=0.058 m Translated ATD to contact the Booster
20	302.9	44.4	Booster: h=0.060, w=0.279, Mass=0.408 kg, ρ=24.373 BSD: k=50, b=1, Length=0.029 m, Current=0.070 m
21	297.3	43.51	BSD: k=50, b=1, Length=0.070 m, Current=0.070 m
22	211.5	31.49	Started with _v2 Booster: h=0.057, w=0.279, Mass=0.408 kg, ρ=25.656 BSD: k=50, b=1, Length=0.043 m, Current=0.043 m

Table D2 (continued)

Version	HIC36	Chest Accel (g)	Version History
23	226.4	33.90	Booster: h=0.05, w=0.279 BSD: k=50, b=1, Length=0.043 m, Current=0.047 m
24	227.5	34.00	BSD: k=50, b=20
25	211.5	31.49	Started with _v22 Booster: μ_s=μ_k=0.3, E=0.0
26	211.9	31.4	BSD: k=50, b=20
27	211.9	31.42	Booster: E=0.5
28	211.9	31.42	Booster: E=2.0
29	n/a	n/a	No change
30	199.0	29.13	Started with _v29 Translated SBSD anchor on seat back mount to Gx=4.407, Gy=-3.116
31	181.4	24.21	Translated SBSD anchor on seat back mount to Gx=4.476, Gy=-3.027
32	269.2	36.84	Translated SBSD anchor on seat back mount to Gx=4.495, Gy=-3.307
33	211.9	31.42	Started with _v29 Added UTSD: k=50, b=1
34	211.1	31.24	UTSD: k=1000, b=100
35	211.8	31.39	UTSD: k=10,000, b=1000
36	211.8	31.39	Seat back: h=0.024, w=0.444

Table D2 (continued)

Version	HIC36	Chest Accel (g)	Version History
37	235.8	33.85	Booster: h=0.048, w=0.279, Mass=0.408 kg, μ_s=μ_k=0.3, E=0.5, ρ=30.404 BSD: k=50, b=20, Length=0.043 m, Current=0.043 m
38	239.1	35.63	BSD: k=500, b=200
39	234.4	33.2	Started with _v36 Booster: h=0.053, w=0.277, Mass=0.408 kg, μ_s=μ_k=0.3, E=2.0, ρ=27.769 NSD: k=1e5, b=1000
40	215.6	33.36	NSD: k=1e5, b=1200
41	243.6	35.27	Booster: h=0.047, w=0.283, Mass=0.408 kg, μ_s=μ_k=1.0, E=1.0, ρ=30.480 BSD: k=1000, b=200, Length=0.053 m, Current=0.053 m
42	211.9	31.42	Booster: h=0.057, w=0.279, Mass=0.408 kg, μ_s=μ_k=0.3, E=0.5, ρ=25.656 BSD: k=50, b=20, Length=0.043 m, Current=0.043 m
43	322.4	41.38	Started with _v3 BSD: k=50, b=1, Length=0.029 m, Current=0.058 m
44	269.2	36.84	Started with _v36 Booster: h=0.057, w=0.279, Mass=0.408 kg, μ_s=μ_k=0.3, E=0.5, ρ=25.656 BSD: k=50, b=20, Length=0.043 m, Current=0.043 m

Table D2 (continued)

Version	HIC36	Chest Accel (g)	Version History
45	276.8	37.68	Started with _v36 Translated SBSD anchor on seat back mount to Gx=4.501, Gy=-3.327
46	241.4	34.37	Translated SBSD anchor on seat back mount to Gx=4.463, Gy=-3.238
47	269.2	36.84	Same as _v32
48	271.9	36.16	Seat: μ_s=μ_k=0.5 Booster: μ_s=μ_k=0.5
49	269.2	36.84	Seat: μ_s=μ_k=0.3 Booster: μ_s=μ_k=0.3
50	269.2	36.84	Same as _v49
51	257.9	37.48	Translated LBSD anchor from torso to femur to Gx=4.797, Gy=-3.315 LBSD: k=7e4, b=4000, Length=0.229 m, Current=0.229 m
52	274.5	38.88	Translated Booster such that distance from seat pan is 0.006 m Translated LBSD anchor from femur to torso to Gx=4.798, Gy=-3.300
53	311.5	39.99	Translated SBSD anchor on torso to Gx=4.653, Gy=-3.068
54	259.9	37.33	Translated SBSD anchor on torso to Gx=4.853, Gy=-3.089

Table D2 (continued)

Version	HIC36	Chest Accel (g)	Version History
55	289.0	35.5	Translated SBSD anchor on torso to Gx=4.671, Gy=-3.079 SBSD: k=15e4, b=20, Length=0.287 m, Current=0.287 m LBSD: k=7e4, b=20, Length=0.244 m, Current=0.244 m
56	320.7	35.00	NSD: b=600 Translated SBSD anchor on seat back mount to Gx=4.494, Gy=-3.307

Note. Chest Accel refers to the Chest Acceleration, 3 ms clip. h refers to height in meters. w refers to width in meters. BSD refers to the Booster spring-dampers. E refers to the modulus of elasticity. ρ refers to material density in kg/m^2. SBSD refers to the shoulder belt spring-damper. LBSD refers to the lap belt spring-damper. k refers to the spring constant in N/m. b refers to the damping coefficient in N-s/m. Gx refers to the Global x position in m. Gy refers to the Global y position in m. UTSD refers to the Travel Vest's upper tether spring damper. NSD refers to the neck spring-damper. _v refers to the model version number. μ_s refers to the coefficient of static friction. μ_k refers to the coefficient of kinetic friction.

Table D3

Working Model Trial C/D Model Versions

Version	HIC36	Chest Accel (g)	Version History
1	176.5	27.72	Started with B_v47 ATD: hip flexion=30°, hip abduction=20°, knee flexion=60° Added bilateral femur fracture cast with 0.0508 m offset from ATD torso. Cast: Mass=3.0 kg, μ_s=μ_k=0.3, E=0.5 Translate Booster car forward 0.095 m to represent positioning on Trial C/D sled tests. Seat pan: h=0.027, w=0.456 Translate and rotate ATD to contact seat back, seat pan, and Booster Translated LBSD anchor on torso to cast to Gx=4.944, Gy=-3.195 SBSD: k=15e4, b=6000, Length=0.249 m, Current=0.249 m LBSD: k=7e4, b=4000, Length=0.393 m, Current=0.393 m
2	182.7	27.08	SBSD: k=15e3, b=6000
3	130.2	29.66	Translated SBSD anchor on seat back mount to Gx=4.395, Gy=-3.061 SBSD: k=15e4, b=6000
4	177.2	11.93	Translated SBSD anchor from torso to cast to Gx=4.771, Gy=-3.108

Table D3 (continued)

Version	HIC36	Chest Accel (g)	Version History
5	n/a	n/a	Translated SBSD anchor on cast to Gx=4.765, Gy=-3.105
6	n/a	n/a	Started with C/D_v2 Translated SBSD anchor from torso cast to Gx=4.787, Gy=-3.097 Added LBSD to Booster with anchors at Gx=4.756, Gy=-3.542, and Gx=4.877, Gy=-3.341 New LBSD: k=7e4, b=4000, Length= 0.233 m, Current=0.233 m
7	122.6	27.97	Started with C/D_v1 SBSD: k=1500, b=6000
8	129.2	30.27	Started with C/D_v1 LBSD: k=7000, b=4000
9	192.2	30.27	Started with C/D_v1 SBSD: k=1500, b=600
10	179.8	34.60	LBSD: k=7000, b=400
11	184.2	36.37	LBSD: k=7000, b=40
12	215.6	39.45	SBSD: k=1500, b=60
13	177.9	52.97	SBSD: k=15e3, b=60 LBSD: k=7e4, b=40

Table D3 (continued)

Version	HIC36	Chest Accel (g)	Version History
14	345.3	40.28	Started with C/D_v12 Translated SBSD anchor on seat back mount to Gx=4.495 Gy=-3.306 SBSD: k=15e3, b=60
15	253.4	42.65	Translated SBSD anchor on seat back mount to Gx=4.463 Gy=-3.232
16	362.9	39.97	Started with C/D_v14 SBSD: k=15e4, b=40 LBSD: k=7e4, b=40
17	376.5	40.12	SBSD: k=15e4, b=20 LBSD: k=7e4, b=20
18	397.5	39.64	SBSD: k=15e4, b=10 LBSD: k=7e4, b=10
19	370.2	52.90	Started with C/D_v17 Cast: Mass=11.1 kg
20	364.0	39.92	Seat: μ_s=μ_k=0.5, E=0.0 Booster: μ_s=μ_k=0.5, E=0.5 Cast: Mass=1.85 kg, μ_s=μ_k=0.33, E=0.5
21	371.9	39.78	Booster: μ_s=μ_k=0.4
22	248.4	36.43	Booster: μ_s=μ_k=0.3

Table D3 (continued)

Version	HIC36	Chest Accel (g)	Version History
23	233.1	37.88	Translated LBSD anchor from cast to torso to Gx=4.918 Gy=-3.208 Seat: μ_s=μ_k=0.5 Booster: μ_s=μ_k=0.5 Cast: μ_s=μ_k=0.5
24	208.2	39.25	Translated LBSD anchor from torso to cast to Gx=4.939 Gy=-3.193
25	268.2	40.21	Seat: μ_s=μ_k=0.3 Booster: μ_s=μ_k=0.3 Cast: μ_s=μ_k=0.3
26	252.9	40.41	Started with C/D_v19 Cast: Mass=1.85 kg
27	304.1	42.12	Translated LBSD anchor on cast to Gx=4.987, Gy=-3.213
28	264.4	42.96	Added cast pieces to cover ankle/foot Cast: Mass=1.85 kg
29	245.6	40.43	Adjustment of seat pan depth to reflect pre-test photos from Trials C & D
30	427.9	49.96	Translation of ATD to reflect pre-test photos from Trials C & D

Note. Chest Accel refers to the Chest Acceleration, 3 ms clip. _v refers to the model version number. h refers to height in meters. w refers to width in meters. E refers to the modulus of elasticity. ρ refers to material density in kg/m^2. SBSD refers to the shoulder belt spring-damper. LBSD refers to the lap belt spring-damper. k refers to the spring constant in N/m. b refers to the damping coefficient in N-s/m. Gx refers to the Global x position in m. Gy refers to the Global y position in m. μ_s refers to the coefficient of static friction. μ_k refers to the coefficient of kinetic friction.

Table D4

Working Model DDH Model Versions

Version	HIC36	Chest Accel (g)	Version History
1	n/a	n/a	Started with B_v47
2	n/a	n/a	ATD: hip flexion=80°, hip abduction=55°, knee flexion=80° Reduce length of femur and foot due to hip abduction angle. Added DDH cast with 0.0508 m offset from ATD torso. Cast: Mass=4.5 kg, μ_s=μ_k=0.3, E=0.5 Translate Booster car forward 0.095 m to represent positioning on Trial C/D sled tests. Seat pan: h=0.027, w=0.456 Translate and rotate ATD to contact seat back and Booster
3	378.0	51.24	Cast: Mass=11.7 kg Translated LBSD anchor to torso to Gx=4.918 Gy=-3.208
4	n/a	n/a	Adjusted cast to better fit along spine and rotated ATD positioning for closer contact with seat back.
5	419.3	85.57	Added rods to cast to ensure fixed distance
6	276.6	41.14	Translated SBSD anchor on seat back mount to Gx=4.441 Gy=-3.165
7	215.4	33.44	SBSD: k=15e4, b=2000

Table D4 (continued)

Version	HIC36	Chest Accel (g)	Version History
8	229.8	34.59	Started with DDH_v6 Cast: Mass=1.3 kg, μ_s=μ_k=0.33 Seat: μ_s=μ_k=0.5 Booster: μ_s=μ_k=0.5
9	257.7	36.00	Translated SBSD anchor on seat back mount to Gx=4.494 Gy=-3.307
10	n/a	n/a	Cast: Mass=11.7 kg, μ_s=μ_k=0.3 Seat: μ_s=μ_k=0.3 Booster: μ_s=μ_k=0.3 Changed pins to rigid joints at knee and ankle Translated LBSD anchor from torso to cast to Gx=4.877 Gy=-3.191
11	291.3	47.13	Started with DDH_v9 Translated LBSD anchor on cast to Gx=4.891 Gy=-3.202
12	321.2	47.09	Cast: Mass=1.305 kg, μ_s=μ_k=0.3 Seat: μ_s=μ_k=0.3 Booster: μ_s=μ_k=0.3
13	382.1	37.71	Adjustment of seat pan depth to reflect pre-test photos from Trials C & D

Note. Chest Accel refers to the Chest Acceleration, 3 ms clip. _v refers to the model version number. h refers to height in meters. w refers to width in meters. E refers to the modulus of elasticity. ρ refers to material density in kg/m^2. SBSD refers to the shoulder belt spring-damper. LBSD refers to the lap belt spring-damper. k refers to the spring constant in N/m. b refers to the damping coefficient in N-s/m. Gx refers to the Global x position in m. Gy refers to the Global y position in m. μ_s refers to the coefficient of static friction. μ_k refers to the coefficient of kinetic friction.

APPENDIX E

Chest G and HIC Calculator Formulas

Figure E1

Raw Data Example from Working Model Simulations

	A	B	C	D	E	F	G	H	I	J	K	L	M	N
1	20250530 - A - Trial A 3yo Vest_v46													
2	5/30/2025 12:20													
3	Sled Acceleration		Head Acceleration					Chest Acceleration					Velocity of Sled 1	
4	t	Ax	t	|A|				t	|A|				t	Vx
5	0	-0.032	0	9.807	-	-	-	0	12.205	-	-	-	0	0
6	0.001	-0.026	0.001	9.825	-	-	-	0.001	9.828	-	-	-	0.001	-2.93E-05
7	0.002	-0.021	0.002	9.804	-	-	-	0.002	9.656	-	-	-	0.002	-5.32E-05
8	0.003	-0.018	0.003	9.769	-	-	-	0.003	9.328	-	-	-	0.003	-7.27E-05
9	0.004	-0.061	0.004	9.713	-	-	-	0.004	8.915	-	-	-	0.004	-9.67E-05
10	0.005	-21.289	0.005	9.626	-	-	-	0.005	8.517	-	-	-	0.005	-0.011
11	0.006	-42.485	0.006	9.507	-	-	-	0.006	8.293	-	-	-	0.006	-0.043
12	0.007	-63.642	0.007	9.38	-	-	-	0.007	8.419	-	-	-	0.007	-0.096
13	0.008	-84.76	0.008	9.272	-	-	-	0.008	9.192	-	-	-	0.008	-0.17
14	0.009	-105.846	0.009	9.209	-	-	-	0.009	11.107	-	-	-	0.009	-0.265
15	0.01	-126.909	0.01	9.218	-	-	-	0.01	14.604	-	-	-	0.01	-0.382
16	0.011	-147.959	0.011	9.347	-	-	-	0.011	19.862	-	-	-	0.011	-0.519
17	0.012	-169.006	0.012	9.668	-	-	-	0.012	27.006	-	-	-	0.012	-0.678
18	0.013	-190.01	0.013	10.299	-	-	-	0.013	36.168	-	-	-	0.013	-0.857
19	0.014	-189.838	0.014	11.453	-	-	-	0.014	47.204	-	-	-	0.014	-1.047
300	0.295	0.221	0.295	31.797	-	-	-	0.295	17.841	-	-	-	0.295	-11.06
301	0.296	0.17	0.296	33.735	-	-	-	0.296	13.607	-	-	-	0.296	-11.06
302	0.297	0.113	0.297	35.059	-	-	-	0.297	9.526	-	-	-	0.297	-11.06
303	0.298	0.042	0.298	35.449	-	-	-	0.298	6.04	-	-	-	0.298	-11.06
304	0.299	-0.03	0.299	34.962	-	-	-	0.299	4.075	-	-	-	0.299	-11.06
305	0.3	-0.098	0.3	33.779	-	-	-	0.3	4.834	-	-	-	0.3	-11.06
306	0.3	-0.054	0.3	13.814	-	-	-	0.3	1.79	-	-	-	0.3	-11.06

Note. Data shown in Excel worksheet after importing from .dta format. Rows 20-299 hidden for clarity.

Figure E2

Chest Acceleration Calculator Example for Working Model Simulations, part 1

	S	T	U	V
1	**Chest Accel CFC**	**time**	**Chest Accel Resultant**	**Partial Filter**
2	180	0	=I5/9.81	
3	**Sample Period**	0.001	=I7/9.81	
4	0.001	0.002	=I8/9.81	=$S$10*U4+$S$12*U3+$S$14*U2+$S$16*V3+$S$18*V2
5	**wd**	0.003	=I9/9.81	=$S$10*U5+$S$12*U4+$S$14*U3+$S$16*V4+$S$18*V3
6	=2*PI()*S2*2.0775	0.004	=I10/9.81	=$S$10*U6+$S$12*U5+$S$14*U4+$S$16*V5+$S$18*V4
7	**wa**	0.005	=I11/9.81	=$S$10*U7+$S$12*U6+$S$14*U5+$S$16*V6+$S$18*V5
8	=(SIN(S6*S4/2))/(COS(S6*S4/2))	0.006	=I12/9.81	=$S$10*U8+$S$12*U7+$S$14*U6+$S$16*V7+$S$18*V6
9	**a0**	0.007	=I13/9.81	=$S$10*U9+$S$12*U8+$S$14*U7+$S$16*V8+$S$18*V7
10	=S8^2/(1+SQRT(2)*S8+S8^2)	0.008	=I14/9.81	=$S$10*U10+$S$12*U9+$S$14*U8+$S$16*V9+$S$18*V8
11	**a1**	0.009	=I15/9.81	=$S$10*U11+$S$12*U10+$S$14*U9+$S$16*V10+$S$18*V9
12	=2*S10	0.01	=I16/9.81	=$S$10*U12+$S$12*U11+$S$14*U10+$S$16*V11+$S$18*V10
13	**a2**	0.011	=I17/9.81	=$S$10*U13+$S$12*U12+$S$14*U11+$S$16*V12+$S$18*V11
14	=S10	0.012	=I18/9.81	=$S$10*U14+$S$12*U13+$S$14*U12+$S$16*V13+$S$18*V12
15	**b1**	0.013	=I19/9.81	=$S$10*U15+$S$12*U14+$S$14*U13+$S$16*V14+$S$18*V13
16	=-2*(S8^2-1)/(1+SQRT(2)*S8+S8^2)	0.014	=I20/9.81	=$S$10*U16+$S$12*U15+$S$14*U14+$S$16*V15+$S$18*V14
17	**b2**	0.015	=I21/9.81	=$S$10*U17+$S$12*U16+$S$14*U15+$S$16*V16+$S$18*V15
18	=(-1+SQRT(2)*S8-S8^2)/(1+SQRT(2)*S8+S8^2)	0.016	=I22/9.81	=$S$10*U18+$S$12*U17+$S$14*U16+$S$16*V17+$S$18*V16
19		0.017	=I23/9.81	=$S$10*U19+$S$12*U18+$S$14*U17+$S$16*V18+$S$18*V17
300		0.298	=I304/9.81	=$S$10*U300+$S$12*U299+$S$14*U298+$S$16*V299+$S$18*V298
301		0.299	=I305/9.81	=$S$10*U301+$S$12*U300+$S$14*U299+$S$16*V300+$S$18*V299
302		0.3	=I306/9.81	=$S$10*U302+$S$12*U301+$S$14*U300+$S$16*V301+$S$18*V300
303				

Note. Rows 20-299 hidden for clarity.

Figure E3

Chest Acceleration Calculator Example for Working Model Simulations, part 2

	S	V	W
1	**Chest Accel CFC**	**Partial Filter**	**Final Filter**
2	180		=$S$10*V2+$S$12*V3+$S$14*V4+$S$16*W3+$S$18*W4
3	**Sample Period**		=$S$10*V3+$S$12*V4+$S$14*V5+$S$16*W4+$S$18*W5
4	0.001	=$S$10*U4+$S$12*U3+$S$14*U2+$S$16*V3+$S$18*V2	=$S$10*V4+$S$12*V5+$S$14*V6+$S$16*W5+$S$18*W6
5	**wd**	=$S$10*U5+$S$12*U4+$S$14*U3+$S$16*V4+$S$18*V3	=$S$10*V5+$S$12*V6+$S$14*V7+$S$16*W6+$S$18*W7
6	=2*PI()*S2*2.0775	=$S$10*U6+$S$12*U5+$S$14*U4+$S$16*V5+$S$18*V4	=$S$10*V6+$S$12*V7+$S$14*V8+$S$16*W7+$S$18*W8
7	**wa**	=$S$10*U7+$S$12*U6+$S$14*U5+$S$16*V6+$S$18*V5	=$S$10*V7+$S$12*V8+$S$14*V9+$S$16*W8+$S$18*W9
8	=(SIN(S6*S4/2))/(COS(S6*S4/2))	=$S$10*U8+$S$12*U7+$S$14*U6+$S$16*V7+$S$18*V6	=$S$10*V8+$S$12*V9+$S$14*V10+$S$16*W9+$S$18*W10
9	**a0**	=$S$10*U9+$S$12*U8+$S$14*U7+$S$16*V8+$S$18*V7	=$S$10*V9+$S$12*V10+$S$14*V11+$S$16*W10+$S$18*W11
10	=S8^2/(1+SQRT(2)*S8+S8^2)	=$S$10*U10+$S$12*U9+$S$14*U8+$S$16*V9+$S$18*V8	=$S$10*V10+$S$12*V11+$S$14*V12+$S$16*W11+$S$18*W12
11	**a1**	=$S$10*U11+$S$12*U10+$S$14*U9+$S$16*V10+$S$18*V9	=$S$10*V11+$S$12*V12+$S$14*V13+$S$16*W12+$S$18*W13
12	=2*S10	=$S$10*U12+$S$12*U11+$S$14*U10+$S$16*V11+$S$18*V10	=$S$10*V12+$S$12*V13+$S$14*V14+$S$16*W13+$S$18*W14
13	**a2**	=$S$10*U13+$S$12*U12+$S$14*U11+$S$16*V12+$S$18*V11	=$S$10*V13+$S$12*V14+$S$14*V15+$S$16*W14+$S$18*W15
14	=S10	=$S$10*U14+$S$12*U13+$S$14*U12+$S$16*V13+$S$18*V12	=$S$10*V14+$S$12*V15+$S$14*V16+$S$16*W15+$S$18*W16
15	**b1**	=$S$10*U15+$S$12*U14+$S$14*U13+$S$16*V14+$S$18*V13	=$S$10*V15+$S$12*V16+$S$14*V17+$S$16*W16+$S$18*W17
16	=-2*(S8^2-1)/(1+SQRT(2)*S8+S8^2)	=$S$10*U16+$S$12*U15+$S$14*U14+$S$16*V15+$S$18*V14	=$S$10*V16+$S$12*V17+$S$14*V18+$S$16*W17+$S$18*W18
17	**b2**	=$S$10*U17+$S$12*U16+$S$14*U15+$S$16*V16+$S$18*V15	=$S$10*V17+$S$12*V18+$S$14*V19+$S$16*W18+$S$18*W19
18	=(-1+SQRT(2)*S8-S8^2)/(1+SQRT(2)*S8+S8^2)	=$S$10*U18+$S$12*U17+$S$14*U16+$S$16*V17+$S$18*V16	=$S$10*V18+$S$12*V19+$S$14*V20+$S$16*W19+$S$18*W20
19		=$S$10*U19+$S$12*U18+$S$14*U17+$S$16*V18+$S$18*V17	=$S$10*V19+$S$12*V20+$S$14*V21+$S$16*W20+$S$18*W21
300		=$S$10*U300+$S$12*U299+$S$14*U298+$S$16*V299+$S$18*V298	=$S$10*V300+$S$12*V301+$S$14*V302+$S$16*W301+$S$18*W302
301		=$S$10*U301+$S$12*U300+$S$14*U299+$S$16*V300+$S$18*V299	
302		=$S$10*U302+$S$12*U301+$S$14*U300+$S$16*V301+$S$18*V300	
303			

Note. Rows 20-299 and Columns T-U hidden for clarity.

Figure E4

Chest Acceleration Calculator Example for Working Model Simulations, part 3

	S	W	X
1	**Chest Accel CFC**	**Final Filter**	**SORT**
2	180	=$S$10*V2+$S$12*V3+$S$14*V4+$S$16*W3+$S$18*W4	=SORT(W2:W300, 1, -1)
3	**Sample Period**	=$S$10*V3+$S$12*V4+$S$14*V5+$S$16*W4+$S$18*W5	
4	0.001	=$S$10*V4+$S$12*V5+$S$14*V6+$S$16*W5+$S$18*W6	
5	**wd**	=$S$10*V5+$S$12*V6+$S$14*V7+$S$16*W6+$S$18*W7	
6	=2*PI()*S2*2.0775	=$S$10*V6+$S$12*V7+$S$14*V8+$S$16*W7+$S$18*W8	
7	**wa**	=$S$10*V7+$S$12*V8+$S$14*V9+$S$16*W8+$S$18*W9	
8	=(SIN(S6*S4/2))/(COS(S6*S4/2))	=$S$10*V8+$S$12*V9+$S$14*V10+$S$16*W9+$S$18*W10	
9	**a0**	=$S$10*V9+$S$12*V10+$S$14*V11+$S$16*W10+$S$18*W11	
10	=S8^2/(1+SQRT(2)*S8+S8^2)	=$S$10*V10+$S$12*V11+$S$14*V12+$S$16*W11+$S$18*W12	
11	**a1**	=$S$10*V11+$S$12*V12+$S$14*V13+$S$16*W12+$S$18*W13	
12	=2*S10	=$S$10*V12+$S$12*V13+$S$14*V14+$S$16*W13+$S$18*W14	
13	**a2**	=$S$10*V13+$S$12*V14+$S$14*V15+$S$16*W14+$S$18*W15	
14	=S10	=$S$10*V14+$S$12*V15+$S$14*V16+$S$16*W15+$S$18*W16	
15	**b1**	=$S$10*V15+$S$12*V16+$S$14*V17+$S$16*W16+$S$18*W17	
16	=-2*(S8^2-1)/(1+SQRT(2)*S8+S8^2)	=$S$10*V16+$S$12*V17+$S$14*V18+$S$16*W17+$S$18*W18	
17	**b2**	=$S$10*V17+$S$12*V18+$S$14*V19+$S$16*W18+$S$18*W19	
18	=(-1+SQRT(2)*S8-S8^2)/(1+SQRT(2)*S8+S8^2)	=$S$10*V18+$S$12*V19+$S$14*V20+$S$16*W19+$S$18*W20	
19		=$S$10*V19+$S$12*V20+$S$14*V21+$S$16*W20+$S$18*W21	
300		=$S$10*V300+$S$12*V301+$S$14*V302+$S$16*W301+$S$18*W302	
301			
302			
303			

Note. Chest Acceleration, 3 ms clip, will be shown in cell X6 once sheet is calculated.

Rows 20-299 and Columns T-U hidden for clarity.

Figure E5

HIC36 Calculator Example for Working Model Simulations, part 1

	AB	AC	AD	AE
1	**Head Accel CFC**	**time**	**Head Accel Resultant**	**Partial Filter**
2	1000	0	=D6/9.81	
3	**Sample Period**	0.001	=D7/9.81	
4	0.001	0.002	=D8/9.81	=$S$10*AD4+$S$12*AD3+$S$14*AD2+$S$16*AE3+$S$18*AE2
5	**wd**	0.003	=D9/9.81	=$S$10*AD5+$S$12*AD4+$S$14*AD3+$S$16*AE4+$S$18*AE3
6	=2*PI()*AB2*2.0775	0.004	=D10/9.81	=$S$10*AD6+$S$12*AD5+$S$14*AD4+$S$16*AE5+$S$18*AE4
7	**wa**	0.005	=D11/9.81	=$S$10*AD7+$S$12*AD6+$S$14*AD5+$S$16*AE6+$S$18*AE5
8	=(SIN(AB6*AB4/2))/(COS(AB6*AB4/2))	0.006	=D12/9.81	=$S$10*AD8+$S$12*AD7+$S$14*AD6+$S$16*AE7+$S$18*AE6
9	**a0**	0.007	=D13/9.81	=$S$10*AD9+$S$12*AD8+$S$14*AD7+$S$16*AE8+$S$18*AE7
10	=AB8^2/(1+SQRT(2)*AB8+AB8^2)	0.008	=D14/9.81	=$S$10*AD10+$S$12*AD9+$S$14*AD8+$S$16*AE9+$S$18*AE8
11	**a1**	0.009	=D15/9.81	=$S$10*AD11+$S$12*AD10+$S$14*AD9+$S$16*AE10+$S$18*AE9
12	=2*AB10	0.01	=D16/9.81	=$S$10*AD12+$S$12*AD11+$S$14*AD10+$S$16*AE11+$S$18*AE10
13	**a2**	0.011	=D17/9.81	=$S$10*AD13+$S$12*AD12+$S$14*AD11+$S$16*AE12+$S$18*AE11
14	=AB10	0.012	=D18/9.81	=$S$10*AD14+$S$12*AD13+$S$14*AD12+$S$16*AE13+$S$18*AE12
15	**b1**	0.013	=D19/9.81	=$S$10*AD15+$S$12*AD14+$S$14*AD13+$S$16*AE14+$S$18*AE13
16	=-2*(AB8^2-1)/(1+SQRT(2)*AB8+AB8^2)	0.014	=D20/9.81	=$S$10*AD16+$S$12*AD15+$S$14*AD14+$S$16*AE15+$S$18*AE14
17	**b2**	0.015	=D21/9.81	=$S$10*AD17+$S$12*AD16+$S$14*AD15+$S$16*AE16+$S$18*AE15
18	=(-1+SQRT(2)*AB8-AB8^2)/(1+SQRT(2)*AB8+AB8^2)	0.016	=D22/9.81	=$S$10*AD18+$S$12*AD17+$S$14*AD16+$S$16*AE17+$S$18*AE16
19		0.017	=D23/9.81	=$S$10*AD19+$S$12*AD18+$S$14*AD17+$S$16*AE18+$S$18*AE17
300		0.298	=D304/9.81	=$S$10*AD300+$S$12*AD299+$S$14*AD298+$S$16*AE299+$S$18*AE298
301		0.299	=D305/9.81	=$S$10*AD301+$S$12*AD300+$S$14*AD299+$S$16*AE300+$S$18*AE299
302		0.3	=D306/9.81	=$S$10*AD302+$S$12*AD301+$S$14*AD300+$S$16*AE301+$S$18*AE300
303				

Note. Rows 20-299 hidden for clarity.

Figure E6

HIC36 Calculator Example for Working Model Simulations, part 2

	AB	AE	AF
1	**Head Accel CFC**	**Partial Filter**	**Final Filter**
2	1000		=$S$10*AE2+$S$12*AE3+$S$14*AE4+$S$16*AF3+$S$18*AF4
3	**Sample Period**		=$S$10*AE3+$S$12*AE4+$S$14*AE5+$S$16*AF4+$S$18*AF5
4	0.001	=$S$10*AD4+$S$12*AD3+$S$14*AD2+$S$16*AE3+$S$18*AE2	=$S$10*AE4+$S$12*AE5+$S$14*AE6+$S$16*AF5+$S$18*AF6
5	**wd**	=$S$10*AD5+$S$12*AD4+$S$14*AD3+$S$16*AE4+$S$18*AE3	=$S$10*AE5+$S$12*AE6+$S$14*AE7+$S$16*AF6+$S$18*AF7
6	=2*PI()*AB2*2.0775	=$S$10*AD6+$S$12*AD5+$S$14*AD4+$S$16*AE5+$S$18*AE4	=$S$10*AE6+$S$12*AE7+$S$14*AE8+$S$16*AF7+$S$18*AF8
7	**wa**	=$S$10*AD7+$S$12*AD6+$S$14*AD5+$S$16*AE6+$S$18*AE5	=$S$10*AE7+$S$12*AE8+$S$14*AE9+$S$16*AF8+$S$18*AF9
8	=(SIN(AB6*AB4/2))/(COS(AB6*AB4/2))	=$S$10*AD8+$S$12*AD7+$S$14*AD6+$S$16*AE7+$S$18*AE6	=$S$10*AE8+$S$12*AE9+$S$14*AE10+$S$16*AF9+$S$18*AF10
9	**a0**	=$S$10*AD9+$S$12*AD8+$S$14*AD7+$S$16*AE8+$S$18*AE7	=$S$10*AE9+$S$12*AE10+$S$14*AE11+$S$16*AF10+$S$18*AF11
10	=AB8^2/(1+SQRT(2)*AB8+AB8^2)	=$S$10*AD10+$S$12*AD9+$S$14*AD8+$S$16*AE9+$S$18*AE8	=$S$10*AE10+$S$12*AE11+$S$14*AE12+$S$16*AF11+$S$18*AF12
11	**a1**	=$S$10*AD11+$S$12*AD10+$S$14*AD9+$S$16*AE10+$S$18*AE9	=$S$10*AE11+$S$12*AE12+$S$14*AE13+$S$16*AF12+$S$18*AF13
12	=2*AB10	=$S$10*AD12+$S$12*AD11+$S$14*AD10+$S$16*AE11+$S$18*AE10	=$S$10*AE12+$S$12*AE13+$S$14*AE14+$S$16*AF13+$S$18*AF14
13	**a2**	=$S$10*AD13+$S$12*AD12+$S$14*AD11+$S$16*AE12+$S$18*AE11	=$S$10*AE13+$S$12*AE14+$S$14*AE15+$S$16*AF14+$S$18*AF15
14	=AB10	=$S$10*AD14+$S$12*AD13+$S$14*AD12+$S$16*AE13+$S$18*AE12	=$S$10*AE14+$S$12*AE15+$S$14*AE16+$S$16*AF15+$S$18*AF16
15	**b1**	=$S$10*AD15+$S$12*AD14+$S$14*AD13+$S$16*AE14+$S$18*AE13	=$S$10*AE15+$S$12*AE16+$S$14*AE17+$S$16*AF16+$S$18*AF17
16	=-2*(AB8^2-1)/(1+SQRT(2)*AB8+AB8^2)	=$S$10*AD16+$S$12*AD15+$S$14*AD14+$S$16*AE15+$S$18*AE14	=$S$10*AE16+$S$12*AE17+$S$14*AE18+$S$16*AF17+$S$18*AF18
17	**b2**	=$S$10*AD17+$S$12*AD16+$S$14*AD15+$S$16*AE16+$S$18*AE15	=$S$10*AE17+$S$12*AE18+$S$14*AE19+$S$16*AF18+$S$18*AF19
18	=(-1+SQRT(2)*AB8-AB8^2)/(1+SQRT(2)*AB8+AB8^2)	=$S$10*AD18+$S$12*AD17+$S$14*AD16+$S$16*AE17+$S$18*AE16	=$S$10*AE18+$S$12*AE19+$S$14*AE20+$S$16*AF19+$S$18*AF20
19		=$S$10*AD19+$S$12*AD18+$S$14*AD17+$S$16*AE18+$S$18*AE17	=$S$10*AE19+$S$12*AE20+$S$14*AE21+$S$16*AF20+$S$18*AF21
300		=$S$10*AD300+$S$12*AD299+$S$14*AD298+$S$16*AE299+$S$18*AE298	=$S$10*AE300+$S$12*AE301+$S$14*AE302+$S$16*AF301+$S$18*AF302
301		=$S$10*AD301+$S$12*AD300+$S$14*AD299+$S$16*AE300+$S$18*AE299	
302		=$S$10*AD302+$S$12*AD301+$S$14*AD300+$S$16*AE301+$S$18*AE300	
303			

Note. Rows 20-299 and Columns AC-AD hidden for clarity.

Figure E7

HIC36 Calculator Example for Working Model Simulations, part 3

	AF	AG	AH
1	**Final Filter**	**=MAX(AH1:AQ1)**	=MAX(AH3:AH300)
2	=$S$10*AE2+$S$12*AE3+$S$14*AE4+$S$16*AF3+$S$18*AF4	**HIC36**	**HIC1**
3	=$S$10*AE3+$S$12*AE4+$S$14*AE5+$S$16*AF4+$S$18*AF5		=0.001*(AVERAGE($AF2:$AF3))^2.5
4	=$S$10*AE4+$S$12*AE5+$S$14*AE6+$S$16*AF5+$S$18*AF6		=0.001*(AVERAGE($AF3:$AF4))^2.5
5	=$S$10*AE5+$S$12*AE6+$S$14*AE7+$S$16*AF6+$S$18*AF7		=0.001*(AVERAGE($AF4:$AF5))^2.5
6	=$S$10*AE6+$S$12*AE7+$S$14*AE8+$S$16*AF7+$S$18*AF8		=0.001*(AVERAGE($AF5:$AF6))^2.5
7	=$S$10*AE7+$S$12*AE8+$S$14*AE9+$S$16*AF8+$S$18*AF9		=0.001*(AVERAGE($AF6:$AF7))^2.5
8	=$S$10*AE8+$S$12*AE9+$S$14*AE10+$S$16*AF9+$S$18*AF10		=0.001*(AVERAGE($AF7:$AF8))^2.5
9	=$S$10*AE9+$S$12*AE10+$S$14*AE11+$S$16*AF10+$S$18*AF11		=0.001*(AVERAGE($AF8:$AF9))^2.5
10	=$S$10*AE10+$S$12*AE11+$S$14*AE12+$S$16*AF11+$S$18*AF12		=0.001*(AVERAGE($AF9:$AF10))^2.5
11	=$S$10*AE11+$S$12*AE12+$S$14*AE13+$S$16*AF12+$S$18*AF13		=0.001*(AVERAGE($AF10:$AF11))^2.5
12	=$S$10*AE12+$S$12*AE13+$S$14*AE14+$S$16*AF13+$S$18*AF14		=0.001*(AVERAGE($AF11:$AF12))^2.5
13	=$S$10*AE13+$S$12*AE14+$S$14*AE15+$S$16*AF14+$S$18*AF15		=0.001*(AVERAGE($AF12:$AF13))^2.5
14	=$S$10*AE14+$S$12*AE15+$S$14*AE16+$S$16*AF15+$S$18*AF16		=0.001*(AVERAGE($AF13:$AF14))^2.5
15	=$S$10*AE15+$S$12*AE16+$S$14*AE17+$S$16*AF16+$S$18*AF17		=0.001*(AVERAGE($AF14:$AF15))^2.5
16	=$S$10*AE16+$S$12*AE17+$S$14*AE18+$S$16*AF17+$S$18*AF18		=0.001*(AVERAGE($AF15:$AF16))^2.5
17	=$S$10*AE17+$S$12*AE18+$S$14*AE19+$S$16*AF18+$S$18*AF19		=0.001*(AVERAGE($AF16:$AF17))^2.5
18	=$S$10*AE18+$S$12*AE19+$S$14*AE20+$S$16*AF19+$S$18*AF20		=0.001*(AVERAGE($AF17:$AF18))^2.5
19	=$S$10*AE19+$S$12*AE20+$S$14*AE21+$S$16*AF20+$S$18*AF21		=0.001*(AVERAGE($AF18:$AF19))^2.5
300	=$S$10*AE300+$S$12*AE301+$S$14*AE302+$S$16*AF301+$S$18*AF302		=0.001*(AVERAGE($AF299:$AF300))^2.5
301			
302			
303			

Note. HIC36 will be shown in cell AG1 once sheet is calculated. Rows 20-299 hidden for clarity.

Figure E8

HIC36 Calculator Example for Working Model Simulations, part 4

	AG	AH	AI	BQ
1	=MAX(AH1:AQ1)	=MAX(AH3:AH300)	=MAX(AI3:AI300)	=MAX(BQ3:BQ300)
2	HIC36	HIC1	HIC2	HIC36
3		=0.001*(AVERAGE($AF2:$AF3))^2.5	=0.002*(AVERAGE($AF2:$AF4))^2.5	=0.036*(AVERAGE($AD2:$AD38))^2.5
4		=0.001*(AVERAGE($AF3:$AF4))^2.5	=0.002*(AVERAGE($AF3:$AF5))^2.5	=0.036*(AVERAGE($AD3:$AD39))^2.5
5		=0.001*(AVERAGE($AF4:$AF5))^2.5	=0.002*(AVERAGE($AF4:$AF6))^2.5	=0.036*(AVERAGE($AD4:$AD40))^2.5
6		=0.001*(AVERAGE($AF5:$AF6))^2.5	=0.002*(AVERAGE($AF5:$AF7))^2.5	=0.036*(AVERAGE($AD5:$AD41))^2.5
7		=0.001*(AVERAGE($AF6:$AF7))^2.5	=0.002*(AVERAGE($AF6:$AF8))^2.5	=0.036*(AVERAGE($AD6:$AD42))^2.5
8		=0.001*(AVERAGE($AF7:$AF8))^2.5	=0.002*(AVERAGE($AF7:$AF9))^2.5	=0.036*(AVERAGE($AD7:$AD43))^2.5
9		=0.001*(AVERAGE($AF8:$AF9))^2.5	=0.002*(AVERAGE($AF8:$AF10))^2.5	=0.036*(AVERAGE($AD8:$AD44))^2.5
10		=0.001*(AVERAGE($AF9:$AF10))^2.5	=0.002*(AVERAGE($AF9:$AF11))^2.5	=0.036*(AVERAGE($AD9:$AD45))^2.5
11		=0.001*(AVERAGE($AF10:$AF11))^2.5	=0.002*(AVERAGE($AF10:$AF12))^2.5	=0.036*(AVERAGE($AD10:$AD46))^2.5
12		=0.001*(AVERAGE($AF11:$AF12))^2.5	=0.002*(AVERAGE($AF11:$AF13))^2.5	=0.036*(AVERAGE($AD11:$AD47))^2.5
13		=0.001*(AVERAGE($AF12:$AF13))^2.5	=0.002*(AVERAGE($AF12:$AF14))^2.5	=0.036*(AVERAGE($AD12:$AD48))^2.5
14		=0.001*(AVERAGE($AF13:$AF14))^2.5	=0.002*(AVERAGE($AF13:$AF15))^2.5	=0.036*(AVERAGE($AD13:$AD49))^2.5
15		=0.001*(AVERAGE($AF14:$AF15))^2.5	=0.002*(AVERAGE($AF14:$AF16))^2.5	=0.036*(AVERAGE($AD14:$AD50))^2.5
16		=0.001*(AVERAGE($AF15:$AF16))^2.5	=0.002*(AVERAGE($AF15:$AF17))^2.5	=0.036*(AVERAGE($AD15:$AD51))^2.5
17		=0.001*(AVERAGE($AF16:$AF17))^2.5	=0.002*(AVERAGE($AF16:$AF18))^2.5	=0.036*(AVERAGE($AD16:$AD52))^2.5
18		=0.001*(AVERAGE($AF17:$AF18))^2.5	=0.002*(AVERAGE($AF17:$AF19))^2.5	=0.036*(AVERAGE($AD17:$AD53))^2.5
19		=0.001*(AVERAGE($AF18:$AF19))^2.5	=0.002*(AVERAGE($AF18:$AF20))^2.5	=0.036*(AVERAGE($AD18:$AD54))^2.5
300		=0.001*(AVERAGE($AF299:$AF300))^2.5	=0.002*(AVERAGE($AF299:$AF301))^2.5	=0.036*(AVERAGE($AD299:$AD335))^2.5
301				
302				
303				

Note. HIC36 will be shown in cell AG1 once sheet is calculated. Rows 20-299 and Columns AJ-BP hidden for clarity.

Figure E9

Raw Sled Data Example from Sled Device's Data Acquisition System

	A	B	F	G	H	I
1	Time	A_10SLED010000ACXP	A_10HEAD0000Y6ACZP	A_10CHST0000Y6ACXP	A_10CHST0000Y6ACYP	A_10CHST0000Y6ACZP
2	-0.2	1.5300049	7.95245	-2.9906838	0.4746173	7.809483
3	-0.19995	-3.680306	8.102172	-2.8409624	0.4746173	7.809483
4	-199.9	-9.968613	8.251892	-2.691241	0.324896	7.6597614
5	-199.85	-12.963044	8.401614	-2.8409624	0.17517444	7.6597614
6	-199.8	-9.429615	8.401614	-2.9906838	-0.124269314	7.51004
7	-199.75	-1.5842042	8.251892	-3.140405	-0.2739909	7.51004
8	-199.7	3.92555	8.102172	-2.9906838	-0.2739909	7.51004
9	-199.65	2.9673321	8.102172	-2.9906838	-0.124269314	7.3603177
10	-199.6	-1.6440927	8.102172	-2.8409624	-0.124269314	7.51004
11	-199.55	-4.3989697	8.102172	-2.691241	-0.2739909	7.51004
12	-199.5	-3.5006404	8.251892	-2.5415196	-0.4237122	7.51004
13	-199.45	-1.8237586	8.251892	-2.691241	-0.57343376	7.3603177
14	-199.4	-1.4644268	8.251892	-2.8409624	-0.57343376	7.3603177
15	-199.35	-0.50620866	8.251892	-2.9906838	-0.57343376	7.3603177
16	-199.3	3.4464407	8.102172	-2.9906838	-0.57343376	7.2105956
17	-199.25	8.596864	7.95245	-2.9906838	-0.57343376	7.2105956
18	-199.2	10.03419	7.802728	-2.9906838	-0.7231559	7.3603177
19	-199.15	6.1414294	7.95245	-3.2901263	-0.57343376	7.51004
14001	499.95	-0.4463201	4.359137	4.6451044	-0.57343376	1.8206155
14002						

Note. Data shown in Excel worksheet after importing from ISOMME data format. Rows 20-14,000 and Columns C-E hidden for clarity.

Figure E10

Raw Sled Data Conversion Example

	M	N	O	P
1	**Sled 1 (g)**	**Sled 2(g)**	**Head Resultant (g)**	**Chest Resultant (g)**
2	=B2/9.81	=C2/9.81	=(SQRT(D2^2+E2^2+F2^2))/9.81	=(SQRT(G2^2+H2^2+I2^2))/9.81
3	=B3/9.81	=C3/9.81	=(SQRT(D3^2+E3^2+F3^2))/9.81	=(SQRT(G3^2+H3^2+I3^2))/9.81
4	=B4/9.81	=C4/9.81	=(SQRT(D4^2+E4^2+F4^2))/9.81	=(SQRT(G4^2+H4^2+I4^2))/9.81
5	=B5/9.81	=C5/9.81	=(SQRT(D5^2+E5^2+F5^2))/9.81	=(SQRT(G5^2+H5^2+I5^2))/9.81
6	=B6/9.81	=C6/9.81	=(SQRT(D6^2+E6^2+F6^2))/9.81	=(SQRT(G6^2+H6^2+I6^2))/9.81
7	=B7/9.81	=C7/9.81	=(SQRT(D7^2+E7^2+F7^2))/9.81	=(SQRT(G7^2+H7^2+I7^2))/9.81
8	=B8/9.81	=C8/9.81	=(SQRT(D8^2+E8^2+F8^2))/9.81	=(SQRT(G8^2+H8^2+I8^2))/9.81
9	=B9/9.81	=C9/9.81	=(SQRT(D9^2+E9^2+F9^2))/9.81	=(SQRT(G9^2+H9^2+I9^2))/9.81
10	=B10/9.81	=C10/9.81	=(SQRT(D10^2+E10^2+F10^2))/9.81	=(SQRT(G10^2+H10^2+I10^2))/9.81
11	=B11/9.81	=C11/9.81	=(SQRT(D11^2+E11^2+F11^2))/9.81	=(SQRT(G11^2+H11^2+I11^2))/9.81
12	=B12/9.81	=C12/9.81	=(SQRT(D12^2+E12^2+F12^2))/9.81	=(SQRT(G12^2+H12^2+I12^2))/9.81
13	=B13/9.81	=C13/9.81	=(SQRT(D13^2+E13^2+F13^2))/9.81	=(SQRT(G13^2+H13^2+I13^2))/9.81
14	=B14/9.81	=C14/9.81	=(SQRT(D14^2+E14^2+F14^2))/9.81	=(SQRT(G14^2+H14^2+I14^2))/9.81
15	=B15/9.81	=C15/9.81	=(SQRT(D15^2+E15^2+F15^2))/9.81	=(SQRT(G15^2+H15^2+I15^2))/9.81
16	=B16/9.81	=C16/9.81	=(SQRT(D16^2+E16^2+F16^2))/9.81	=(SQRT(G16^2+H16^2+I16^2))/9.81
17	=B17/9.81	=C17/9.81	=(SQRT(D17^2+E17^2+F17^2))/9.81	=(SQRT(G17^2+H17^2+I17^2))/9.81
18	=B18/9.81	=C18/9.81	=(SQRT(D18^2+E18^2+F18^2))/9.81	=(SQRT(G18^2+H18^2+I18^2))/9.81
19	=B19/9.81	=C19/9.81	=(SQRT(D19^2+E19^2+F19^2))/9.81	=(SQRT(G19^2+H19^2+I19^2))/9.81
10041	=B10041/9.81	=C10041/9.81	=(SQRT(D10041^2+E10041^2+F10041^2))/9.81	=(SQRT(G10041^2+H10041^2+I10041^2))/9.81
10042				

Note. Rows 20-10,040 hidden for clarity.

Figure E11

Raw Sled Data Sample Period Conversion

	Q	R	S	T	U	V	W	X	Y
1			ROW #				Sled 1 Accel	time	Sled 1 Accel
2			4002				60	0	=INDIRECT("M"&S2)
3			4022				Sample Period	0.001	=INDIRECT("M"&S3)
4			4042				0.001	0.002	=INDIRECT("M"&S4)
5			4062				wd	0.003	=INDIRECT("M"&S5)
6			4082				=2*PI()*W2*2.0775	0.004	=INDIRECT("M"&S6)
7			4102				wa	0.005	=INDIRECT("M"&S7)
8			4122				=(SIN(W6*W4/2))/(COS(W6*W4/2))	0.006	=INDIRECT("M"&S8)
9			4142				a0	0.007	=INDIRECT("M"&S9)
10			4162				=W8^2/(1+SQRT(2)*W8+W8^2)	0.008	=INDIRECT("M"&S10)
11			4182				a1	0.009	=INDIRECT("M"&S11)
12			4202				=2*W10	0.01	=INDIRECT("M"&S12)
13			4222				a2	0.011	=INDIRECT("M"&S13)
14			4242				=W10	0.012	=INDIRECT("M"&S14)
15			4262				b1	0.013	=INDIRECT("M"&S15)
16			4282				=-2*(W8^2-1)/(1+SQRT(2)*W8+W8^2)	0.014	=INDIRECT("M"&S16)
17			4302				b2	0.015	=INDIRECT("M"&S17)
18			4322				=(-1+SQRT(2)*W8-W8^2)/(1+SQRT(2)*W8+W8^2)	0.016	=INDIRECT("M"&S18)
19			4342					0.017	=INDIRECT("M"&S19)
300			9962					0.298	=INDIRECT("M"&S300)
301			9982					0.299	=INDIRECT("M"&S301)
302			10002					0.3	=INDIRECT("M"&S302)
303									

Note. Rows 20-299 hidden for clarity.

Figure E12

Sled Test Acceleration Filter Example, part 1

	W	X	Y	Z
1	Sled 1 Accel	time	Sled 1 Accel	Partial Filter
2	60	0	=INDIRECT("M"&S2)	
3	Sample Period	0.001	=INDIRECT("M"&S3)	
4	0.001	0.002	=INDIRECT("M"&S4)	=$W$10*Y4+$W$12*Y3+$W$14*Y2+$W$16*Z3+$W$18*Z2
5	wd	0.003	=INDIRECT("M"&S5)	=$W$10*Y5+$W$12*Y4+$W$14*Y3+$W$16*Z4+$W$18*Z3
6	=2*PI()*W2*2.0775	0.004	=INDIRECT("M"&S6)	=$W$10*Y6+$W$12*Y5+$W$14*Y4+$W$16*Z5+$W$18*Z4
7	wa	0.005	=INDIRECT("M"&S7)	=$W$10*Y7+$W$12*Y6+$W$14*Y5+$W$16*Z6+$W$18*Z5
8	=(SIN(W6*W4/2))/(COS(W6*W4/2))	0.006	=INDIRECT("M"&S8)	=$W$10*Y8+$W$12*Y7+$W$14*Y6+$W$16*Z7+$W$18*Z6
9	a0	0.007	=INDIRECT("M"&S9)	=$W$10*Y9+$W$12*Y8+$W$14*Y7+$W$16*Z8+$W$18*Z7
10	=W8^2/(1+SQRT(2)*W8+W8^2)	0.008	=INDIRECT("M"&S10)	=$W$10*Y10+$W$12*Y9+$W$14*Y8+$W$16*Z9+$W$18*Z8
11	a1	0.009	=INDIRECT("M"&S11)	=$W$10*Y11+$W$12*Y10+$W$14*Y9+$W$16*Z10+$W$18*Z9
12	=2*W10	0.01	=INDIRECT("M"&S12)	=$W$10*Y12+$W$12*Y11+$W$14*Y10+$W$16*Z11+$W$18*Z10
13	a2	0.011	=INDIRECT("M"&S13)	=$W$10*Y13+$W$12*Y12+$W$14*Y11+$W$16*Z12+$W$18*Z11
14	=W10	0.012	=INDIRECT("M"&S14)	=$W$10*Y14+$W$12*Y13+$W$14*Y12+$W$16*Z13+$W$18*Z12
15	b1	0.013	=INDIRECT("M"&S15)	=$W$10*Y15+$W$12*Y14+$W$14*Y13+$W$16*Z14+$W$18*Z13
16	=-2*(W8^2-1)/(1+SQRT(2)*W8+W8^2)	0.014	=INDIRECT("M"&S16)	=$W$10*Y16+$W$12*Y15+$W$14*Y14+$W$16*Z15+$W$18*Z14
17	b2	0.015	=INDIRECT("M"&S17)	=$W$10*Y17+$W$12*Y16+$W$14*Y15+$W$16*Z16+$W$18*Z15
18	=(-1+SQRT(2)*W8-W8^2)/(1+SQRT(2)*W8+W8^2)	0.016	=INDIRECT("M"&S18)	=$W$10*Y18+$W$12*Y17+$W$14*Y16+$W$16*Z17+$W$18*Z16
19		0.017	=INDIRECT("M"&S19)	=$W$10*Y19+$W$12*Y18+$W$14*Y17+$W$16*Z18+$W$18*Z17
300		0.298	=INDIRECT("M"&S300)	=$W$10*Y300+$W$12*Y299+$W$14*Y298+$W$16*Z299+$W$18*Z298
301		0.299	=INDIRECT("M"&S301)	=$W$10*Y301+$W$12*Y300+$W$14*Y299+$W$16*Z300+$W$18*Z299
302		0.3	=INDIRECT("M"&S302)	=$W$10*Y302+$W$12*Y301+$W$14*Y300+$W$16*Z301+$W$18*Z300
303				

Note. Rows 20-299 hidden for clarity.

Figure E13

Sled Test Acceleration Filter Example, part 2

	W	Z	AA
1	**Sled 1 Accel**	**Partial Filter**	**Final Filter**
2	60		=$W$10*Z2+$W$12*Z3+$W$14*Z4+$W$16*AA3+$W$18*AA4
3	**Sample Period**		=$W$10*Z3+$W$12*Z4+$W$14*Z5+$W$16*AA4+$W$18*AA5
4	0.001	=$W$10*Y4+$W$12*Y3+$W$14*Y2+$W$16*Z3+$W$18*Z2	=$W$10*Z4+$W$12*Z5+$W$14*Z6+$W$16*AA5+$W$18*AA6
5	**wd**	=$W$10*Y5+$W$12*Y4+$W$14*Y3+$W$16*Z4+$W$18*Z3	=$W$10*Z5+$W$12*Z6+$W$14*Z7+$W$16*AA6+$W$18*AA7
6	=2*PI()*W2*2.0775	=$W$10*Y6+$W$12*Y5+$W$14*Y4+$W$16*Z5+$W$18*Z4	=$W$10*Z6+$W$12*Z7+$W$14*Z8+$W$16*AA7+$W$18*AA8
7	**wa**	=$W$10*Y7+$W$12*Y6+$W$14*Y5+$W$16*Z6+$W$18*Z5	=$W$10*Z7+$W$12*Z8+$W$14*Z9+$W$16*AA8+$W$18*AA9
8	=(SIN(W6*W4/2))/(COS(W6*W4/2))	=$W$10*Y8+$W$12*Y7+$W$14*Y6+$W$16*Z7+$W$18*Z6	=$W$10*Z8+$W$12*Z9+$W$14*Z10+$W$16*AA9+$W$18*AA10
9	**a0**	=$W$10*Y9+$W$12*Y8+$W$14*Y7+$W$16*Z8+$W$18*Z7	=$W$10*Z9+$W$12*Z10+$W$14*Z11+$W$16*AA10+$W$18*AA11
10	=W8^2/(1+SQRT(2)*W8+W8^2)	=$W$10*Y10+$W$12*Y9+$W$14*Y8+$W$16*Z9+$W$18*Z8	=$W$10*Z10+$W$12*Z11+$W$14*Z12+$W$16*AA11+$W$18*AA12
11	**a1**	=$W$10*Y11+$W$12*Y10+$W$14*Y9+$W$16*Z10+$W$18*Z9	=$W$10*Z11+$W$12*Z12+$W$14*Z13+$W$16*AA12+$W$18*AA13
12	=2*W10	=$W$10*Y12+$W$12*Y11+$W$14*Y10+$W$16*Z11+$W$18*Z10	=$W$10*Z12+$W$12*Z13+$W$14*Z14+$W$16*AA13+$W$18*AA14
13	**a2**	=$W$10*Y13+$W$12*Y12+$W$14*Y11+$W$16*Z12+$W$18*Z11	=$W$10*Z13+$W$12*Z14+$W$14*Z15+$W$16*AA14+$W$18*AA15
14	=W10	=$W$10*Y14+$W$12*Y13+$W$14*Y12+$W$16*Z13+$W$18*Z12	=$W$10*Z14+$W$12*Z15+$W$14*Z16+$W$16*AA15+$W$18*AA16
15	**b1**	=$W$10*Y15+$W$12*Y14+$W$14*Y13+$W$16*Z14+$W$18*Z13	=$W$10*Z15+$W$12*Z16+$W$14*Z17+$W$16*AA16+$W$18*AA17
16	=-2*(W8^2-1)/(1+SQRT(2)*W8+W8^2)	=$W$10*Y16+$W$12*Y15+$W$14*Y14+$W$16*Z15+$W$18*Z14	=$W$10*Z16+$W$12*Z17+$W$14*Z18+$W$16*AA17+$W$18*AA18
17	**b2**	=$W$10*Y17+$W$12*Y16+$W$14*Y15+$W$16*Z16+$W$18*Z15	=$W$10*Z17+$W$12*Z18+$W$14*Z19+$W$16*AA18+$W$18*AA19
18	=(-1+SQRT(2)*W8-W8^2)/(1+SQRT(2)*W8+W8^2)	=$W$10*Y18+$W$12*Y17+$W$14*Y16+$W$16*Z17+$W$18*Z16	=$W$10*Z18+$W$12*Z19+$W$14*Z20+$W$16*AA19+$W$18*AA20
19		=$W$10*Y19+$W$12*Y18+$W$14*Y17+$W$16*Z18+$W$18*Z17	=$W$10*Z19+$W$12*Z20+$W$14*Z21+$W$16*AA20+$W$18*AA21
300		=$W$10*Y300+$W$12*Y299+$W$14*Y298+$W$16*Z299+$W$18*Z298	=$W$10*Z300+$W$12*Z301+$W$14*Z302+$W$16*AA301+$W$18*AA302
301		=$W$10*Y301+$W$12*Y300+$W$14*Y299+$W$16*Z300+$W$18*Z299	
302		=$W$10*Y302+$W$12*Y301+$W$14*Y300+$W$16*Z301+$W$18*Z300	
303			

Note. Rows 20-299 and Columns X-Y hidden for clarity.

Figure E14

Chest Acceleration Calculator Example for Sled Test, part 1

	AO	AP	AQ	AR
1	**Chest Resultant Accel**	**time**	**Chest Res Accel**	**partial filter**
2	180	0	=INDIRECT("P"&S2)	
3	**Sample Period**	0.001	=INDIRECT("P"&S3)	
4	0.001	0.002	=INDIRECT("P"&S4)	=$AO$10*AQ4+$AO$12*AQ3+$AO$14*AQ2+$AO$16*AR3+$AO$18*AR2
5	**wd**	0.003	=INDIRECT("P"&S5)	=$AO$10*AQ5+$AO$12*AQ4+$AO$14*AQ3+$AO$16*AR4+$AO$18*AR3
6	=2*PI()*AO2*2.0775	0.004	=INDIRECT("P"&S6)	=$AO$10*AQ6+$AO$12*AQ5+$AO$14*AQ4+$AO$16*AR5+$AO$18*AR4
7	**wa**	0.005	=INDIRECT("P"&S7)	=$AO$10*AQ7+$AO$12*AQ6+$AO$14*AQ5+$AO$16*AR6+$AO$18*AR5
8	=(SIN(AO6*AO4/2))/(COS(AO6*AO4/2))	0.006	=INDIRECT("P"&S8)	=$AO$10*AQ8+$AO$12*AQ7+$AO$14*AQ6+$AO$16*AR7+$AO$18*AR6
9	**a0**	0.007	=INDIRECT("P"&S9)	=$AO$10*AQ9+$AO$12*AQ8+$AO$14*AQ7+$AO$16*AR8+$AO$18*AR7
10	=AO8^2/(1+SQRT(2)*AO8+AO8^2)	0.008	=INDIRECT("P"&S10)	=$AO$10*AQ10+$AO$12*AQ9+$AO$14*AQ8+$AO$16*AR9+$AO$18*AR8
11	**a1**	0.009	=INDIRECT("P"&S11)	=$AO$10*AQ11+$AO$12*AQ10+$AO$14*AQ9+$AO$16*AR10+$AO$18*AR9
12	=2*AO10	0.01	=INDIRECT("P"&S12)	=$AO$10*AQ12+$AO$12*AQ11+$AO$14*AQ10+$AO$16*AR11+$AO$18*AR10
13	**a2**	0.011	=INDIRECT("P"&S13)	=$AO$10*AQ13+$AO$12*AQ12+$AO$14*AQ11+$AO$16*AR12+$AO$18*AR11
14	=AO10	0.012	=INDIRECT("P"&S14)	=$AO$10*AQ14+$AO$12*AQ13+$AO$14*AQ12+$AO$16*AR13+$AO$18*AR12
15	**b1**	0.013	=INDIRECT("P"&S15)	=$AO$10*AQ15+$AO$12*AQ14+$AO$14*AQ13+$AO$16*AR14+$AO$18*AR13
16	=-2*(AO8^2-1)/(1+SQRT(2)*AO8+AO8^2)	0.014	=INDIRECT("P"&S16)	=$AO$10*AQ16+$AO$12*AQ15+$AO$14*AQ14+$AO$16*AR15+$AO$18*AR14
17	**b2**	0.015	=INDIRECT("P"&S17)	=$AO$10*AQ17+$AO$12*AQ16+$AO$14*AQ15+$AO$16*AR16+$AO$18*AR15
18	=(-1+SQRT(2)*AO8-AO8^2)/(1+SQRT(2)*AO8+AO8^2)	0.016	=INDIRECT("P"&S18)	=$AO$10*AQ18+$AO$12*AQ17+$AO$14*AQ16+$AO$16*AR17+$AO$18*AR16
19		0.017	=INDIRECT("P"&S19)	=$AO$10*AQ19+$AO$12*AQ18+$AO$14*AQ17+$AO$16*AR18+$AO$18*AR17
300		0.298	=INDIRECT("P"&S300)	=$AO$10*AQ300+$AO$12*AQ299+$AO$14*AQ298+$AO$16*AR299+$AO$18*AR298
301		0.299	=INDIRECT("P"&S301)	=$AO$10*AQ301+$AO$12*AQ300+$AO$14*AQ299+$AO$16*AR300+$AO$18*AR299
302		0.3	=INDIRECT("P"&S302)	=$AO$10*AQ302+$AO$12*AQ301+$AO$14*AQ300+$AO$16*AR301+$AO$18*AR300
303				

Note. Rows 20-299 hidden for clarity.

Figure E15

Chest Acceleration Calculator Example for Sled Test, part 2

	AO	AR	AS
1	**Chest Resultant Accel**	**partial filter**	**final filter**
2	180		=$AO$10*AR2+$AO$12*AR3+$AO$14*AR4+$AO$16*AS3+$AO$18*AS4
3	**Sample Period**		=$AO$10*AR3+$AO$12*AR4+$AO$14*AR5+$AO$16*AS4+$AO$18*AS5
4	0.001	=$AO$10*AQ4+$AO$12*AQ3+$AO$14*AQ2+$AO$16*AR3+$AO$18*AR2	=$AO$10*AR4+$AO$12*AR5+$AO$14*AR6+$AO$16*AS5+$AO$18*AS6
5	**wd**	=$AO$10*AQ5+$AO$12*AQ4+$AO$14*AQ3+$AO$16*AR4+$AO$18*AR3	=$AO$10*AR5+$AO$12*AR6+$AO$14*AR7+$AO$16*AS6+$AO$18*AS7
6	=2*PI()*AO2*2.0775	=$AO$10*AQ6+$AO$12*AQ5+$AO$14*AQ4+$AO$16*AR5+$AO$18*AR4	=$AO$10*AR6+$AO$12*AR7+$AO$14*AR8+$AO$16*AS7+$AO$18*AS8
7	**wa**	=$AO$10*AQ7+$AO$12*AQ6+$AO$14*AQ5+$AO$16*AR6+$AO$18*AR5	=$AO$10*AR7+$AO$12*AR8+$AO$14*AR9+$AO$16*AS8+$AO$18*AS9
8	=(SIN(AO6*AO4/2))/(COS(AO6*AO4/2))	=$AO$10*AQ8+$AO$12*AQ7+$AO$14*AQ6+$AO$16*AR7+$AO$18*AR6	=$AO$10*AR8+$AO$12*AR9+$AO$14*AR10+$AO$16*AS9+$AO$18*AS10
9	**a0**	=$AO$10*AQ9+$AO$12*AQ8+$AO$14*AQ7+$AO$16*AR8+$AO$18*AR7	=$AO$10*AR9+$AO$12*AR10+$AO$14*AR11+$AO$16*AS10+$AO$18*AS11
10	=AO8^2/(1+SQRT(2)*AO8+AO8^2)	=$AO$10*AQ10+$AO$12*AQ9+$AO$14*AQ8+$AO$16*AR9+$AO$18*AR8	=$AO$10*AR10+$AO$12*AR11+$AO$14*AR12+$AO$16*AS11+$AO$18*AS12
11	**a1**	=$AO$10*AQ11+$AO$12*AQ10+$AO$14*AQ9+$AO$16*AR10+$AO$18*AR9	=$AO$10*AR11+$AO$12*AR12+$AO$14*AR13+$AO$16*AS12+$AO$18*AS13
12	=2*AO10	=$AO$10*AQ12+$AO$12*AQ11+$AO$14*AQ10+$AO$16*AR11+$AO$18*AR10	=$AO$10*AR12+$AO$12*AR13+$AO$14*AR14+$AO$16*AS13+$AO$18*AS14
13	**a2**	=$AO$10*AQ13+$AO$12*AQ12+$AO$14*AQ11+$AO$16*AR12+$AO$18*AR11	=$AO$10*AR13+$AO$12*AR14+$AO$14*AR15+$AO$16*AS14+$AO$18*AS15
14	=AO10	=$AO$10*AQ14+$AO$12*AQ13+$AO$14*AQ12+$AO$16*AR13+$AO$18*AR12	=$AO$10*AR14+$AO$12*AR15+$AO$14*AR16+$AO$16*AS15+$AO$18*AS16
15	**b1**	=$AO$10*AQ15+$AO$12*AQ14+$AO$14*AQ13+$AO$16*AR14+$AO$18*AR13	=$AO$10*AR15+$AO$12*AR16+$AO$14*AR17+$AO$16*AS16+$AO$18*AS17
16	=-2*(AO8^2-1)/(1+SQRT(2)*AO8+AO8^2)	=$AO$10*AQ16+$AO$12*AQ15+$AO$14*AQ14+$AO$16*AR15+$AO$18*AR14	=$AO$10*AR16+$AO$12*AR17+$AO$14*AR18+$AO$16*AS17+$AO$18*AS18
17	**b2**	=$AO$10*AQ17+$AO$12*AQ16+$AO$14*AQ15+$AO$16*AR16+$AO$18*AR15	=$AO$10*AR17+$AO$12*AR18+$AO$14*AR19+$AO$16*AS18+$AO$18*AS19
18	=(-1+SQRT(2)*AO8-AO8^2)/(1+SQRT(2)*AO8+AO8^2)	=$AO$10*AQ18+$AO$12*AQ17+$AO$14*AQ16+$AO$16*AR17+$AO$18*AR16	=$AO$10*AR18+$AO$12*AR19+$AO$14*AR20+$AO$16*AS19+$AO$18*AS20
19		=$AO$10*AQ19+$AO$12*AQ18+$AO$14*AQ17+$AO$16*AR18+$AO$18*AR17	=$AO$10*AR19+$AO$12*AR20+$AO$14*AR21+$AO$16*AS20+$AO$18*AS21
300		=$AO$10*AQ300+$AO$12*AQ299+$AO$14*AQ298+$AO$16*AR299+$AO$18*AR298	=$AO$10*AR300+$AO$12*AR301+$AO$14*AR302+$AO$16*AS301+$AO$18*AS302
301		=$AO$10*AQ301+$AO$12*AQ300+$AO$14*AQ299+$AO$16*AR300+$AO$18*AR299	
302		=$AO$10*AQ302+$AO$12*AQ301+$AO$14*AQ300+$AO$16*AR301+$AO$18*AR300	
303			

Note. Rows 20-299 and Columns AP-AQ hidden for clarity.

Figure E16

Chest Acceleration Calculator Example for Sled Test, part 3

	AO	AS	AT
1	**Chest Resultant Accel**	**final filter**	**SORT**
2	180	=$AO$10*AR2+$AO$12*AR3+$AO$14*AR4+$AO$16*AS3+$AO$18*AS4	=SORT(AS2:AS300,1,-1)
3	**Sample Period**	=$AO$10*AR3+$AO$12*AR4+$AO$14*AR5+$AO$16*AS4+$AO$18*AS5	
4	0.001	=$AO$10*AR4+$AO$12*AR5+$AO$14*AR6+$AO$16*AS5+$AO$18*AS6	
5	**wd**	=$AO$10*AR5+$AO$12*AR6+$AO$14*AR7+$AO$16*AS6+$AO$18*AS7	
6	=2*PI()*AO2*2.0775	=$AO$10*AR6+$AO$12*AR7+$AO$14*AR8+$AO$16*AS7+$AO$18*AS8	
7	**wa**	=$AO$10*AR7+$AO$12*AR8+$AO$14*AR9+$AO$16*AS8+$AO$18*AS9	
8	=(SIN(AO6*AO4/2))/(COS(AO6*AO4/2))	=$AO$10*AR8+$AO$12*AR9+$AO$14*AR10+$AO$16*AS9+$AO$18*AS10	
9	**a0**	=$AO$10*AR9+$AO$12*AR10+$AO$14*AR11+$AO$16*AS10+$AO$18*AS11	
10	=AO8^2/(1+SQRT(2)*AO8+AO8^2)	=$AO$10*AR10+$AO$12*AR11+$AO$14*AR12+$AO$16*AS11+$AO$18*AS12	
11	**a1**	=$AO$10*AR11+$AO$12*AR12+$AO$14*AR13+$AO$16*AS12+$AO$18*AS13	
12	=2*AO10	=$AO$10*AR12+$AO$12*AR13+$AO$14*AR14+$AO$16*AS13+$AO$18*AS14	
13	**a2**	=$AO$10*AR13+$AO$12*AR14+$AO$14*AR15+$AO$16*AS14+$AO$18*AS15	
14	=AO10	=$AO$10*AR14+$AO$12*AR15+$AO$14*AR16+$AO$16*AS15+$AO$18*AS16	
15	**b1**	=$AO$10*AR15+$AO$12*AR16+$AO$14*AR17+$AO$16*AS16+$AO$18*AS17	
16	=-2*(AO8^2-1)/(1+SQRT(2)*AO8+AO8^2)	=$AO$10*AR16+$AO$12*AR17+$AO$14*AR18+$AO$16*AS17+$AO$18*AS18	
17	**b2**	=$AO$10*AR17+$AO$12*AR18+$AO$14*AR19+$AO$16*AS18+$AO$18*AS19	
18	=(-1+SQRT(2)*AO8-AO8^2)/(1+SQRT(2)*AO8+AO8^2)	=$AO$10*AR18+$AO$12*AR19+$AO$14*AR20+$AO$16*AS19+$AO$18*AS20	
19		=$AO$10*AR19+$AO$12*AR20+$AO$14*AR21+$AO$16*AS20+$AO$18*AS21	
300		=$AO$10*AR300+$AO$12*AR301+$AO$14*AR302+$AO$16*AS301+$AO$18*AS302	
301			
302			
303			

Note. Chest Acceleration, 3 ms clip, will be shown in cell AT6 once sheet is calculated.

Rows 20-299 and Columns AP-AR hidden for clarity.

Figure E17

HIC36 Calculator Example for Sled Test, part 1

	AX	AY	AZ	BA
1				
2	**Head Accel CFC**	**time**	**Head Accel Resultant**	**Partial Filter**
3	1000	0	=INDIRECT("O"&S2)	
4	**Sample Period**	0.001	=INDIRECT("O"&S3)	
5	0.001	0.002	=INDIRECT("O"&S4)	=$AX$11*AZ5+$AX$13*AZ4+$AX$15*AZ3+$AX$17*BA4+$AX$19*BA3
6	**wd**	0.003	=INDIRECT("O"&S5)	=$AX$11*AZ6+$AX$13*AZ5+$AX$15*AZ4+$AX$17*BA5+$AX$19*BA4
7	=2*PI()*AX3*2.0775	0.004	=INDIRECT("O"&S6)	=$AX$11*AZ7+$AX$13*AZ6+$AX$15*AZ5+$AX$17*BA6+$AX$19*BA5
8	**wa**	0.005	=INDIRECT("O"&S7)	=$AX$11*AZ8+$AX$13*AZ7+$AX$15*AZ6+$AX$17*BA7+$AX$19*BA6
9	=(SIN(AX7*AX5/2))/(COS(AX7*AX5/2))	0.006	=INDIRECT("O"&S8)	=$AX$11*AZ9+$AX$13*AZ8+$AX$15*AZ7+$AX$17*BA8+$AX$19*BA7
10	**a0**	0.007	=INDIRECT("O"&S9)	=$AX$11*AZ10+$AX$13*AZ9+$AX$15*AZ8+$AX$17*BA9+$AX$19*BA8
11	=AX9^2/(1+SQRT(2)*AX9+AX9^2)	0.008	=INDIRECT("O"&S10)	=$AX$11*AZ11+$AX$13*AZ10+$AX$15*AZ9+$AX$17*BA10+$AX$19*BA9
12	**a1**	0.009	=INDIRECT("O"&S11)	=$AX$11*AZ12+$AX$13*AZ11+$AX$15*AZ10+$AX$17*BA11+$AX$19*BA10
13	=2*AX11	0.01	=INDIRECT("O"&S12)	=$AX$11*AZ13+$AX$13*AZ12+$AX$15*AZ11+$AX$17*BA12+$AX$19*BA11
14	**a2**	0.011	=INDIRECT("O"&S13)	=$AX$11*AZ14+$AX$13*AZ13+$AX$15*AZ12+$AX$17*BA13+$AX$19*BA12
15	=AX11	0.012	=INDIRECT("O"&S14)	=$AX$11*AZ15+$AX$13*AZ14+$AX$15*AZ13+$AX$17*BA14+$AX$19*BA13
16	**b1**	0.013	=INDIRECT("O"&S15)	=$AX$11*AZ16+$AX$13*AZ15+$AX$15*AZ14+$AX$17*BA15+$AX$19*BA14
17	=-2*(AX9^2-1)/(1+SQRT(2)*AX9+AX9^2)	0.014	=INDIRECT("O"&S16)	=$AX$11*AZ17+$AX$13*AZ16+$AX$15*AZ15+$AX$17*BA16+$AX$19*BA15
18	**b2**	0.015	=INDIRECT("O"&S17)	=$AX$11*AZ18+$AX$13*AZ17+$AX$15*AZ16+$AX$17*BA17+$AX$19*BA16
19	=(-1+SQRT(2)*AX9-AX9^2)/(1+SQRT(2)*AX9+AX9^2)	0.016	=INDIRECT("O"&S18)	=$AX$11*AZ19+$AX$13*AZ18+$AX$15*AZ17+$AX$17*BA18+$AX$19*BA17
300		0.297	=INDIRECT("O"&S299)	=$AX$11*AZ300+$AX$13*AZ299+$AX$15*AZ298+$AX$17*BA299+$AX$19*BA298
301		0.298	=INDIRECT("O"&S300)	=$AX$11*AZ301+$AX$13*AZ300+$AX$15*AZ299+$AX$17*BA300+$AX$19*BA299
302		0.299	=INDIRECT("O"&S301)	=$AX$11*AZ302+$AX$13*AZ301+$AX$15*AZ300+$AX$17*BA301+$AX$19*BA300
303		0.3	=INDIRECT("O"&S302)	=$AX$11*AZ303+$AX$13*AZ302+$AX$15*AZ301+$AX$17*BA302+$AX$19*BA301
304				

Note. Rows 20-299 hidden for clarity.

Figure E18

HIC36 Calculator Example for Sled Test, part 2

	AX	BA	BB
1			
2	**Head Accel CFC**	**Partial Filter**	**Final Filter**
3	1000		=$AX$11*BA3+$AX$13*BA4+$AX$15*BA5+$AX$17*BB4+$AX$19*BB5
4	**Sample Period**		=$AX$11*BA4+$AX$13*BA5+$AX$15*BA6+$AX$17*BB5+$AX$19*BB6
5	0.001	=$AX$11*AZ5+$AX$13*AZ4+$AX$15*AZ3+$AX$17*BA4+$AX$19*BA3	=$AX$11*BA5+$AX$13*BA6+$AX$15*BA7+$AX$17*BB6+$AX$19*BB7
6	**wd**	=$AX$11*AZ6+$AX$13*AZ5+$AX$15*AZ4+$AX$17*BA5+$AX$19*BA4	=$AX$11*BA6+$AX$13*BA7+$AX$15*BA8+$AX$17*BB7+$AX$19*BB8
7	=2*PI()*AX3*2.0775	=$AX$11*AZ7+$AX$13*AZ6+$AX$15*AZ5+$AX$17*BA6+$AX$19*BA5	=$AX$11*BA7+$AX$13*BA8+$AX$15*BA9+$AX$17*BB8+$AX$19*BB9
8	**wa**	=$AX$11*AZ8+$AX$13*AZ7+$AX$15*AZ6+$AX$17*BA7+$AX$19*BA6	=$AX$11*BA8+$AX$13*BA9+$AX$15*BA10+$AX$17*BB9+$AX$19*BB10
9	=(SIN(AX7*AX5/2))/(COS(AX7*AX5/2))	=$AX$11*AZ9+$AX$13*AZ8+$AX$15*AZ7+$AX$17*BA8+$AX$19*BA7	=$AX$11*BA9+$AX$13*BA10+$AX$15*BA11+$AX$17*BB10+$AX$19*BB11
10	**a0**	=$AX$11*AZ10+$AX$13*AZ9+$AX$15*AZ8+$AX$17*BA9+$AX$19*BA8	=$AX$11*BA10+$AX$13*BA11+$AX$15*BA12+$AX$17*BB11+$AX$19*BB12
11	=AX9^2/(1+SQRT(2)*AX9+AX9^2)	=$AX$11*AZ11+$AX$13*AZ10+$AX$15*AZ9+$AX$17*BA10+$AX$19*BA9	=$AX$11*BA11+$AX$13*BA12+$AX$15*BA13+$AX$17*BB12+$AX$19*BB13
12	**a1**	=$AX$11*AZ12+$AX$13*AZ11+$AX$15*AZ10+$AX$17*BA11+$AX$19*BA10	=$AX$11*BA12+$AX$13*BA13+$AX$15*BA14+$AX$17*BB13+$AX$19*BB14
13	=2*AX11	=$AX$11*AZ13+$AX$13*AZ12+$AX$15*AZ11+$AX$17*BA12+$AX$19*BA11	=$AX$11*BA13+$AX$13*BA14+$AX$15*BA15+$AX$17*BB14+$AX$19*BB15
14	**a2**	=$AX$11*AZ14+$AX$13*AZ13+$AX$15*AZ12+$AX$17*BA13+$AX$19*BA12	=$AX$11*BA14+$AX$13*BA15+$AX$15*BA16+$AX$17*BB15+$AX$19*BB16
15	=AX11	=$AX$11*AZ15+$AX$13*AZ14+$AX$15*AZ13+$AX$17*BA14+$AX$19*BA13	=$AX$11*BA15+$AX$13*BA16+$AX$15*BA17+$AX$17*BB16+$AX$19*BB17
16	**b1**	=$AX$11*AZ16+$AX$13*AZ15+$AX$15*AZ14+$AX$17*BA15+$AX$19*BA14	=$AX$11*BA16+$AX$13*BA17+$AX$15*BA18+$AX$17*BB17+$AX$19*BB18
17	=-2*(AX9^2-1)/(1+SQRT(2)*AX9+AX9^2)	=$AX$11*AZ17+$AX$13*AZ16+$AX$15*AZ15+$AX$17*BA16+$AX$19*BA15	=$AX$11*BA17+$AX$13*BA18+$AX$15*BA19+$AX$17*BB18+$AX$19*BB19
18	**b2**	=$AX$11*AZ18+$AX$13*AZ17+$AX$15*AZ16+$AX$17*BA17+$AX$19*BA16	=$AX$11*BA18+$AX$13*BA19+$AX$15*BA20+$AX$17*BB19+$AX$19*BB20
19	=(-1+SQRT(2)*AX9-AX9^2)/(1+SQRT(2)*AX9+AX9^2)	=$AX$11*AZ19+$AX$13*AZ18+$AX$15*AZ17+$AX$17*BA18+$AX$19*BA17	=$AX$11*BA19+$AX$13*BA20+$AX$15*BA21+$AX$17*BB20+$AX$19*BB21
300		=$AX$11*AZ300+$AX$13*AZ299+$AX$15*AZ298+$AX$17*BA299+$AX$19*BA298	=$AX$11*BA300+$AX$13*BA301+$AX$15*BA302+$AX$17*BB301+$AX$19*BB302
301		=$AX$11*AZ301+$AX$13*AZ300+$AX$15*AZ299+$AX$17*BA300+$AX$19*BA299	=$AX$11*BA301+$AX$13*BA302+$AX$15*BA303+$AX$17*BB302+$AX$19*BB303
302		=$AX$11*AZ302+$AX$13*AZ301+$AX$15*AZ300+$AX$17*BA301+$AX$19*BA300	
303		=$AX$11*AZ303+$AX$13*AZ302+$AX$15*AZ301+$AX$17*BA302+$AX$19*BA301	
304			

Note. Rows 20-299 and Columns AY-AZ hidden for clarity.

Figure E19

HIC36 Calculator Example for Sled Test, part 3

	BB	BC	BD
1		=MAX(BD1:CM1)	=MAX(BD3:BD301)
2	Final Filter	HIC36	HIC1
3	=$AX$11*BA3+$AX$13*BA4+$AX$15*BA5+$AX$17*BB4+$AX$19*BB5		=0.001*(AVERAGE($BB3:$BB4))^2.5
4	=$AX$11*BA4+$AX$13*BA5+$AX$15*BA6+$AX$17*BB5+$AX$19*BB6		=0.001*(AVERAGE($BB4:$BB5))^2.5
5	=$AX$11*BA5+$AX$13*BA6+$AX$15*BA7+$AX$17*BB6+$AX$19*BB7		=0.001*(AVERAGE($BB5:$BB6))^2.5
6	=$AX$11*BA6+$AX$13*BA7+$AX$15*BA8+$AX$17*BB7+$AX$19*BB8		=0.001*(AVERAGE($BB6:$BB7))^2.5
7	=$AX$11*BA7+$AX$13*BA8+$AX$15*BA9+$AX$17*BB8+$AX$19*BB9		=0.001*(AVERAGE($BB7:$BB8))^2.5
8	=$AX$11*BA8+$AX$13*BA9+$AX$15*BA10+$AX$17*BB9+$AX$19*BB10		=0.001*(AVERAGE($BB8:$BB9))^2.5
9	=$AX$11*BA9+$AX$13*BA10+$AX$15*BA11+$AX$17*BB10+$AX$19*BB11		=0.001*(AVERAGE($BB9:$BB10))^2.5
10	=$AX$11*BA10+$AX$13*BA11+$AX$15*BA12+$AX$17*BB11+$AX$19*BB12		=0.001*(AVERAGE($BB10:$BB11))^2.5
11	=$AX$11*BA11+$AX$13*BA12+$AX$15*BA13+$AX$17*BB12+$AX$19*BB13		=0.001*(AVERAGE($BB11:$BB12))^2.5
12	=$AX$11*BA12+$AX$13*BA13+$AX$15*BA14+$AX$17*BB13+$AX$19*BB14		=0.001*(AVERAGE($BB12:$BB13))^2.5
13	=$AX$11*BA13+$AX$13*BA14+$AX$15*BA15+$AX$17*BB14+$AX$19*BB15		=0.001*(AVERAGE($BB13:$BB14))^2.5
14	=$AX$11*BA14+$AX$13*BA15+$AX$15*BA16+$AX$17*BB15+$AX$19*BB16		=0.001*(AVERAGE($BB14:$BB15))^2.5
15	=$AX$11*BA15+$AX$13*BA16+$AX$15*BA17+$AX$17*BB16+$AX$19*BB17		=0.001*(AVERAGE($BB15:$BB16))^2.5
16	=$AX$11*BA16+$AX$13*BA17+$AX$15*BA18+$AX$17*BB17+$AX$19*BB18		=0.001*(AVERAGE($BB16:$BB17))^2.5
17	=$AX$11*BA17+$AX$13*BA18+$AX$15*BA19+$AX$17*BB18+$AX$19*BB19		=0.001*(AVERAGE($BB17:$BB18))^2.5
18	=$AX$11*BA18+$AX$13*BA19+$AX$15*BA20+$AX$17*BB19+$AX$19*BB20		=0.001*(AVERAGE($BB18:$BB19))^2.5
19	=$AX$11*BA19+$AX$13*BA20+$AX$15*BA21+$AX$17*BB20+$AX$19*BB21		=0.001*(AVERAGE($BB19:$BB20))^2.5
300	=$AX$11*BA300+$AX$13*BA301+$AX$15*BA302+$AX$17*BB301+$AX$19*BB302		=0.001*(AVERAGE($BB300:$BB301))^2.5
301	=$AX$11*BA301+$AX$13*BA302+$AX$15*BA303+$AX$17*BB302+$AX$19*BB303		=0.001*(AVERAGE($BB301:$BB302))^2.5
302			
303			
304			

Note. HIC36 will be shown in cell BC1 once sheet is calculated. Rows 20-299 hidden for clarity.

Figure E20

HIC36 Calculator Example for Sled Test, part 4

	BC	BD	BE	CM
1	=MAX(BD1:CM1)	=MAX(BD3:BD301)	=MAX(BE3:BE301)	=MAX(CM3:CM301)
2	HIC36	HIC1	HIC2	HIC36
3		=0.001*(AVERAGE($BB3:$BB4))^2.5	=0.002*(AVERAGE($BB3:$BB5))^2.5	=0.036*(AVERAGE($BB3:$BB39))^2.5
4		=0.001*(AVERAGE($BB4:$BB5))^2.5	=0.002*(AVERAGE($BB4:$BB6))^2.5	=0.036*(AVERAGE($BB4:$BB40))^2.5
5		=0.001*(AVERAGE($BB5:$BB6))^2.5	=0.002*(AVERAGE($BB5:$BB7))^2.5	=0.036*(AVERAGE($BB5:$BB41))^2.5
6		=0.001*(AVERAGE($BB6:$BB7))^2.5	=0.002*(AVERAGE($BB6:$BB8))^2.5	=0.036*(AVERAGE($BB6:$BB42))^2.5
7		=0.001*(AVERAGE($BB7:$BB8))^2.5	=0.002*(AVERAGE($BB7:$BB9))^2.5	=0.036*(AVERAGE($BB7:$BB43))^2.5
8		=0.001*(AVERAGE($BB8:$BB9))^2.5	=0.002*(AVERAGE($BB8:$BB10))^2.5	=0.036*(AVERAGE($BB8:$BB44))^2.5
9		=0.001*(AVERAGE($BB9:$BB10))^2.5	=0.002*(AVERAGE($BB9:$BB11))^2.5	=0.036*(AVERAGE($BB9:$BB45))^2.5
10		=0.001*(AVERAGE($BB10:$BB11))^2.5	=0.002*(AVERAGE($BB10:$BB12))^2.5	=0.036*(AVERAGE($BB10:$BB46))^2.5
11		=0.001*(AVERAGE($BB11:$BB12))^2.5	=0.002*(AVERAGE($BB11:$BB13))^2.5	=0.036*(AVERAGE($BB11:$BB47))^2.5
12		=0.001*(AVERAGE($BB12:$BB13))^2.5	=0.002*(AVERAGE($BB12:$BB14))^2.5	=0.036*(AVERAGE($BB12:$BB48))^2.5
13		=0.001*(AVERAGE($BB13:$BB14))^2.5	=0.002*(AVERAGE($BB13:$BB15))^2.5	=0.036*(AVERAGE($BB13:$BB49))^2.5
14		=0.001*(AVERAGE($BB14:$BB15))^2.5	=0.002*(AVERAGE($BB14:$BB16))^2.5	=0.036*(AVERAGE($BB14:$BB50))^2.5
15		=0.001*(AVERAGE($BB15:$BB16))^2.5	=0.002*(AVERAGE($BB15:$BB17))^2.5	=0.036*(AVERAGE($BB15:$BB51))^2.5
16		=0.001*(AVERAGE($BB16:$BB17))^2.5	=0.002*(AVERAGE($BB16:$BB18))^2.5	=0.036*(AVERAGE($BB16:$BB52))^2.5
17		=0.001*(AVERAGE($BB17:$BB18))^2.5	=0.002*(AVERAGE($BB17:$BB19))^2.5	=0.036*(AVERAGE($BB17:$BB53))^2.5
18		=0.001*(AVERAGE($BB18:$BB19))^2.5	=0.002*(AVERAGE($BB18:$BB20))^2.5	=0.036*(AVERAGE($BB18:$BB54))^2.5
19		=0.001*(AVERAGE($BB19:$BB20))^2.5	=0.002*(AVERAGE($BB19:$BB21))^2.5	=0.036*(AVERAGE($BB19:$BB55))^2.5
300		=0.001*(AVERAGE($BB300:$BB301))^2.5	=0.002*(AVERAGE($BB300:$BB302))^2.5	=0.036*(AVERAGE($BB300:$BB336))^2.5
301		=0.001*(AVERAGE($BB301:$BB302))^2.5	=0.002*(AVERAGE($BB301:$BB303))^2.5	=0.036*(AVERAGE($BB301:$BB337))^2.5
302				
303				
304				

Note. HIC36 will be shown in cell BC1 once sheet is calculated. Rows 20-299 and Columns BF-CL hidden for clarity.

APPENDIX F

MATLAB Script for Data Visualization

```
% _*Kristy Brinker Brouwer*_ _*Sled_vs_Model.mlx*_


% Importing Final Filter Data from the Chest G and HIC Calculator.
A_sled_model=csvread("A_sled_model.csv");
B_sled_model=csvread("B_sled_model.csv");
CD_sled_model=csvread("CD_sled_model.csv");
DDH_model=csvread("DDH_model.csv");


% Comparing Deceleration Pulses from Sled Testing Trials
c = [
    0.267 0.467 0.667  % Blue
    0.400 0.800 0.933  % Cyan
    0.133 0.533 0.200  % Green
    0.533 0.667 0.467  % Light Green
    0.800 0.733 0.267  % Yellow
    0.933 0.400 0.467  % Red
    0.667 0.200 0.467  % Purple
    0.933 0.467 0.200  % Orange
    0.067 0.467 0.467  % Teal
    ];

figure(1)
clf
hold on
xlim([0 0.2])
xticks(0:0.02:0.2)
ylim([0 35])
yticks(0:5:35)
grid on
plot(A_sled_model(1:201,1), A_sled_model(1:201,2),'-', "LineWidth",1)
plot(A_sled_model(1:201,1), A_sled_model(1:201,3),'--',
"LineWidth",1.5)
colororder(c)
title('Sled Trial A Deceleration Pulse', 'FontSize',12)
legend("A Ch1", "A Ch2", "location","southoutside", "NumColumns", 2)
xlabel('Time (s)', 'FontSize',12)
ylabel('Acceleration (g)', 'FontSize',12)
hold off
print("Sled_Trial_A_Deceleration_Pulse_1","-dpng")

figure(2)
clf
hold on
xlim([0 0.2])
xticks(0:0.02:0.2)
ylim([0 35])
yticks(0:5:35)
```

```
grid on
plot(B_sled_model(1:201,1), B_sled_model(1:201,2),'-', "LineWidth",1)
plot(B_sled_model(1:201,1), B_sled_model(1:201,3),'--',
"LineWidth",1.5)
colororder(c)
title('Sled Trial B Deceleration Pulse', 'FontSize',12)
legend("B Ch1", "B Ch2", "location","southoutside", "NumColumns", 2)
xlabel('Time (s)', 'FontSize',12)
ylabel('Acceleration (g)', 'FontSize',12)
hold off
print("Sled_Trial_B_Deceleration_Pulse_2","-dpng")

figure(3)
clf
hold on
xlim([0 0.2])
xticks(0:0.02:0.2)
ylim([0 35])
yticks(0:5:35)
grid on
plot(CD_sled_model(1:201,1), CD_sled_model(1:201,2),'-', "LineWidth",1)
plot(CD_sled_model(1:201,1), CD_sled_model(1:201,3),'--',
"LineWidth",1.5)
plot(CD_sled_model(1:201,1), CD_sled_model(1:201,9),'-', "LineWidth",1)
plot(CD_sled_model(1:201,1), CD_sled_model(1:201,10),'--',
"LineWidth",1.5)
colororder(c)
title('Sled Trials C & D Deceleration Pulse', 'FontSize',12)
legend("C Ch1", "C Ch2", "D Ch1", "D Ch2", "location","southoutside",
"NumColumns", 2)
xlabel('Time (s)', 'FontSize',12)
ylabel('Acceleration (g)', 'FontSize',12)
hold off
print("Sled_Trials_CD_Deceleration_Pulse_3","-dpng")

figure(4)
clf
hold on
xlim([0 0.2])
xticks(0:0.02:0.2)
ylim([0 35])
yticks(0:5:35)
grid on
plot(A_sled_model(1:201,1), A_sled_model(1:201,2), '-', "LineWidth",1)
plot(B_sled_model(1:201,1), B_sled_model(1:201,2), '-', "LineWidth",1)
plot(CD_sled_model(1:201,1), CD_sled_model(1:201,2), '-',
"LineWidth",1)
plot(CD_sled_model(1:201,1), CD_sled_model(1:201,9), '-',
"LineWidth",1)
colororder(c)
title('Sled Channel 1 Deceleration Pulse Comparison', 'FontSize',12)
legend("Sled A", "Sled B", "Sled C", "Sled D",
"location","southoutside", "NumColumns", 2)
xlabel('Time (s)', 'FontSize',12)
ylabel('Acceleration (g)', 'FontSize',12)
```

```
hold off
print("Sled_Ch1_Deceleration_Pulse_4","-dpng")

figure(5)
clf
hold on
xlim([0 0.2])
xticks(0:0.02:0.2)
ylim([0 35])
yticks(0:5:35)
grid on
plot(A_sled_model(1:201,1), A_sled_model(1:201,3), '-', "LineWidth",1)
plot(B_sled_model(1:201,1), B_sled_model(1:201,3), '-', "LineWidth",1)
plot(CD_sled_model(1:201,1), CD_sled_model(1:201,3), '-',
"LineWidth",1)
plot(CD_sled_model(1:201,1), CD_sled_model(1:201,10), '-',
"LineWidth",1)
colororder(c)
title('Sled Channel 2 Deceleration Pulse Comparison', 'FontSize',12)
legend("Sled A", "Sled B", "Sled C", "Sled D",
"location","southoutside", "NumColumns", 2)
xlabel('Time (s)', 'FontSize',12)
ylabel('Acceleration (g)', 'FontSize',12)
hold off
print("Sled_Ch2_Deceleration_Pulse_5","-dpng")


% Comparing Deceleration Pulses from Sled Testing Trials
% to the Simulation Models
figure(6)
clf
hold on
xlim([0 0.2])
xticks(0:0.02:0.2)
ylim([0 35])
yticks(0:5:35)
grid on
plot(A_sled_model(1:201,1), A_sled_model(1:201,2), '-', "LineWidth",1)
plot(A_sled_model(1:201,1), A_sled_model(1:201,6)*-0.1019368, '-',
"LineWidth",1)
colororder(c)
title('A: Sled vs Model Deceleration Pulse Comparison', 'FontSize',12)
legend("Sled A", "Model A", "location","southoutside", "NumColumns", 2)
xlabel('Time (s)', 'FontSize',12)
ylabel('Acceleration (g)', 'FontSize',12)
hold off
print("Sled_Model_A_Deceleration_Pulse_6","-dpng")

figure(7)
clf
hold on
xlim([0 0.2])
xticks(0:0.02:0.2)
ylim([0 35])
yticks(0:5:35)
```

```
grid on
plot(B_sled_model(1:201,1), B_sled_model(1:201,2), '-', "LineWidth",1)
plot(B_sled_model(1:201,1), B_sled_model(1:201,6)*-0.1019368, '-',
"LineWidth",1)
colororder(c)
title('B: Sled vs Model Deceleration Pulse Comparison', 'FontSize',12)
legend("Sled B", "Model B", "location","southoutside", "NumColumns", 2)
xlabel('Time (s)', 'FontSize',12)
ylabel('Acceleration (g)', 'FontSize',12)
hold off
print("Sled_Model_B_Deceleration_Pulse_7","-dpng")

figure(8)
clf
hold on
xlim([0 0.2])
xticks(0:0.02:0.2)
ylim([0 35])
yticks(0:5:35)
grid on
plot(CD_sled_model(1:201,1), CD_sled_model(1:201,2), '-',
"LineWidth",1)
plot(CD_sled_model(1:201,1), CD_sled_model(1:201,9), '--',
"LineWidth",1.5)
plot(CD_sled_model(1:201,1), CD_sled_model(1:201,6)*-0.1019368, '-',
"LineWidth",1)
colororder(c)
title('CD: Sled vs Model Deceleration Pulse Comparison', 'FontSize',12)
legend("Sled C", "Sled D", "Model CD", "location","southoutside",
"NumColumns", 2)
xlabel('Time (s)', 'FontSize',12)
ylabel('Acceleration (g)', 'FontSize',12)
hold off
print("Sled_Model_CD_Deceleration_Pulse_8","-dpng")

figure(9)
clf
hold on
xlim([0 0.2])
xticks(0:0.02:0.2)
ylim([0 35])
yticks(0:5:35)
grid on
plot(A_sled_model(1:201,1), A_sled_model(1:201,2), '-', "LineWidth",1)
plot(B_sled_model(1:201,1), B_sled_model(1:201,2), '-', "LineWidth",1)
plot(CD_sled_model(1:201,1), CD_sled_model(1:201,2), '-',
"LineWidth",1)
plot(CD_sled_model(1:201,1), CD_sled_model(1:201,9), '-',
"LineWidth",1.5)
plot(A_sled_model(1:201,1), A_sled_model(1:201,6), '--', "LineWidth",2)
plot(B_sled_model(1:201,1), B_sled_model(1:201,6)*-0.1019368, '--',
"LineWidth",2)
plot(CD_sled_model(1:201,1), CD_sled_model(1:201,6)*-0.1019368, '--',
"LineWidth",2)
```

```
plot(DDH_model(1:201,1), DDH_model(1:201,6)*-0.1019368, '--',
"LineWidth",2)
colororder(c)
title('Sled vs Model Deceleration Pulse Comparison', 'FontSize',12)
legend("Sled A", "Sled B", "Sled C", "Sled D", "Model A", "Model B",
"Model CD", "Model DDH", "location","southoutside", "NumColumns", 2)
xlabel('Time (s)', 'FontSize',12)
ylabel('Acceleration (g)', 'FontSize',12)
hold off
print("Sled_Model_Deceleration_Pulse_9","-dpng")


% Comparing Chest Acceleration from Sled Testing Trials
% to the Simulation Models
figure(10)
clf
hold on
xlim([0 0.2])
xticks(0:0.02:0.2)
ylim([0 70])
yticks(0:10:70)
grid on
plot(A_sled_model(1:201,1), A_sled_model(1:201,4)+0.5, '-',
"LineWidth",1)
plot(A_sled_model(1:201,1), A_sled_model(1:201,7), '-', "LineWidth",1)
yline([60], "k--", "FMVSS213 Limiting Value")
colororder(c)
title('A: Sled vs Model Chest Acceleration Comparison', 'FontSize',12)
legend("Sled A", "Model A", "location","southoutside", "NumColumns", 2)
xlabel('Time (s)', 'FontSize',12)
ylabel('Acceleration (g)', 'FontSize',12)
hold off
print("Sled_Model_A_Chest_10","-dpng")

figure(11)
clf
hold on
xlim([0 0.2])
xticks(0:0.02:0.2)
ylim([0 70])
yticks(0:10:70)
grid on
plot(B_sled_model(1:201,1), B_sled_model(1:201,4), '-', "LineWidth",1)
plot(B_sled_model(1:201,1), B_sled_model(1:201,7), '-', "LineWidth",1)
yline([60], "k--", "FMVSS213 Limiting Value")
colororder(c)
title('B: Sled vs Model Chest Acceleration Comparison', 'FontSize',12)
legend("Sled B", "Model B", "location","southoutside", "NumColumns", 2)
xlabel('Time (s)', 'FontSize',12)
ylabel('Acceleration (g)', 'FontSize',12)
hold off
print("Sled_Model_B_Chest_11","-dpng")

figure(12)
clf
```

```
hold on
xlim([0 0.2])
xticks(0:0.02:0.2)
ylim([0 100])
yticks(0:10:100)
grid on
plot(CD_sled_model(1:201,1), CD_sled_model(1:201,4)-2, '-',
"LineWidth",1)
plot(CD_sled_model(1:201,1), CD_sled_model(1:201,11)-5, '--',
"LineWidth",1.5)
plot(CD_sled_model(1:201,1), CD_sled_model(1:201,7), '-',
"LineWidth",1)
yline([60], "k--", "FMVSS213 Limiting Value")
colororder(c)
title('CD: Sled vs Model Chest Acceleration Comparison', 'FontSize',12)
legend("Sled C", "Sled D", "Model CD", "location","southoutside",
"NumColumns", 2)
xlabel('Time (s)', 'FontSize',12)
ylabel('Acceleration (g)', 'FontSize',12)
hold off
print("Sled_Model_CD_Chest_12","-dpng")

figure(13)
clf
hold on
xlim([0 0.2])
xticks(0:0.02:0.2)
ylim([0 100])
yticks(0:10:100)
grid on
plot(A_sled_model(1:201,1), A_sled_model(1:201,4)+0.5, '-',
"LineWidth",1)
plot(B_sled_model(1:201,1), B_sled_model(1:201,4), '-', "LineWidth",1)
plot(CD_sled_model(1:201,1), CD_sled_model(1:201,4)-2, '-',
"LineWidth",1)
plot(CD_sled_model(1:201,1), CD_sled_model(1:201,11)-5, '-',
"LineWidth",1)
plot(A_sled_model(1:201,1), A_sled_model(1:201,7), '-', "LineWidth",1)
plot(B_sled_model(1:201,1), B_sled_model(1:201,7), '-', "LineWidth",1)
plot(CD_sled_model(1:201,1), CD_sled_model(1:201,7), '-',
"LineWidth",1)
plot(DDH_model(1:201,1), DDH_model(1:201,7), '-', "LineWidth",1)
yline([60], "k--", "FMVSS213 Limiting Value")
colororder(c)
title('Sled vs Model Chest Acceleration Comparison', 'FontSize',12)
legend("Sled A", "Sled B", "Sled C", "Sled D", "Model A", "Model B",
"Model CD", "Model DDH", "location","southoutside","NumColumns", 3)
xlabel('Time (s)', 'FontSize',12)
ylabel('Acceleration (g)', 'FontSize',12)
hold off
print("Sled_Model_Chest_13","-dpng")
```

```
% Comparing Head Acceleration from Sled Testing Trials
% to the Simulation Models
figure(14)
clf
hold on
xlim([0 0.2])
xticks(0:0.02:0.2)
ylim([0 120])
yticks(0:10:120)
grid on
plot(A_sled_model(1:201,1), A_sled_model(1:201,5)+2.8, '-',
"LineWidth",1)
plot(A_sled_model(1:201,1), A_sled_model(1:201,8), '-', "LineWidth",1)
colororder(c)
title('A: Sled vs Model Head Acceleration Comparison', 'FontSize',12)
legend("Sled A", "Model A", "location","southoutside", "NumColumns", 2)
xlabel('Time (s)', 'FontSize',12)
ylabel('Acceleration (g)', 'FontSize',12)
hold off
print("Sled_Model_A_Head_14","-dpng")

figure(15)
clf
hold on
xlim([0 0.2])
xticks(0:0.02:0.2)
ylim([0 120])
yticks(0:10:120)
grid on
plot(B_sled_model(1:201,1), B_sled_model(2:202,5)+3.5, '-',
"LineWidth",1)
plot(B_sled_model(1:201,1), B_sled_model(1:201,8), '-', "LineWidth",1)
colororder(c)
title('B: Sled vs Model Head Acceleration Comparison', 'FontSize',12)
legend("Sled B", "Model B", "location","southoutside", "NumColumns", 2)
xlabel('Time (s)', 'FontSize',12)
ylabel('Acceleration (g)', 'FontSize',12)
hold off
print("Sled_Model_B_Head_15","-dpng")

figure(16)
clf
hold on
xlim([0 0.2])
xticks(0:0.02:0.2)
ylim([0 120])
yticks(0:10:120)
grid on
plot(CD_sled_model(1:201,1), CD_sled_model(3:203,5)+7, '-',
"LineWidth",1)
plot(CD_sled_model(1:201,1), CD_sled_model(1:201,12)+6, '--',
"LineWidth",1.5)
plot(CD_sled_model(1:201,1), CD_sled_model(1:201,8), '-',
"LineWidth",1)
colororder(c)
```

```
title('CD: Sled vs Model Head Acceleration Comparison', 'FontSize',12)
legend("Sled C", "Sled D", "Model CD", "location","southoutside",
"NumColumns", 3)
xlabel('Time (s)', 'FontSize',12)
ylabel('Acceleration (g)', 'FontSize',12)
hold off
print("Sled_Model_CD_Head_16","-dpng")

figure(17)
clf
hold on
xlim([0 0.2])
xticks(0:0.02:0.2)
ylim([0 120])
yticks(0:10:120)
grid on
plot(A_sled_model(1:201,1), A_sled_model(1:201,5)+2.8, '-',
"LineWidth",1)
plot(B_sled_model(1:201,1), B_sled_model(2:202,5)+3.5, '-',
"LineWidth",1)
plot(CD_sled_model(1:201,1), CD_sled_model(3:203,5)+7, '-',
"LineWidth",1)
plot(CD_sled_model(1:201,1), CD_sled_model(1:201,12)+6, '-',
"LineWidth",1)
plot(A_sled_model(1:201,1), A_sled_model(1:201,8), '-', "LineWidth",1)
plot(B_sled_model(1:201,1), B_sled_model(1:201,8), '-', "LineWidth",1)
plot(CD_sled_model(1:201,1), CD_sled_model(1:201,8), '-',
"LineWidth",1)
plot(DDH_model(1:201,1), DDH_model(1:201,8), '-', "LineWidth",1)
colororder(c)
title('Sled vs Model Head Acceleration Comparison', 'FontSize',12)
legend("Sled A", "Sled B", "Sled C", "Sled D", "Model A", "Model B",
"Model CD", "Model DDH", "location","southoutside","NumColumns", 4)
xlabel('Time (s)', 'FontSize',12)
ylabel('Acceleration (g)', 'FontSize',12)
hold off
print("Sled_Model_Head_17","-dpng")


% Additional Comparisons
d = [
    0.267 0.467 0.667  % Blue
    0.133 0.533 0.200  % Green
    0.800 0.733 0.267  % Yellow
    0.933 0.400 0.467  % Red
    0.667 0.200 0.467  % Purple
    0.933 0.467 0.200  % Orange
    0.067 0.467 0.467  % Teal
    ];

figure(20)
clf
hold on
xlim([0 0.2])
xticks(0:0.02:0.2)
```

```
ylim([0 120])
yticks(0:10:120)
grid on
plot(A_sled_model(1:201,1), A_sled_model(1:201,7), '-', "LineWidth",1)
plot(B_sled_model(1:201,1), B_sled_model(1:201,7), '-', "LineWidth",1)
plot(CD_sled_model(1:201,1), CD_sled_model(1:201,7), '-',
"LineWidth",1)
plot(DDH_model(1:201,1), DDH_model(1:201,7), '-', "LineWidth",1)
yline([60], "k--", "FMVSS213 Limiting Value")
colororder(d)
title('Model Chest Acceleration Comparison', 'FontSize',12)
legend("Model A", "Model B", "Model CD", "Model DDH",
"location","southoutside","NumColumns", 3)
xlabel('Time (s)', 'FontSize',12)
ylabel('Acceleration (g)', 'FontSize',12)
hold off
print("Model_Chest_20","-dpng")

figure(21)
clf
hold on
xlim([0 0.2])
xticks(0:0.02:0.2)
ylim([0 120])
yticks(0:10:120)
grid on
plot(A_sled_model(1:201,1), A_sled_model(1:201,8), '-', "LineWidth",1)
plot(B_sled_model(1:201,1), B_sled_model(1:201,8), '-', "LineWidth",1)
plot(CD_sled_model(1:201,1), CD_sled_model(1:201,8), '-',
"LineWidth",1)
plot(DDH_model(1:201,1), DDH_model(1:201,8), '-', "LineWidth",1)
colororder(d)
title('Model Head Acceleration Comparison', 'FontSize',12)
legend("Model A", "Model B", "Model CD", "Model DDH",
"location","southoutside","NumColumns", 3)
xlabel('Time (s)', 'FontSize',12)
ylabel('Acceleration (g)', 'FontSize',12)
hold off
print("Model_Head_21","-dpng")


% Sled Chest Accelerations with Peaks
figure(181)
clf
hold on
xlim([0 0.2])
xticks(0:0.02:0.2)
ylim([0 80])
yticks(0:10:80)
grid on
plot(A_sled_model(1:201,1), A_sled_model(1:201,4)+0.5, '-',
"LineWidth",1)
plot(B_sled_model(1:201,1), B_sled_model(1:201,4), '-', "LineWidth",1)
plot(CD_sled_model(1:201,1), CD_sled_model(1:201,4)-2, '-',
"LineWidth",1)
```

```
plot(CD_sled_model(1:201,1), CD_sled_model(1:201,11)-5, '-',
"LineWidth",1)
yline([60], "k--", "FMVSS213 Limiting Value")
colororder(d)
title('Sled Trials Chest Acceleration Comparison', 'FontSize',12)
legend("Sled A", "Sled B", "Sled C", "Sled D",
"location","southoutside","NumColumns", 3)
xlabel('Time (s)', 'FontSize',12)
ylabel('Acceleration (g)', 'FontSize',12)
hold off
print("Sled_Chest_181","-dpng")

figure(191)
clf
hold on
xlim([0 0.2])
xticks(0:0.02:0.2)
ylim([0 80])
yticks(0:10:80)
grid on
plot(A_sled_model(1:201,1), A_sled_model(1:201,5)+2.8, '-',
"LineWidth",1)
plot(B_sled_model(1:201,1), B_sled_model(2:202,5)+3.5, '-',
"LineWidth",1)
plot(CD_sled_model(1:201,1), CD_sled_model(3:203,5)+7, '-',
"LineWidth",1)
plot(CD_sled_model(1:201,1), CD_sled_model(1:201,12)+6, '-',
"LineWidth",1)
colororder(d)
title('Sled Trials Head Acceleration Comparison', 'FontSize',12)
legend("Sled A", "Sled B", "Sled C", "Sled D",
"location","southoutside","NumColumns", 3)
xlabel('Time (s)', 'FontSize',12)
ylabel('Acceleration (g)', 'FontSize',12)
hold off
print("Sled_Head_191","-dpng")

figure(222)
clf
hold on
xlim([0 0.2])
xticks(0:0.02:0.2)
ylim([0 80])
yticks(0:10:80)
grid on
plot(A_sled_model(1:201,1), A_sled_model(1:201,5)+2.8, '-',
"LineWidth",1)
xline([0.056], "--", "t = 56 ms")
xline([0.083], "--", "t = 83 ms")
xline([0.120], "--", "t = 120 ms")
colororder(d)
title('Sled Trial A Head Acceleration', 'FontSize',12)
legend("Sled A", "location","southoutside","NumColumns", 3)
xlabel('Time (s)', 'FontSize',12)
ylabel('Acceleration (g)', 'FontSize',12)
```

```
hold off
print("Sled_Head_APeaks_222","-dpng")

figure(221)
clf
hold on
xlim([0 0.2])
xticks(0:0.02:0.2)
ylim([0 80])
yticks(0:10:80)
grid on
plot(A_sled_model(1:201,1), A_sled_model(1:201,5)+2.8, '-',
"LineWidth",1)
plot(B_sled_model(1:201,1), B_sled_model(2:202,5)+3.5, '-.',
"LineWidth",1)
xline([0.076], "--")
text(0.075, 60, "t = 76 ms",'Rotation', 90, 'VerticalAlignment',
'bottom', 'HorizontalAlignment', 'left');
xline([0.083], "--", "t = 83 ms")
colororder(d)
title('Sled Trial A & B Head Acceleration', 'FontSize',12)
legend("Sled A", "Sled B" ,"location","southoutside","NumColumns", 3)
xlabel('Time (s)', 'FontSize',12)
ylabel('Acceleration (g)', 'FontSize',12)
hold off
print("Sled_Head_ABPeaks_221","-dpng")

figure(231)
clf
hold on
xlim([0 0.2])
xticks(0:0.02:0.2)
ylim([0 80])
yticks(0:10:80)
grid on
plot(B_sled_model(1:201,1), B_sled_model(2:202,5)+3.5, '-',
"LineWidth",1)
xline([0.056], "--", "t = 56 ms")
xline([0.076], "--", "t = 76 ms")
xline([0.120], "--", "t = 120 ms")
colororder(d)
title('Sled Trial B Head Acceleration', 'FontSize',12)
legend("Sled B", "location","southoutside","NumColumns", 3)
xlabel('Time (s)', 'FontSize',12)
ylabel('Acceleration (g)', 'FontSize',12)
hold off
print("Sled_Head_BPeaks_231","-dpng")

figure(241)
clf
hold on
xlim([0 0.2])
xticks(0:0.02:0.2)
ylim([0 80])
yticks(0:10:80)
```

```
grid on
plot(CD_sled_model(1:201,1), CD_sled_model(3:203,5)+7, '-',
"LineWidth",1)
xline([0.058], "--", "t = 58 ms")
xline([0.080], "--", "t = 80 ms")
xline([0.120], "--", "t = 120 ms")
colororder(d)
title('Sled Trial C Head Acceleration', 'FontSize',12)
legend("Sled C", "location","southoutside","NumColumns", 3)
xlabel('Time (s)', 'FontSize',12)
ylabel('Acceleration (g)', 'FontSize',12)
hold off
print("Sled_Head_CPeaks_241","-dpng")

figure(251)
clf
hold on
xlim([0 0.2])
xticks(0:0.02:0.2)
ylim([0 80])
yticks(0:10:80)
grid on
plot(CD_sled_model(1:201,1), CD_sled_model(1:201,12)+6, '-',
"LineWidth",1)
xline([0.057], "--", "t = 57 ms")
xline([0.081], "--", "t = 81 ms")
xline([0.120], "--", "t = 120 ms")
colororder(d)
title('Sled Trial D Head Acceleration', 'FontSize',12)
legend("Sled D", "location","southoutside","NumColumns", 3)
xlabel('Time (s)', 'FontSize',12)
ylabel('Acceleration (g)', 'FontSize',12)
hold off
print("Sled_Head_DPeaks_251","-dpng")

figure(252)
clf
hold on
xlim([0 0.2])
xticks(0:0.02:0.2)
ylim([0 80])
yticks(0:10:80)
grid on
plot(CD_sled_model(1:201,1), CD_sled_model(3:203,5)+7, '-',
"LineWidth",1)
plot(CD_sled_model(1:201,1), CD_sled_model(1:201,12)+6, '-.',
"LineWidth",1)
xline([0.080], "--")
text(0.080, 1, "t = 80 ms",'Rotation', 90, 'VerticalAlignment',
'bottom', 'HorizontalAlignment', 'left');
colororder(d)
title('Sled Trial C & D Head Acceleration', 'FontSize',12)
legend("Sled C", "Sled D", "location","southoutside","NumColumns", 3)
xlabel('Time (s)', 'FontSize',12)
ylabel('Acceleration (g)', 'FontSize',12)
```

```
hold off
print("Sled_Head_CDPeaks_252","-dpng")

figure(261)
clf
hold on
xlim([0 0.2])
xticks(0:0.02:0.2)
ylim([0 80])
yticks(0:10:80)
grid on
plot(A_sled_model(1:201,1), A_sled_model(1:201,4)+0.5, '-',
"LineWidth",1)
xline([0.056], "--", "t = 56 ms")
yline([60], "k--", "FMVSS213 Limiting Value")
colororder(d)
title('Sled Trial A Chest Acceleration', 'FontSize',12)
legend("Sled A", "location","southoutside","NumColumns", 3)
xlabel('Time (s)', 'FontSize',12)
ylabel('Acceleration (g)', 'FontSize',12)
hold off
print("Sled_Chest_APeaks_261","-dpng")

figure(271)
clf
hold on
xlim([0 0.2])
xticks(0:0.02:0.2)
ylim([0 80])
yticks(0:10:80)
grid on
plot(B_sled_model(1:201,1), B_sled_model(1:201,4), '-', "LineWidth",1)
xline([0.056], "--", "t = 56 ms")
yline([60], "k--", "FMVSS213 Limiting Value")
colororder(d)
title('Sled Trial B Chest Acceleration', 'FontSize',12)
legend("Sled B", "location","southoutside","NumColumns", 3)
xlabel('Time (s)', 'FontSize',12)
ylabel('Acceleration (g)', 'FontSize',12)
hold off
print("Sled_Chest_BPeaks_271","-dpng")

figure(272)
clf
hold on
xlim([0 0.2])
xticks(0:0.02:0.2)
ylim([0 80])
yticks(0:10:80)
grid on
plot(A_sled_model(1:201,1), A_sled_model(1:201,4)+0.5, '-',
"LineWidth",1)
plot(B_sled_model(1:201,1), B_sled_model(1:201,4), '-.', "LineWidth",1)
xline([0.056], "--", "t = 56 ms")
yline([60], "k--", "FMVSS213 Limiting Value")
```

```
colororder(d)
title('Sled Trial A & B Chest Acceleration', 'FontSize',12)
legend("Sled A", "Sled B", "location","southoutside","NumColumns", 3)
xlabel('Time (s)', 'FontSize',12)
ylabel('Acceleration (g)', 'FontSize',12)
hold off
print("Sled_Chest_ABPeaks_272","-dpng")

figure(281)
clf
hold on
xlim([0 0.2])
xticks(0:0.02:0.2)
ylim([0 80])
yticks(0:10:80)
grid on
plot(CD_sled_model(1:201,1), CD_sled_model(1:201,4)-2, '-',
"LineWidth",1)
xline([0.058], "--", "t = 58 ms")
yline([60], "k--", "FMVSS213 Limiting Value")
colororder(d)
title('Sled Trial C Chest Acceleration', 'FontSize',12)
legend("Sled C", "location","southoutside","NumColumns", 3)
xlabel('Time (s)', 'FontSize',12)
ylabel('Acceleration (g)', 'FontSize',12)
hold off
print("Sled_Chest_CPeaks_281","-dpng")

figure(291)
clf
hold on
xlim([0 0.2])
xticks(0:0.02:0.2)
ylim([0 80])
yticks(0:10:80)
grid on
plot(CD_sled_model(1:201,1), CD_sled_model(1:201,11)-5, '-',
"LineWidth",1)
xline([0.057], "--", "t = 57 ms")
yline([60], "k--", "FMVSS213 Limiting Value")
colororder(d)
title('Sled Trial D Chest Acceleration', 'FontSize',12)
legend("Sled D", "location","southoutside","NumColumns", 3)
xlabel('Time (s)', 'FontSize',12)
ylabel('Acceleration (g)', 'FontSize',12)
hold off
print("Sled_Chest_DPeaks_291","-dpng")

figure(292)
clf
hold on
xlim([0 0.2])
xticks(0:0.02:0.2)
ylim([0 80])
yticks(0:10:80)
```

```
grid on
plot(CD_sled_model(1:201,1), CD_sled_model(1:201,4)-2, '-',
"LineWidth",1)
plot(CD_sled_model(1:201,1), CD_sled_model(1:201,11)-5, '-.',
"LineWidth",1)
xline([0.058], "--", "t = 58 ms")
yline([60], "k--", "FMVSS213 Limiting Value")
colororder(d)
title('Sled Trial D Chest Acceleration', 'FontSize',12)
legend("Sled C", "Sled D", "location","southoutside","NumColumns", 3)
xlabel('Time (s)', 'FontSize',12)
ylabel('Acceleration (g)', 'FontSize',12)
hold off
print("Sled_Chest_CDPeaks_292","-dpng")

figure(30)
clf
hold on
xlim([0 0.2])
xticks(0:0.02:0.2)
ylim([0 70])
yticks(0:10:70)
grid on
plot(DDH_model(1:201,1), DDH_model(1:201,7), '-', "LineWidth",1)
yline([60], "k--", "FMVSS213 Limiting Value")
xline([0.060], "--", "t = 60 ms")
colororder(d)
title('Model DDH Chest Acceleration', 'FontSize',12)
legend("Model DDH", "location","southoutside","NumColumns", 3)
xlabel('Time (s)', 'FontSize',12)
ylabel('Acceleration (g)', 'FontSize',12)
hold off
print("Model_DDH_Chest_30","-dpng")


figure(31)
clf
hold on
xlim([0 0.2])
xticks(0:0.02:0.2)
ylim([0 120])
yticks(0:10:120)
grid on
plot(DDH_model(1:201,1), DDH_model(1:201,8), '-', "LineWidth",1)
xline([0.067], "--", "t = 67 ms")
colororder(d)
title('Model DDH Head Acceleration', 'FontSize',12)
legend("Model DDH",  "location","southoutside","NumColumns", 3)
xlabel('Time (s)', 'FontSize',12)
ylabel('Acceleration (g)', 'FontSize',12)
hold off
print("Model_DDH_Head_31","-dpng")
```

```
% _*Kristy Brinker Brouwer*_ _*Nursemaid.mlx*_


% Importing NEISS data.
neiss=csvread("neiss.csv");

% Figures for Part 2
figure(1)
clf
hold on
colororder({'k','k'})
xlim([2014 2024])
xticks(2015:1:2023)
grid on
box on
yyaxis left
ylim([0 425])
yticks(0:50:400)
bar(neiss(1:9,1), neiss(1:9,2), 'FaceColor',[0.267 0.467
0.667],'EdgeColor',[0.400 0.800 0.933],'LineWidth',1)
ylabel('NEISS Raw Count of Injury Events','Color',[0.267 0.467
0.667],'FontSize',10)
yyaxis right
ylim([0 8500])
yticks(0:1000:8000)
plot(neiss(1:9,1), neiss(1:9,3), '-o', 'Color',[0.533 0.667
0.467],'MarkerFaceColor',[0.133 0.533 0.200],"LineWidth", 4)
ylabel('Weighted National Frequency of Injury Events', 'Color', [0.533
0.667 0.467],'FontSize',10)
title('Yearly Non-Transportation Related CSS Injuries Reported in the
United States', 'FontSize',12)
legend("Raw", "Weighted", "location","southoutside","NumColumns", 2)
hold off
print("Yearly_NonT_Injuries_1","-dpng")

figure(2)
clf
hold on
grid on
box on
ylim([0 3000])
yticks(0:500:3000)
xlim([0 11])
xticks([1:10])
xtickangle(45)
xticklabels({['1' char(8804) '6'],['7' char(8804) '12'],['13'
char(8804) '18'],['19' char(8804) '23'],'2', '3', '4', '5', '6', '7'})
plot(neiss(12:21,1), neiss(12:21,2), '-o', 'Color',[0.267 0.467
0.667],'MarkerFaceColor',[0.400 0.800 0.933],"LineWidth",4)
xlabel(' ', 'FontSize',20)
ylabel('Injury Events', 'FontSize',12)
title('Predicted Yearly Frequency for CSS Fall Related Injuries in the
United States', 'FontSize',12)
hold off
print("Yearly_CSS_Falls_2","-dpng")
```

```
figure(3)
clf
hold on
grid on
box on
ylim([0 2500])
yticks(0:500:2500)
xlim([0 11])
xticks([1:10])
xtickangle(45)
xticklabels({['1' char(8804) '6'],['7' char(8804) '12'],['13'
char(8804) '18'],['19' char(8804) '23'],'2', '3', '4', '5', '6', '7'})
plot(neiss(24:33,1), neiss(24:33,2), '-o', 'Color',[0.267 0.467
0.667],'MarkerFaceColor',[0.400 0.800 0.933],"LineWidth",4)
xlabel(' ', 'FontSize',20)
ylabel('Injury Events', 'FontSize',12)
title('Predicted Yearly Frequency for CSS Non-Crash Event Head Injuries
in the United States', 'FontSize',12)
hold off
print("Yearly_CSS_Head_3","-dpng")

figure(4)
clf
hold on
grid on
box on
ylim([0 200])
yticks(0:50:200)
xlim([0 8])
xticks([1:7])
xtickangle(45)
xticklabels({['1' char(8804) '6'],['7' char(8804) '12'],['13'
char(8804) '18'],['19' char(8804) '23'],'2', '3', '4', '5', '6', '7'})
plot(neiss(35:41,1), neiss(35:41,2), '-o', 'Color',[0.267 0.467
0.667],'MarkerFaceColor',[0.400 0.800 0.933],"LineWidth",4)
xlabel(' ', 'FontSize',20)
ylabel('Injury Events', 'FontSize',12)
%title('Predicted Yearly Frequency of Nurse-maid's Elbow Cases in the
United States ', 'FontSize',12)
hold off
print("Yearly_CSS_Nursemaid_4","-dpng")
```

APPENDIX G

In-Vehicle DOE Outcome Summaries

Figure G1

DOE Outcomes for the Compact Vehicle Type

Full Design of Experiments: 4 factors, Multi-levels **Non-CPST vs. Non-CPST + CPST-STAC guidance**				Trial #	**Initial fit check by CPST**	Trial #	**non-CPST**	Trial #	**non-CPST + STAC CPST**
Compact: Toyota Corolla	Merritt Wallenberg	1yo	Hip	1.01	PASS	1.16	PASS	1.31	cancel
			Femur	1.02	FAIL	1.17	cancel	1.32	cancel
			Walking	1.03	PASS	1.18	PASS	1.33	cancel
		3yo	Hip	1.04	PASS	1.19	PASS	1.34	cancel
			Femur	1.05	PASS	1.20	PASS	1.35	cancel
			Walking	1.06	Cond PASS	1.21	Cond PASS	1.36	cancel
	Diono Radian R100	1yo	Hip	1.07	PASS	1.22	PASS	1.37	cancel
			Femur	1.08	FAIL	1.23	cancel	1.38	cancel
			Walking	1.09	FAIL	1.24	cancel	1.39	cancel
		3yo	Hip	1.10	PASS	1.25	PASS	1.40	cancel
			Femur	1.11	PASS	1.26	PASS	1.41	cancel
			Walking	1.12	Cond PASS	1.27	Cond PASS	1.42	cancel
	RideSafer + BubbleBum	3yo	Hip	1.13	PASS	1.28	FAIL	1.43	PASS
			Femur	1.14	FAIL	1.29	cancel	1.44	cancel
			Walking	1.15	Cond FAIL	1.30	cancel	1.45	cancel

Figure G2

DOE Outcomes for the SUV Vehicle Type

Full Design of Experiments:
4 factors, Multi-levels
Non-CPST vs. Non-CPST + CPST-STAC guidance

				Trial #	Initial fit check by CPST	Trial #	non-CPST	Trial #	non-CPST + STAC CPST
SUV: Toyota Rav4	Merritt Wallenberg	1yo	Hip	2.01	PASS	2.16	FAIL	2.31	PASS
			Femur	2.02	PASS	2.17	FAIL	2.32	PASS
			Walking	2.03	PASS	2.18	PASS	2.33	cancel
		3yo	Hip	2.04	PASS	2.19	PASS	2.34	cancel
			Femur	2.05	PASS	2.20	PASS	2.35	cancel
			Walking	2.06	Cond PASS	2.21	Cond PASS	2.36	cancel
	Diono Radian R100	1yo	Hip	2.07	PASS	2.22	FAIL	2.37	PASS
			Femur	2.08	FAIL	2.23	cancel	2.38	cancel
			Walking	2.09	FAIL	2.24	cancel	2.39	cancel
		3yo	Hip	2.10	PASS	2.25	PASS	2.40	cancel
			Femur	2.11	PASS	2.26	FAIL	2.41	PASS
			Walking	2.12	Cond PASS	2.27	Cond FAIL	2.42	Cond PASS
	RideSafer + BubbleBum	3yo	Hip	2.13	PASS	2.28	FAIL	2.43	PASS
			Femur	2.14	FAIL	2.29	cancel	2.44	cancel
			Walking	2.15	Cond FAIL	2.30	cancel	2.45	cancel

Figure G3

DOE Outcomes for the Truck Vehicle Type

Full Design of Experiments:
4 factors, Multi-levels
Non-CPST vs. Non-CPST + CPST-STAC guidance

Vehicle	Seat	Age	Placement	Trial #	Initial fit check by CPST	Trial #	non-CPST	Trial #	non-CPST + STAC CPST
Truck: Ford F-150 Crew Cab	Merritt Wallenberg	1yo	Hip	3.01	FAIL	3.16	cancel	3.31	cancel
			Femur	3.02	FAIL	3.17	cancel	3.32	cancel
			Walking	3.03	FAIL	3.18	cancel	3.33	cancel
		3yo	Hip	3.04	PASS	3.19	PASS	3.34	cancel
			Femur	3.05	PASS	3.20	PASS	3.35	cancel
			Walking	3.06	Cond PASS	3.21	Cond PASS	3.36	cancel
	Diono Radian R100	1yo	Hip	3.07	PASS	3.22	FAIL	3.37	PASS
			Femur	3.08	FAIL	3.23	cancel	3.38	cancel
			Walking	3.09	Cond FAIL	3.24	cancel	3.39	cancel
		3yo	Hip	3.10	PASS	3.25	PASS	3.40	cancel
			Femur	3.11	PASS	3.26	PASS	3.41	cancel
			Walking	3.12	Cond PASS	3.27	Cond PASS	3.42	cancel
	RideSafer + BubbleBum	3yo	Hip	3.13	PASS	3.28	FAIL	3.43	PASS
			Femur	3.14	FAIL	3.29	cancel	3.44	cancel
			Walking	3.15	Cond FAIL	3.30	cancel	3.45	cancel

Figure G4

DOE Outcomes for the Minivan Vehicle Type

Full Design of Experiments: 4 factors, Multi-levels **Non-CPST vs. Non-CPST + CPST-STAC guidance**				Trial #	**Initial fit check by CPST**	Trial #	**non-CPST**	Trial #	**non-CPST + STAC CPST**
Minivan: Toyota Sienna	Merritt Wallenberg	1yo	Hip	4.01	PASS	4.16	PASS	4.31	cancel
			Femur	4.02	PASS	4.17	Cond PASS	4.32	cancel
			Walking	4.03	PASS	4.18	PASS	4.33	cancel
		3yo	Hip	4.04	PASS	4.19	PASS	4.34	cancel
			Femur	4.05	PASS	4.20	PASS	4.35	cancel
			Walking	4.06	PASS	4.21	PASS	4.36	cancel
	Diono Radian R100	1yo	Hip	4.07	PASS	4.22	**FAIL**	4.37	PASS
			Femur	4.08	FAIL	4.23	cancel	4.38	cancel
			Walking	4.09	FAIL	4.24	cancel	4.39	cancel
		3yo	Hip	4.10	PASS	4.25	PASS	4.40	cancel
			Femur	4.11	PASS	4.26	**FAIL**	4.41	PASS
			Walking	4.12	Cond PASS	4.27	**Cond FAIL**	4.42	Cond PASS
	RideSafer + BubbleBum	3yo	Hip	4.13	PASS	4.28	**FAIL**	4.43	PASS
			Femur	4.14	PASS	4.29	**FAIL**	4.44	PASS
			Walking	4.15	Cond PASS	4.30	**Cond FAIL**	4.45	Cond PASS

APPENDIX H

In-Vehicle Post-Installation Photos

Figure H1

Post-Installation Photos #1 for the Compact Vehicle Type, PASS

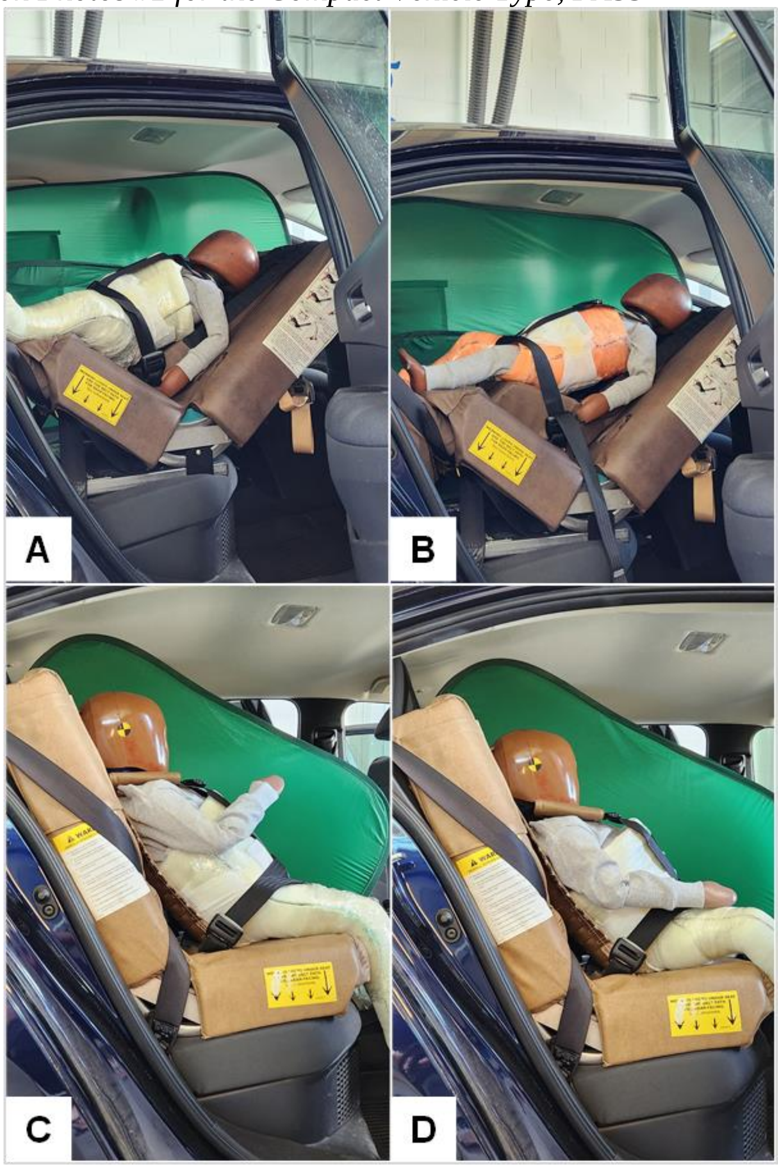

Note. (A) 1.01: Wallenberg, 1-year-old, DDH Cast. (B) 1.03: Wallenberg, 1-year-old, Walking Cast. (C) 1.05: Wallenberg, 3-year-old, Femur Cast. (D) 1.04: Wallenberg, 3-year-old, DDH Cast.

Figure H2

Post-Installation Photos #2 for the Compact Vehicle Type, PASS

Note. (A) 1.07: Radian, 1-year-old, DDH Cast. (B) 1.10: Radian, 3-year-old, DDH Cast. (C) 1.11: Radian, 3-year-old, Femur Cast. (D) 1.13: RideSafer + BubbleBum, 3-year-old, DDH Cast.

Figure H3

Post-Installation Photos for the Compact Vehicle Type, FAIL

Note. (A) 1.02: Wallenberg, 1-year-old, Femur Cast. (B) 1.08: Radian, 1-year-old, Femur Cast. (C) 1.09: Radian, 1-year-old, Walking Cast. (D) 1.13: RideSafer + BubbleBum, 3-year-old, Femur Cast.

Figure H4

Post-Installation Photos #1 for the SUV Vehicle Type, PASS

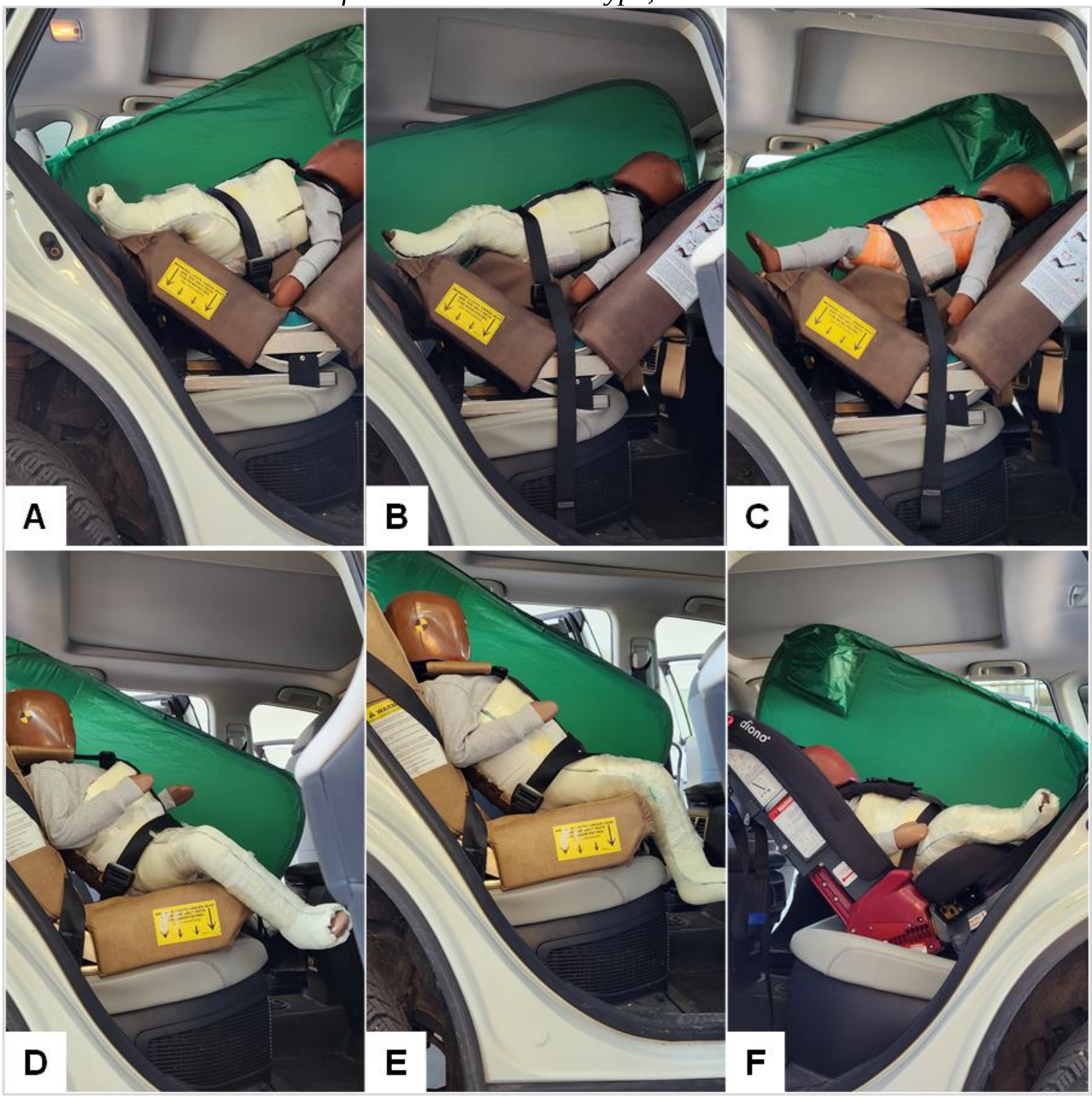

Note. (A) 2.01: Wallenberg, 1-year-old, DDH Cast. (B) 2.02: Wallenberg, 1-year-old, Femur Cast. (C) 2.03: Wallenberg, 1-year-old, Walking Cast. (D) 2.04: Wallenberg, 3-year-old, DDH Cast. (E) 2.05: Wallenberg, 3-year-old, Femur Cast. (F) 2.07: Radian, 1-year-old, DDH Cast.

Figure H5

Post-Installation Photos #2 for the SUV Vehicle Type, PASS

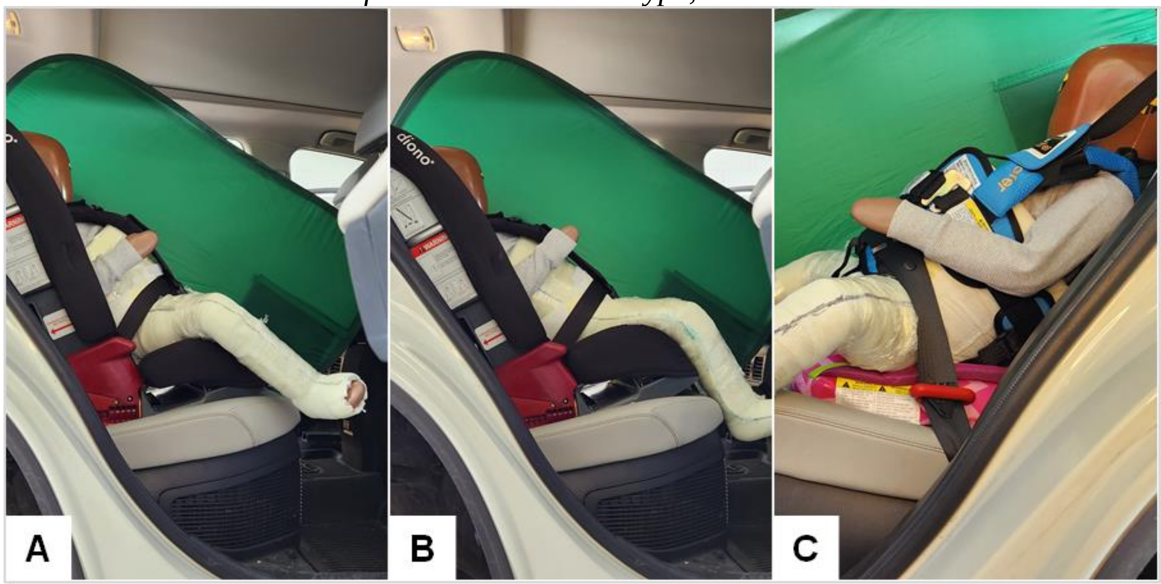

Note. (A) 2.10: Radian, 3-year-old, DDH Cast. (B) 2.11: Radian, 3-year-old, Femur Cast. (C) 1.13: RideSafer + BubbleBum, 3-year-old, DDH Cast.

Figure H6

Post-Installation Photos for the SUV Vehicle Type, FAIL

Note. (A) 2.08: Radian, 1-year-old, Femur Cast. (B) 2.09: Radian, 1-year-old, Walking Cast. (C) 2.14: RideSafer + BubbleBum, 3-year-old, Femur Cast.

Figure H7

Post-Installation Photos for the Truck Vehicle Type, PASS

Note. (A) 3.04: Wallenberg, 3-year-old, DDH Cast. (B) 3.05: Wallenberg, 3-year-old, Femur Cast. (C) 3.07: Radian, 1-year-old, DDH Cast. (D) 3.10: Radian, 3-year-old, DDH Cast. (E) 3.11: Radian, 3-year-old, Femur Cast. (F) 3.13: RideSafer + BubbleBum, 3-year-old, DDH Cast.

Figure H8

Post-Installation Photos for the Truck Vehicle Type, FAIL

Note. (A) 3.01: Wallenberg, 1-year-old, DDH Cast. (B) 3.08: Radian, 1-year-old, Femur Cast. (C) 3.14: RideSafer + BubbleBum, 3-year-old, Femur Cast.

Figure H9

Post-Installation Photos #1 for the Minivan Vehicle Type, PASS

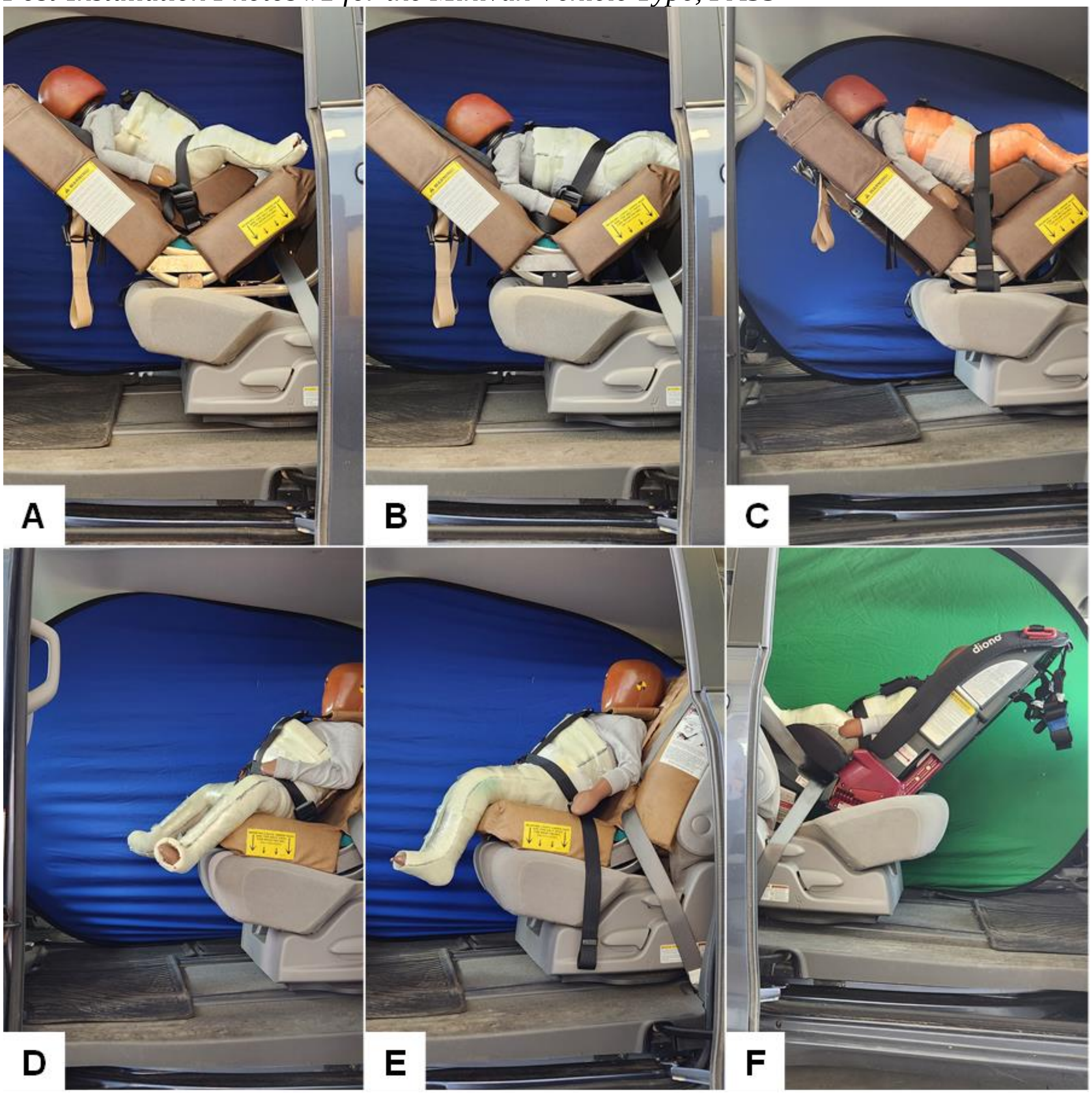

Note. (A) 4.01: Wallenberg, 1-year-old, DDH Cast. (B) 4.02: Wallenberg, 1-year-old, Femur Cast. (C) 4.03: Wallenberg, 1-year-old, Walking Cast. (D) 4.04: Wallenberg, 3-year-old, DDH Cast. (E) 4.05: Wallenberg, 3-year-old, Femur Cast. (F) 4.07: Radian, 1-year-old, DDH Cast.

Figure H10

Post-Installation Photos #2 for the Minivan Vehicle Type, PASS

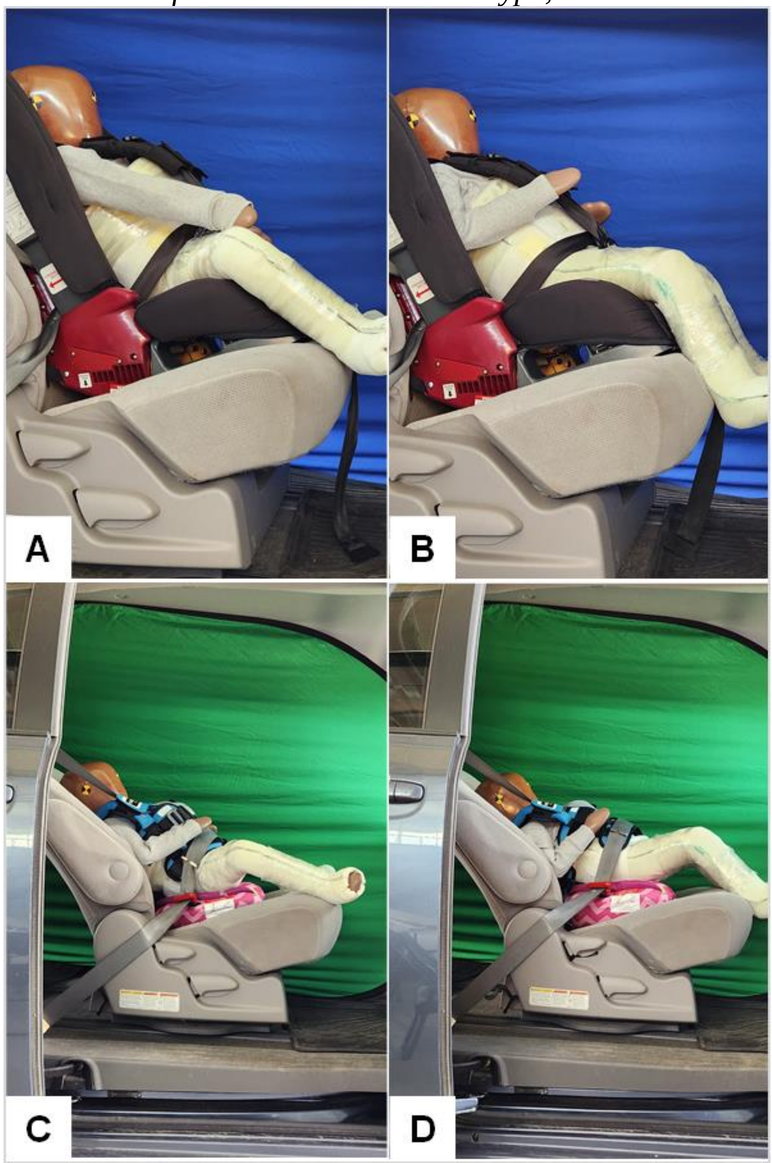

Note. (A) 4.10: Radian, 3-year-old, DDH Cast. (B) 4.11: Radian, 3-year-old, Femur Cast. (C) 4.13: RideSafer + BubbleBum, 3-year-old, DDH Cast. (D) 4.14: RideSafer + BubbleBum, 3-year-old, Femur Cast.

Figure H11

Post-Installation Photos for the Minivan Vehicle Type, FAIL

Note. 4.09: Radian, 1-year-old, Walking Cast.

APPENDIX I

Spica Cast Discharge Planning

Figure I1

Spica Cast Discharge Planning Decision Tree

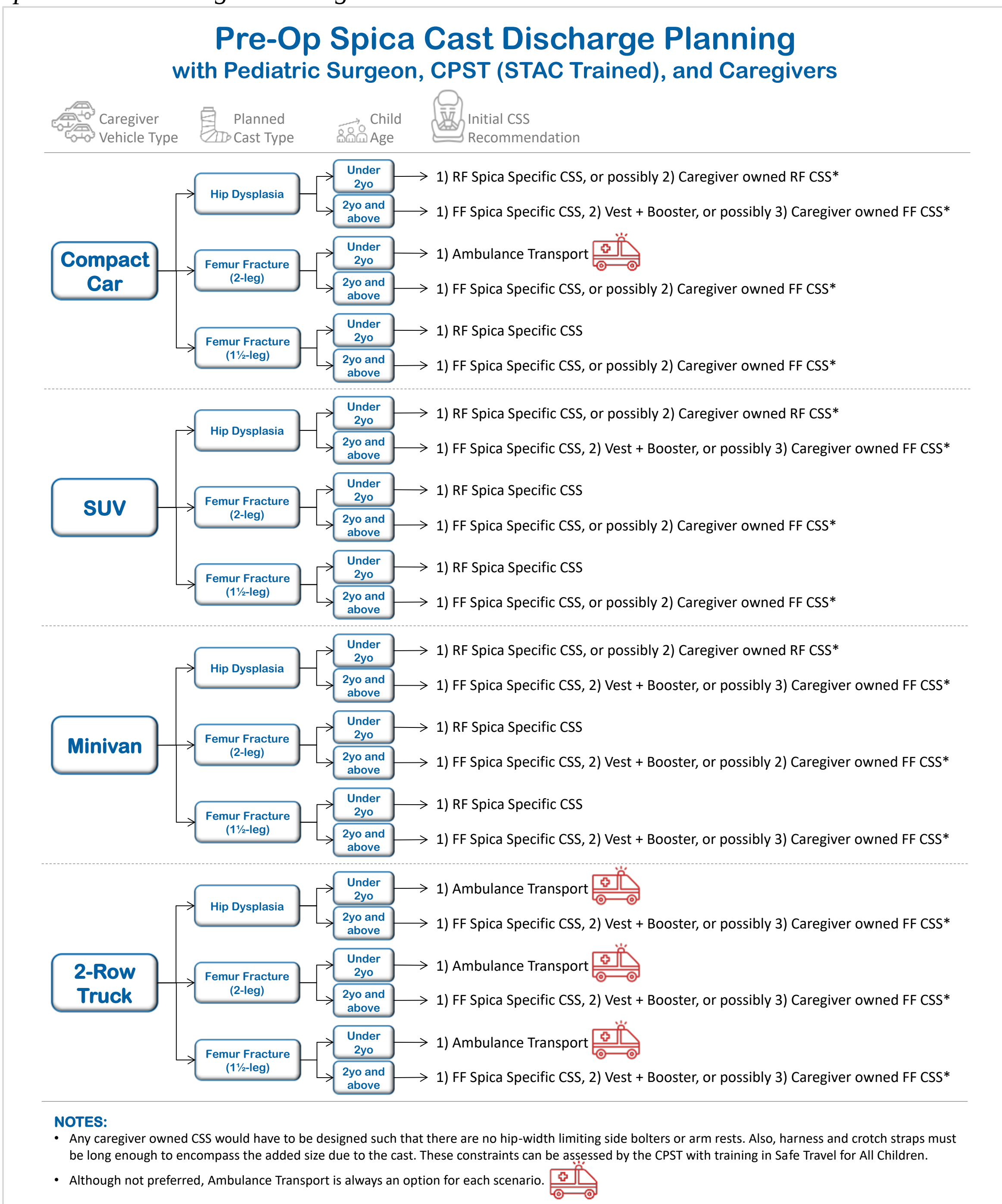

REFERENCES

Adams, A.J., Johnson, M.A., Ryan, K.A., Farrell, S.B., Morro, M., & Sankar, W.N. (2019). Safe Transportation in-Spica Following Surgical Treatment of Infantile DDH: Solutions and Threats. *J Pediatr Orthop*, 39(7), e488–e493. https://doi.org/10.1097/BPO.0000000000001317

Adaptive Specialties. (2025a, February 18). Inspired By Drive Spirit Spica Car Seat. https://www.adaptivespecialties.com/inspired-by-drive-spirit-spica-car-seat.aspx

Adaptive Specialties. (2025b, February 18). The Wallenberg Hip Cast Seat by Merritt. https://www.adaptivespecialties.com/the-wallenberg-hip-cast-car-seat-by-merritt.aspx

Ames, S.G., Salvi, A., Lin, A., Malveau, S., Mann, N.C., Jenkins, P., Hansen, M., Papa, L., Schmitz, S., Sabogal, C., & Newgard, C. (2024). Timing and causes of death to 1 year among children presenting to emergency departments. *Academic Emergency Medicine: Official Journal of the Society for Academic Emergency Medicine*, 31(6), 555–563. https://doi.org/10.1111/acem.14875

Bae, J. Y., Anderson, E., Silver, D., & Macinko, J. (2014). Child Passenger Safety Laws in the United States, 1978-2010: Policy Diffusion in the Absence of Strong Federal Intervention. *Social Science & Medicine*, 100(1), 30–37. https://doi.org/10.1016/j.socscimed.2013.10.035

Babyark. (2025, March 6). Babyark Smart User Manual. https://babyark.com/pages/user-guides

Batra, E., Midgett, J., Moon, R. (2015). Hazards Associated with Sitting and Carrying Devices for Children Two Years and Younger. *J Pediatr*, 167(1), 183-7. https://doi.org/10.1016/j.jpeds.2015.03.044

BubbleBum USA LLC. (n.d.). *BubbleBum Booster Seat (Model BB0012) [Child restraint system]*. Orlando, FL.

BubbleBum USA LLC. (2013, May 13). *Booster Seat Owner's Manual.* BubbleBum USA LLC.

Budziszewski, R., Thompson, R., Lucido, T., Walker, J., Meyer, L. K., Arthur, L. G., & Grewal, H. (2021). Measuring the Effectiveness of a Car Seat Program in an Urban, Level One Pediatric Trauma Center. *Injury Epidemiology*, 8(Suppl 1), 19. https://doi.org/10.1186/s40621-021-00313-1

Bull, M., Agran, P., Laraque, D., Pollack, S., Smith, G., Spivak, H., Tenenbein, M., & Tully, S. (1999). Transporting children with special health care needs. *Pediatrics*, 104(1), 988-992.

City of Livonia. (2025, February 18). Ambulance Transport Information. https://www.livonia.gov/ 283/Ambulance-Transport-Information

Collins, A.C., Caskey, S., Peck, J.B., Walter, N., Atkinson, T.S., & Atkinson, P.J. (2020). Frontal Crash Injury Metrics Are Below Mandated Limits for a Spica Casted Child Dummy in Currently Available Restraints. *J Pediatr Orthop*, 40(5), e394–e400. https://doi.org/10.1097/BPO.0000000000001477

Collins, A., Adams, N., Ostrander, J., Atkinson, P., & Atkinson, T. (2022). Safe transport of spica casted infants: Reducing the risk of traumatic injury in side impact collisions. *Am J Surg*, 223(1),164–169. https://doi.org/10.1016/j.amjsurg.2021.08.039

Collins, A., McKean, L., Ostrander, J., Nagarajan, S., Atkinson, P., & Atkinson, T. (2022). Crash Performance of Rear-facing Restraints with a Fracture Type Spica Casted 1-Year-Old Dummy. *J Pediatr Orthop*, 42(1), e1–e7. https://doi.org/10.1097/BPO.0000000000001978

Decina, L.E., & Lococo, K.H. (2005). Child Restraint System Use and Misuse in Six States. *Accident Analysis & Prevention.* 37(3), 583-590. https://doi.org/10.1016/j.aap.2005.01.006

Desapriya, E., Joshi, P., Subzwari, S., & Nolan, M. (2008). Infant injuries from child restraint safety seat misuse at British Columbia Children's Hospital. *Pediatr Int,* 50(5), 674-678. https://doi.org/10.1111/j.1442-200X.2008.02635.x

Diono US. (n.d.). *Radian R100, Model 50602 [Child restraint system]*. Sumner, WA.

Diono US. (2016, July 26). *Radian R100 Convertible + Booster Instruction Manual*. Diono US.

Durbin, D.R., Hoffman, B.D., &, COUNCIL ON INJURY, VIOLENCE, AND POISON PREVENTION. (2018a); Child Passenger Safety, Policy Statement. *Pediatrics,* 142(5), e20182460. https://doi.org/10.1542/peds.2018-2460

Durbin, D., Hoffman, B., & COUNCIL ON INJURY, VIOLENCE, AND POISON PREVENTION. (2018b). Child Passenger Safety, Technical Report. *Pediatrics*, 142(5), 1-18. https://doi.org/10.1542/peds.2018-2461 eSpecial Needs. (2025, February 18). EZ-ON 503 Lay Down Vest. https://www.especialneeds.com/ez-on-503-lay-down-vest.html

Ford Motor Company. (2018, September). 2018 F-150 Owner's Manual. https://www.toyota.com/owners/warranty-owners-manuals/vehicle/rav4/2019

Gadd, C. W. (1966, February). *Use of a Weighted-Impulse Criterion for Estimating Injury Hazard.* SAE Technical Paper 660793. https://doi.org/10.4271/660793

GoodCarBadCar. (2024). U.S. Sub-Segment Sales Data & Reports, 2003-2023 [Data Set]. https://www.goodcarbadcar.net/us-auto-sales-hub/u-s-automotive-segment-sales-hub

Gockley, A., Hennrikus, W., Lavin, S., Rzucidlo, S., & Rieghard, C. (2015). Transportation of children in spica casts in the USA. *J Pediatr Orthop B*, 24(4), 277-280. https://doi.org/10.1097/BPB.0000000000000169

Goldstick, J. E., Cunningham, R. M., & Carter, P. M. (2022). Current Causes of Death in Children and Adolescents in the United States. *The New England Journal of Medicine*, 386(20), 1955–1956. https://doi.org/10.1056/NEJMc2201761

Herman, M. J., Abzug, J. M., Krynetskiy, E. E., & Guzzardo, L. V. (2011). Motor vehicle transportation in hip spica casts: are our patients safely restrained? *J Pediatr Orthop,* 31(4), 465–468. https://doi.org/10.1097/BPO.0b013e31821996b2

Hu, J., Klinich, K. D., Reed, M. P., Ebert-Hamilton, S. M., & Rupp, J. D. (2014). Characterizing Child Head Motions Relative to Vehicle Rear Seat Compartment in Motor Vehicle Crashes. (Report No. DOT HS 812 105). National Highway Traffic Safety Administration

Jiang, L., Zhao, M., Lin, H., Xu, H., Chen, X., & Xu, J. (2022). Will Smart Improvements to Child Restraints Increase Their Popularity? *International Journal of Environmental Research and Public Health*, 19(23), 15727. https://doi.org/10.3390/ijerph192315727

Kistler Group. (2025). *CrashDesigner* (Version 2.11) [Data acquisition and analysis software]. Kistler Instrumente GmbH. https://www.kistler.com

Maltese, M., Tylko, S., Belwadi, A., Locey, C., & Arbogast, K.B. (2014). Comparative Performance of Forward-Facing Child Restraint Systems on the C/FMVSS No. 213Bench and Vehicle Seats. *Traffic Inj Prev*, 15(sup1), S103–S110. https://doi.org/10.1080/15389588.2014.935358

Mead, M., Caskey, S., Walter, N., Atkinson, P., Atkinson, T., & Collins, A. (2020). Injury metrics are altered in spica-casted versus non-casted child ATDs in side-impact collisions with door intrusion. *Traffic Inj Prev*, 21(6), 341–346. https://doi.org/10.1080/15389588.2020.1755969

Meriam, J. L., Kraige, L. G., & Bolton, J. N. (2018). *Engineering Mechanics: Statics* (9th ed.). Wiley.

Merritt Manufacturing, Inc. (n.d.). *Wallenberg Hip Cast Car Seat [Child restraint system]*. Franklin, IN.

Merritt Manufacturing, Inc. (2024, April). The Wallenberg Instructions for Use. https://merrittcarseat.com/the-wallenberg

MSC Software Corporation. (2004). *Working Model 2004 SP1* (Version 7.0.0.0) [Physics simulation software]. MSC Software. https://www.mscsoftware.com

Nardi, N.M., & Schaefer, T.J. (2023). Nursemaid Elbow. *StatPearls [Internet]*. https://www.ncbi.nlm.nih.gov/books/NBK430777/

National Highway Traffic Safety Administration. (2010). Special Crash Investigations—A Model for Future Corrective Action: First Generation Frontal Air Bags. *Ann of Emerg Med*, 55(4), 373-374. https://doi.org/10.1016/j.annemergmed.2010.01.028

National Highway Traffic Safety Administration. (2023). *Laboratory test procedure for FMVSS No. 213: TP-213-11*. U.S. Department of Transportation.

National Highway Traffic Safety Administration. (2024a). *Federal Motor Vehicle Safety Standard No. 208; Occupant crash protection* (49 C.F.R. § 571.208). U.S. Department of Transportation. https://www.ecfr.gov/current/title-49/subtitle-B/chapter-V/part-571/subpart-B/section-571.208

National Highway Traffic Safety Administration. (2024b). *Federal Motor Vehicle Safety Standard No. 213; Child restraint systems* (49 C.F.R. § 571.213). U.S. Department of Transportation. https://www.ecfr.gov/current/title-49/subtitle-B/chapter-V/part-571/subpart-B/section-571.213

Oliver II, G., Zielinski, J., Walter, N.E., Fornari, J., & Atkinson, P.J. (2009). The Influence of Hip Spica Casts on Child Dummies in Dynamic Crash Tests. *Traffic Inj Prev*, 10(3), 204-208. https://doi.org/10.1080/15389580802506592

O'Neil, J., Yonkman, J., Talty, J., & Bull, M. (2009). Transporting Children with Special Health Care Needs: Comparing Recommendations and Practice. *Pediatrics*, 124(2), 596–603. https://doi.org/10.1542/peds.2008-1124

Patton, D. A., Maheshwari, J., & Arbogast, K. (2022). Interactions Between Rearward-Facing Child Restraint Systems and the Front Row Seatback in Frontal Impact Sled Tests. *Traffic Inj Prev*, 23(sup1), S99–S104. https://doi.org/10.1080/15389588.2022.2078812

Parikh, S., & Wilson, L. (2010). Hazardous Use of Car Seats Outside the Car in the United States, 2003-2007. *Pediatrics*, 126(2), 352-357. https://doi.org/10.1542/peds.2010-0333

SAE International. (1995, March 1). "Instrumentation for Impact Test Part 1 - Electronic Instrumentation," SAE Recommended Practice J211/1. https://doi.org/10.4271/J211/1_199503

SAE International. (2015, March, 27). "Securing Child Restraint Systems in Motor Vehicles," SAE Recommended Practice J1819. https://doi.org/10.4271/J1819_201503

SAE International. (2021, April 30). "Taxonomy and Definitions for Terms Related to Driving Automation Systems for On-Road Motor Vehicles," SAE Recommended Practice J3016. https://doi.org/10.4271/J3016_202104

Safe Kids Worldwide. (2018a, October 17). Blue Ribbon Panel: Now Is The Time To Consider Child Passenger Safety In Self Driving Vehicles. https://www.safekids.org/press-release/blue-ribbon-panel-now-time-consider-child-passenger-safety-self-driving-vehicles

Safe Kids Worldwide. (2018b). Children in Autonomous Vehicles: Blue Ribbon Panel. https://www.safekids.org/sites/default/files/children_in_av-blue_ribbon_panel_report-final.pdf

Safe Kids Worldwide. (2019, May 14). Safe Kids Worldwide Convenes First-Ever “Children In Autonomous Vehicles” Consortium. https://www.safekids.org/press-release/safe-kids-worldwide-convenes-first-ever-children-autonomous-vehicles-consortium

Safe Kids in Automated Vehicles Alliance. (2024). White Paper: Emerging Technologies on the Road and Child Safety Implications. https://7324bcc31b4ecc63e0a9-ef9d298d888d34a4dc00b88cdd7c87b7.ssl.cf5.rackcdn.com/SKAVA%20White%20Paper%202024%20v2.3.pdf

Safe Traffic System, Inc. (n.d.). *RideSafer Travel Vest Gen 5, Model JD14101BLB [Child restraint system]*. Franklin, IL.

Safe Traffic System, Inc. (2023, June). RideSafer Gen 5 Owner’s Manual. https://ridesafertravelvest.com/manuals

Singhal, A., Adams, E., & Desapriya, E. (2012). Improper Use of Child Restraint Seats as a Sleeping Environment: Two Cases of Childhood Death. *Paediatrics & Child Health*, 17(9). 498-500. https://doi.org/10.1093/pch/17.9.498

Smith, A., & AAP Committee on Injury, Violence, and Poison Prevention. (2006). Shopping Cart–Related Injuries to Children. *Pediatrics,* 118(2), e540–e544. https://doi.org/10.1542/peds.2006-1216

Toyota Motor Sales. (2019, January). Toyota 2019 RAV4 Owner’s Manual (OM0R009U). https://www.toyota.com/owners/warranty-owners-manuals/vehicle/rav4/2019

Toyota Motor Sales. (2020a, February). Toyota 2017 Sienna Owner's Manual (OM08007U). https://www.toyota.com/owners/warranty-owners-manuals/vehicle/sienna/2017

Toyota Motor Sales. (2020b, July). Toyota 2021 Corolla Owner's Manual (OM02582U). https://www.toyota.com/owners/warranty-owners-manuals/vehicle/corolla/2021

Wang, D., Zhang, J., Wang, S., & Hu, L. (2022). Frontal Vehicular Crash Energy Management Using Analytical Model in Multiple Conditions. *Sustainability*, 14(24), 16913. https://doi.org/10.3390/su142416913

Weaver, N.L., Brixey, S.N., Williams, J., & Nansel, T.R. (2013). Promoting Correct Car Seat Use in Parents of Young Children: Challenges, Recommendations, and Implications for Health Communication. *Health Promotion Practice,* 14(2), 301-307. https://doi.org/10.1177/1524839912457567

Wietholter, K., Louden, A., & Echemendia, C. (2021). *Development of a Representative Seat Assembly for FMVSS No. 213.* (Report No. DOT HS 813 096). National Highway Traffic Safety Administration

Zaloshnja, E., Miller, T. R., & Hendrie, D. (2007). Effectiveness of child safety seats vs safety belts for children aged 2 to 3 years. *Archives of Pediatrics & Adolescent Medicine, 161*(1), 65–68. https://doi.org/10.1001/archpedi.161.1.65

Zielinski, J., Oliver, G., Sybesma, J., Walter, N., & Atkinson, P. (2009). Casting Technique and Restraint Choice Influence Child Safety During Transport of Body Casted Children Subjected to a Simulated Frontal MVA. *J Trauma,* 66(6), 1653–1665. https://doi.org/10.1097/TA.0b013e3181a4c0f4